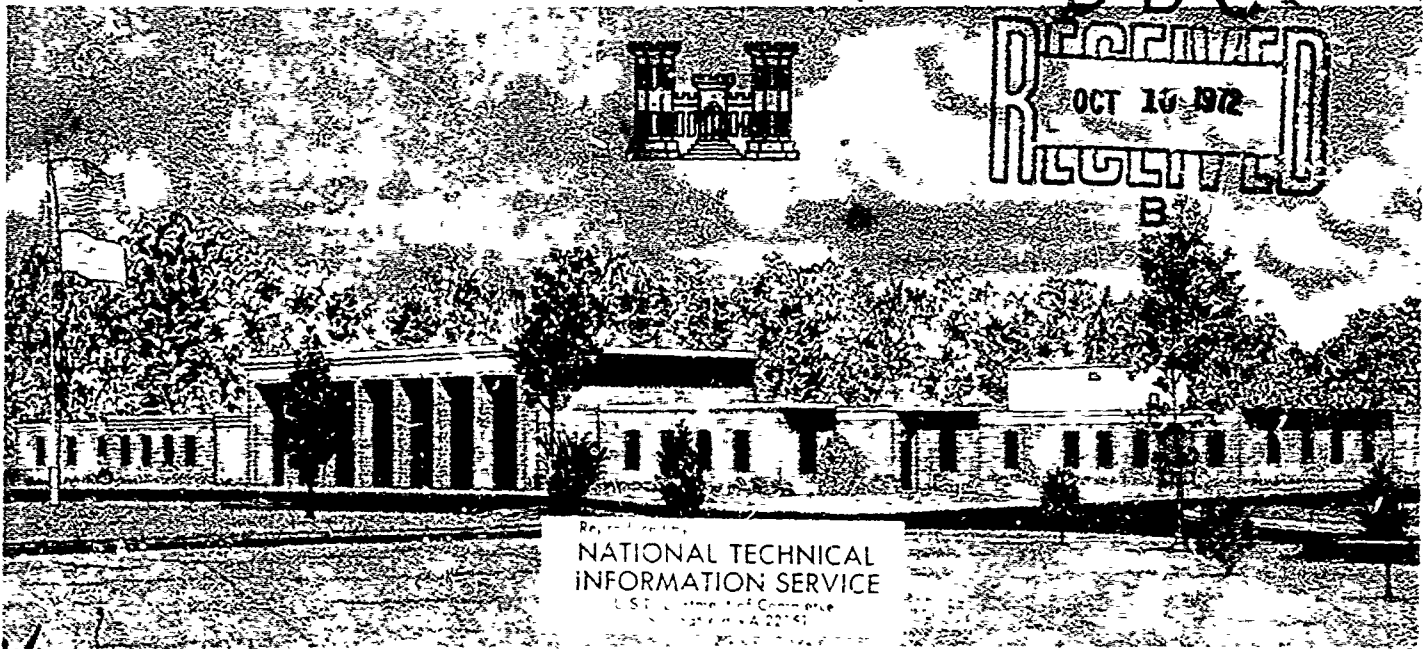TECHNICAL REPORT S-71-14

# EARTH VIBRATION EFFECTS AND ABATEMENT FOR MILITARY FACILITIES

Report 3

## ANALYSIS METHOD FOR FOOTING VIBRATIONS THROUGH LAYERED MEDIA

by

G. Waas

Destroy this report when no longer needed. Do not return
it to the originator.

The findings in this report are not to be construed as an official
Department of the Army position unless so designated
by other authorized documents.

This program is furnished by the Government and is accepted and used
by the recipient with the express understanding that the United States
Government makes no warranties, expressed or implied, concerning the
accuracy, completeness, reliability, usability, or suitability for any
particular purpose of the information and data contained in this pro-
gram or furnished in connection therewith, and the United States shall
be under no liability whatsoever to any person by reason of any use
made thereof. The program belongs to the Government. Therefore, the
recipient further agrees not to assert any proprietary rights therein or
to represent this program to anyone as other than a Government program.

## DOCUMENT CONTROL DATA - R & D

(Security classification of title, body of abstract and indexing annotation must be entered when the overall report is classified)

| 1. ORIGINATING ACTIVITY (Corporate author) | 2a. REPORT SECURITY CLASSIFICATION |
|---|---|
| College of Engineering, Office of Research Services University of California Berkeley, California | Unclassified |
| | 2b. GROUP |

3. REPORT TITLE

EARTH VIBRATION EFFECTS AND ABATEMENT FOR MILITARY FACILITIES; Report 3, ANALYSIS METHOD FOR FOOTING VIBRATIONS THROUGH LAYERED MEDIA

4. DESCRIPTIVE NOTES (Type of report and inclusive dates)

Report 3 of a series

5. AUTHOR(S) (First name, middle initial, last name)

Günter Waas

| 6. REPORT DATE | 7a. TOTAL NO. OF PAGES | 7b. NO. OF REFS |
|---|---|---|
| September 1972 | 190 | 52 |

| 8a. CONTRACT OR GRANT NO. DACA39-70-C-0023 | 9a. ORIGINATOR'S REPORT NUMBER(S) |
|---|---|
| b. PROJECT NO. | Technical Report S-71-14, Report 3 |
| c. | 9b. OTHER REPORT NO(S) (Any other numbers that may be assigned this report) |
| d. | |

10. DISTRIBUTION STATEMENT

Approved for public release; distribution unlimited.

| 11. SUPPLEMENTARY NOTES | 12. SPONSORING MILITARY ACTIVITY |
|---|---|
| Prepared under contract for U. S. Army Engineer Waterways Experiment Station, CE, Vicksburg, Mississippi. | Chief of Research and Development, Department of the Army Office, Chief of Engineers, U. S. Army |

13. ABSTRACT

A numerical method is presented for the analysis of steady-state wave propagation problems in linearly elastic or viscoelastic media of infinite extent. Plane and axisymmetric geometries are considered which consist of a finite irregular region joined to semi-infinite layered regions. By this method, torsional and vertical vibrations of circular footings on, or embedded in, homogeneous and inhomogeneous soil layers over rock are studied. The irregular region is discretized by compatible finite elements, while the semi-infinite layered regions are discretized by subdividing the layers into thin sublayers and by assuming that within each sublayer the displacements vary linearly in the direction normal to the layers. In the direction parallel to the layers, the displacements are expanded into a finite number of plane or axisymmetric propagating and decaying wave modes which are determined by the solution of algebraic eigenvalue problems. Dynamic stiffness matrices are developed which uniquely relate nodal forces to simultaneous nodal displacements at the boundary between the irregular and the layered regions and thus represent the dynamic response of the semi-infinite layered regions. The dynamic stiffness of the combined regions is computed by the direct stiffness method. The equations of motion are derived from the principle of virtual work which is formulated to facilitate the use of complex variables in the analysis of the harmonic motion. Solutions obtained by this numerical method show good agreement with known analytical solutions. The response of circular footings, which are supported by soil layers over rock and are excited to vibrate in the torsional and vertical mode, are investigated; the effects of the thickness of the supporting layer, embedment of the footing and increasing shear modulus with depth are studied. The screening effect of trenches on horizontally polarized shear waves is explored by varying the trench depth and the frequency of the wave motion.

1a

| 14 KEY WORDS | LINK A | | LINK B | | LINK C | |
|---|---|---|---|---|---|---|
| | ROLE | WT | ROLE | WT | ROLE | WT |
| Footings | | | | | | |
| Ground motion | | | | | | |
| Layered systems | | | | | | |
| Military facilities | | | | | | |
| Numerical analysis | | | | | | |
| Vibration | | | | | | |
| Wave propagation | | | | | | |

TECHNICAL REPORT S-71-14

# EARTH VIBRATION EFFECTS AND ABATEMENT FOR MILITARY FACILITIES

Report 3

## ANALYSIS METHOD FOR FOOTING VIBRATIONS THROUGH LAYERED MEDIA

by

G. Waas

September 1972

ARMY-MRC VICKSBURG MISS

# ABSTRACT

A numerical method is presented for the analysis of steady-state wave propagation problems in linearly elastic or viscoelastic media of infinite extent. Plane and axisymmetric geometries are considered which consist of a finite irregular region joined to semi-infinite layered regions. By this method, torsional and vertical vibrations of circular footings on, or embedded in, homogeneous and inhomogeneous soil layers over rock are studied.

The irregular region is discretized by compatible finite elements, while the semi-infinite layered regions are discretized by subdividing the layers into thin sublayers and by assuming that within each sublayer the displacements vary linearly in the direction normal to the layers. In the direction parallel to the layers, the displacements are expanded into a finite number of plane or axisymmetric propagating and decaying wave modes which are determined by the solution of algebraic eigenvalue problems. Dynamic stiffness matrices are developed which uniquely relate nodal forces to simultaneous nodal displacements at the boundary between the irregular and the layered regions and thus represent the dynamic response of the semi-infinite layered regions. The dynamic stiffness of the combined regions is computed by the direct stiffness method. The equations of motion are derived from the principle of virtual work which is formulated to facilitate the use of complex variables in the analysis of the harmonic motion.

Solutions obtained by this numerical method show good agreement with known analytical solutions. The response of circular footings, which are supported by soil layers over rock and are excited to vibrate in the torsional and vertical mode, are investigated; the effects of the thickness of the supporting layer, embedment of the footing and increasing shear modulus with depth are studied. The screening effect of trenches on horizontally polarized shear waves is explored by varying the trench depth and the frequency of the wave motion.

## FOREWORD

The research described in this report was performed under Contract No. DACA39-70-C-0023, "Dynamic Analysis of Embedded Footings on Layered Subsoil," between the U. S. Army Engineer Waterways Experiment Station (WES) and The Regents of the University of California during the period 1 June 1970 to 30 June 1972.

The objective of the research, which was begun in June 1970, was to compute steady state displacements generated within a layered soil system by forced vibrations of a rigid circular footing located on, or embedded in, this sytem. The stated objective has been achieved and in addition a new very general method has been developed for steady state analysis of infinite plane and axisymmetric structures. The major part of the research described was performed by Mr. Günter Waas as part of his doctoral research under the supervision of the principal investigator, Dr. John Lysmer, Associate Professor of Civil Engineering.

The project was administered by the Office of Research Services of the College of Engineering. The contracting officer for WES was Mr. John J. Kirschenbaum, Jr., represented by Dr. Lyman W. Heller of the Soils and Pavements Laboratory. During the period of this work, Mr. J. P. Sale was Chief of the Soils and Pavements Laboratory, Mr. R. G. Ahlvin was Assistant Chief of the Soils and Pavements Laboratory, and Mr. R. W. Cunny was Chief of the Soil Dynamics Branch.

COL Ernest D. Peixotto, CE, was the Director of the WES and Mr. F. R. Brown was the Technical Director.

**Preceding page blank**

# TABLE OF CONTENTS

**Preceding page blank**

Table of Contents (Continued)

Table of Contents (Continued)

# LIST OF ILLUSTRATIONS

# 1. INTRODUCTION

## 1.1 Foundation Vibration Problems

The designer of foundations for machinery must be able to predict whether or not the response of a foundation to dynamic loads from the machine will meet certain design criteria and if the vibrations transmitted through the ground will be small enough as not to affect other machines, vibration sensitive equipment and humans in the neighborhood. The prediction of the vibration amplitudes involves the determination of the dynamic loads and soil properties, the selection of a mathematical model and its analysis.

Discussions and data on dynamic loads from machines are presented in Refs. [9, 27]. Periodic loads caused by combustion engines, compressors and turbins are to be distinguished from transient loads caused by forge hammers and testing machines. If the soil-foundation system behaves linearly under dynamic loading, the response to periodic loads can be obtained by superposition of the harmonic response at different frequencies. Transient loads may be treated similarly by employing the Fourier transformation, possibly in a discretized form.

The determination of the dynamic soil properties is discussed briefly in Chapter 2. The dynamic stress-strain behavior of soils is approximately linear for small strain amplitudes and can therefore be represented by elastic moduli. To incorporate material damping in harmonic motion complex moduli may be employed.

The geometry involved is often quite complicated. It may consist of the foundation, several soil layers with different material properties, rock at some depth and adjacent foundations and structures. To make the problem amenable to analysis the geometry must therefore be strongly idealized.

Many problems which are actually three-dimensional in space can be reduced with some justification to either plane or axisymmetric

1

problems. For instance, the soil-foundation interaction of a turbine pedestal, which is ten times as long as it is wide, may be treated as a plane problem if the motion of the foundation slab in a plane perpendicular to the turbine axis is studied. Thus a cross-section of the soil-foundation system is considered which is plane and of unit thickness. On the other hand, the vertical vibration of a machine foundation which is square in plan may be treated as an axisymmetric problem. For this purpose the square footing is approximated by a circular footing of equal area in plan.

Many problems in soil dynamics can be characterized as wave propagation problems, because the motion in the soil is dominated by propagating waves. The waves are generated at some source, for instance by the vibration of a machine footing, and from there they propagate into the underlying medium which is unbounded except at the surface of the ground. The effect of the propagating waves is to disperse energy into the infinite medium and at the same time to carry disturbances a long distance away from the source. Due to energy dissipation by the waves, the footing response to dynamic loads is damped and the displacement amplitudes of the footing are considerably reduced, especially at frequencies corresponding to maximum amplitudes.

The depth profile at a construction site commonly consists of horizontally layered soil deposits underlain by rock. The lower soil layers are usually stiffer than the upper layers, because the overburden and thus the confining or consolidation pressure increases with depth. Waves generated somewhere close to the surface of the ground are therefore reflected and refracted at the layer interfaces. Since the soil layers generally become stiffer with depth, the pattern of reflections and refractions causes the waves to propagate mainly in the horizontal direction and most of the dispersed energy is transmitted in the softer layers close to the surface. Even in the case of a vertically vibrating circular footing which is supported by a homogeneous elastic half space, Fig. 1, 67 percent of the energy is dispersed by Rayleigh waves which travel along the surface of the half space [28]. Therefore an even higher percentage of the energy will be dispersed in the horizontal direction if the medium is stratified as

described above. If the rock underlying the soil deposits is much harder than the soil, as is usually the case, it may be assumed for practical purposes that the rock is completely rigid and that the waves are totally reflected at the surface of the rock.

## 1.2 Existing Methods of Analysis

The dynamic analysis of machine foundations is often based on the mathematical model shown in Fig. 1. A circular footing is supported by a homogeneous, isotropic, linearly elastic, semi-infinite half space. This model was first studied by Reissner [39, 40, 41] in the 1930's. He derived analytical solutions for the forced vertical and torsional vibration of the footing. Subsequently, the model has been studied by some 20 researchers who have directed almost their entire attention to the dynamic compliances of the vertical, torsional, rocking and horizontal vibration of the circular footing. A recently published paper by Luco and Westmann [23] presents a summary of the various solutions and numerical results for the compliances over a large frequency range. The paper also contains some information on the stress distribution under the footing and on the displacements in the far field.

A more satisfactory model for many foundation vibration problems where rock is situated at shallow depth is shown in Fig. 2. Here, a circular footing is supported by a homogeneous elastic layer over a rigid base. This model is more difficult to deal with by analytical methods than the half space model because additional boundary conditions have to be satisfied at the rigid base. The forced torsional motion of the footing was studied by Arnold et al. [6], Bycroft [10] and Awojobi [8]. The forced vertical motion of the footing was investigated by Bycroft [10] and Warburton [46]. No methods of analysis for the rocking and sliding motion are available.

Problems which include layering of the soil or embedment of the foundation, two significant features of most foundation vibration problems, have not been solved by analytical methods, since the inherent boundary conditions are too complex.

3

Numerical methods such as the finite difference and the finite element method are not directly applicable to steady-state wave propagation problems in an infinite medium, because only a finite number of nodal points can be considered and therefore the discrete model is confined to a finite region. This poses the problem as to how wave reflections can be prevented at an artificial boundary. which is introduced to confine the model.

Lysmer and Kuhlemeyer [25] developed a viscous boundary which absorbes much of the impinging wave energy. At the boundary they applied viscous forces which they computed from one-dimensional wave propagation theory. The dashpots can be designed to perfectly absorb the energy contained in P-waves (compressional waves) and S-waves (shear waves) if the incident angles of the waves are known. However, the incident angles are usually unknown and therefore must be anticipated. If the actual incident angles differ from those anticipated by not more than about 60 degrees, the dashpots are very effective [25].

Lysmer and Kuhlemeyer obtained good results with discrete models of the type shown in Fig. 3 when applied to the analysis of steady-state vertical vibrations of circular footings embedded in a homogeneous elastic half space. They designed the dashpots at the lower horizontal boundary for perpendicular incident angles and the dashpots at the vertical boundary for the frequency dependent incident angles of the P and S-wave components that form a Rayleigh wave.

Kuhlemeyer [22] extended the method to the case of a layered half space. He obtained good results in the low frequency range for cases in which the elastic moduli of the layers decreased with depth. However, he observed that in general it is difficult to predict the incident angles of P and S-waves at the artificial boundary, because the P and S-waves undergo multiple reflections and refractions at the layer interfaces and at the free surface. To complicate the matter, the incident angles often change drastically with frequency.

Ang and Newmark [4] developed a "transmitting boundary" at about the same time that Lysmer and Kuhlemeyer developed their viscous boundary. In essence, both boundaries are the same. They are based on one-dimensional wave propagation theory and require some advance

4

knowledge of the incident angles. Ang and Newmark used the transmitting boundary in the analysis of ground shock waves caused by nuclear blasts. They demonstrated the effectiveness of the boundary in cases in which the wave motion was mainly one-dimensional, but they presented little evidence of the boundary's performance in two-dimensional wave propagation problems.

However, studies by Hadala [18] show that the transmitting boundary is useful in certain two-dimensional shock wave problems in layered semi-infinite media, when only a very short time period after the blast is considered. The degree of perfection required of a transmitting boundary in these problems is less stringent than in steady-state wave propagation problems.

Another method of analyzing steady-state wave propagation problems in infinite media is to employ a very large discrete model with a considerable amount of damping. Thus, the waves generated at the source are strongly attenuated before they reach the artificial boundary, and after reflection, are further attenuated so that they are almost dissipated before they return to the zone of interest. This approach is physically justified if the chosen amount of damping is reasonable and if the model is large enough. But in practice, it is prohibitively expensive in computational time and storage requirements despite the dramatic advances in the development of digital computers.

A new discrete model which is particularly suited for the analysis of foundation vibration problems is described below.

## 1.3    A Finite Dynamic Model for Layered Semi-Infinite Media

The discrete method developed in this dissertation is designed to solve plane and axisymmetric wave propagation problems in semi-infinite, linearly viscoelastic media of the type illustrated in Figs. 4 and 5.

Fig. 4 shows the cross-section of a typical plane problem in which the geometry, the material properties and the external loads do not change in the direction perpendicular to the cross-section. The region I is joined along vertical planes to the regions L and R which

5

extend infinitely to the left and to the right, respectively.

The regions L and R consist of horizontal layers which are welded together at their interfaces and may differ in their material properties and thickness. They are called the layered or semi-infinite regions. The region I contains all geometrical irregularities and is therefore called the irregular region. The regions L, R and I are welded to a rigid base which is fixed in space.

The materials involved may be linearly elastic or linearly visco-elastic. For simplicity, they are assumed to be isotropic.

All external forces act within the irregular regions and vary harmonically with time. They generate harmonic motion which consists of propagating and standing waves. The propagating waves transmit energy. This energy is either dissipated due to material damping within a finite distance from its source or is propagated outward to infinity if the layered regions are ideally elastic.

Fig. 5 shows a typical cross-section of the analogous axisymmetric problem in which the geometry, the material properties and the loads do not vary in the angular direction.

Since there is no hope to find closed form solutions to problems as complicated as this, numerical methods which reduce the difficulty by discretization must be resorted to.

The finite element method is the most flexible numerical method available for solving complex boundary value problems in continuum mechanics, because it is easily adaptable to complicated geometries and local changes in material properties. Therefore it is employed to analyze the motion in the irregular region. It is applied to the present problem in the displacement formulation. The application is outlined in Chapter 3.

The layered regions, however, cannot be treated by the finite element method, because these regions are of infinite extent and their discretization by finite elements would result in an infinite number of elements and degrees of freedom.

Since the geometry of the layered region, L or R, does not vary in the horizontal direction, a numerical method is suggested which reduces the analysis of harmonic motion in the layered region to a

6

discrete problem with typically 20 to 60 degrees of freedom. To this
end, the region is discretized in the following way. The natural
layers are subdivided into thin sublayers as shown in Fig. 6 and it is
assumed that the displacements within each sublayer vary linearly in
the vertical direction. But in the horizontal direction the displace-
ments are required to satisfy the pertinent, ordinary differential
equations which are obtained from the governing, partial differential
equations by separating the variables. This method is similar to
Lysmer's original lumped mass method for the analysis of Rayleigh
waves [26].

At a given frequency, the free motion in the thus discretized
layered region consists of a finite number of wave modes which are
obtained by the solution of an algebraic eigenvalue problem. These
wave modes serve as shape functions for expanding the displacements in
the region in terms of mode participation factors.

If the layered region is separated from the irregular region,
nodal forces have to be applied at the boundary as shown in Figs. 11 and
12 in order to preserve dynamic equilibrium. These nodal forces are
derived from the displacement expansion by observing the strain-
displacement and stress-strain relations. The nodal forces are
uniquely related to the simultaneous nodal displacements at the boundary
through a dynamic stiffness matrix which represents the elastic and
the viscous response of the semi-infinite region. The dynamic stiffness
matrix is complex symmetric and frequency dependent.

Once the dynamic stiffness matrices of the layered regions are
established, the analysis of the combined regions L, I and R follows
the usual procedure of the direct stiffness method. The analysis
yields the displacements and stresses in the irregular and the layered
regions.

The dynamic stiffness matrix of a layered region is developed in
Chapters 4 through 7 for the plane and the axisymmetric case. In each
case the motions in the plane and perpendicular to the plane of the
cross-section, shown in Figs. 4 and 5, are treated separately since
they are independent.

In the layered regions, the motions in the plane and perpendicular to the plane of the cross-section consist of generalized Rayleigh and Love waves, respectively.

A generalized Rayleigh wave in the plane case is here defined by

$$\left.\begin{aligned} \delta_x &= u(z) \exp (i\omega t - ikx) \\ \delta_z &= w(z) \exp (i\omega t - ikx) \end{aligned}\right\} \tag{1.1}$$

in which $\delta_x$ and $\delta_z$ are the displacements in the x and z-direction, $u(z)$ and $w(z)$ are the corresponding vertical mode shapes, $\omega$ is the frequency, k is called the wave number and $i = \sqrt{-1}$. The wave defined by Eq. (1.1) is called a generalized Rayleigh wave, because Rayleigh waves in layered media are described mathematically in the same way, but are usually understood as having real wave numbers [16], whereas the wave number in Eq. (1.1) may be real, imaginary or complex.

A generalized Love wave in the plane case is defined by

$$\delta_y = v(z) \exp (i\omega t - ikx) \tag{1.2}$$

in which $\delta_y$ is the displacement in the y-direction and $v(z)$ is the vertical mode shape. The wave number may again be real, imaginary or complex, while Love waves in layered media are usually understood as having real wave numbers [16].

Axisymmetric generalized Rayleigh and Love waves are described similarly in Chapters 5 and 7. Henceforth, the cases in which the motion occurs either in the plane or perpendicular to the plane of the cross-section are called the Rayleigh wave case or the Love wave case according to the type of wave generated.

# 2. DYNAMIC SOIL PROPERTIES

## 2.1 Introduction

Successful determination of the response of soil-foundation systems to dynamic loads is critically dependent on the incorporation of representative soil-properties in the analysis. Thus considerable effort has been directed towards the determination of soil properties in recent years. Several techniques for measuring dynamic soil properties have been either newly developed or improved and a considerable amount of data has been collected [42, 43].

The stress-strain relationships of most soils subjected to symmetric cyclic loading conditions are curvi-linear as shown in Fig. 7. The secant modulus, which is determined by the extreme points on the hysteresis loop, and the damping factor, which is proportional to the area inside the loop, may be selected to represent the hysteretic stress-strain behavior in analyses. Both the modulus and the damping factor depend to some degree on the magnitude of the strain as the axis and the area of the loop vary with the strain amplitude.

## 2.2 Experimental Determination

The main procedures for determining the moduli and damping characteristics at low to moderately high strain levels are summarized below [43].

a) Direct determination of stress-strain relationships

Hysteretic stress-strain curves of the type shown in Fig. 7 can be obtained in the laboratory from triaxial compression tests, simple shear tests or torsional shear tests conducted under cyclic loading conditions. The strain amplitudes in these tests may vary from about $10^{-2}$ to 5 percent.

9

b)  Forced vibration tests

Forced vibration tests may be performed on cylindrical samples by subjecting them to longitudinal vibrations and torsional vibrations with strain amplitudes from about $10^{-4}$ to $10^{-2}$ percent. The tests involve the determination of the resonant frequencies and measurement of the response at other frequencies.

c)  Free vibration tests

In these tests cylindrical soil samples are set into longitudinal or torsional vibrations as in the forced vibration tests and thereafter the decay of the amplitudes is observed. These tests are particularly suited for the determination of the damping factor since the logarithmic decrement at any given strain level is obtained directly from successive amplitudes of free vibration.

d)  Field measurement of wave velocities

Field tests have been used to measure the velocity of propagation of P-waves, S-waves and Rayleigh waves. The soil moduli for low strains of about $5 \times 10^{-4}$ percent can be determined from the wave velocities, but damping factors have not been obtained from these tests.


## 2.3  Linearity

The strain amplitudes in soils beneath foundations for vibratory machines are usually small [42]. Test data for soils under cyclic loading conditions have shown that the soil response is approximately linear for small strains, say $10^{-3}$ percent [43]. Thus the secant moduli and the damping factors used in analyses of foundation vibration problems may well be assumed to be independent of the strain amplitude. Even in the case of large strains which are developed in soils during earthquakes, researchers have successfully employed linear analyses using soil properties based on observed strain amplitudes [20].

## 2.4 Complex Modulus Representation

Though the internal damping in soils is not considered to be
caused by viscosity, the stress-strain behavior of soils under vibratory
loading is similar to that of viscoelastic materials.  This permits
the use of complex moduli in representing the stress-strain behavior
of soils that are subjected to loads varying harmonically in time.
The stress-strain relation under uniaxial conditions can be expressed by

$$\sigma^c \exp(i\omega t) = E^c \, \varepsilon^c \exp(i\omega t) \tag{2.1}$$

in which

$$\sigma^c = \sigma_1 + i\,\sigma_2 \tag{2.2}$$

$$\varepsilon^c = \varepsilon_1 + i\,\varepsilon_2 \tag{2.3}$$

$$E^c(\omega) = E_1(\omega) + i\,E_2(\omega) \tag{2.4}$$

are the complex stress, the complex strain and the complex modulus,
respectively, $\omega$ is the circular frequency and $i = \sqrt{-1}$.  The superscript
$c$ denotes a complex quantity.

The complex stress and strain may be visualized as a pair of
vectors rotating at the frequency $\omega$ about the origin of the complex
plane as shown in Fig. 8.  At any given time, the actual stress and
strain are the projections of the vectors onto the real axis.  The
complex modulus is generally frequency dependent.  Its real component,
$E_1$, is the modulus of strain which is in phase with the stress and its
imaginary component, $E_2$, is the modulus of strain which is $90^\circ$ out of
phase with the stress.  $E_1$ is associated with the elastic phenomenon in
which energy is stored in a recoverable form while $E_2$ is associated
with the viscous phenomenon in which energy is dissipated.

Due to the viscous effect, the strain vector lags behind the
stress vector by an angle $\phi_L$ which lies between $0^\circ$ and $90^\circ$.  This
angle is called the "loss angle" and its tangent is called the "loss
tangent" because it is associated with energy loss.  The loss tangent
is defined by

$$\tan\phi_L = E_2/E_1 \tag{2.5}$$

and is related to the damping factor or fraction of critical damping,

11

β, and the logarithic decrement, D, by [42]

$$\tan\phi_L \approx 2 \beta \approx D/3.14 \tag{2.6}$$

if the damping is small.  This is the case in foundation vibration problems.

Since most data on damping characteristics of soils has been presented in terms of the fraction of critical damping, β will also be used here as the measure for material damping.  The complex modulus may be written accordingly

$$E^c = E_1 (1 + i\ 2\ \beta) \tag{2.7}$$

The use of a complex modulus implies that the actual hysteresis loops of the type shown in Fig. 7 are approximated by elliptical hysteresis loops which are equivalent with respect to the slope of the principle axes and the areas enclosed by the loops.  Thus the secant modulus, determined as shown in Fig. 7, equals the real component of the corresponding complex modulus, and the energy losses per cycle, which are proportional to the areas of the hysteresis loops, are also matched.

The complex modulus $E^c$ used above may represent any of the usual moduli, Young's modulus, shear modulus or bulk modulus.  The relations between the complex moduli of an isotropic, linearly viscoelastic material at a given frequency are analogous to those between the real moduli of an isotropic, linearly elastic material.  Thus, a complex Lame's constant $\lambda^c$ and a complex Poisson's ratio $\nu^c$ may be defined by

$$\lambda^c = \lambda_1 + i\ \lambda_2 = \frac{G^c\ (E^c - 2\ G^c)}{3G^c - E^c} \tag{2.8}$$

$$\nu^c = \nu_1 + i\ \nu_2 = \frac{E^c}{2\ G^c} - 1 \tag{2.9}$$

in which $E^c = E_1 + i\ E_2$ and $G^c = G_1 + i\ G_2$ denote the complex Young's modulus and shear modulus, respectively.

Values for $E^c$ and $G^c$ can be directly determined from longitudinal and torsional vibrations of cylindrical soil samples in forced and free vibration tests.  However,  later in the analyses it is more convenient

12

to use the complex Lame's constants $\lambda^c$ and $G^c$.

Henceforth, the superscript $^c$ will be omitted to simplify the notation. It is understood that $\lambda$ and $G$ denote complex moduli unless otherwise stated.

## 2. Wave Velocities

The velocity of P-waves, $V_P$, and the velocity of S-waves, $V_S$, in linearly viscoelastic media are [17]

$$V_P = \left[ \text{Re } \sqrt{\rho/(\lambda + 2G)} \right]^{-1} \tag{2.10}$$

$$V_S = \left[ \text{Re } \sqrt{\rho/G} \right]^{-1} \tag{2.11}$$

in which $\rho$ is the mass density and the symbol Re specifies the real part. $V_P$ and $V_S$ vary with frequency as do the complex Lame's constants. If the imaginary parts of the complex Lame's constants are small, $V_P \simeq \text{Re } \sqrt{(\lambda+2G)/\rho}$ and $V_S \simeq \text{Re } \sqrt{G/\rho}$.

In linearly elastic media, the P-wave and S-wave velocities are independent of frequency. They are

$$V_P = \sqrt{(\lambda + 2G)/\rho} \tag{2.12}$$

$$V_S = \sqrt{G/\rho} \tag{2.13}$$

in which $G$ and $\lambda$ denote real Lame's constants.

## 2.6 Material Damping in Foundation Vibrations

The frequency of motion hardly affects the secant moduli and the damping values of soils throughout the practical frequency range. Therefore the complex moduli may be considered frequency independent. This means that the damping forces in soils are proportional to the strain amplitudes rather than to the strain velocities [43].

The fraction of critical damping in foundation vibration problems is usually small. Its values for shear deformations may typically vary from 2 to 5 percent, and its values for compressional deformations

13

are even less. Therefore, it might be argued that a viscoelastic theory for analyses of foundation vibration problems is not warranted, especially so, as relative errors in the determination of the secant moduli usually exceed 10 to 20 percent. However, it takes little effort to include damping in the analyses, since most of the computations will have to be performed using complex algebra. Furthermore, the incorporation of damping avoids possible singularities in the analyses, which might be troublesome, and it provides a more realistic model.

## 3. METHOD OF ANALYSIS

### 3.1 Method of Complex Variables for Harmonic Motion

It is convenient to represent the forces, displacements, strains
and stresses of harmonic motion by complex variables. If $f(t)$ is
harmonic in time it can be defined by

$$f(t) = f_o \cos(\omega t + \phi) \tag{3.1}$$

or

$$f(t) = f_1 \cos\omega t - f_2 \sin\omega t \tag{3.2}$$

or

$$f(t) = \text{Re} \ (f^c \exp\lambda\omega t) \tag{3.3}$$

in which $\omega$ is the circular frequency and $f^c$ is the complex variable

$$f^c = f_1 + i \ f_2 \tag{3.4}$$

with $i = \sqrt{-1}$. The amplitude $f_o$ is

$$f_o = \sqrt{f_1^2 + f_2^2} \tag{3.5}$$

and the phase angle $\phi$ is

$$\phi = \tan^{-1}(f_2/f_1) \tag{3.6}$$

### Equation of Motion for Discrete Systems

The equation of motion for a simple damped oscillator with a mass
M, a spring constant K, and a dashpot constant C is

$$K \ u(t) + C \ \dot{u}(t) + M \ \ddot{u}(t) = P(t) \tag{3.7}$$

in which $u$, $\dot{u}$, and $\ddot{u}$ are the displacement, velocity and acceleration of
the mass, respectively, and $P(t)$ is the driving force. For harmonic
motion at the frequency $\omega$, Eq. (3.7) can be reduced to

$$(K^c - \omega^2 M) \ u^c = P^c \tag{3.8}$$

in which

$$K^c = K_1 + i K_2 = K + i C \omega \qquad (3.9)$$

$$u^c = u_1 + i u_2 \qquad (3.10)$$

$$P^c = P_1 + i P_2$$

Eq. (3.8) is a time independent, complex, linear equation which is equivalent to the two real equations

$$K_1 u_1 - K_2 u_2 - \omega^2 M u_1 = P_1 \qquad (3.12)$$

$$K_1 u_2 + K_2 u_1 - \omega^2 M u_2 = P_2 \qquad (3.13)$$

The first equation states equilibrium when $\sin\omega t = 0$, the second when $\cos\omega t = 0$. If both equations are satisfied then equilibrium prevails at any time.

The equations of harmonic motion for a system of n degrees of freedom are, in generalization of Eq. (3.8),

$$([K^c] - \omega^2 [M]) \{u^c\} = \{P^c\} \qquad (3.14)$$

in which the mass matrix [M] and the complex stiffness matrix $[K^c] = [K_1]$ + $i[K_2]$ are of order n x n. $[K_1]$ contains the stiffness coefficients and $[K_2]$ the damping coefficients multiplied by $\omega$. The vectors $\{u^c\}$ and $\{P^c\}$ contain the complex displacements and forces, $u_j^c$ and $P_j^c$, $j=1, \ldots,$ n, respectively. The complex stiffness matrix $[K^c]$ may be generated in the same manner as a real stiffness matrix, the only difference being that complex moduli are used instead of real moduli.

## Equation of Motion for Continuous System

The equilibrium conditions for an infinitesimal element together with the strain-displacement relations and the stress-strain relations yield the field equations of motions in terms of the displacements.

If the motion is harmonic the field equations can be reduced to time independent equations in the same way as shown above. Using rectangular Cartesian coordinates, x, y, z, as indicated in Fig. 4, and assuming plane strain conditions, i.e. all derivatives with respect to y vanish, the field equations for the homogeneous case, in which no external body forces act on the element, are

16

$$G\left(\frac{\partial^2 u_x^c}{\partial x^2} + \frac{\partial^2 u_x^c}{\partial z^2}\right) + (\lambda + G)\left(\frac{\partial^2 u_x^c}{\partial x^2} + \frac{\partial^2 u_z^c}{\partial x \partial z}\right) + \rho\omega^2 u_x^c = 0 \tag{3.15a}$$

$$G\left(\frac{\partial^2 u_z^c}{\partial x^2} + \frac{\partial^2 u_z^c}{\partial z^2}\right) + (\lambda + G)\left(\frac{\partial^2 u_x^c}{\partial x \partial z} + \frac{\partial^2 u_z^c}{\partial z^2}\right) + \rho\omega^2 u_z^c = 0 \tag{3.15b}$$

$$G\left(\frac{\partial^2 u_y^c}{\partial x^2} + \frac{\partial^2 u_y^c}{\partial z^2}\right) + \rho\omega^2 u_y^c = 0 \tag{3.15c}$$

$u_x^c$, $u_y^c$, and $u_z^c$ are the complex displacements in the x, y, and z-directions, respectively, $\rho$ is the mass density and $\lambda$ and $G$ are the complex moduli introduced in Section 2.2. Eqs. (3.15) are valid for small deformations in an isotropic, linearly viscoelastic medium. Eqs. (3.15a) and (3.15b) are coupled. They govern the motion in the x-z-plane, while Eq. (3.15c) governs the motion in the y-direction.

The analogous equations for axisymmetric conditions, when all derivatives with respect to the angular direction $\theta$ vanish, are

$$(\lambda + 2G)\left(\frac{\partial^2 u_r^c}{\partial r^2} + \frac{1}{r}\frac{\partial u_r^c}{\partial r} - \frac{u_r^c}{r^2} + \frac{\partial u_z^c}{\partial r \partial z}\right) + G\left(\frac{\partial^2 u_r^c}{\partial z^2} - \frac{\partial^2 u_z^c}{\partial r \partial z}\right) + \rho\omega^2 u_r^c = 0$$
$$\tag{3.16a}$$

$$(\lambda + 2G)\left(\frac{\partial^2 u_r^c}{\partial r \partial z} + \frac{1}{r}\frac{\partial u_r^c}{\partial z} + \frac{\partial^2 u_z^c}{\partial z^2}\right) + G\left(\frac{\partial^2 u_z^c}{\partial r^2} + \frac{1}{r}\frac{\partial u_z^c}{\partial r} - \frac{\partial^2 u_r^c}{\partial r \partial z} - \frac{1}{r}\frac{\partial u_r^c}{\partial r}\right)$$
$$+ \rho\omega^2 u_r^c = 0 \tag{3.16b}$$

$$G\left(\frac{\partial^2 u_\theta^c}{\partial r^2} + \frac{1}{r}\frac{\partial u_\theta^c}{\partial r} - \frac{u_\theta^c}{r^2} + \frac{\partial^2 u_\theta^c}{\partial z^2}\right) + \rho\omega^2 u_\theta^c = 0 \tag{3.16c}$$

in which $u_r^c$, $u_\theta^c$, and $u_z^c$ are the complex displacements in the r, $\theta$, and z-directions of a cylindrical coordinate system as indicated in Fig. 5. Eqs. (3.16a) and (3.16b) are coupled. They govern the motion in the r-z-plane, whereas the motion in the $\theta$-direction is governed by Eq. (3.16c).

17

## Principle of Virtual Work

It is expedient to have a stationary principle available for the viscoelastic medium as discretized by the finite element method. To this end, the well known principle of virtual work will be specialized for application to harmonic motion. The principle of virtual work for the dynamic case can be stated in the following form [17]

$$\int_V \{\hat{\epsilon}\}^T\{\sigma\}dV - \int_V \{\hat{u}\}^T(\{F\} - \rho\{\ddot{u}\})dV - \int_S \{\hat{u}\}^T\{T\}dS = 0 \qquad (3.17)$$

in which the stress vector $\{\sigma\}$, the body force vector $\{F\}$, the surface force vector $\{T\}$, and the acceleration vector $\{\ddot{u}\}$ are functions of space and time. The vectors $\{\hat{u}\}$ and $\{\hat{\epsilon}\}$ contain the virtual displacements and virtual strains, respectively. The integration $\int_V \ldots dV$ is performed over the total volume of the body and the integration $\int_S \ldots dS$ is performed over that part of the surface of the body where no displacements are prescribed. The virtual displacements are small, triply differentiable functions of space and must vanish over the surface of the body where displacements are prescribed [17]. Accordingly, the virtual strains are small, twice differentiable functions of space.

Eq. (3.17) states that equilibrium prevails if the sum of the virtual work, performed by the actual forces and actual strains on the virtual displacements and virtual strains, vanishes.

Alternatively, the rate of the virtual work may be considered. This leads to the equation of motion in the following stationary form

$$\int_V \{\hat{\dot{\epsilon}}\}^T\{\sigma\}dV - \int_V \{\hat{\dot{u}}\}^T(\{F\} - \rho\{\ddot{u}\})dV - \int_S \{\hat{\dot{u}}\}^T\{T\}dS = 0 \qquad (3.18)$$

in which the vectors $\{\hat{\dot{u}}\}$ and $\{\hat{\dot{\epsilon}}\}$ contain the virtual velocities of the displacements and strains, respectively.

If the motion is harmonic with the circular frequency $\omega$, each variable in Eqs. (3.17) and (3.18), including the virtual displacements and the virtual strains, can be described in time as is $f(t)$ in Eq. (3.2). The time derivatives in Eqs. (3.17) and (3.18) are

$$\{\ddot{u}\} = -\omega^2(\{u_1\} \cos\omega t - \{u_2\} \sin\omega t) \tag{3.19}$$

$$\{\hat{u}\} = -\omega(\{\hat{u}_1\} \sin\omega t + \{\hat{u}_2\} \cos\omega t) \tag{3.20}$$

$$\{\hat{\varepsilon}\} = -\omega(\{\hat{\varepsilon}_1\} \sin\omega t + \{\hat{\varepsilon}_2\} \cos\omega t) \tag{3.21}$$

The integration of Eqs. (3.17) and (3.18) over the time of one period leads to

$$\int_V \left[ \{\hat{\varepsilon}_1\}^T\{\sigma_1\} + \{\hat{\varepsilon}_2\}^T\{\sigma_2\} - \{\hat{u}_1\}^T(\{F_1\} + \rho\omega^2\{u_1\}) - \{\hat{u}_2\}^T(\{F_2\} + \rho\omega^2\{u_2\}) \right] dV$$

$$- \int_S (\{\hat{u}_1\}^T\{T_1\} + \{\hat{u}_2\}\{T_2\})dS = 0 \tag{3.22}$$

and

$$\int_V \left[ \{\hat{\varepsilon}_1\}^T\{\sigma_2\} - \{\hat{\varepsilon}_2\}^T\{\sigma_1\} - \{\hat{u}_1\}^T(\{F_2\} + \rho\omega^2\{u_2\}) + \{\hat{u}_2\}^T(\{F_1\} + \rho\omega^2\{u_1\}) \right] dV$$

$$- \int_S (\{\hat{u}_1\}^T\{T_2\} - \{\hat{u}_2\}^T\{T_1\})dS = 0 \tag{3.23}$$

respectively, since

$$\int_0^{2\pi/\omega} \sin^2\omega t\, dt = \int_0^{2\pi/\omega} \cos^2\omega t\, dt = \pi/\omega \tag{3.24}$$

$$\int_0^{2\pi/\omega} \sin\omega t \cdot \cos\omega t\, dt = 0 \tag{3.25}$$

Now, Eq. (3.23) is multiplied by $i = \sqrt{-1}$ and added to Eq. (3.22). If complex variables are introduced according to Eqs. (3.3) and (3.4), this leads to the equation of harmonic motion in the stationary form

$$\int_V \{\hat{\varepsilon}\}^*\{\sigma^c\}dV - \int_V \{\hat{u}\}^* (\{F^c\} + \rho\omega^2\{u^c\})dV - \int_S \{\hat{u}\}^*\{T^c\}dS = 0 \tag{3.26}$$

in which the superscript $^c$ indicates a complex variable, as before, and the $^*$ indicates the transposed complex conjugate (e.g. $\{u^c\} = \{u_1\} + i\{u_2\}$ and $\{\hat{u}\}^* = \{\hat{u}_1\}^T - i\{\hat{u}_2\}^T$).

19

Henceforth, however, the superscript $^c$ will be omitted for convenience, and it is understood that the quantities of harmonic motion are represented by complex variables as is f(t) in Eq. (3.3).

## 3.2    Finite Element Method

The finite element method is a numerical technique for obtaining approximate solutions to complex boundary value problems. The development of the method in the field of structural mechanics began in the early 1950's with the work of Turner et al. [45]. Since then the method has been developed extensively and is now widely used in structural and continuum mechanics. It has also been applied successfully to various other physical problems.

A recently published text by Zienkiewicz [53] describes in detail the application of the finite element method in structural and continuum mechanics. The text also contains an extensive list of references on the subject. The finite element method has been used very successfully in static and dynamic analyses of plane and axisymmetric problems [12, 13, 50, 51]. It has also been applied to quasi-static and dynamic analyses of viscoelastic continua with considerable success [1, 3, 11, 32, 35].

Since the finite element method is widely known, only the principal steps involved in the particular application of the method to the analysis of harmonic motion in a viscoelastic medium are summarized below.

## (i)    Discretization:

The irregular region I is subdivided into subregions, called finite elements, as shown in Fig. 6. The finite elements are prisms in the plane case and rings in the axisymmetric case and have arbitrary quadrilateral cross-sections. They are interconnected at straight or circular nodal joints, which are located at the edges of the elements. Because the strains are either plane or axisymmetric, the displacements vary only over the cross-section of the elements. It is assumed that the displacement field of an element is restricted to a finite number of degrees of freedom. Here, the displacements of the nodal joints are

20

introduced as the degrees of freedom. Each degree of freedom of an element is associated with a shape function which defines the displacement variation within the element. The shape functions vary linearly along the boundary of an element, see Section 3.3. Hence, the displacements across the boundary between adjacent elements remain continuous during deformation if the elements are interconnected at their nodal joints.

(ii) Element matrices:

The influence coefficients of an individual element with respect to unit nodal displacements are derived from the principle of virtual work, Eq. (3.26). This step is performed in Section 3.3. The influence coefficients are collected in the element stiffness matrix [K'] and the element mass matrix [M']. Because harmonic motion of a viscoelastic body is considered, [K'] is here a complex matrix representing the viscous as well as the elastic resistance of the element against deformation. The matrix [M'] is real and represents the inertia forces of the element.

(iii) Assemblage of finite elements:

The elements are assembled by matching the displacements of adjacent elements at common nodal joints. The global stiffness and mass matrices of the assemblage, [K] and [M], are accordingly formed by addition of the element matrices while observing the global numbering system of the nodal displacements. The procedure is that of the direct stiffness method [53].

(iv) Equation of motion:

Nodal displacements are prescribed which provide the kinematic stability of the body and external loads are applied as discrete forces acting at the nodal joints or as prescribed nodal displacements. The loads vary harmonically with time at the circular frequency $\omega$. The equation of motion is therefore

$$[A] \{u\} = \{b\} \tag{3.27}$$

in which

$$[A] = [K] - \omega^2 [M] \tag{3.28}$$

21

is a symmetric banded matrix with complex coefficients. The vector $\{u\}$ contains the complex nodal displacements and the vector $\{b\}$ the complex nodal forces.

Eq. (3.28) can be partitioned in the following way

$$\begin{bmatrix} A_{ff} & A_{fs} \\ A_{fs}^T & A_{ss} \end{bmatrix} \begin{Bmatrix} u_f \\ u_s \end{Bmatrix} = \begin{Bmatrix} b_f \\ b_s \end{Bmatrix} \qquad (3.29)$$

in which $\{u_f\}$ contains the unconstrained or free nodal displacements and $\{u_s\}$ the prescribed nodal displacements. Accordingly, $\{b_f\}$ contains the prescribed nodal forces and $\{b_s\}$ the reaction forces. Hence, Eq. (3.29) can be reduced to

$$[A_{ff}] \{u_f\} = \{b_f\} - [A_{fs}] \{u_s\} \qquad (3.30)$$

(v)   Solution of equation:

Eq. (3.30) constitutes a set of simultaneous complex linear equations. The coefficient matrix is symmetric, sparse and also narrowly banded if a favorable numbering system of the nodal displacements is used. The equations may be solved by a Gaussian elimination algorithm without pivots using complex arithmetic. Once the displacement vector $\{u_f\}$ is known the reaction forces $\{b_s\}$ can be computed by

$$\{b_s\} = [A_{fs}]^T \{u_f\} + [A_{ss}] \{u_s\} \qquad (3.31)$$

Further details of the procedure outlined above are given in Ref. [53]. However, a few points need additional discussion.

The semi-infinite layered regions R and L must also be considered. Dynamic stiffness matrices for these regions are derived in Chapters 4 through 7 for the cases of plane and axisymmetric Love and Rayleigh wave motion. When these matrices are added by the direct stiffness method into the global matrix [A] of Eq. (3.2/), the influence of the semi-infinite regions on the motion in the irregular region is properly accounted for.

The accuracy of the analysis depends upon the fineness of the finite element mesh. In general, the larger the strain gradient the finer should be the mesh. Therefore the mesh should be refined in areas

22

where large strain gradients are to be expected.

Characteristic features of harmonic motion in elastic or visco-elastic media are the wave lengths of P and S-waves. In order to obtain a good approximation to the actual wave motion, the maximum cross-sectional dimension of any finite element should be small compared to the length of S-waves, which is always shorter than the length of P-waves in the same medium at any given frequency. Lysmer and Kuhlemeyer [25] recommended that the maximum dimension of a rectangular finite element with a linear strain field be not greater than about 1/10 of the length of S-waves in the medium. This recommendation also applies to the quadrilateral finite elements presented in Section 3.3.

Numerical solutions are compared with analytical solutions in Chapters 9 and 11. The comparisons show clearly that very good results can be obtained by the proposed method for steady-state wave propagation problems in semi-infinite elastic and viscoelastic media.

It was mentioned earlier that the set of complex linear equations, Eq. (3.30), may be solved by a Gaussian elimination algorithm without pivots. The algorithms, used in the computer programs of Appendix 5 and 6, are coded in the FORTRAN IV language and employ the complex arithmetic capabilities of FORTRAN IV. By utilizing complex arithmetic, computer storage requirements are half that required for the equivalent real arithmetic computation, in which the complex matrix and the complex vectors are decomposed into real and imaginary parts. Since the co-efficient matrix is banded and symmetric, only half of the band needs to be stored in the computer memory.

No numerical sensitivity has been noted in the solution of the equations. Numerical sensitivity could arise when the frequency of excitation is extremely close to the natural frequency of a subsystem of the discretized model. But this cannot be the case if the model contains some viscous damping associated with each degree of freedom, because then none of the subsystems possesses a real natural frequency whereas the frequency of excitation is always real. If the model contains no damping, the natural frequency of a subsystem could coincide with the exciting frequency. But this is very unlikely. Therefore an algorithm without pivots is used and the extra computation time and storage needed for pivoting are saved.

23

## 3.3 Element Stiffness and Mass Matrices

In order to assemble the matrices [K] and [M] appearing in Eq. (3.28) it is necessary to first determine the matrices [K'] and [M'] for the individual elements of the assemblage. The plane or axisymmetric cross-section of a typical element is shown in Fig. 9, which also shows the global coordinate system $(r, z)$ and a local coordinate system $(\eta, \xi)$. The two sets of coordinates are related through the transformation

$$\langle r \ z \rangle = \{b\}^T \begin{bmatrix} r_1 & z_1 \\ r_2 & z_2 \\ r_3 & z_3 \\ r_4 & z_4 \end{bmatrix} \quad (3.32)$$

in which $r_m$, $z_m$, m=1,2,3,4, are the coordinates of the four nodal points of the element cross-section and $\{b\}$ is the column vector defined by

$$\{b\} = \frac{1}{4} \begin{Bmatrix} (1-\xi)(1-\eta) \\ (1-\xi)(1+\eta) \\ (1+\xi)(1+\eta) \\ (1+\xi)(1-\eta) \end{Bmatrix} \quad (3.33)$$

The Jacobian matrix of the transformation is

$$[J] = \begin{bmatrix} \dfrac{\partial r}{\partial \xi} & \dfrac{\partial z}{\partial \xi} \\ \dfrac{\partial r}{\partial \eta} & \dfrac{\partial z}{\partial \eta} \end{bmatrix} = [D] \begin{bmatrix} r_1 & z_1 \\ r_2 & z_2 \\ r_3 & z_3 \\ r_4 & z_4 \end{bmatrix} \quad (3.34)$$

in which

$$[D] = \frac{1}{4} \begin{bmatrix} -(1-\eta) & -(1+\eta) & (1+\eta) & (1-\eta) \\ -(1-\xi) & (1-\xi) & (1+\xi) & -(1+\xi) \end{bmatrix} \quad (3.35)$$

The determinant of [J] is denoted J.

For both the Love wave case and the Rayleigh wave case the assumption will be made that the displacements within the element vary according to

24

$$\delta(r,z) = \delta(\xi,\eta) = \{b\}^T \begin{Bmatrix} \delta_1 \\ \delta_2 \\ \delta_3 \\ \delta_4 \end{Bmatrix} \qquad (3.36)$$

in which $\delta_1$, $\delta_2$, $\delta_3$ and $\delta_4$ are the nodal displacements in some coordinate direction of the element shown in Fig. 10. Due to the special properties of the chosen transformation, Eq. (3.32), this implies that all displacements vary linearly along the boundaries of the element and that all elements remain compatible as the nodal joints are displaced.

## Element Matrices for Axisymmetric Love Wave Case

In the Love wave case, the quadrilateral element shown in Fig. 10a has four degrees of freedom which are the nodal displacements in the $\theta$-direction. The displacement field $\delta_\theta = \delta(\xi, \eta)$ is defined by Eq. (3.36).

The strain-displacement relations in cylindrical coordinates are

$$\gamma_{r\theta} = \frac{\partial \delta}{\partial r} - \frac{\delta}{r} \quad \text{and} \quad \gamma_{z\theta} = \frac{\partial \delta}{\partial z} \qquad (3.37)$$

Differentiation by the chain rule yields

$$\begin{Bmatrix} \dfrac{\partial \delta}{\partial r} \\[2mm] \dfrac{\partial \delta}{\partial z} \end{Bmatrix} = [T] \{\delta\} \qquad (3.38)$$

in which [T] is the 2 x 4 matrix

$$[T] = [J]^{-1}[D] \qquad (3.39)$$

and the matrices [J] and [D] are those defined in Eqs. (3.34) and (3.35). The strains expressed in terms of the nodal displacements are

$$\{\varepsilon\} = \begin{Bmatrix} \gamma_{r\theta} \\ \gamma_{rz} \end{Bmatrix} = [S] \{\delta\} \qquad (3.40)$$

25

in which [S] is the 2 x 4 matrix

$$[S] = \begin{bmatrix} t_{11} - b_1/r & t_{12} - b_2/r & t_{13} - b_3/r & t_{14} - b_4/r \\ t_{21} & t_{22} & t_{23} & t_{24} \end{bmatrix} \tag{3.41}$$

The elements $t_{ij}$, $i=1$, 2, $j=1$, 2, 3, 4, are the elements of [T] and $b_j$, $j=1$, 2, 3, 4, are the elements of $\{b\}$, defined by Eq. (3.33).

The stress-strain relation of an isotropic material is

$$\{\sigma\} = \begin{Bmatrix} \tau_{r\theta} \\ \tau_{rz} \end{Bmatrix} = G\{\varepsilon\} \tag{3.42}$$

in which G represents the complex shear modulus if harmonic motion in a viscoelastic material is considered.

The nodal forces $Q_j$, $j=1$, 2, 3, 4, which are shown in Fig. 10a and are collected in the vector $\{Q\}$, are the only external forces acting on the element. They vary harmonically in time. Since [S] and $\{b\}$ are real, the principle of virtual work, Eq. (3.26), yields

$$G \int_V \{\hat{\delta}\}^*[S]^T[S]\{\delta\}dV - \rho\omega^2 \int_V \{\hat{\delta}\}^*\{b\}\{b\}^T\{\delta\}dV = \{\hat{\delta}\}^*\{Q\} \tag{3.43}$$

in which the vector $\{\hat{\delta}\}$ contains the virtual displacements of the nodal joints and the $*$ denotes the conjugate transposed.

The four virtual displacement states in each of which a single component of $\{\hat{\delta}\}$ is assigned the value 1 while the other three components are 0 yield the matrix equation

$$([K'] - \omega^2[M'])\{\delta\} = \{Q\} \tag{3.44}$$

in which [K'] is the 4 x 4 element stiffness matrix

$$[K'] = G \int_V [S]^T[S]dV \tag{3.45}$$

and [M'] is the 4 x 4 consistent element mass matrix [5]

$$[M'] = \rho \int_V \{b\}\{b\}^T dV \tag{3.46}$$

The volume integral can be converted to an area integral since $dV=r\ d\theta\ dA$ for an axisymmetric element. In the $\xi$-$\eta$ coordinate system $dA=J\ d\xi\ d\eta$. The stiffness and mass matrices for a one radian segment of the element are therefore

26

$$[K'] = \int_{-1}^{1} \int_{-1}^{1} G[S]^T [S] \; r \; J \; d\xi \; d\eta \qquad (3.47)$$

$$[M'] = \int_{-1}^{1} \int_{-1}^{1} \rho\{b\}\{b\}^T \; r \; J \; d\xi \; d\eta \qquad (3.48)$$

The integration is performed numerically by Gaussian quadrature with a four point scheme [53].

## Element Matrices for Plane Love Wave Case

Axisymmetric strain conditions become plane strain conditions at large distance from the axis of symmetry. The matrices for a plane strain element can therefore be deduced from Eqs. (3.47) and (3.48) by considering a segment of infinite radius subtending a unit arc. Since [S] reduces to [T], defined by Eq. 3.39, the matrices are

$$[K'] = \int_{-1}^{1} \int_{-1}^{1} G[T]^T [T] \; J \; d\xi \; d\eta \qquad (3.49)$$

$$[M'] = \int_{-1}^{1} \int_{-1}^{1} \rho\{b\}\{b\}^T \; J \; d\xi \; d\eta \qquad (3.50)$$

## Element Matrices for Axisymmetric Rayleigh Wave Case

The Rayleigh wave case involves two displacements and two forces per nodal joint as shown in Fig. 10b.

The r and z displacements within the element are, according to Eq. (3.36),

$$\begin{Bmatrix} \delta_r \\ \delta_z \end{Bmatrix} = [N]\{\delta\} \qquad (3.51)$$

in which $\{\delta\}$ contains the nodal displacements $\delta_j$, j=1, ..., 8, and [N] is the 2 x 8 matrix

27

$$[N] = \begin{bmatrix} b_1 & 0 & b_2 & 0 & b_3 & 0 & b_4 & 0 \\ 0 & b_1 & 0 & b_2 & 0 & b_3 & 0 & b_4 \end{bmatrix} \qquad (3.52)$$

The elements $b_j$, j=1, 2, 3, 4, are the components of $\{b\}$ defined in Eq. (3.33).

The strain-displacement relations are

$$\varepsilon_r = \frac{\partial \delta_r}{\partial r} \quad ; \quad \varepsilon_z = \frac{\partial \delta_z}{\partial z} \qquad (3.53a)$$

$$\varepsilon_\theta = \frac{\delta_r}{r} \quad ; \quad \gamma_{rz} = \frac{\partial \delta_r}{\partial z} + \frac{\partial \delta_z}{\partial r} \qquad (3.53b)$$

Differentiation by the chain rule leads to

$$\{\varepsilon\} = \begin{Bmatrix} \varepsilon_r \\ \varepsilon_z \\ \varepsilon_\theta \\ \gamma_{rz} \end{Bmatrix} = [S]\{\delta\} \qquad (3.54)$$

in which [S] is now the 4 x 8 matrix

$$[S] = \begin{bmatrix} t_{11} & 0 & t_{12} & 0 & t_{13} & 0 & t_{14} & 0 \\ 0 & t_{21} & 0 & t_{22} & 0 & t_{23} & 0 & t_{24} \\ b_1/r & 0 & b_2/r & 0 & b_3/r & 0 & b_4/r & 0 \\ t_{21} & t_{11} & t_{22} & t_{12} & t_{23} & t_{13} & t_{24} & t_{14} \end{bmatrix} \qquad (3.55)$$

The elements $t_{ij}$, i=1, 2, j=1, 2, 3, 4, are the elements of [T] defined in Eq. (3.39) and $b_j$, j=1, 2, 3, 4, are the elements of $\{b\}$ defined in Eq. (3.33).

The stress-strain relation for an isotropic material is

$$\{\sigma\} = \begin{Bmatrix} \sigma_r \\ \sigma_z \\ \sigma_\theta \\ \tau_{rz} \end{Bmatrix} = [C]\{\varepsilon\} \qquad (3.56)$$

28

in which

$$[C] = \begin{bmatrix} \lambda + 2G & \lambda & \lambda & 0 \\ \lambda & \lambda + 2G & \lambda & 0 \\ \lambda & \lambda & + 2G & 0 \\ 0 & 0 & 0 & G \end{bmatrix} \qquad (3.57)$$

If harmonic motion in a viscoelastic material is considered, the Lame's constants $\lambda$ and $G$ are complex moduli, which are generally frequency dependent.

The further derivation of the stiffness and mass matrices is analogous to that in the Love wave case and leads to the 8 x 8 matrices for a one radian segment of the element

$$[K'] = \int_{-1}^{1} \int_{-1}^{1} [S]^T [C][S] \, r \, J \, d\xi \, d\eta \qquad (3.58)$$

$$[M'] = \int_{-1}^{1} \int_{-1}^{1} \rho [N]^T [N] \, r \, J \, d\xi \, d\eta \qquad (3.59)$$

in which [S] is the matrix defined by Eq. (3.55).

The integration is again performed numerically by Gaussian quadrature with a four point scheme.

## Element Matrices for Plane Rayleigh Wave Case

The stiffness and mass matrices for the plane strain element can be deduced from those for the axisymmetric element by considering an element segment of infinite radius subtending a unit arc. This leads to

$$[K'] = \int_{-1}^{1} \int_{-1}^{1} [\breve{S}]^T [\breve{C}][\breve{S}] \, J \, d\xi \, d\eta \qquad (3.60)$$

$$[M'] = \int_{-1}^{1} \int_{-1}^{1} \rho [N]^T [N] \, J \, d\xi \, d\eta \qquad (3.61)$$

in which [$\breve{S}$] is the 3 x 8 matrix obtained by deleting the third row in matrix [S] and [$\breve{C}$] is the 3 x 3 matrix obtained by deleting the third row and the third column in matrix [C].

29

# 4. PLANE LOVE WAVE MOTION

## 4.1  Eigenvalue Problem for Continuous Layered Region

Free harmonic motion under plane strain conditions in a semi-infinite layered region of the type shown in Fig. 4 is considered.  The region consists of n isotropic linearly elastic or viscoelastic layers, which are welded together at their interfaces.  The jth layer has the mass density $\rho_j$ and the complex shear modulus $G_j$.  All displacements are perpendicular to the x-z-plane and are described by

$$\delta = \delta_y(x,z,t) = u(x,z)\ \exp(i\omega t) \tag{4.1}$$

in which $\omega$ is the circular frequency.

The governing homogeneous differential equations for the spatial part of the displacements in the n layers are, according to Eq. (3.15c),

$$G_j\left(\frac{\partial^2 u}{\partial x^2} + \frac{\partial^2 u}{\partial z^2}\right) + \rho_j\,\omega^2 u = 0 \qquad j=1,\ \ldots,\ n \tag{4.2}$$

These partial differential equations may be reduced to ordinary differential equations by separation of the variables.  The assumption that

$$u(x,z) = v(z) \cdot g(x) \tag{4.3}$$

leads to

$$\frac{\partial^2 v}{\partial z^2}\ \frac{1}{v} + \frac{\rho_j}{G_j}\ \omega^2 = -\frac{\partial^2 g}{\partial x^2}\ \frac{1}{g} \qquad j=1,\ \ldots,\ n \tag{4.4}$$

which can only be valid for all values of x and z in the respective layer if both sides of Eq. (4.4) are equal to the same constant.  Setting this constant equal to $k^2$ yields the ordinary differential equations

$$\frac{d^2 v}{dz^2} + (\omega^2\rho_j/G_j - k^2)v = 0 \qquad j=1,\ \ldots,\ n \tag{4.5}$$

30

and

$$\frac{d^2g}{dx^2} + k^2g = 0 \qquad (4.6)$$

The latter equation has a solution

$$g = \exp(-ikx) \qquad (4.7)$$

in which $i = \sqrt{-1}$. The parameter $k$ is called the wave number, which, if real, is related to the phase velocity, $c$, and to the apparent wavelength in the x-direction, $\ell$, by

$$k = \frac{\omega}{c} = \frac{2\pi}{\ell} \qquad (4.8)$$

Thus, a solution to Eq. (4.2) may be expressed in the form of a wave

$$\delta = v(z) \exp(i\omega t - ikx) \qquad (4.9)$$

The function in the z-direction, $v(z)$, which will be called the mode shape of the wave, must satisfy the n ordinary differential equations, Eq. (4.5). In addition, the boundary conditions at the planes, $z=z_j$, $j=1, \ldots, n+1$, i.e. continuity of the displacements and shear stresses at the interfaces between the n layers, zero displacements at the rough rigid base and zero shear stresses at the free surface, must also be satisfied. Since the shear stress on a horizontal plane is

$$\tau_{zy} = G \frac{\partial \hat{\delta}}{\partial z} = G \frac{dv}{dz} \exp(i\omega t - ikx) \qquad (4.10)$$

these boundary conditions may be expressed in the form

$$v(z_j') = v(z_j'') \qquad j=2,3, \ldots, n \qquad (4.11a)$$

$$G_j \frac{d}{dz} v(z_j') = G_{j+1} \frac{d}{dz} v(z_j'') \qquad j=2,3, \ldots n \qquad (4.11b)$$

$$\frac{d}{dz} v(z=0) = 0 \qquad (4.11c)$$

and

$$v(z=H) = 0 \qquad (4.11d)$$

in which $z_j'$ and $z_j''$ refer respectively to planes immediately above and immediately below the interface $z_j$.

31

The general solution to Eq. (4.5) for $z_j \leq z \leq z_{j+1}$ is

$$v(z) = a_j \cos\gamma_j z + b_j \sin\gamma_j z \qquad (4.12)$$

in which

$$\gamma_j^2 = \omega^2 \rho_j / G_j - k^2 \qquad (4.13)$$

The shear stresses at the interfaces $j$ and $j+1$ in terms of $v_j = v(z_j)$ and $v_{j+1} = v(z_{j+1})$ follow from Eqs. (4.10) and (4.12) and, after some algebra, reduce to

$$-\tau_{zy}(z_j'') = (c_j v_j + d_j v_{j+1}) \exp(i\omega t - ikx) \qquad (4.14a)$$

and

$$\tau_{zy}(z_{j+1}') = (d_j v_j + c_j v_{j+1}) \exp(i\omega t - ikx) \qquad (4.14b)$$

in which

$$c_j = + G_j \gamma_j \cot\gamma_j h_j \qquad (4.15a)$$

$$d_j = - G_j \gamma_j / \sin\gamma_j h_j \qquad (4.15b)$$

and $\quad h_j = z_{j+1} - z_j.$

Substitution of Eqs. (4.14) into Eqs. (4.11) leads to a set of n homogeneous transcendental equations

$$c_1 v_1 + d_2 v_2 \qquad\qquad = 0$$

$$d_{j-1} v_{j-1} + (c_{j-1} + c_j) v_j + d_j v_{j+1} = 0 \qquad j=2, \ldots, n$$

$$d_{n-1} v_{n-1} + (c_{n-1} + c_n) v_n \qquad = 0$$

$$(4.16)$$

Non-trivial solutions to these equations can be obtained only for eigen-values, $k^2$, which cause the determinant of the coefficient matrix to vanish. Eq. (4.16) states a difficult eigenvalue problem, because the eigenvalues are "hidden" in the arguments of the transcendental ex-pressions $c_j$ and $d_j$. Infinitely many different eigenvalues and associated eigenfunctions exist; but it is difficult to obtain even a few of them, because they can be found only by search procedures.

In the study of the earth's crust, seismologists face eigenvalue problems of this type when they calculate dispersion curves for Love waves in a layered medium [16]. Dispersion curves show the relation between the frequency or period of a harmonic wave and its phase velocity or wave number. Only the fundamental wave mode, which is the mode of greatest phase velocity or smallest wave number at any given frequency, and one or two higher modes are usually considered. Haskell [19] has formulated a matrix transfer method suited for automatic computation that permits finding a few of the lower wave modes in a layered elastic medium.

## Expansion of Displacements into Eigenfunctions

The actual displacements in the layered region R shown in Fig. 4 may be expanded into eigenfunctions, which are determined from the solutions to Eq. (4.16) and which satisfy the differential equations, Eq. (4.2), and the boundary conditions at horizontal planes, Eq. (4.11). According to Eq. (4.9), the expansion is of the form

$$\delta(x,z,t) = \sum_{s=1}^{\infty} \alpha_s v_s(z) \exp(i\omega t - ik_s x) \tag{4.17}$$

in which $v_s(z)$, $k_s$ and $\alpha_s$ are the mode shape, the wave number and the mode participation factor of the sth mode or eigenfunction, respectively.

The mode participation factors have to be chosen so that displacement and stress conditions at the boundary between the irregular and the layered region are satisfied. In addition, only those modes which transmit energy in the positive x-direction and do not increase in amplitude with x can be included in the expansion. These latter conditions follow from energy considerations. Since the motion is generated by external forces in the irregular region and since the layered region R is open to the right, the energy transmission must be positive in the x-direction and the energy density cannot increase with x.

The method outlined above, which is based on continuum theory, was employed to solve a very simple boundary value problem involving a line load on a homogeneous layer, see Appendix 3. However, major difficulties arise when a more complicated problem is to be solved by this method. In actual analyses, the number of eigenfunctions included in the expansion, Eq. (4.17), will be small, instead of infinite, because the determination of any one eigenfunction takes a considerable effort. In addition, it is difficult to ensure that none of the more important eigenfunctions is omitted in the expansion and that a good approximate solution is obtained.

Therefore, a discrete method will be developed for the analysis of harmonic motion in the layered region. This method is suited to automatic computation, provides accurate results and is easy to use in connection with the finite element analysis of the irregular region.

## 4.2 Eigenvalue Problem for Discretized Layered Region

The layered region is discretized in the vertical direction by subdividing the region into thin layers as shown in Fig. 11 and assuming that $v(z)$ varies linearly within each layer. In order for this assumption to be reasonable the thickness, $h$, of each layer must be chosen small compared to the wavelength of shear waves in the layer. For this reason the number of layers, $n$, in the discrete system is usually larger than the number of natural layers; a typical analysis involves from 10 to 40 layers. The region is subdivided into layers so that the interfaces between the layers coincide with the nodal joints at the vertical boundary with the irregular region. The layered and the irregular regions can then be connected at these nodal joints. As the displacements at the vertical boundary vary linearly between the nodal joints of the finite elements and between the layer interfaces, the displacements will be continuous across the boundary.

The assumption of linear variation of $v(z)$ within each layer implies that $v(z)$ is defined by its values $v_j = v(z_j)$, $j=1, \ldots, n$, at the layer interfaces. Therefore, the displacements of a generalized

34

Love wave may be represented by

$$\{\delta\} = \alpha\{v\} \exp(i\omega t - ikx) \tag{4.18}$$

in which the vector $\{\delta\}$ contains the displacements $\delta_j$, $j=1, \ldots, n$, of the layer interfaces. The vector $\{v\}$ represents the mode shape and $\alpha$ is the mode participation factor as before.

The displacement function for $z_j \leq z \leq z_{j+1}$ is accordingly

$$u(x,z) = v(z) \exp(-ikx) \tag{4.19}$$

in which

$$v(z) = (z_{j+1} - z)/h_j \cdot v_j + (z - z_j)/h_j \cdot v_{j+1} \tag{4.20}$$

Omitting the common factor $\exp(i\omega t)$, these displacements produce the shear strains

$$\varepsilon_{xy} = \frac{\partial u}{\partial x} = - iku \tag{4.21a}$$

$$\varepsilon_{zy} = \frac{\partial u}{\partial z} = (-v_j + v_{j+1})/h_j \cdot \exp(-ikx) \tag{4.21b}$$

shear stresses

$$\tau_{xy} = G_j \, \varepsilon_{xy} \tag{4.22a}$$

$$\tau_{zy} = G_j \, \varepsilon_{zy} \tag{4.22b}$$

and inertia forces

$$f_I = \rho_j \, \omega^2 u \tag{4.23}$$

If a section of the layered region between the planes $x=0$ and $x=\xi$ is considered separately, see Fig. 11, the surface tractions

$$p_o(z) = - \tau_{xy}(0,z) \tag{4.24a}$$

and

$$p_\xi(z) = + \tau_{xy}(\xi,z) \tag{4.24b}$$

must be applied at the boundaries $x=0$ and $x=\xi$ in order to preserve dynamic equilibrium. They are the only external forces acting on this section.

The application of the principle of virtual work as expressed by Eq. (3.26) yields

$$\int_0^\xi \int_{z_1}^{z_{n+1}} (\hat{\epsilon}^*_{xy}\tau_{xy} + \hat{\epsilon}^*_{zy}\tau_{zy} - \hat{u}^*f_I)dz\ dx = \int_{z_1}^{z_{n+1}} \hat{u}^*(p_o + p_\xi)dz \qquad (4.25)$$

in which $\hat{\epsilon}^*_{xy}$, $\hat{\epsilon}^*_{zy}$ and $\hat{u}^*$ are the complex conjugates of the virtual strains and displacements, respectively.

According to Eq. (4.18), the only degrees of freedom in the discretized region are the nodal displacements $v_j$, $j=1, \ldots, n$. From the virtual displacement state "j", i.e.

$$\hat{v}_j = 1 \quad \text{and} \quad \hat{v}_\ell = 0 \quad \text{for} \quad \ell \neq j \qquad (4.26)$$

and from Eqs. (4.19 - 4.21) it follows that

$$\hat{u}^* = \begin{cases} (z-z_{j-1})/h_{j-1} \cdot \exp(i\bar{k}x) & \text{for } z_{j-1} \leq z \leq z_j \\ (z_{j+1}-z)/h_j \cdot \exp(i\bar{k}x) & \text{for } z_j \leq z \leq z_{j+1} \\ 0 & \text{elsewhere} \end{cases} \qquad (4.27a)$$

$$\hat{\epsilon}^*_{xy} = i\bar{k}\ u^* \qquad (4.27b)$$

and

$$\hat{\epsilon}^*_{zy} = \begin{cases} 1/h_{j-1} \cdot \exp(i\bar{k}x) & \text{for } z_{j-1} < z < z_j \\ -1/h_j \cdot \exp(i\bar{k}x) & \text{for } z_j < z < z_{j+1} \\ 0 & \text{elsewhere} \end{cases} \qquad (4.27c)$$

in which $\bar{k}$ is the complex conjugate of $k$.

Substitution of Eqs. (4.19 - 4.24) and (4.27) into Eq. (4.25) leads to the equilibrium equations for the section considered. The n virtual displacement states "j", $j=1, 2, \ldots, n$, produce a set of simultaneous linear equations in the n unknowns $v_j$. When the simple integrations defined in Eq. (4.25) are performed, the equilibrium equations can be reduced to the matrix equation

$$(k^2[A] + [G] - \omega^2[M])\{v\} = \{0\} \qquad (4.28)$$

in which $\{v\}$ is the displacement vector with the elements $v_j$, $j=1, \ldots, n$. The n x n matrices [A], [G], and [M] consist of the contributions from the individual layers and can therefore be conveniently assembled from

the layer submatrices as demonstrated in Fig. 13. The submatrices to be substituted for $[X]_j$, $j=1, \ldots, n$, in Fig. 13 are

$$[A]_j = h_j G_j \begin{bmatrix} \frac{1}{3} & \frac{1}{6} \\ \frac{1}{6} & \frac{1}{3} \end{bmatrix} \qquad j=1, \ldots, n \qquad (4.29a)$$

$$[G]_j = \frac{G_j}{h_j} \begin{bmatrix} 1 & -1 \\ -1 & 1 \end{bmatrix} \qquad j=1, \ldots, n \qquad (4.29b)$$

and

$$[M]_j = \rho_j h_j \begin{bmatrix} \frac{1}{3} & \frac{1}{6} \\ \frac{1}{6} & \frac{1}{3} \end{bmatrix} \qquad j=1, \ldots, n \qquad (4.29c)$$

for the matrices [A], [G], and [M], respectively. The first two matrices are obviously related to the stiffness of the layers. They are real in the undamped case, when all shear moduli $G_j$, $j=1, \ldots,$ are real. The mass matrix [M] is always real since $\rho_j$, the mass density of the jth layer, is real.

Eq. (4.28) is independent of $\xi$. Hence, the solutions to Eq. (4.28) satisfy equilibrium in the layered region between the vertical planes $x=0$ and $x=\xi$ where $\xi$ may take any value greater than zero. In the following it will be assumed that $\xi$ is infinitely large.

As the circular frequency $\omega$ is a given parameter, it is convenient to introduce the n x n matrix

$$[C] = [G] - \omega^2 [M] \qquad (4.30)$$

and write Eq. (4.28) in the form

$$([A]k^2 + [C])\{v\} = \{0\} \qquad (4.31)$$

which states an algebraic eigenvalue problem with n eigenvalues $k_s^2$, $s=1, \ldots, n$, and the corresponding eigenvectors $\{v\}_s$.

The matrices [A] and [C] are tridiagonal and symmetric. In the undamped case they are real and matrix [A] is positive definite, giving Eq. (4.31) the convenient property that all the eigenvalues and eigenvectors are real [49].

37

A procedure for computing the complete set of eigenvalues and corresponding vectors in the damped and undamped case is presented in Appendix 1 and a FORTRAN IV subroutine for automatic computation is listed in Appendix 5. The procedure uses Newton's method to find the roots of the determinant $|[A]k^2 + [C]|$ and inverse iteration to obtain the eigenvectors.

The orthogonality conditions of the eigenvectors can be derived from any two solutions to Eq. (4.31) such as

$$([A]k_r^2 + [C])\{v\}_r = \{0\} \tag{4.32a}$$

and

$$([A]k_s^2 + [C])\{v\}_s = \{0\} \tag{4.32b}$$

The first equation is premultiplied by $\{v\}_s^T$, the second equation is transposed, post-multiplied by $\{v\}_r$ and then subtracted from the first equation. This gives

$$(k_r^2 - k_s^2)\{v\}_s^T [A]\{v\}_r = 0 \tag{4.33}$$

which implies

$$\{v\}_s^T [A]\{v\}_r = \begin{cases} 1 & \text{for } r=s \\ 0 & \text{for } r \neq s \end{cases} \tag{4.34}$$

when the case r=s is used to normalize the vectors.

The general motion of the discretized layered region can be described by a linear combination of Love modes. Hence, if only one each of the modes corresponding to the pairs $\pm k_s$, s=1, ..., n, exist in the system, the displacements at x=0 are

$$\{u\}^R = \sum_{s=1}^{n} \alpha_s \{v\}_s = [V]\{\alpha\} \tag{4.35}$$

in which $\{\alpha\}$ is a column vector containing the generally complex participation factors $\alpha_s$, s=1, ..., n, and [V] is an n x n matrix which contains the mode shapes $\{v\}_s$ in its columns.

The orthogonality properties, Eq. (4.34), imply that

$$[V]^{-1} = [V]^T [A] \tag{4.36}$$

38

and Eq. (4.35) can therefore be inverted to

$$\{\alpha\} = [V]^T[A]\{u\}^R \qquad (4.37)$$

which is used to compute the mode participation factors $\alpha_s$, s=1, ..., n, when the displacements at x=0 are known.

## 4.3 Wave Types

Each eigenvalue $k_s^2$ yields two possible wave numbers, $+ k_s$ and $- k_s$. One sign corresponds to a generalized Love wave which propagates or decays to the left, the other sign to a wave which propagates or decays to the right. Both waves have the same mode shape.

In the undamped case all eigenvalues and mode shapes are real, as the matrices [A] and [C] are real. Hence, by Eq. (4.18), positive eigenvalues, $k^2 > 0$, correspond to propagating waves of the type

$$\{\delta\}_s = \alpha_s\{v\}_s \exp(i\omega t \pm i|k_s|x) \qquad (4.38a)$$

Negative eigenvalues, $k_s^2 < 0$, yield purely imaginary wave numbers and motions of the type

$$\{\delta\}_s = \alpha_s\{v\}_s \exp(i\omega t \pm |k_s|x) \qquad (4.38b)$$

which decay or increase exponentially in amplitude with x and do not propagate.

In the damped case, when the matrices [A] and [C] are complex, all eigenvalues and therefore all wave numbers are complex, i.e. $k_s = k_1^s + ik_2^s$. The motion is a wave

$$\{\delta\}_s = \alpha_s\{v\}_s \exp(i\omega t - ik_1^s x + k_2^s x) \qquad (4.38c)$$

which propagates in the x-direction with the phase velocity $c_s = \omega/k_1^s$ and a decaying or increasing amplitude, depending on the sign of $k_2^s$.

In the undamped case the possibility exists that $k_s = 0$ and that the motion degenerates to

$$\{\delta\}_s = \alpha_s\{v\}_s \exp(i\omega t) \qquad (4.38d)$$

This motion is independent of x and consists of a shear wave travelling

39

vertically up and down through the layers, being reflected at the rigid base and the free surface. This wave type can only occur at certain frequencies which are the natural frequencies for one-dimensional vertical waves in the layered system. The natural frequencies can be found from the secular equation

$$\left| [G] - \omega^2 [M] \right| = 0 \tag{4.39}$$

which follows from Eqs. (4.30) and (4.31).

## 4.4 Dynamic Stiffness Matrix for Layered Region

In order to develop the dynamic stiffness matrix for the layered region R in Fig. 11 it is first assumed that only those modes which decay or propagate energy in the positive x-direction exist in R. This requires choosing those n wave numbers out of the 2n numbers $\pm k_s = \pm(k_1^s + i\, k_2^s)$, $s=1, \ldots, n$, that have a negative imaginary part or, if the imaginary part is zero, have a positive real part, i.e. for $s=1, \ldots, n$

$$k_s = \begin{cases} k_1^s - i|k_2^s| & \text{if} \quad k_2^s \neq 0 \\[2mm] + |k_1^s| & \text{if} \quad k_2^s = 0 \end{cases} \tag{4.40}$$

The displacements in the layered region are then expressed by super-position of the corresponding modes

$$\{\delta\} = \sum_{s=1}^{n} \{v\}_s \exp(i\omega t - i k_s x)\, \alpha_s \tag{4.41}$$

The only stress on the plane x=0, see Fig. 15, is the shear stress

$$\tau_{xy} = G \frac{\partial \delta}{\partial x} (x=0) = -\, i\, G \sum_{s=1}^{n} k_s v_s(z)\, \alpha_s \tag{4.42}$$

in which G is the shear modulus. The time factor $\exp(i\omega t)$ is understood. The assumption that $v(z)$ varies linearly within a layer implies that

$\tau_{xy}$ also varies linearly with z as shown in Fig. 15a. The nodal forces which are in equilibrium with the stresses at the vertical face of the jth layer are

$$P'_j = \frac{i}{6} G_j h_j \sum_{s=1}^{n} k_s (2 v_j^s + v_{j+1}^s) \alpha_s \qquad (4.43a)$$

$$P''_{j+1} = \frac{i}{6} G_j h_j \sum_{s=1}^{n} k_s (v_j^s + 2 v_{j+1}^s) \alpha_s \qquad (4.43b)$$

in which $v_j^s$ is the jth element of the eigenvector $\{v\}_s$.

These forces, which are also shown in Fig. 15a, act on the region $x > 0$. The total forces acting at the boundary nodal joints of the layered region at x=0 are

$$P_j = P'_j + P''_j \qquad j=1, \ldots, n \qquad (4.44)$$

with $P''_1 = 0$. These forces can be expressed in matrix notation by

$$\{P\}^R = i[A][V][K]\{\alpha\} \qquad (4.45)$$

in which $\{P\}^R$ contains the forces $P_j$, j=1, ..., n, and [K] is a diagonal matrix with the elements $k_s$, s=1, .... n, which are chosen according to Eq. (4.40). Matrix [V] contains the eigenvectors $\{v\}_s$, s=1, ..., n, columnwise and [A] is the matrix defined above by Eq. (4.29a).

The boundary forces $\{P\}^R$ are expressed in Eq. (4.45) in terms of the mode participation factors $\alpha_s$. However, in the finite element analysis of the irregular region the nodal displacements are introduced as the unknowns. The coordinate transformation according to Eq. (4.27) yields

$$\{P\}^R = [R]\{u\}^R \qquad (4.46)$$

in which

$$[R] = i[A][V][K][V]^T[A] \qquad (4.47)$$

is the dynamic stiffness matrix of the semi-infinite layered region. The matrix [R] relates the nodal forces acting on the layered region to the simultaneous nodal displacements at the boundary x=0. The attribute

"dynamic" indicates that the effect of the inertia forces is included in [R]. Matrix [R] is symmetric, as it should be according to the theorem of reciprocity [14]. Its elements are generally complex. The real part of [R] exactly represents the elastic resistance of the discretized semi-infinite layered region to the displacement of the nodal joints. Whereas the imaginary part of [R] represents the damping effect of the layered region on the displacements of the nodal joints. This damping is caused by dissipation of energy to infinity or by viscosity of the material.

The dynamic stiffness matrix changes with the frequency of the harmonic motions because the displacement functions chosen are the frequency dependent eigenfunctions of the layered system. Eq. (4.46) is also valid for the static case, $\omega=0$.

The dynamic stiffness matrix becomes singular if any one of the wave numbers $k_s$ of the diagonal matrix [K] vanishes. If this is the case no forces are required to excite the mode corresponding to $k_s=0$. However, this can happen only in the undamped case and then only at the natural frequencies determined by Eq. (4.39).

The analysis of a left layered region L, as shown in Fig. 4, is analogous to that of a right layered region. The only difference between a left and a similar right layered region is due to their positions with respect to the global coordinate system introduced in Fig. 4. Thus the dynamic stiffness matrix, [L], of a left layered region is also given by the right hand side of Eq. (4.47).

4.5 Energy Transmission

Consider a set of harmonic external forces

$$\{F\} = \{P\} \, \exp(i\omega t) = (\{P_1\} + i\{P_2\}) \, \exp(i\omega t) \qquad (4.48)$$

which act on the nodal points of a discrete system and produce the nodal displacements

$$\{\delta\} = \{u\} \, \exp(i\omega t) = (\{u_1\} + i\{u_2\}) \, \exp(i\omega t) \qquad (4.49)$$

The time average of the rate of work done by the forces on the displacements is

$$E = \frac{1}{T} \int_0^T \text{Re } \{\dot{\delta}\}^T \text{ Re } \{F\} \, dt \tag{4.50}$$

in which $T = 2\pi/\omega$ is the period and $\{\dot{\delta}\}$ is the time derivative of $\{\delta\}$. Substitution of

$$\text{Re } \{\dot{\delta}\} = - \omega(\{u_1\} \sin\omega t + \{u_2\} \cos\omega t) \tag{4.51}$$

and

$$\text{Re } \{F\} = \{P_1\} \cos\omega t - \{P_2\} \sin\omega t \tag{4.52}$$

into Eq. (4.50) and integration over one period yields

$$E = \frac{\omega}{2} (\{u_1\}^T\{P_2\} - \{u_2\}^T\{P_1\}) \tag{4.53}$$

which is identical to

$$E = \frac{\omega}{2} \text{ Im } (\{u\}^*\{P\}) \tag{4.54}$$

The * indicates the conjugate transpose and Im denotes the imaginary part.

The energy transmission from the irregular region I to the layered region R at the boundary x=0 is now considered, see Fig. 11. Substitution of Eqs. (4.35) and (4.45) into Eq. (4.54) gives the time average

$$E = \frac{\omega}{2} \text{ Im } (i\{\alpha\}^*[V]^*[A][V][K]\{\alpha\}) \tag{4.55}$$

This expression can be simplified in the undamped case, when [A] and therefore [V] are real, to

$$E = \frac{\omega}{2} \text{ Im } (i\{\alpha\}^*[K]\{\alpha\}) \tag{4.56}$$

since $[V]^T[A][V] = [I]$ according to Eq. (4.34). As [K] is a diagonal matrix, Eq. (4.56) may also be written in the form

$$E = \frac{\omega}{4} \sum_{s=1}^{n} (\bar{k}_s + k_s)|\alpha_s|^2 = \sum_{s=1}^{n} E_s \tag{4.57}$$

43

in which

$$E_s = \begin{cases} \dfrac{\omega}{2} k_s |\alpha_s|^2 & \text{if } k_s \text{ is real} \\\\ 0 & \text{if } k_s \text{ is imaginary} \end{cases} \qquad (4.58)$$

and represents the energy transmitted by a single mode s.

# 5. AXISYMMETRIC LOVE WAVE MOTION

## 5.1 Motion in Layered Region

The analysis of axisymmetric Love wave motion in a layered region as shown in Fig. 5 is similar to the analysis of plane Love wave motion presented in Chapter 4.

Any point $(r,z)$ in the region undergoes displacements in the angular $\theta$-direction only. The displacements of harmonic motion at the frequency $\omega$,

$$\delta = \delta_\theta(r,z,t) = u(r,z) \exp(i\omega t) \tag{5.1}$$

are governed, according to Eq. (3.16c), by the homogeneous differential equations for the n layers

$$G_j \left( \frac{\partial^2 u}{\partial r^2} + \frac{1}{r} \frac{\partial u}{\partial r} - \frac{u}{r^2} + \frac{\partial^2 u}{\partial z^2} \right) + \rho_j \omega^2 u = 0 \qquad j=1, \ldots, n \tag{5.2}$$

The assumption that

$$u(r,z) = v(z) \cdot g(r) \tag{5.3}$$

leads to

$$\frac{\partial^2 v}{\partial z^2} \frac{1}{v} + \frac{\rho_j}{G_j} \omega^2 = - \frac{1}{g} \left( \frac{\partial^2 g}{\partial r^2} + \frac{1}{r} \frac{\partial g}{\partial r} - \frac{1}{r^2} \right) \qquad j=1, \ldots, n \tag{5.4}$$

which can only be valid for all values of r and z in the respective layers if both sides of the equation are equal to the same constant. Setting the constant equal to $k^2$, the following ordinary differential equations

$$\frac{d^2 v}{dz^2} + (\rho_j \omega^2 / G_j - k^2) v = 0 \qquad j=1, \ldots, n \tag{5.5}$$

45

and

$$\frac{d^2 g}{dr^2} + \frac{1}{r} \frac{dg}{dr} - (\frac{1}{r^2} - k^2)g = 0 \tag{5.6}$$

are obtained. Eq. (5.6) is a Bessel equation [2] which has a solution

$$g(r) = H_1^{(2)}(kr) \tag{5.7}$$

in which $H_1^{(2)}$ is the Hankel function of the first order and second kind
[2]. Eq. (5.7) can easily be verified by substitution into Eq. (5.6)
and observing the following derivatives

$$\frac{d}{dr} H_0^{(2)}(kr) = - k H_1^{(2)}(kr) \tag{5.8a}$$

$$\frac{d}{dr} H_1^{(2)}(kr) = - \frac{1}{r} H_1^{(2)}(kr) + k H_0^{(2)}(kr) \tag{5.8b}$$

$$\frac{d^2}{dr^2} H_1^{(2)}(kr) = (\frac{2}{r^2} - k^2) H_1^{(2)}(kr) - \frac{k}{r} H_0^{(2)}(kr) \tag{5.8c}$$

The Hankel functions $H_0^{(2)}(kr)$ and $H_1^{(2)}(kr)$ tend to zero in the
sector $-\pi < \arg (kr) < 0$ as $|kr| \to \infty$. They are related to the Bessel
functions of the first and second kind, $J_m$ and $Y_m$, respectively, by

$$H_m^{(2)} = J_m - i Y_m \tag{5.9}$$

in which the subscript m indicates the order of the functions and
$i = \sqrt{-1}$. However, Eq. (5.9) should not be used to compute values of
$H_m^{(2)}(kr)$ in the sector $-\pi < \arg (kr) < 0$ from values of $J_m$ and $Y_m$ because
severe cancellations may occur in the subtraction $J_m - i Y_m$ and may
result in the loss of all significant digits. A method for computing
the functions $H_0^{(2)}$ and $H_1^{(2)}$ by ascending and asymptotic series is
presented in Appendix 4 and a Fortran IV subroutine for automatic com-
putation of these functions is listed in Appendix 5.

A solution to Eq. (5.2) may be expressed in the form of an axi-
symmetric wave

$$\delta = v(z) \, H_1^{(2)}(kr) / H_1^{(2)}(kr_o) \cdot \exp(i\omega t) \tag{5.10}$$

46

which is similar to a plane wave at some distance from the origin. In this expression $r_o$ defines the distance of the boundary between the irregular and layered regions from the origin. If $|kr|$ is large the asymptotic approximation to the Hankel function [2]

$$H_1^{(2)}(kr) \simeq \sqrt{2/(kr\pi)} \, \exp(-ikr+i3\pi/4) \qquad (5.11)$$

may be used to obtain

$$\delta \simeq v(z) \exp(i\omega t-ikr) \ \sqrt{2/(\pi kr)} \ \exp(i3\pi/4)/H_1^{(2)}(kr_o) \qquad (5.12)$$

which is similar to Eq. (4.9) except for the decay factor $\sqrt{2/(\pi kr)}$ and a complex number indicating a phase shift. The similarity to a plane wave shows that Eq. (5.10) describes a wave travelling away from the origin if the real part of the wave number k is positive.

The boundary conditions at the horizontal planes $z_j$, $j=1,2, \ldots,$ $n+1$, are, as in the plane case, the continuity of the displacements and the stresses at the layer interfaces, zero shear stresses at the free surface and zero displacements at the fixed base. As the stress-displacement relation is

$$\tau_{z\theta} = G \, \frac{\partial \delta}{\partial z} = G \, \frac{dv}{dz} \, H_1^{(2)}(kr)/H_1^{(2)}(kr_o) \cdot \exp(i\omega t) \qquad (5.13)$$

the boundary conditions take the form

$$v(z_j') \quad = v(z_j'') \qquad\qquad j=2, \ldots, n \qquad (5.14a)$$

$$G_j \frac{d}{dz} \, v(z_j') \ = G_{j+1} \, \frac{d}{dz} \, v(z_j'') \qquad\qquad j=2, \ldots, n \qquad (5.14b)$$

$$v(z_{n+1}') \ = 0 \qquad (5.14c)$$

and

$$\frac{d}{dz} \, v(z_1'') = 0 \qquad (5.14d)$$

The function v(z) is determined by the n ordinary differential equations, Eq. (5.5), and the boundary conditions, Eq. (5.14), which are identical to the corresponding differential equations and boundary conditions for the plane case, Eqs. (4.5) and (4.11). Therefore, the resulting eigenvalue problem and its solutions are the same for the plane

47

and axisymmetric cases. This holds not only for the continuum theory but also for the discrete theory because in the axisymmetric case the layered region is discretized in the same manner as in the plane case.

It is again assumed that $v(z)$ varies linearly within each layer according to Eq. (4.20). Hence, the displacements in the layered region may be defined by the displacements of the layer interfaces which are collected in the vector $\{\delta\}$, i.e.

$$\{\delta\}^T = <\delta_1\delta_2 \ldots \delta_n> \tag{5.15}$$

The sth axisymmetric mode is obtained from the sth solution to Eqs. (4.31) and, by Eq. (5.10), takes the form

$$\{\delta\}_s = \{v\}_s \, H_1^{(2)}(k_s r)/H_1^{(2)}(k_1 r_o) \cdot \exp(i\omega t) \tag{5.16}$$

Thus, the displacements in the layered region may be expressed by the linear combination

$$\{\hat{c}\} = \sum_{s=1}^{n} \alpha_s \{v\}_s \, H_1^{(2)}(k_s r)/H_1^{(2)}(k_s r_o) \cdot \exp(i\omega t) \tag{5.17}$$

The rule for the selection of the n wave numbers $k_s$ from the 2n values $\pm k_s$, s=1, ..., n, is the same as in the plane case, i.e. Eq. (4.40). This follows from the properties of $H_1^{(2)}$ and its similarity to the exponential function for large arguments.

## 5.2   Dynamic Stiffness Matrix for Layered Region

The nodal displacement at the cylindrical boundary $r=r_o$ between the layered and irregular regions are, omitting the time factor $\exp(i\omega t)$,

$$\{u\}^R = \sum_{s=1}^{n} \{v\}_s \alpha_s = [V]\{\alpha\} \tag{5.18}$$

in which the vector $\{u\}^R$ has the elements $u_j$, j=1, ..., n, the n x n matrix [V] contains the eigenvectors $\{v\}_s$ columnwise, and the vector $\{\alpha\}$ contains the mode participation factors $\alpha_s$.

48

The inversion of Eq. (5.18) gives, according to Eq. (4.36),

$$\{\alpha\} = [V]^T [A] \{u\}^R \tag{5.19}$$

which serves to obtain the mode participation factors from a known vector $\{u\}^R$.

The only stress at the boundary $r=r_o$ is the shear stress $\tau_{r\theta}$. By using the stress-displacement relation

$$\tau_{r\theta} = G \left( \frac{\partial \delta}{\partial r} - \frac{\delta}{r} \right) \tag{5.20}$$

and Eq. (5.17), the shear stress in the jth layer at $r=r_o$ is obtained, i.e.

$$\tau_{r\theta} = G \sum_{s=1}^{n} v_s(z) \left\{ k_s H_0^{(2)}(k_s r_o) / H_1^{(2)}(k_s r_o) - \frac{2}{r_o} \right\} \alpha_s \tag{5.21}$$

when the time factor $\exp(i\omega t)$ is omitted. The assumption that $v(z)$ varies linearly within a layer implies that $\tau_{r\theta}$ also varies linearly with z as shown in Fig. 15a. The nodal forces which are equivalent to the stresses acting on the vertical boundary of a one radian segment of the jth layer are

$$P'_j = G_j h_j / 6 \cdot \sum_{s=1}^{n} (2v_j^s + v_{j+1}^s)\{-k_s r_o \cdot H_0^{(2)}(k_s r_o)/H_1^{(2)}(k_s r_o) + 2\} \alpha_s \tag{5.22}$$

and

$$P''_{j+1} = G_j h_j / 6 \cdot \sum_{s=1}^{n} (v_j^s + 2v_{j+1}^s)\{-k_s r_o \cdot H_0^{(2)}(k_s r_o)/H_1^{(2)}(k_s r_o) + 2\} \alpha_s \tag{5.23}$$

in which $v_j^s$ is the jth element of the eigenvector $\{v\}_s$. These forces, which are also shown in Fig. 15a, act on the region $r > r_o$.

The total forces acting on a one radian segment of the layered region are

$$P_j = P'_j + P''_j \qquad\qquad j=1, \ldots, n \tag{5.24}$$

49

with $P''_1 = 0$. In matrix notation these forces may be expressed by

$$\{P\}^R = [A][V][H]\{\alpha\} \qquad (5.25)$$

The vector $\{P\}^R$ contains the forces $P_j$, $j=1, \ldots, n$; the $n \times n$ matrix [V] contains the eigenvectors $\{v\}_s$, $s=1, \ldots, n$, columnwise; [A] is the matrix defined by Eq. (4.29) and [H] is the diagonal matrix

$$[H] = \text{Diag} \{-k_s r_o \, H_0^{(2)}(k_s r_o)/H_1^{(2)}(k_s r_o) + 2\} \qquad (5.26)$$

Substitution of Eq. (5.19) into (5.22) gives

$$\{P\}^R = [R]\{u\}^R \qquad (5.27)$$

in which

$$[R] = [A][V][H][V]^T[A] \qquad (5.28)$$

The matrix [R] is the dynamic stiffness matrix for a one radian segment of the axisymmetric layered region which extends in the radial direction from $r_o$ to infinity. It relates the nodal forces to the simultaneous nodal displacements at the boundary $r=r_o$ and is valid for axisymmetric harmonic motion including the static case. Matrix [R] changes with frequency and depends on $r_o$. It cannot become singular, because none of the diagonal elements of [H] can vanish at any given frequency and matrices [A] and [V] are always non-singular.

## 6. PLANE RAYLEIGH WAVE MOTION

### 6.1 Eigenvalue Problem

Free harmonic Rayleigh wave motion under plane strain conditions in a semi-infinite layered region as shown in Fig. 5 is considered. Any point in the region undergoes displacements in the x and z-directions, i.e.

$$\delta_x = q_x(x,z) \ \exp(i\omega t) \tag{6.1a}$$

$$\delta_z = q_z(x,z) \ \exp(i\omega t) \tag{6.1b}$$

The homogeneous differential equations of motion for the spatial parts of the displacements are according to Eq. (3.15), for the jth layer,

$$G_j \left( \frac{\partial^2 q_x}{\partial x^2} + \frac{\partial^2 q_x}{\partial z^2} \right) + (\lambda_j + G_j) \left( \frac{\partial^2 q_x}{\partial x^2} + \frac{\partial^2 q_z}{\partial x \partial z} \right) + \rho_j \ \omega^2 q_x = 0 \tag{6.2a}$$

and

$$G_j \left( \frac{\partial^2 q_z}{\partial x^2} + \frac{\partial^2 q_z}{\partial z^2} \right) + (\lambda_j + G_j) \left( \frac{\partial^2 q_x}{\partial x \partial z} + \frac{\partial^2 q_z}{\partial z^2} \right) + \rho_j \ \omega^2 q_z = 0 \tag{6.2b}$$

Separation of the variables x and z with the assumptions that

$$q_x(x,z) = u(z) \ g(x) \tag{6.3a}$$

and

$$q_z(x,z) = w(z) \ g(x) \tag{6.3b}$$

leads to the coupled ordinary differential equations

$$\{k^2(\lambda_j + 2G_j) - \omega^2\rho_j\} \ u - G_j \ \frac{d^2u}{dz^2} + ik \ (\lambda_j + G_j) \ \frac{dw}{dz} = 0 \tag{6.4a}$$

and

$$\{k^2 G_j - \omega^2\rho_j\} \ w - (\lambda_j + 2G_j) \ \frac{d^2w}{dz^2} + ik \ (\lambda_j + G_j) \ \frac{du}{dz} = 0 \tag{6.4b}$$

for each of the n layers, $j=1, \ldots, n$, and to the differential equation

$$\frac{d^2 g}{dx^2} + k^2 g = 0 \tag{6.5}$$

Since a solution to Eq. (6.5) is

$$g(x) = \exp(-ikx) \tag{6.6}$$

the displacements in the layered region may be expressed in the form of a wave by

$$\delta_x = u(z) \exp(i\omega t - ikx) \tag{6.7a}$$

$$\delta_z = w(z) \exp(i\omega t - ikx) \tag{6.7b}$$

The mode shapes $u(z)$ and $w(z)$ are determined by the 2n differential equations, Eq. (6.4), and by the boundary conditions at the horizontal planes $z=z_j$, $j=1, \ldots, n+1$, i.e. the continuity of the displacements and the stresses at the layer interfaces, zero stresses at the free surface and zero displacements at the fixed base. Using the stress-displacement relations

$$\sigma_z = (\lambda + 2G) \frac{\partial \delta_z}{\partial z} + \lambda \frac{\partial \delta_x}{\partial x} = \{(\lambda + 2G) \frac{dw}{dz} - ik\lambda u\} \exp(i\omega t - ikx) \tag{6.8a}$$

and

$$\tau = G\left(\frac{\partial \delta_z}{\partial x} + \frac{\partial \delta_x}{\partial z}\right) = G \{- ikw + \frac{du}{dz}\} \exp(i\omega t - ikx) \tag{6.8b}$$

these conditions can be written

$$u(z_j') = u(z_j'') \quad \text{and} \quad w(z_j') = w(z_j'') \qquad j=2, \ldots, n \tag{6.9a}$$

$$u(z_{n+1}'') = 0 \qquad \text{and} \quad w(z_{n+1}') = 0 \tag{6.9b}$$

$$(\lambda_{j-1} + 2G_{j-1}) \frac{d}{dz} w(z_j') - ik \lambda_{j-1} u(z_j') = (\lambda_j + 2G_j) \frac{d}{dz} w(z_j'') - ik \lambda_j u(z_j'')$$
$$\text{for} \quad j=2, \ldots, n \tag{6.9c}$$

$$G_{j-1} \left(-ik w(z_j') + \frac{d}{dz} u(z_j')\right) = G_j \left(-ik w(z_j'') + \frac{d}{dz} u(z_j'')\right)$$
$$\text{for} \quad j=2, \ldots, n \tag{6.9d}$$

52

$$(\lambda_1 + 2G_1) \frac{d}{dz} w(z_1'') - ik \lambda_1 u(z_1'') = 0 \qquad (6.9e)$$

and

$$-ik \, w(z_1'') + \frac{d}{dz} u(z_1'') = 0 \qquad (6.9f)$$

in which $z_j'$ and $z_j''$ respectively refer to planes immediately above and immediately below the interface $z_j$.

Eqs. (6.4) and (6.9) lead to an eigenvalue problem similar to that for Love waves. In continuum theory, this problem consists of 2n simultaneous homogeneous equations with coefficients which contain the eigenvalue $k^2$ in the argument of transcendental functions. A derivation of the eigenvalue problem can be found in Ref. [22]. Finding solutions to this problem is even more difficult than finding solutions to the corresponding eigenvalue problem for Love waves, Eq. (4.16), because in the Rayleigh wave case the number of equations for n layers is 2n and the coefficients are more complicated than those in the Love wave case. For the same reasons given in Section 4.1, a discrete theory is preferred to the continuum theory and will now be developed.

## Discretization

As in the Love wave case, the layered region is treated as a continuum in the horizontal direction but discretized in the vertical direction by assuming that $u(z)$ and $w(z)$ in Eq. (6.7) vary linearly within each layer. In order for this assumption to be reasonable the layers have to be chosen thin compared to the length of S-waves in the layer.

The displacements in the layered region may be defined by

$$\{\delta\}^T = <\delta_{x1} \; \delta_{z1} \; \delta_{z2} \; \cdots \; \delta_{xn} \; \delta_{zn}> \qquad (6.10)$$

in which $\delta_{xj}$ and $\delta_{zj}$, j=1, ..., n, are the horizontal and vertical interface displacements, respectively. If the elements of the corresponding mode shape $\{v\}$ are

$$v_{2j-1} = u(z_j) \quad \text{and} \quad v_{2j} = w(z_j) \qquad j=1, \ldots, n \qquad (6.11)$$

the discrete representation of a plane generalized Rayleigh wave is

$$\{\delta\} = \{v\} \, \exp(i\omega t - ikx) \tag{6.12}$$

The displacement functions in terms of interface displacements are

$$q_x(x,z) = u(z) \, \exp(-ikx) \tag{6.13a}$$

$$q_z(x,z) = w(z) \, \exp(-ikx) \tag{6.13b}$$

in which, for $z_j \leq z \leq z_{j+1}$,

$$u(z) = (z_{j+1} - z)/h_j \cdot v_{2j-1} + (z-z_j)/h_j \cdot v_{2j+1} \tag{6.14a}$$

$$w(z) = (z_{j+1} - z)/h_j \cdot v_{2j} + (z-z_j)/h_j \cdot v_{2j+2} \tag{6.14b}$$

Omitting the common factor $\exp(i\omega t)$, these displacements produce the strains

$$\varepsilon_x = \frac{\partial q_x}{\partial x} = -ikq_x \tag{6.15a}$$

$$\varepsilon_z = \frac{\partial q_z}{\partial z} = (-v_{2j} + v_{2j+2})/h_j \cdot \exp(-ikx) \tag{6.15b}$$

$$\gamma_{xz} = \frac{\partial q_x}{\partial z} + \frac{\partial q_z}{\partial x} = (-v_{2j-1} + v_{2j+1})/h_j \cdot \exp(-ikx) - ikq_z \tag{6.15c}$$

stresses

$$\sigma_x = (\lambda_j + 2G_j) \, \varepsilon_x + \lambda_j \, \varepsilon_z \tag{6.16a}$$

$$\sigma_z = (\lambda_j + 2G_j) \, \varepsilon_z + \lambda_j \, \varepsilon_x \tag{6.16b}$$

$$\tau = G_j \, \gamma_{xz} \tag{6.16c}$$

and inertia forces

$$f_x^I = \omega^2 \, \rho_j \, q_x \tag{6.17a}$$

$$f_z^I = \omega^2 \, \rho_j \, q_z \tag{6.17b}$$

If a section of the layered region between the planes $x=0$ and $z=\xi$ is considered separately, see Fig. 12, one has to apply as surface traction $-\sigma_x(0,z)$ and $-\tau(0,z)$ at the left boundary, $x=0$, and $\sigma_x(\xi,z)$ and $\tau(\xi,z)$ at the right boundary, $x=\xi$. The surface tractions are the only

external forces acting on this section of the layered region.

The application of the principle of virtual work as expressed by Eq. (3.20) yields

$$\int_{x=0}^{\ell} \int_{z=z_1}^{z_{n+1}} \left[ \hat{\varepsilon}_x^* \sigma_x + \hat{\varepsilon}_z^* \sigma_z + \hat{\gamma}_{xz}^* \tau - \hat{q}_z^* f_z^I - \hat{q}_x^* f_x^I \right] dz\,dx$$

$$= \int_{z=z_1}^{z_{n+1}} \left[ - \hat{q}_x^*(0,z)\ \sigma_x(0,z) - \hat{q}_z^*(0,z)\ \tau(0,z) \right.$$

$$\left. + \hat{q}_x^*(\xi,\ z)\ \sigma_x(\xi,\ z) + \hat{q}_z^*(\xi,\ z)\ \tau(\xi,\ z) \right] dz \qquad (6.18)$$

in which $\hat{\varepsilon}_x^*$, $\hat{\varepsilon}_z^*$, and $\hat{\gamma}_{xz}^*$ are the complex conjugates of the virtual strains and $\hat{q}_x^*$ and $\hat{q}_z^*$ are the complex conjugates of the virtual displacements.

The degrees of freedom in the discretized region are $v_j$, $j=1, \ldots,$ $2n$, according to Eq. (6.11). The virtual displacement state "$\ell$" defined by

$$\hat{v}_\ell = 1 \quad ; \quad \hat{v}_m = 0 \qquad \text{for } m \neq \ell \qquad (6.19)$$

yields, with Eqs. (6.13 - 6.15), for odd values of $\ell$, i.e. $\ell = 2j-1$

$$\hat{q}_x^* = \begin{cases} (z-z_{j-1})/h_{j-1} \cdot \exp(i\bar{k}x) & \text{for } z_{j-1} \leq z \leq z_j \\ (z_{j+1}-z)/h_j \cdot \exp(i\bar{k}x) & \text{for } z_j \leq z \leq z_{j+1} \\ 0 & \text{elsewhere} \end{cases} \qquad (6.20a)$$

$$\hat{q}_z^* = 0 \quad ; \quad \hat{\varepsilon}_x^* = i\bar{k}\,\hat{q}_x^* \quad ; \quad \hat{\varepsilon}_z^* = 0 \qquad (6.20b)$$

$$\hat{\gamma}_{xz}^* = \begin{cases} 1/h_{j-1} \cdot \exp(i\bar{k}x) & \text{for } z_{j-1} < z < z_j \\ -1/h_j \cdot \exp(i\bar{k}x) & \text{for } z_j < z < z_{j+1} \\ 0 & \text{elsewhere} \end{cases} \qquad (6.20c)$$

55

and for even values of $\ell$, i.e. $\ell=2j$

$$\hat{q}_z^* = \begin{cases} (z-z_{j-1})/h_{j-1} \cdot \exp(i\bar{k}x) & \text{for } z_{j-1} \leq z \leq z_j \\ (z_{j+1}-z)/h_j \cdot \exp(i\bar{k}x) & \text{for } z_j \leq z \leq z_{j+1} \\ 0 & \text{elsewhere} \end{cases} \qquad (6.20\text{d})$$

$$\hat{q}_x^* = 0 \quad ; \quad \hat{\epsilon}_x^* = 0 \quad ; \quad \hat{\gamma}_{xz}^* = +ik\,\hat{q}_z^* \qquad (6.20\text{e})$$

$$\hat{\epsilon}_z^* = \begin{cases} 1/h_{j-1} \cdot \exp(i\bar{k}x) & \text{for } z_{j-1} < z < z_j \\ -1/h_j \cdot \exp(i\bar{k}x) & \text{for } z_j < z < z_{j+1} \\ 0 & \text{elsewhere} \end{cases} \qquad (6.20\text{f})$$

Substitution of Eqs. (6.13 - 6.17) and Eqs. (6.20) into Eq. (6.18) leads to one equilibrium equation for each of the $2n$ virtual displacement states "$\ell$". The $2n$ equilibrium equations are simultaneous complex linear equations in the $2n$ complex unknowns $v_\ell$, $\ell=1, \ldots, 2n$. When the simple integrations defined in Eq. (6.18) are performed, the set of equations may be written in matrix notation as

$$(k^2[A] - ik[D] + ik[D]^T + [G] - \omega^2[M])\{v\} = \{c\} \qquad (6.21)$$

The vector $\{v\}$ contains the complex displacements $v_j$, $j=1, \ldots, 2n$. The $2n \times 2n$ matrices $[A]$, $[D]$, $[G]$ and $[M]$ consist of the contributions from the individual layers and can therefore be assembled by addition of layer submatrices as indicated in Fig. 14. The submatrices to be substituted for $[X]_j$ in Fig. 14 are

$$[A]_j = \frac{1}{6} h_j \begin{bmatrix} 2(2G_j+\lambda_j) & 0 & (2G_j+\lambda_j) & 0 \\ 0 & 2G_j & 0 & G_j \\ (2G_j+\lambda_j) & 0 & 2(2G_j+\lambda_j) & 0 \\ 0 & G_j & 0 & 2G_j \end{bmatrix} \qquad j=1, \ldots, n \qquad (6.22\text{a})$$

$$[D]_j = \frac{1}{2} \begin{bmatrix} 0 & \lambda_j & 0 & -\lambda_j \\ G_j & 0 & -G_j & 0 \\ 0 & \lambda_j & 0 & -\lambda_j \\ G_j & 0 & -G_j & 0 \end{bmatrix} \qquad j=1, \ldots, n \qquad (6.22b)$$

$$[G]_j = \frac{1}{h_j} \begin{bmatrix} G_j & 0 & -G_j & 0 \\ 0 & (2G_j+\lambda_j) & 0 & -(2G_j+\lambda_j) \\ -G_j & 0 & G_j & 0 \\ 0 & -(2G_j+\lambda_j) & 0 & (2G_j+\lambda_j) \end{bmatrix} \qquad j=1, \ldots, n \qquad (6.22c)$$

$$[M]_j = \rho_j h_j \begin{bmatrix} 1/3 & 0 & 1/6 & 0 \\ 0 & 1/3 & 0 & 1/6 \\ 1/6 & 0 & 1/3 & 0 \\ 0 & 1/6 & 0 & 1/3 \end{bmatrix} \qquad j=1, \ldots, n \qquad (6.22d)$$

for the matrices [A], [D], [G] and [M], respectively. The first three matrices are obviously related to the stiffness of the layers and are real in the undamped case when the shear moduli $G_j$ and the Lame's constants $\lambda_j$, $j=1, \ldots, n$, are real. Matrix [M] is a consistent mass matrix [5].

Eq. (6.21) is independent of $\xi$. Hence, the solutions to Eq. (6.21) satisfy equilibrium in the layered region between the vertical planes $x=0$ and $x=\xi$ where $\xi$ may take any value greater than zero. In the following it will be assumed that $\xi$ is infinitely large.

The circular frequency $\omega$ is a given parameter. When the 2n x 2n matrices

$$[C] = [G] - \omega^2 [M] \qquad (6.24)$$

57

and

$$[B] = [D]^T - [D] \tag{6.25}$$

are introduced, Eq. (6.23) can be written

$$([A]k^2 + i[B]\, k + [C])\{v\} = 0 \tag{6.26}$$

The matrices $[A]$ and $[C]$ are symmetric and the matrix $[B]$ is skew symmetric. $[A]$, $[B]$ and $[C]$ are real in the undamped case and complex in the damped case. Eq. (6.26) differs from a similar matrix equation obtained by Lysmer [26] in that it includes a consistent mass matrix, while Lysmer employed a lumped mass matrix. Eq. (6.26) constitutes a set of $2n$ linear homogeneous equations which have non-trivial solutions $\{v\}$ only if the determinant of the coefficient matrix vanishes. Hence, for any given frequency $\omega$, the secular equation

$$\left|[A]k^2 + i[B]\, k + [C]\right| = 0 \tag{6.27}$$

defines the possible wave numbers for generalized Rayleigh waves in the layered region.

Because the determinant, Eq. (6.27), is a polynomial in $k$ of order $4n$, Eq. (6.26) states an algebraic eigenvalue problem which has $4n$ generally complex roots $k_s$, $s=1, 2, \ldots, 4n$. The corresponding solution vectors $\{v\}_s$, $s=1, \ldots, 4n$ are called eigenvectors or mode shapes. A numerical method for finding all of the eigenvalues and eigenvectors is presented in Appendix 2 and a FORTRAN IV subroutine for this task is listed in Appendix 6.

It is convenient for the following wave interpretation to rewrite Eq. (6.26) in the partitioned form

$$\begin{bmatrix} k^2 A_x + C_x & ik\, B_{xz} \\ -ik\, B_{xz}^T & k^2 A_z + C_z \end{bmatrix} \begin{Bmatrix} v_x \\ v_z \end{Bmatrix} = \begin{Bmatrix} 0 \\ 0 \end{Bmatrix} \tag{6.28}$$

where the elements of $\{v_x\}$ are the horizontal displacements $v_j$, $j=1, 3, \ldots, 2n-1$, and the elements of $\{v_z\}$ are the vertical displacements $v_j$, $j=2, 4, \ldots, 2n$. The $n \times n$ submatrices $[A_x]$, $[A_z]$, $[C_x]$, $[C_z]$ and $[B_{xz}]$ are obtained from the matrices $[A]$, $[C]$ and $[B]$, respectively, by permuting the rows and columns in the same way as the vector elements

58

are permuted.

## 6.2  Wave Types

Each eigenvalue $k_s$ and its corresponding eigenvector $\{v\}_s$ define a Rayleigh wave mode which can exist in the layered region and has the displacements

$$\{\delta\}_s = \alpha_s\{v\}_s \cdot \exp(i\omega t - ik_s x) \tag{6.29}$$

The nature of this motion depends on the wave number $k_s$. As in the Love wave case four wave types can be distinguished.

a) If k is complex, $k = k_1 + i\,k_2$, $k_1 \neq 0$, $k_2 \neq 0$, the motion is of the form

$$\{\delta\} = \alpha\{v\} \cdot \exp(k_2 x) \cdot \exp(i\omega t - ik_1 x) \tag{6.30a}$$

which propagates in the x-direction with the phase velocity $c = \omega/k_1$ and decays or increases in amplitude depending on the sign of $k_2$. The mode shape $\{v\}$ is complex and generally neither the horizontal nor the vertical displacements are in phase on vertical planes.

b) If k is real, $k = k_1$, $k_2 = 0$, the motion is a wave which propagates in the x-direction with a constant amplitude and the phase velocity $c = \omega/k_1$ and is of the form

$$\{\delta\} = \alpha\{v\} \exp(i\omega t - ik_1 x) \tag{6.30b}$$

Inspection of Eq. (6.28) shows that for a real k the vector $\{v_x\}$ is purely real while the vector $\{v_z\}$ is purely imaginary. This means that all horizontal displacements are in phase at constant x and 90° out of phase with the vertical displacements. The particle motion describes an ellipse with its major axis either parallel or normal to the surface.

c) If k is purely imaginary, $k = ik_2$, $k_2 \neq 0$, the motion is

$$\{\delta\} = \alpha\{v\} \exp(i\omega t) \tag{6.30c}$$

which varies exponentially in the x-direction and does not propagate. As the coefficient matrix of Eq. (6.23) is real for a purely imaginary k,

59

and as the phase does not change in x, the horizontal and vertical displacements of all points in the layered region have the same phase. In this case particles oscillate along straight lines.

d) If k=0 the motion is independent of x, i.e.

$$\{\delta\} = \alpha\{v\} \exp(i\omega t) \qquad (6.30d)$$

and degenerates to a one-dimensional standing wave. This wave type can occur only at certain frequencies of a layered medium without viscous damping. The natural frequencies can be found from the secular equation

$$\left| [G] - \omega^2[M] \right| = 0 \qquad (6.31)$$

which follows from Eqs. (6.24) and (6.26). When $\cdot=0$, Eq. (6.28) shows that the horizontal and vertical displacements are uncoupled. The motion corresponding to the natural frequencies therefore consists either of standing S-waves with horizontal displacements or of standing P-wave with vertical displacements. The standing S-waves are identical to the degenerated Love waves with a vanishing wave number discussed in Chapter 4, except that the displacements occur here in the x-direction.

Waves of the types b) and d) do not exist in the damped case because all waves attenuate with distance from their source due to damping and thus $k_2$ cannot vanish.

A study of the structure of Eq. (6.26) with reference to Eq. (6.28) shows that if k is an eigenvalue of Eq. (6.26) and $\{v\}$ the corresponding eigenvector, which contains the elements $v_j$, j=1, ..., 2n, then -k is also an eigenvalue and its corresponding eigenvector in transposed form is

$$\{v\}^T = <-v_1 \; v_2 \; -v_3 \; v_4 \; \cdots \; -v_{2n-1} \; v_{2n}> \qquad (6.32)$$

which is obtained from $\{v\}$ by changing the sign on all horizontal displacements. The vector $\{\tilde{v}\}$ is the adjoined of $\{v\}$.

The two solutions describe the motions

$$\{\delta\} = \alpha\{v\} \exp(i\omega t - ikx) \qquad (6.33a)$$

and

$$\{\delta\} = \alpha\{\tilde{v}\} \exp(i\omega t + ikx) \qquad (6.33b)$$

which are identical waves propagating or decaying in opposite directions. Substitution of the second solution, $-k$ with $\{\tilde{v}\}$, into Eq. (6.26) yields

$$([A]k^2 - i[B]k + [C])\{\tilde{v}\} = \{0\} \tag{6.34}$$

In the undamped case, when [A], [B] and [C] are real, the complex eigenvalues occur in conjugate pairs, $k$ and $\bar{k}$. For this case the complex conjugate of Eq. (6.34) is

$$([A]\bar{k}^2 + i[B]\bar{k} + [C])\{\overline{\tilde{v}}\} = \{0\} \tag{6.35}$$

which shows that $\bar{k}$ with $\{\overline{\tilde{v}}\}$ satisfies Eq. (6.26). From the complex conjugate of Eq. (6.26) it may also be shown that $-\bar{k}$ with $\{\bar{v}\}$ is another solution.

Summing up, the eigenvalue problem, Eq. (6.26), has the property that if

a)  $k$ with $\{v\}$

is a solution to Eq. (6.26) then

b)  $-k$ with $\{\tilde{v}\}$

is another solution and, in the undamped case,

c)  $\bar{k}$ with $\{\overline{\tilde{v}}\}$

d)  $-\bar{k}$ with $\{\bar{v}\}$

are also solutions. These solutions are linearly independent with the exception that the solutions c) and d) depend on a) and b) if $k$ is purely real or purely imaginary.


## Orthogonality of Eigenvectors

Two solutions to Eq. (6.26), $\{v\}_r$ with $k_r \neq 0$ and $\{\tilde{v}\}_s$ with $k_s \neq 0$, are considered, i.e.

$$([A]k_r^2 + i[B]k_r + [C])\{v\}_r = \{0\} \tag{6.36a}$$

and

$$([A]k_s^2 - i[B]k_s + [C])\{\tilde{v}\}_s = \{0\} \tag{6.36b}$$

Premultiplying the first equation by $\{\tilde{v}\}_s^T / k_r$ and the second by $\{v\}_r^T / k_s$, then subtracting the transposed second equation from the first gives

$$\{\tilde{v}\}_s^T \Big( [A](k_r - k_s) - [C](k_r - k_s)/(k_r k_s) \Big) \{v\}_r = 0 \tag{6.37}$$

61

Division by $(k_r - k_s)$, provided $k_r \neq k_s$, yields the orthogonality relations

$$\{\tilde{v}\}_s^T [A] \{v\}_r - \{\tilde{v}\}_s^T [C] \{v\}_r / (k_r k_s) = \begin{cases} 2 \text{ if } k_r = k_s \\ 0 \text{ if } k_r \neq k_s \end{cases} \qquad (6.38)$$

in which the case $k_r = k_s$ is used to normalize the eigenvectors. Eq. (6.38) may be expressed by the matrix equation

$$[K][\tilde{V}]^T [A][V][K] - [\tilde{V}]^T [C][V] = 2[K]^2 \qquad (6.39)$$

in which $[K]$ is a 2n x 2n diagonal matrix containing one each of the pairs of eigenvalues $\pm k_s$, s=1, ..., 2n, and $[V]$ and $[\tilde{V}]$ are 2n x 2n nodal matrices containing the corresponding mode shapes $\{v\}_s$ and $\{\tilde{v}\}_s$, s=1, ..., 2n, columnwise.

## 6.3   Dynamic Stiffness Matrix for Layered Region

The "energy conditions" discussed in Section 4.1 demand that only those 2n generalized Rayleigh waves which decay or propagate energy in the positive x-direction are chosen from among the 4n solutions to Eq. (6.26). Thus, among the waves possessing complex wave numbers, those waves which have a wave number with a negative imaginary part are selected. If wave numbers are real the selection must be based on the direction of energy propagation. While for Love waves the directions in which the energy and the "phase" travel are always identical, it some-times occurs that the "phase" of Rayleigh waves travels backwards, i.e. the directions of the phase velocity $c = \omega/k$ and of the energy propagation are opposed. This phenomenon was also observed by Lysmer [26].

It will be shown in Section 6.4 that the energy transmission is positive for waves with a positive wave number $k_s$ and a corresponding mode shape $\{v\}_s$ if the complex conjugate of the mode shape, $\{\bar{v}\}_s$, is equal to the adjoined mode shape $\{\tilde{v}\}_s$ after normalization by Eq. (6.38), i.e. $\{\bar{v}\}_s = \{\tilde{v}\}_s$. If $\{\bar{v}\}_s = -\{\tilde{v}\}_s$, the direction of energy transmission is opposite to that of the phase velocity. Hence, the rules for the selection of the 2n wave numbers $k_s$, s=1, ..., 2n, from the 4n wave

numbers $\pm k_s = \cdot(k_1^S + i\, k_2^S)$ are

$$k_s = \begin{cases} + k_s & \text{if } k_2^S < 0 \text{ or if } k_2^S = 0 \text{ and } \{\bar{v}\}_s = \{\tilde{v}\}_s \\ - k_s & \text{if } k_2^S > 0 \text{ or if } k_2^S = 0 \text{ and } \{\bar{v}\}_s = -\{\tilde{v}\}_s \end{cases} \qquad (6.40)$$

The displacements in the layered region, when expanded into waves corresponding to the selected wave numbers $k_s$, are

$$\{\delta\} = \sum_{s=1}^{2n} \{v\}_s \exp(i\omega t - ik_s x)\, \alpha_s \qquad (6.41)$$

and the displacements $u_j$, $j=1, \ldots, 2n$, of the nodal points at the boundary $x=0$ are, omitting the time factor $\exp(i\omega t)$,

$$\{u\}^R = \sum_{s=1}^{2n} \{v\}_s\, \alpha_s = [V]\{\alpha\} \qquad (6.42)$$

in which the vectors $\{u\}^R$ and $\{\alpha\}$ are of equal dimension, $2n$, and contain the elements $u_j$ and $\alpha_s$, respectively. The matrix $[V]$ is the $2n \times 2n$ modal matrix containing the mode shapes $\{v\}_s$ columnwise. The inversion of Eq. (6.42) yields the mode participation factors in terms of the nodal displacements, i.e.

$$\{\alpha\} = [V]^{-1}\{u\}^R \qquad (6.43)$$

The normal stress $\sigma_x$ and the shear stress $\tau_{xz}$ at the boundary $x=0$ are by Eqs.(6.16) and (6.41) for $z_j < z < z_{j+1}$

$$\sigma_x = \sum_{s=1}^{2n} \left[ -ik_s(\lambda_j + 2G_j)[(z_{j+1}-z)/h_j \cdot v_{2j-1}^s + (z-z_j)/h_j \cdot v_{2j+1}^s] \right. $$
$$\left. + \lambda_j/h_j \cdot (-v_{2j}^s + v_{2j+2}^s) \right] \alpha_s \qquad (6.44a)$$

and

$$\tau_{xz} = \sum_{s=1}^{2n} G_j/h_j \cdot \left[ (-v_{2j-1}^s + v_{2j+1}^s) - ik_s[(z_{j+1}-z) v_{2j}^s + (z-z_j) v_{2j+2}^s] \right] \alpha_s$$

$$(6.44b)$$

in which $v_j^s$ is the jth element of $\{v\}_s$. The time factor $\exp(i\omega t)$ is implied.

The nodal forces which are in equilibrium with these stresses and act on the region $x>0$ as shown in Fig. 15b are

$$\begin{Bmatrix} P'_{2j-1} \\ P'_{2j} \\ P''_{2j+1} \\ P''_{2j+2} \end{Bmatrix} = \sum_{s=1}^{2n} (i[A]_j k_s + [D]_j) \begin{Bmatrix} v^s_{2j-1} \\ v^s_{2j} \\ v^s_{2j+1} \\ v^s_{2j+2} \end{Bmatrix} \alpha_s \qquad (6.45)$$

in which $[A]_j$ and $[D]_j$ are the layer matrices defined by Eq. (6.22). The total forces, $P_j$, acting on the layered region each consist of the force components from the layer above and below the respective nodal point, i.e.

$$P_j = P'_j + P''_j \qquad\qquad j=1, \ldots. 2n \qquad (6.46)$$

with $P''_1 = P''_2 = 0$. Expressed in matrix notation they are

$$\{P\}^R = (i[A][V][K] + [D][V])\{\alpha\} \qquad (6.47)$$

in which $\{P\}^R$ is the vector containing the elements $P_j$, $j=1, \ldots, 2n$, and $[K]$ is the diagonal matrix containing the wave numbers $k_s$, $s=1, \ldots, 2n$.

Substitution of Eq. (6.43) into Eq. (6.47) gives

$$\{P\}^R = [R]\{u\}^R \qquad (6.48)$$

in which

$$[R] = i[A][V][K][V]^{-1} + [D] \qquad (6.49)$$

The 2n x 2n matrix $[R]$ is the dynamic stiffness matrix of the semi-infinite layered region R. It relates the nodal forces to the simultaneous nodal displacement at the boundary $x=0$.

Matrix $[R]$ is symmetric, as it should be, according to the theorem of reciprocity [14]. Because the symmetry is not apparent from Eq. (6.49) it is proved below.

The analysis of a left layered region I. shown in Fig. 4 is analogous to that of a right layered region R. The only difference between a left

64

and a similar right layered region is due to their positions with respect to the global coordinate system. Thus the dynamic stiffness matrix, [L], of a left layered region may be computed from the right hand side of Eq. (6.49) by changing only the sign on all the coefficients that relate horizontal forces to vertical displacements or vertical forces to horizontal displacements.

## Proof that [R] is Symmetric

Eqs. (6.49) and (6.25) yield

$$[R]^T - [R] = i[V]^{-T}[K][V]^T[A] + [D]^T - i[A][V][K][V]^{-1} - [D]$$

$$= i[V]^{-T}[X][V]^{-1} \tag{6.50}$$

in which

$$[X] = [K][V]^T[A][V] - [V]^T[A][V][K] - i[V]^T[B][V] \tag{6.51}$$

In order to show that each element $x_{rs}$ of [X] vanishes, two solutions to Eq. (6.26) are considered, i.e.

$$([A]k_s^2 + i[B]k_s + [C])\{v\}_s = \{0\} \tag{6.52a}$$

and

$$([A]k_r^2 + i[B]k_r + [C])\{v\}_r = \{0\} \tag{6.52b}$$

Pre-multiplying the first equation by $\{v\}_r^T$ and the second by $\{v\}_s^T$, then subtracting the transposed second equation from the first yields

$$\{v\}_r^T \left( [A](k_s^2 - k_r^2) + i[B](k_s + k_r) \right)\{v\}_s = 0 \tag{6.53}$$

Since $(k_s + k_r) \neq 0$ for any two k of matrix [K], Eq. (6.53) gives

$$\{v\}_r^T \left( [A](k_r - k_s) - i[B] \right)\{v\}_s = 0 \tag{6.54}$$

The left hand side of Eq. (6.54) is identical to element $x_{rs}$. Hence, it is shown that

$$[R] = [R]^T \tag{6.55}$$

## 6.4 Energy Transmission

The energy transmission from the irregular region to the layered region at the boundary $x=0$, shown in Fig. 12, is by Eqs. (4.54), (6.42) and (6.47)

$$E = \frac{\omega}{2} \text{Im} (\{u\}^*\{P\}) = \frac{i\omega}{4} (\{P\}^*\{u\} - \{u\}^*\{P\})$$

$$= i\frac{\omega}{4}\{\alpha\}^*\left(-i[K]^*[V]^*[A]^*[V] + [V]^*[D]^*[V]\right.$$

$$\left.-i[V]^*[A][V][K] - [V]^*[D][V]\right)\{\alpha\} \qquad (6.56)$$

in which $^*$ indicates the conjugate transposed.

In the undamped case, when $[A]$ and $[D]$ are real, Eq. (6.56) can be simplified to

$$E = \frac{\omega}{4}\{\alpha\}^*([K]^*[V]^*[A][V] + [V]^*[A][V][K] + i[V]^*[B][V])\{\alpha\} \quad (6.57)$$

because $[B] = [D]^T - [D]$ by Eq. (6.25), and Eq. (6.57) can be further reduced when the orthogonality relation

$$\{v\}_r^*[A]\{v\}_s(\bar{k}_r + k_s) + i\{v\}_r^*[B]\{v\}_s = 0 \quad \text{for } k_r \neq k_s \qquad (6.58)$$

is observed, in which $\bar{k}_r$ is the conjugate of $k_r$. The result obtained is

$$E = \sum_{s=1}^{2n} E_s \qquad (6.59)$$

in which

$$E_s = \frac{\omega}{4}|\alpha_s|^2\{v\}_s^*([A](\bar{k}_s + k_s) + i[B])\{v\}_s \qquad (6.60)$$

is the energy transmitted by the $s$th mode. Hence, in the absence of viscous damping, the generalized Rayleigh waves are orthogonal with respect to energy transmission as were the generalized Love waves.

In order to prove Eq. (6.58) two solutions to Eq. (6.26) are considered, i.e.

$$([A]k_s^2 + i[B]k_s + [C])\{v\}_s = \{0\} \qquad (6.61a)$$

and

$$([A]k_r^2 + i[B]k_r + [C])\{v\}_r = \{0\} \qquad (6.61b)$$

Pre-multiplying the first equation by $\{v\}_r^*$, the second by $\{v\}_s^*$, then subtracting the conjugate transposed of the second equation from the first yields

$$\{v\}_r^* \Big([A](k_s^2 - \bar{k}_r^2) + i[B](k_s - \bar{k}_r)\Big)\{v\}_s = 0 \tag{6.62}$$

Division by $(k_s - \bar{k}_r)$, provided $k_s \neq \bar{k}_r$, proves Eq. (6.58).

In evaluating Eq. (6.60) for the wave types discussed in Section 6.2 it is of assistance to consider the conditions under which the wave number k is complex, real or imaginary in the undamped case. Pre-multiplying Eq. (6.26) with $\{v\}^*$ and introducing the abbreviations

$$A = \{v\}^*[A]\{v\} \; ; \quad B = -i\{v\}^*[B]\{v\} \; ; \quad C = \{v\}^*[C]\{v\} \tag{6.63}$$

gives the quadratic equation

$$A k^2 - B k + C = 0 \tag{6.64}$$

which has the solutions

$$k_{1,2} = \Big(B \pm \sqrt{B^2 - 4AC}\Big)/(2A) \tag{6.65}$$

As [A] and [C] are real symmetric and [B] is real skew symmetric, the numbers A, B and C are real, A being positive, because matrix [A] is positive definite. With the above abbreviations, Eq. (6.60) can be written

$$E_s = \frac{\omega}{4} |\alpha_s|^2 \Big((k_s + \bar{k}_s) A - B\Big) \tag{6.66}$$

The results obtained from Eqs. (6.65) and (6.66) are:

a) $k_s$ is complex if $B \neq 0$ and $B^2 - 4AC < 0$ and from $k_s + \bar{k}_s = B/A$ it follows that

$$E_s = 0$$

b) $k_s$ is imaginary if $B = 0$ and $C > 0$ and from $k_s + \bar{k}_s = 0$ it follows that

$$E_s = 0$$

c) $k_s$ is real if $B^2 - 4AC > 0$ and from $(k_s + \bar{k}_s) = 2k_s$ and Eq. (6.66) it follows that

$$E_s = \frac{\omega}{4} |\alpha_s|^2 (Ak_s - C/k_s) = \frac{\omega}{4} |\alpha_s|^2 \{v\}_s^* ([A]k_s - [C]/k_s)\{v\}_s \tag{6.67}$$

67

In Section 6.2 it was shown that the horizontal and vertical displacements of $\{v\}_s$ are 90° out of phase if $k_s$ is real and that in this case $\{\bar{v}\}_s = \pm\{\tilde{v}\}_s$ after normalization by Eq. (6.33). Eqs. (6.67) and (6.38) therefore yield

$$E_s = \begin{cases} +\dfrac{\omega}{2} k_s \left|\alpha_s\right|^2 & \text{if} \quad \{\bar{v}\}_s = + \{\tilde{v}\} \\[3mm] -\dfrac{\omega}{2} k_s \left|\alpha_s\right|^2 & \text{if} \quad \{\bar{v}\}_s = - \{\tilde{v}\} \end{cases} \qquad (6.68)$$

which is of the same form as the corresponding expression for the energy transmission of Love waves, Eq. (4.58).

68

# 7. AXISYMMETRIC RAYLEIGH WAVE MOTION

## 7.1 Motion in the Layered Region

The analysis of axisymmetric Rayleigh wave motion in a layered region of the type shown in Fig. 5 is similar to that for plane Rayleigh wave motion presented in Chapter 6.

Any point $(r,z)$ in the region undergoes displacements in the radial direction, $r$, and in the vertical direction, $z$. For harmonic motion at the frequency $\omega$ the displacements can be expressed by

$$\delta_r(r,z,t) = q_r(r,z,\ \exp(i\omega t) \tag{7.1a}$$

and

$$\delta_z(r,z,t) = q_z(r,z)\ \exp(i\omega t) \tag{7.1b}$$

The governing homogeneous differential equations for the spatial part of the displacements are, by Eq. (3.16), for the jth layer

$$(\lambda_j + 2G_j)\left(\frac{\partial^2 q_r}{\partial r^2} + \frac{1}{r}\frac{\partial q_r}{\partial r} - \frac{q_r}{r^2} + \frac{\partial^2 q_z}{\partial z \partial r}\right) + G_j\left(\frac{\partial^2 q_r}{\partial z^2} - \frac{\partial^2 q_z}{\partial z \partial r}\right)$$
$$+ \rho_j \omega^2 q_r = 0 \tag{7.2a}$$

and

$$(\lambda_j + 2G_j)\left(\frac{\partial^2 q_r}{\partial z \partial r} + \frac{1}{r}\frac{\partial q_r}{\partial z} + \frac{\partial^2 q_z}{\partial z^2}\right) + G_j\left(\frac{\partial^2 q_z}{\partial r^2} + \frac{1}{r}\frac{\partial q_z}{\partial r} - \frac{\partial q_r}{\partial z \partial r} - \frac{1}{r}\frac{\partial q_r}{\partial z}\right)$$
$$+ \rho_j \omega^2 q_z = 0 \tag{7.2b}$$

Separation of the variables $r$ and $z$ leads to a particular solution to Eqs. (7.2) of the form

$$q_r(r,z) = u(z)\ H_1^{(2)}(kr) \tag{7.3a}$$

$$q_z(r,z) = w(z)\ i\ H_0^{(2)}(kr) \tag{7.3b}$$

in which $H_0^{(2)}$ and $H_1^{(2)}$ are the Hankel functions which were introduced in

69

Chapter 5. The functions $u(z)$ and $w(z)$ are unknown functions which must satisfy the coupled ordinary differential equations for $j=1, \ldots, n$

$$\{k^2(\lambda_j + 2G_j) - \omega^2 \rho_j\} u - G_j \frac{d^2 u}{dz^2} + ik(\lambda_j + G_j) \frac{dw}{dz} = 0 \qquad (7.4a)$$

$$\{k^2 G_j - \omega^2 \rho_j\} w - (\lambda_j + 2G_j) \frac{d^2 w}{dz^2} + ik(\lambda_j + G_j) \frac{du}{dz} = 0 \qquad (7.4b)$$

Eqs. (7.3) and (7.4) are easily verified by substituting Eqs. (7.3) into Eqs. (7.2) and observing Eqs. (5.8). Eqs. (7.4) are identical to the corresponding equations for plane Rayleigh waves, Eqs. (6.4).

The boundary conditions at the horizontal planes $z_j$, $j=1, \ldots, n+1$, are

$$u(z_j') = u(z_j'') \quad ; \quad w(z_j') = w(z_j'') \qquad j=2, \ldots, n$$
$$u(z_{n+1}) = 0 \quad ; \quad w(z_{n+1}) = 0 \qquad (7.5)$$

and

$$\sigma_z(z_1'') = 0 \quad ; \quad \tau_{zr}(z_1'') = 0$$
$$\sigma_z(z_j') = \sigma_z(z_j'') \quad ; \quad \tau_{zr}(z_j') = \tau_{zr}(z_j'') \qquad j=2, \ldots, n \qquad (7.6)$$

When the stress displacement relations

$$\sigma_z = (\lambda + 2G) \frac{\partial \delta_z}{\partial z} + \lambda \left( \frac{\partial \delta_r}{\partial r} + \frac{\delta_r}{r} \right)$$
$$= \left( (\lambda + 2G) \frac{dw}{dz} - k \lambda u \right) i H_0^{(2)}(kr) \exp(i\omega t) \qquad (7.7a)$$

and

$$\tau_{zr} = G \left( \frac{\partial \delta_r}{\partial z} + \frac{\partial \delta_z}{\partial r} \right)$$
$$= G \left( \frac{du}{dz} - ikw \right) H_1^{(2)}(kr) \exp(i\omega t) \qquad (7.7b)$$

are substituted into Eq. (7.6), these boundary conditions reduce to those of the plane case, Eq. (6.9).

As the differential equations, Eqs. (6.4) or (7.4), and the boundary conditions, Eq. (6.9), are identical for plane and axisymmetric Rayleigh waves, the resulting eigenvalue problem and its solutions are the same in both the plane and axisymmetric case. This holds not only for

70

the continuum theory but also for the discrete theory, because the layered region is discretized in the axisymmetric case in the same manner as in the plane case.

It is again assumed that $u(z)$ and $w(z)$ vary linearly within each layer according to Eq. (6.14). The displacements in the layered region can then be defined by the displacements of the layer interfaces which are collected in the vector $\{\delta\}$, i.e.

$$\{\delta\}^T = <\delta_{r1} \ \delta_{z1} \ \delta_{r2} \ \delta_{z2} \ \cdots \ \delta_{rn} \ \delta_{zn}> \tag{7.8}$$

in which $\delta_{rj}$ and $\delta_{zj}$ are the radial and the vertical displacements of the interfaces.

The displacements may be expressed as a linear combination of the $2n$ modes that propagate or decay in the positive r-direction, i.e.

$$\{\delta\} = \sum_{s=1}^{2n} \{\delta\}_s \ \alpha_s \tag{7.9}$$

in which $\alpha_s$ is the participation factor of the sth mode $\{\delta\}_s$.

The sth mode $\{\delta\}_s$ is obtained from the sth solution to Eq. (6.26) i.e. from $\{v\}_s$ and $k_s$, when Eqs. (7.3) are observed. The displacements of the sth mode are accordingly

$$\delta_j^s = v_j^s \ H_1^{(2)}(k_s r) \cdot \exp(i\omega t) \qquad j=1,3, \ \ldots, \ 2n-1 \tag{7.10a}$$

and

$$\delta_j^s = v_j^s i H_0^{(2)}(k_s r) \cdot \exp(i\omega t) \qquad j=2,4, \ \ldots, \ 2n \tag{7.10b}$$

The $2n$ modes used in the expansion, Eq. (7.9), are selected according to the rules of Eq. (6.40) which were derived for the plane case. From the properties of the Hankel functions and from the similarity of axisymmetric waves to plane waves at large values of $|k_s r|$ it follows that these rules also hold for the axisymmetric case.

## 7.2 Dynamic Stiffness Matrix for Layered Region

The displacements at the cylindrical boundary, $r=r_o$, between the irregular and the layered region are, if the time factor $\exp(i\omega t)$ is omitted,

$$\{u\}^R = [\Phi]\{\alpha\} \tag{7.11}$$

in which the vector $\{u\}^R$ contains the displacements of the layer interfaces at $r=r_o$, i.e. $u_j$, $j=1, \ldots, 2n$, and the vector $\{\alpha\}$ contains the mode participation factors $\alpha_s$, $s=1, \ldots, 2n$. The $2n \times 2n$ matrix $[\Phi]$ contains the vectors $\{\phi\}_s$, $s=1, \ldots, 2n$, columnwise. The elements of $\{\phi\}_s$ are by Eq. (7.10)

$$\phi_j^s = v_j^s a_s \qquad j=1,3, \ldots, 2n-1 \tag{7.12a}$$

and

$$\phi_j^s = v_j^s b_s \qquad j=2,4, \ldots, 2n \tag{7.12b}$$

with

$$a_s = H_1^{(2)}(k_s r_o) \quad \text{and} \quad b_s = i\, H_0^{(2)}(k_s r_o) \tag{7.13}$$

The inversion of Eq. (7.11), i.e.

$$\{\alpha\} = [\Phi]^{-1}\{u\}^R \tag{7.14}$$

yields the mode participation factors if the boundary displacements are known.

The stresses at the boundary $r=r_o$ are

$$\sigma_x = (\lambda + 2G)\frac{\partial \delta_r}{\partial r} + \lambda\left(\frac{\partial \delta_z}{\partial z} + \frac{\delta_r}{r}\right) \tag{7.15a}$$

and

$$\tau_{rz} = G\left(\frac{\partial \delta_r}{\partial z} + \frac{\partial \delta_z}{\partial r}\right) \tag{7.15b}$$

According to Eqs. (7.3) and (7.9) the stresses are, for $z_j < z < z_{j+1}$,

$$\sigma_x = \sum_{s=1}^{2n} \left([-ik_s(\lambda_j + 2G_j)\, u_s(z) + \lambda_j\, \frac{d}{dz} w_s(z)]b_s - 2G_j/r_o \cdot u_s(z)a_s\right)\alpha_s$$

$$\tag{7.16a}$$

and

$$\tau_{rz} = \sum_{s=1}^{2n} G_j \left( \frac{d}{dz} u_s(z) - ik_s w_s(z) \right) a_s \alpha_s \qquad (7.16b)$$

in which

$$u_s(z) = (z_{j+1} - z)/h_j \cdot v^s_{2j-1} + (z-z_j)/h_j \cdot v^s_{2j+1} \qquad (7.17a)$$

and

$$w_s(z) = (z_{j+1} - z)/h_j \cdot v^s_{2j} + (z-z_j)/h_j \cdot v^s_{2j+2} \qquad (7.17b)$$

The nodal forces which are in equilibrium with the stresses on a segment of unit radian are

$$\begin{Bmatrix} P'_{2j-1} \\ P'_{2j} \\ P''_{2j+1} \\ P''_{2j+2} \end{Bmatrix} = \sum_{s=1}^{2n} ik_s r_o [A]_j \begin{Bmatrix} v^s_{2j-1} \cdot b_s \\ v^s_{2j} \cdot a_s \\ v^s_{2j+1} \cdot b_s \\ v^s_{2j+2} \cdot a_s \end{Bmatrix} \alpha_s + \sum_{s=1}^{2n} r_o ([D]_j + [E]_j) \begin{Bmatrix} \phi^s_{2j-1} \\ \phi^s_{2j} \\ \phi^s_{2j+1} \\ \phi^s_{2j+2} \end{Bmatrix} \alpha_s$$

$$(7.18)$$

in which the layer matrices $[A]_j$ and $[D]_j$ are those defined by Eqs. (6.22) and layer matrix $[E]_j$ is

$$[E]_j = \frac{1}{3} \frac{G_j}{r_o} \begin{bmatrix} 2 & 0 & 1 & 0 \\ 0 & 0 & 0 & 0 \\ 1 & 0 & 2 & 0 \\ 0 & 0 & 0 & 0 \end{bmatrix} \qquad (7.19)$$

The total forces acting on the layered region $r > r_o$ at the boundary nodal joints each consist of the force contributions from the layer above and below the respective nodal joint, i.e.

$$P_j = P'_j + P''_j \qquad\qquad j=1, \ldots, 2n \qquad (7.20)$$

with $P'_1 = P''_2 = 0$. The forces expressed in matrix notation are

$$\{P\}^R = r_o \left( i[A][\Psi][K] + [D][\Phi] + [E][\Phi] \right)\{ \iota\} \qquad (7.21)$$

73

in which the vector $\{P\}^R$ contains the nodal forces $P_j$, $j=1, \ldots, 2n$.
Matrices [A], [K] and [D] were defined in Chapter 6. Matrix [E] is
assembled by addition of the layer matrices $[E]_j$ as shown in Fig. 14
by substituting $[E]_j$ for $[X]_j$. Matrix $[\Psi]$ consist of the column vectors
$\{\psi\}_s$, $s=1, \ldots, 2n$, which have the elements

$$\psi_j^s = v_j^s \, b_s \qquad\qquad j=1, 3, \ldots, 2n-1 \qquad (7.22a)$$

and

$$\psi_j^s = v_j^s \, a_s \qquad\qquad j=2, 4, \ldots, 2n \qquad (7.22b)$$

Substitution of Eq. (7.14) into Eq. (7.21) gives

$$\{P\}^R = [R]\{u\}^R \qquad\qquad (7.23)$$

in which [R] is the dynamic stiffness matrix for the semi-infinite
layered region R, i.e.

$$[R] = r_o(i[A][\Psi][K][\Phi]^{-1} + [D] + [E]) \qquad\qquad (7.24)$$

which relates the nodal forces per radian to the simultaneous nodal dis-
placements at the boundary $r=r_c$. The matrix [R] has properties similar
to those of the dynamic stiffness matrix for the plane case; in parti-
cular, matrix [R] is symmetric in accordance with the theorem of
reciprocity [14]. This may be shown by a proof similar to that presented
for the plane case in Section 6.3.

# 8.  SUMMARY OF PROCEDURE

The theory for the proposed method of analysis is now completed and the steps involved in analyzing plane or axisymmetric systems of the type shown in Figs. 4 and 5 are summarized below.

I.  Idealization

1.  Subdivide the layered regions R and L into sublayers so that the thickness of each sublayer is less than about 1/10 of the length of S-waves travelling in it at the frequencies considered.

2.  Cover the irregular region I by a finite element mesh and specify the coordinates and reference numbers of the nodal joints.  The nodal joints at the boundaries between the irregular region and the layered regions must coincide with the interfaces of the sublayers, see Fig. 6.  The maximum dimension of each element should again be less than 1/10 of the length of S-waves and perhaps smaller near stress concentrations.

3.  Define the material properties of the finite elements and sublayers.  Viscous damping is included by the use of complex moduli.

4.  Define the prescribed nodal displacements and the external forces acting on nodal joints of Region I and specify the frequency of the harmonic loading.

II. Dynamic Stiffness Matrix for Layered Regions

1.  Formulate the eigenvalue problem for region R, i.e.  Eqs. (4.31) and (6.26) in the Love and Rayleigh wave cases, respectively.

2.  Solve the eigenvalue problem by the methods outlined in Appendix 1 and 2.

3. Form the dynamic stiffness matrix [R] for region R according to Eqs. (4.47), (5.28), (6.49) and (7.24) in the plane and axisymmetric Love and Rayleigh wave cases, respectively.

4. In the plane cases, perform steps 1., 2. and 3. in a similar manner to obtain the dynamic stiffness matrix [L] for region L.

III. Analysis of Irregular Region

1. Form element mass and stiffness matrices [M'] and [K']. Use complex moduli to include viscous damping in [K'].

2. Assemble the global matrix $[A] = [K] - \omega^2 [M]$ by the direct stiffness method from the element matrices of region I and the frequency dependent dynamic stiffness matrices [R] and [L] for the layered regions.

3. Compute the nodal displacements by solving Eq. (3.27). The amplitudes and phase angles of the nodal displacements are determined by Eqs. (3.5) and (3.6). Reaction forces may be computed by Eq. (3.31).

IV. Displacements in Layered Regions

1. Compute mode participation factors for region R by Eqs. (4.37), (5.19), (6.43) and (7.14) in the plane ⌐ axisymmetric Love and Rayleigh wave cases, respectively.

2 Compute displacements of the sublayer interfaces in region R by Eqs. (4.41), (5.17), (6.41) or (7.9).

3. In the plane cases, perform steps 1. and 2. for region L.

Computer programs which accomplish steps II, III and IV of the above procedure for systems of the type shown in Figs. 4 and 5 have been developed. The major part of the computation required is performed in complex variables utilizing the complex arithmetic capabilities of FORTRAN IV. Results from the analysis of several examples are presented in the following chapters.

# 9. LINE LOADS ON HOMOGENEOUS LAYER

The accuracy of the presented method is studied by application to the following problem. A harmonic line load of unit amplitude acts on the surface of a homogeneous layer of unit thickness as shown in Fig. 16. The layer material has a unit mass density and a Poisson's ratio $\nu=0.3$. If no material damping is assumed, the shear modulus $G=1$ unit, and if a fraction of critical damping $\beta=0.05$ is chosen, the stress-strain behavior is represented by the complex shear modulus $G=(1 + i2\beta)$ units.

## 9.1 Love Wave Case

Fig. 16 shows a line load, $P=1 \cdot \exp(i\omega t)$ per unit length, which acts in the direction perpendicular to the specified x-z-plane and thus generates plane generalized Love waves. The correct solution to this problem, labelled E, is derived in Appendix 3 and serves to check the numerical solutions which are computed by the presented method for three different discrete models. Each of these models makes use of the symmetry of the problem about the z-axis.

Model A, shown in Fig. 17, consists of a region I with 18 x 18 rectangular finite elements and a region R with 18 sublayers. The finite element mesh is condensed near the line load and the maximum mesh size is 1/15 of the wave length of shear waves at the highest frequency considered ($\omega = 2\pi$).

Model B contains no finite element region; the layered region R extends from x=0 to infinity and consists of 18 sublayers as does region R in Model A.

Model C is obtained from Model B by dividing each sublayer into two sublayers of equal thickness resulting in a total of 36 sublayers.

The solutions obtained from these models are referred to as solutions A, B, and C respectively.

Displacements for the static case, $\omega=0$, and displacement amplitudes for harmonic motion with and without material damping at the frequency

77

$\omega=2\pi$ are shown in Table 1 for several points. The phase shifts of the displacements with respect to the phase of the line load are presented in Table 2.

Table 1 and Table 2 show that the solutions A and B are about equally close to the correct solutions, E, and satisfactorily accurate in the neighborhood of the line load and at some distance from it. The solution C is significantly better than the solution B because the sublayers in Model C are only half as thick as in Model B.

The errors in the displacements, displacement amplitudes and phase shifts of the solution C are almost precisely four times smaller than the errors of the solution B. This is true for all the values presented in Table 1 and Table 2 and is therefore a strong indication that the errors, if they are small, are essentially proportional to $1/h^2$ where h is the thickness of a sublayer.

This observation can be utilized to obtain a much improved solution, called D, from the solutions B and C by adding one third of the difference between the solutions C and B to the solution C. Values of the solution D are also listed in Table 1 and Table 2. They have one or two more correct digits than the values of solution C and agree very well with the values of the correct solution.

The approximate solutions for the layered regions consist of finite series of approximate wave modes, Eq. (4.41), while the correct solutions are infinite series of exact wave modes, Eq. (A3.13). Some wave numbers of corresponding approximate and exact modes are listed in Table 3, in which the letters B, C, D, and E indicate, as before, the respective models and solutions.

The values C, obtained with 36 layers, are again almost exactly four times closer to the correct values E than the values B obtained with 18 layers. The very precise values D are computed by adding one third of the difference between the values C and B to the values C.

One may recall that the displacements of the sth wave mode are $\delta_s(x,z,t) = v_s(z) \exp(i\omega t - ik_s x)$. In the undamped case, $\beta=0$, the wave numbers $k_s$ are either real or imaginary and correspond to waves which propagate with constant amplitude or decay exponentially in the x-direction. The rapidly decaying waves, which have a wave number with a large negative imaginary part, contribute significantly to the total displacements only at small values of x, i.e. close to the line load.

At some distance from the line load only the propagating modes are important.

When damping is introduced, as in the case $\beta=0.05$, all waves propagate and attenuate in the x-direction because all wave numbers are complex. However, the exponential decay is relatively small for the waves which would propagate with constant amplitude in the undamped case and the wave lengths of the modes which would decay exponentially in the undamped case are relatively long, as the real parts of their wave numbers are small.

## 9.2   Rayleigh Wave Case

The case in which the harmonic line load $P=1 \cdot \exp(i\omega t)$ per unit length is applied at $x=z=0$ and acts in the z-direction, rather than in the y-direction as shown in Fig. 16, is now considered. Generalized plane Rayleigh waves are generated by the force.

The correct solution to this problem is not known and cannot be found easily. Approximate solutions are obtained for the discrete models A, B, and C described in the Love wave case. Their values for displacements, displacement amplitudes and phase shifts are shown in Table 5 and Table 6 for several points.

The agreement between the solutions A, B, and C is about as good as in the Love wave case. It shows that the numerical results change only very slightly as the left boundary of the layered region R is moved from $x=1$ (Model A) to $x=0$ (Model B) and as the discretization of the region R is refined by reducing the thickness of the sublayers (Model C). The solutions differ significantly only at points very close to the line load, see point ($x=0.01$, $z=0$). This must be expected, because the strain directly under the line load ($x=z=0$) is infinitively large in a linearly elastic continuum.

Some approximate wave numbers which were computed from Model B and C are compared with correct wave numbers in Table 4. The correct numbers are the roots of a difficult secular equation with transcendental terms [22]. They were computed iteratively by the secant method using as initial guess the wave numbers obtained from Model C.

The values C, obtained with 36 layers, are again almost exactly

79

four times closer to the correct values E than are the values B, obtained with 18 layers. As in the Love wave case, this indicates that the errors, if they are small, are essentially proportional to $1/h^2$ where h is the thickness of a sublayer.

The values D are computed by adding one third of the difference between the values C and B to the values C. This extrapolation improves the accuracy by one or two digits.

## 10. SCREENING EFFECT OF TRENCHES

Many attempts have been made to reduce ground-transmitted vibrations by the installation of wave barriers in the form of trenches or walls. Barkan [9] reviewed several installations and came to the conclusion that such barriers are often practically useless. He attributed the limited success to the absence of a rational design procedure for this type of installation. Recent experimental studies by Woods [52] and by Dolling [15] have greatly improved the understanding of the screening problem. But a rational design procedure which includes a sound analysis of the screening is still not available.

The method developed in this dissertation is capable of analyzing plane strain and axisymmetric screening problems. A relatively simple example is presented below in which the ground transmitted disturbance consists of plane generalized Love waves.

Figs. 18 and 19 show computed surface displacements near a strip footing embedded in a homogeneous linearly elastic soil layer over a rigid base. The footing is excited by a harmonic force $P = \omega^2 \cdot \cos\omega t$ per unit length. This type of loading is typical for foundations supporting rotatory machines.

The finite element mesh used in the analysis contained 450 rectangular elements and extended from the left edge of the footing to the right edge of the trench. The semi-infinite layered regions to the left and to the right of the finite element mesh were represented by 18 sublayers each.

Fig. 19 shows the effect of trench depth at the frequency $\omega = 1$. At this frequency a trench is quite effective in reducing the surface vibrations. Its effectiveness increases with increasing trench depth. A, perhaps, unexpected result is that the presence of the trench causes a reduction in the displacement amplitude of the footing. This reduction is due to reflections from the trench wall. However, the reflections might just as well cause an amplification of the footing

81

displacement depending on the frequency of the exciting force and on the distance between the footing and the trench. The curve labeled $\omega = 1.5$ in Fig. 18 illustrates this point.

Fig. 18 shows the effect of changing the frequency for the case in which the trench penetrates half way through the soil layer. At the lower frequencies $\omega = 0.5$ and $\omega = 1.0$ the trench is quite effective but as the frequency is increased to $\omega = 1.5$ the trench becomes useless. This phenomenon is associated with the number of propagating Love modes in the system. At frequencies below $\omega = \pi/8 \simeq .39$ no propagating modes exist and the displacement amplitudes in the far field, i.e. beyond the trench, decay exponentially according to Eq. (4.38b). In the frequency range 0.39 to 1.18 one propagating mode exists. Its mode shape, shown in Fig. 18, indicates that most of the energy is transmitted in the upper half of the layer. The trench is therefore quite effective in reflecting the Love wave. This is demonstrated by the curves labeled $\omega = 0.5$ and 1.0 in Fig. 18. As the frequency is increased into the range 1.18 to 1.96 a second propagating mode appears. Its mode shape, shown in Fig. 18, indicates that a significant part of the energy is transmitted below the bottom of the trench. Consequently, the trench is not an effective barrier for the second mode. This is illustrated by the curves labeled $\omega = 1.5$ in Fig. 18. At frequencies beyond $\omega = 1.96$ additional modes will appear and the displacement in the far field becomes more complicated.

## 11. TORSIONAL MOTION OF RIGID CIRCULAR FOOTINGS

### 11.1 Introduction

A rigid circular footing on an axisymmetric medium has four
distinct degrees of freedom; they are the vertical and horizontal trans-
lations and the rotations about a horizontal and a vertical axis. The
rotational motion about the vertical axis of symmetry, called torsional
motion, is of considerable importance to precision tracking radar towers
and communication antennas [47, 48].

Radar towers are often supported on spread footings of approximately
circular plan. The footings are stiff compared to the soil underneath
and may therefore be treated as rigid circular disks.

A solution for the harmonic torsional motion of a rigid circular
disk fixed to the surface of a homogeneous linearly elastic half space,
Fig. 1, was first obtained by Reissner and Sagoci [41]. Stallybras
[44] derived a solution to the same problem which is easier to evaluate
for high frequencies. Weissmann [47] considered the effect of material
damping and slippage between the footing and the surface of the half
space.

The assumption that the footing is supported by a homogeneous
half space is mathematically convenient and for practical purposes
suitable if the subsoil is homogeneous to a depth of a few footing
diameters. But this condition is not often encountered in practice.

Arnold et al. [6] obtained a solution for the torsional motion of
a rigid circular footing supported by an elastic layer which extends
laterally to infinity and is fixed at its bottom to a rigid base, see
Fig. 2. They assumed that the dynamic stress distribution under the
footing on a layer is similar to the static stress distribution under a
rigid footing on a half space. This assumption loses its validity as
the frequency of the motion increases and the thickness of the layer
decreases. Awojobi [ 8] treated the same problem by reducing it to the

solution of an integral equation without assuming a priori a stress distribution under the rigid footing. However, he substituted the kernel of the integral by an approximation for which he could find a closed form solution.

The half space solution based on the model in Fig. 1 and the layer solution based on the model in Fig. 2 are currently used in design practice. But as footings are always embedded in the ground and are usually supported by layered soil, the applicability of the half space and layer solutions is often questionable. No methods of analysis have been published so far which can quantitatively account for the effect of embedment and layering of the soil.

The method presented herein has the flexibility to analyze the response of footings embedded in layered soil. In the following examples the effect of the thickness of a homogeneous layer over a rigid base, the effect of damping, the effect of embedment and the effect of an increase in the shear modulus of the soil with depth are studied.

First, a few terms used in the presentation and the discussion of the examples have to be explained.

The harmonic torsional motion of a massless rigid footing is described by

$$\Theta = \frac{T_o}{k_\theta} F \exp(i\omega t) \qquad (11.1)$$

in which $\Theta$ is the angle of rotation about the axis, $T_o$ is the amplitude of the external torque on the footing, and $k_\theta$ is the static spring constant. The dimensionless complex quantity $F = F_1 + i\,F_2$, designated as the displacement function, depends on the circular frequency $\omega$ or on the dimensionless frequency ratio

$$a_o = \omega r_o/V_s \qquad (11.2)$$

in which $r_o$ is the radius of the footing and $V_s$ is the shear wave velocity in the soil.

If the displacement function $F$ for a footing without inertia is known one can calculate the response of a footing with the mass moment of inertia, $I_\theta$, about the axis of rotation, as shown by Lysmer and Richart [24], by

$$\Theta = \frac{T_o}{k_\theta} M \cos(\omega t + \phi) \tag{11.3}$$

in which M is the dynamic magnification factor

$$M = \sqrt{\frac{F_1^2 + F_2^2}{(1 - \omega^2 I_\theta F_1/k_\theta)^2 + (\omega^2 I_\theta F_2/k_\theta)^2}} \tag{11.4}$$

and $\phi$ is the phase shift

$$\phi = \tan^{-1} \frac{F_2}{F_1 - \omega^2 I_\theta (F_1^2 + F_2^2)/k_\theta} \tag{11.5}$$

It is often convenient to employ a dimensionless inertia ratio, which can be defined by [42]

$$B_\theta = \frac{I_\theta}{\rho r_o^5} \tag{11.6}$$

where $\rho$ is the mass density of the soil.

If the mass density and the shear wave velocity of the soil vary with depth, $\rho$ and $V_s$ in Eqs. (11.2) and (11.6) are the values of the density and the shear wave velocity at a designated reference depth. In all the following examples, in which soil properties vary with depth, this reference depth will be taken to be equal to one footing radius.

## 11.2 Comparison of Numerical Results with Analytical Solutions and Experimental Results

Arnold et al. [6] performed model tests to check their analytical solutions for the torsional motion of a rigid circular disk on an elastic layer against experimental results. They glued a disk to the surface of a sheet of foam rubber and forced the disk to vibrate in the torsional mode .

Fig. 20 shows their experimental and their analytical results for the following parameters. The ratio of the layer thickness to the disk radius is $H/r_o = 0.97$ and the inertia ratio of the disk is $B_\theta = 0.79$.

85

The analytical and experimental results agree well with respect to the resonance frequency and the general shape of the response curve; but they differ in the maximum amplitude.

Awojobi [8] also compared his analytical solution with Arnold's experimental results. The comparison, see Fig. 20, shows a good agreement in the ascending part of the response curve, but a difference of about 10 percent in the resonance frequency.

The same example was studied numerically by the finite element method with a fine mesh, which is shown in Fig. 21. The maximum dimension of the elements and the maximum thickness of the sublayers are less than 1/25 of the length of shear waves at the frequency ratio $a_o$ = 2.5. Numerical results are presented in Fig. 20 for an elastic material without damping, $\beta$ = 0%, and for a viscoelastic material with a fraction of critical damping $\beta$ = 7.5%. The numerical solution for the undamped material and Arnold's experimental results agree very well with respect to the resonance frequency and the general shape of the response curve. The deviation in the peak amplitude is apparently caused by the internal damping of the foam rubber. The numerical solution for $\beta$ = 7.5%, which takes the damping of the foam rubber into account, fits the experimental results exceptionally well throughout the given frequency range.

The small difference between Arnold's analytical solution and the finite element solution for $\beta$ = 0% can be attributed mainly to the deviation of the stress distribution assumed by Arnold et al. from the actual dynamic stress distribution under the rigid footing. The error resulting from the finite element discretization is expected be small because the chosen mesh is fine.

The computational time needed for the finite element analysis at one frequency was approximately 4 seconds on the CDC 6 computer.

11.3 Effect of Layer Thickness

Fig. 22 shows the displacement function F for the torsional motion of a massless footing on a homogeneous elastic layer without material

86

damping. The figure also shows the geometry of the vibrating system. The radius of the footing is $r_o$ and the thickness of the layer is H. Displacement functions are presented for the ratios $H/r_o = 1, 2, 4, 8,$ and $\infty$. The function for $H/r_o = \infty$ is the Reissner-Sagoci solution for the elastic half space [41].

Fig. 22 shows that the $F_2$-curves are zero for frequency ratios below certain values which can be computed from Eq. (A3.6). No Love waves can exist which propagate through the layer and no energy is dissipated away from the footing, if

$$a_o < \frac{\pi}{2} \frac{r_o}{H} \qquad (11.7)$$

or

$$\ell_s = 2\pi \, V_s/\omega = 2\pi \, r_o/a_o > 4H \qquad (11.8)$$

in which $\ell_s$ is the length of a shear wave and $V_s$ is the shear wave velocity. This means that there is no geometric or radiation damping, that the rotation of the footing is in phase with the applied torque, and that the $F_2$-curve is zero. In this range where $\ell_s > 4H$, the response of a footing with inertia can become infinitely large as the denominator in Eq. (11.4) may vanish, depending upon the moment of inertia of the footing and on the frequency.

The waviness of the displacement function Fig. 22 is caused by the change of wave modes from the decaying type to the propagating type as the frequency ratio increases, see Section 4.3. The change of the sth mode occurs at

$$a_o = \frac{2s-1}{2} \pi \frac{r_o}{H} \qquad (11.9)$$

according to Eq. (A3.6). The wave number $k_s$ of the sth mode vanishes at this $a_o$ value, while it is purely imaginary and purely real for smaller and for larger frequency ratios, respectively.

As pointed out in Section 5.2, the dynamic stiffness of a layer against torsional motion does not become singular if one of the wave numbers vanishes.

The displacement functions for small ratios $H/r_o$ differ significantly from the half space solution; the smaller $H/r_o$ the greater they differ. However, the displacement function for $H/r_o = 8$ shows good agreement with

87

the half space solution in the range $a_o < 2$, which is the range of interest for most footings.

The values of the static spring constants are also presented in Fig. 22. For $H/r_o > 2$ the static spring constant is close to that of a footing on a half space.

The discrete models used in the computation of the displacement functions were similar to the one shown in Fig. 21. The maximum mesh size was, in all cases, smaller than $1/12$ of the length of a shear wave. Values of the displacement functions were computed at frequency ratios in intervals of 0.2.

## 11.4 Effect of Embedment

It was shown in the previous example that a footing on a homogeneous elastic layer with a thickness of several footing radii responds to torsional excitation very much the same as does a footing on a homogeneous elastic half space.

The effect of embedment will be demonstrated for a footing on a thick layer, $H/r_o = 8$. The response curves for three different footings, each with inertia ratios $B_\theta = 2$ and $B_\theta = 4$, are shown in Fig. 23.

Footing 1 is placed on the surface of the layer. Footing 2 is embedded to a depth of $0.4 \times r_o$ and has a free periphery. Footing 3 is embedded to the same depth as Footing 2 but its periphery is in contact with the surrounding soil. No slippage occurs where the footings and the layer are in contact.

The static stiffness coefficients of Footing 1, 2 and 3 are $k_\theta = 5.34$, 7.04 and $11.9 \times G r_o^3$, respectively, where $G$ is the shear modulus and $r_o$ is the footing radius. This means that the static compliance is strongly reduced by the embedment of the footing and by side friction.

The above value for the static stiffness of Footing 3 agrees well with Kaldjian's [21] results for the torsional stiffness of embedded circular footings.

The reduction of the static compliance causes the resonance

88

frequency to increase and, as the amount of geometric or radiation
damping grows with frequency, this results in an increased damping of
the footing motion. The peak amplitude is therefore even further reduced
by embedment of the footing than is the static compliance.

A comparison of the response curves for the inertia ratios $B_\theta = 2$
and $B_\theta = 4$ shows that a decrease of the inertia ratio has a similar effect
on the footing response as have embedment and side friction.

The displacement functions from which the response curves in Fig.
23 were calculated by Eqs. (11.3), (11.4) and (11.6) are presented in
Fig. 24.

The $F_1$-curves are changed only insignificantly by embedment and
side friction. The $F_2$-curve for Footing 3 is somewhat higher than those
for Footing 1 and 2. This means that the radiation damping is increased
by embedment with side friction.

## 11.5 Shear Modulus Increasing with Depth

In the previous example it was assumed that the medium supporting
the footing was homogeneous with respect to the mass density and the
shear modulus. However, the elastic moduli of soils usually vary with
depth even though the mass density and other properties of the soil may
be fairly constant within the zone of interest.

The shear moduli of sands and gravels increase approximately as
the square root of the effective confining pressure [43] and therefore
with the depth below the surface. In the following examples, the relation
between the shear modulus and the depth is assumed, accordingly, to be

$$G(z) = G_o \sqrt{z/r_o} \qquad (11.10)$$

in which $z$ is the depth below the surface, $r_o$ is the footing radius and
$G_o$ is the shear modulus at $z = r_o$.

The confining pressure in the soil below the footing is decreased
by the load of the footing. To account for this fact in a very simple
manner it is assumed that the modulus under the footing, $r < r_o$, is

$$G(z) = G_o \sqrt{p} \quad \text{for } \gamma z < q \qquad (11.11)$$

89

in which $\gamma$ is the unit weight of the soil, $q$ is the average contact
pressure under the footing, and $p$ is the dimensionless load ratio de-
fined by

$$p = \frac{q}{\gamma r_o} \qquad (11.12)$$

Fig. 25 shows the assumed variation of the shear modulus with depth for
$r < r_o$ at $p=0.5$, 1 and 2 and for $r > r_o$.

Displacement functions for the torsional motion of three footings
without inertia are shown in Figs. 27, 28 and 29. One footing sits on
the surface of the ground, the other two are embedded in the soil to a
depth of $0.4 \times r_o$, one with and one without soil contact at their sides.
Each footing is supported by a thick soil layer over a rigid base,
$H/r_o = 8$. The shear modulus in the layer increases with depth according
to Fig. 25 and its value under the footing is determined by the parameter
$p$. Displacement functions for $p = 0.5$, 1.0 and 2.0 are presented and
for comparison the displacement functions for a homogeneous layer are
also shown in Figs. 27, 28 and 29.

The displacement functions for the layer, in which the shear
modulus increases with depth, differ somewhat from the displacement
functions for the homogeneous layer. The difference is pronounced in the
case where the footing sits on the surface of the layer, but is less
significant in the more practical cases of embedment either with or
without side friction.

The parameter $p$ has hardly any influence on the displacement
functions, but it affects the static spring constant $k_\theta$, values of which
are also presented in Figs. 27, 28 and 29 for the various cases.

11.6  Displacements in the Far Field

Displacement amplitudes versus depth at different distances from
the axis of symmetry and along the surface are shown for three particular
cases in Figs. 30-33. In Case A the footing sits on the surface of a
homogeneous layer; in Case B the footing is embedded in the same homo-
geneous layer; in Case C the footing is embedded in a layer in which

90

the shear modulus increases with depth as shown in Fig. 26 (p=1.18). In each case the thickness of the layer is equal to 18 footing radii, the material damping of the layers is $\beta$ = 3% of critical damping, and the footings are exc the at the frequency $\omega$ = 60$\pi$ so that the amplitudes of the footing rotation are one radian.

Figs. 30 and 31 show that the displacement amplitudes close to the axis (r=4$r_o$) are, as expected, much larger at the surface than at some depth. But the displacement amplitudes at greater distance from the axis (r=36$r_o$) do not decrease with depth. This can be explained by the fact that the generalized Love waves generated by the torsional vibrations of the footings are not surface waves, as are the Rayleigh waves, which have large amplitudes close to the surface and attenuate with depth, but consist of S-waves which are reflected at the free surface and the rigid base.

A comparison of Figs. 30 and 31 shows that for Case B the displacement amplitudes in the far field are almost exactly twice as large as for case A. The reason for this is that the torque applied through the footing to the layer is 2.04 times larger in Case B than in Case A. Since the wave length of S-waves, $\ell_s$, is large compared to the footing radius at the considered frequency, ($\ell_s$=8.6$r_o$), Saint-Venant's principle applies. A different distribution of the shear stresses around the footing has a negligible effect on the displacements at some distance from the footing if the applied total torque is the same. For high frequencies at which the length of S-waves is not long compared to the footing dimension, this is not true.

In Case C, Fig. 32, the displacement amplitudes attenuate with depth even at large distance from the axis of symmetry (r=36$r_o$), because the shear modulus increases with depth. Most of the energy is propagated through the softer part of the layer near the surface.

This is also the reason for the amplitudes of the surface displacements, Fig. 33, being much larger in Case C than in Case A or Case B.

## 12. VERTICAL MOTION OF RIGID CIRCULAR FOOTINGS

### 12.1 Introduction

The vertical motion of a rigid circular footing which is supported
by a homogeneous, linearly elastic half space, Fig. 1, and excited by a
harmonic vertical force was first studied by Reissner [39] in 1936, who
assumed, for simplicity, a uniform stress distribution under the footing.
Bycroft [10] investigated the same problem. He assumed that the dynamic
stress distribution beneath the rigid footing is similar to that for the
static case and obtained an approximate solution valid for low frequencies.
Lysmer [24] and Awojobi and Grootenhuis [7] derived solutions for the
same problem by accounting properly for the frequency dependence of the
stress distribution beneath the footing.

The application of the half space theory to the analysis of footing-
soil systems implies the assumption that the subsoil under the footing
is fairly homogeneous down to a depth of several footing diameters.
Often, this assumption cannot be justified, especially if large footings
are to be analyzed. Considerable deviations from the half space theory
occur in cases in which rock or hard layers are encountered at shallow
depth below the footing [29].

Warburton [46] studied the vertical vibration of a rigid circular
footing supported by a homogeneous elastic layer which extends infinitely
in the horizontal direction and rests on a rigid base, Fig. 2. He assumed
a frictionless interface between the layer and the rigid base and made
an approximation regarding the stress distribution beneath the footing.
Paul [38] studied the same problem without assuming a priori a stress
distribution beneath the footing. But he did not present a readily
useable solution and left the results in implicit form.

In each of the analytical half space and layer solutions referenced
above, it was assumed that the interface between the footing and the
supporting medium is frictionless.

92

Lysmer and Kuhlemeyer [25] used successfully a finite element method with an energy absorbing boundary (see Chapter 1) to study the effect of embedment on the vertical motion of a footing which is supported by a homogeneous elastic half space. Kuhlmeyer [22] used the same method to study the vertical motion of a footing supported by a stratified half space and found that the method gave inconclusive results when the deeper layers were stiffer than the surface layer, which is usually the case in foundation vibration problems.

In the following examples the vertical motion of rigid circular footings on the surface of a homogeneous layer and of those embedded in a layer in which the elastic moduli increase with depth are investigated by the method presented in this dissertation.

Before the examples can be discussed a few terms need to be explained. The harmonic vertical motion of a rigid, massless footing is described by

$$w = \frac{P_o}{k_z} \, F \, \exp(i\omega t) \tag{12.1}$$

in which $w$ is the vertical displacement of the footing, $P_o$ is the amplitude of the vertical force exciting the footing motion and $k_z$ is the static spring constant. The dimensionless complex quantity $F = F_1 + i \, F_2$ is the displacement function as before and depends on the circular frequency $\omega$ or the dimensionless frequency ratio $a_o$ defined by Eq. 11.2.

If the displacement function $F$ for a massless footing is known, one can calculate the response of a footing with the mass $m$, as shown by Lysmer and Richart [24], by

$$w = \frac{P_o}{k_z} \, M \, \cos(\omega t + \phi) \tag{12.2}$$

in which $M$ is the dynamic magnification factor

$$M = \sqrt{\frac{F_1^2 + F_2^2}{(1-\omega^2 m \, F_1/k_z)^2 + (\omega^2 m \, F_2/k_z)^2}} \tag{12.3}$$

and $\phi$ is the phase shift

93

$$\phi = \tan^{-1} \frac{F_2}{F_1 - \omega^2 m \, (F_1^2 + F_2^2)/k_z} \qquad (12.4)$$

A dimensionless mass ratio may be defined by

$$B_z = \frac{m}{\rho \, r^3} \cdot \frac{G \, r_o}{k_z} \qquad (12.5)$$

in which $\rho$ and $G$ are the mass density and the shear modulus of the soil, respectively, and $r_o$ is the footing radius.

## 12.2 Footing on Homogeneous Layer

The vertical motion of a rigid circular footing supported by a homogeneous layer, Fig. 2, is studied. The footing has the radius $r_o$ and is smooth at its interface with the layer, permitting free horizontal displacements of the layer surface beneath the footing. The layer has the thickness H and is welded to the rigid base. Poisson's ratio of the layer material is $\nu = 0.25$ and the complex shear modulus $G = (1 + i \, 2 \, \beta)$ units, where $\beta$ is the fraction of critical damping.

Displacement functions for the ratio of layer thickness to footing radius $H/r_o = 10$ and 6 are presented in Figs. 34 and 35 for different values of $\beta$. The curves for $H/r_o = 10$ and $H/r_o = 6$ look similar if the abscissas in Figs. 34 and 35 are scaled by the layer thicknesses. In the undamped case, $\beta = 0\%$, the displacement functions show singularities, but in the damped case, $\beta = 5\%$ or $10\%$, they are "smooth."

To explain the singularities in the undamped case it is best to look at the spectral lines of the wave numbers which characterizes the wave modes used in the displacement expansion according to Eq. (7.9).

The first five spectral lines are presented in Fig. 36 which shows a three-dimensional space. The axes in Fig. 36 are labeled $\xi = \mathrm{Re}(k) \cdot H$, $\eta = \mathrm{Im}(k) \cdot H$ and $\Omega = \omega H/V_S$ where H is the thickness of the layer. The long dashed lines lie in the $\xi$-$\Omega$- plane and represent real wave numbers. The short dashed lines lie in the $\eta$-$\Omega$- plane and represent imaginary wave numbers. The full lines are curves in the $\xi$-$\eta$-$\Omega$- space and occur in pairs which are symmetric about the $\eta$-$\Omega$- plane; each pair represents a

pair of complex wave numbers, $k = k_1-ik_2$ and $-\bar{k} = -k_1-ik_2$.

The spectral lines intersect the planes $\Omega=0$, $\xi=0$ and $\eta=0$ at right angles. This follows from the fact that the secular equation, Eq. 6.27, is an analytical function of $\omega^2$ and $k^2$ in the undamped case. A proof can be performed in a similar manner to that given by McNiven et al. [31] for the spectral lines of waves in axisymmetric rods and will therefore not be presented.

The points at which the spectral lines intersect the $\Omega$-axis define natural frequencies of the layer corresponding to vertically propagating waves which are reflected at the free surface and the rigid base resulting in a standing wave. At these frequencies the dsiplacements in the layer vary only with the depth z and any plane parallel to the surface remains plane during motion because k=0.

The natural frequencies labelled a, c and d in Fig. 36 are associated with pure S-waves producing only horizontal displacements. They can be computed by

$$\omega_n = \frac{2n-1}{2} \pi V_s/H. \qquad n=1,2, \ldots \qquad (12.6)$$

in which $V_s$ is the shear wave velocity. Because the waves corresponding to the points a, c and d have no displacement components in the vertical direction, they do not affect the vertical motion of the footing.

The natural frequencies labelled b and e in Fig. 36 are associated with pure P-waves producing only vertical displacements in the layer. The layer surface can move up and down at these frequencies without being excited by external forces, and since it remains plane the boundary conditions under the massless footing are identical to those of the free surface. Therefore, these frequencies are natural frequencies of the footing-layer system if the footing is massless. Consequently, the displacement functions for $\beta=0$ in Figs. 34 and 35 have singularities at the corresponding frequency ratios. The natural frequencies in question are

$$\omega_n = \frac{2n-1}{2} \pi V_p/H \qquad n=1,2, \ldots \qquad (12.7)$$

in which $V_p$ is the velocity of P-waves.

The first two natural frequencies for the vertical motion of the massless footing in the case $H/r_o = 10$ occur at $a_o = 0.272$ and $a_o = 0.816$.

95

Fig. 34 shows clearly the singularity at $a_o \approx 0.272$, but the singularity at $a_o \approx 0.816$ is hardly noticeable.

In Fig. 34 one observes another irregularity at $a_o \approx 0.746$ which corresponds to the frequency at g and g' in Fig. 36. At this frequency two wave modes exist in the layer which have equal and opposite phase velocities. The group velocity, which is

$$U = \frac{d\omega}{dk} \tag{12.8}$$

if k is real [16], vanishes at g and g'. The two wave modes have, therefore, zero group velocities at this frequency and do not transmit energy, because the rate of energy transmitted by a wave is the product of the group velocity and the energy density in the wave [17].

If the amplitudes of the two wave modes are equal, the modes combine to a standing wave and the horizontal and vertical displacements in the axisymmetric case vary along the free surface as

$$\delta_x \propto J_1 \ (kr) \ \exp(i\omega t) \tag{12.9a}$$

$$\delta_z \propto J_0 \ (kr) \ \exp(i\omega t) \tag{12.9b}$$

in which $J_0$ and $J_1$ are the Bessel functions of order zero and one, respectively. Eq. (12.9) follows from Eqs. (6.32, 7.1, 7.3) and from the properties of the Hankel functions [2].

$$H_0^{(2)}(kr) - H_0^{(2)}(-kr) = 2J_0 \ (kr) \tag{12.10a}$$

$$H_1^{(2)}(kr) + H_1^{(2)}(-kr) = 2J_1 \ (kr) \tag{12.10b}$$

Because the wave number corresponding to point g in Fig. 36 is relatively small, $kr_o \approx 0.208$ for $H/r_o = 10$, the free surface in the area $r < r_o$ remains approximately plane during vibration in these two modes. The difference in the vertical displacements at $r = r_o$ and $r = 0$ is only one percent. This means that the displacements of the free surface are almost compatible with those under the rigid massless footing. Therefore it takes only a small force to completely satisfy the boundary conditions under the footing and to produce a large footing displacement at this frequency. Consequently, the $F_1$-curve for $\beta = 0\%$ in Fig. 34 shows a peak at $a_o = 0.746$. The peak is finite in height; but it is difficult to

determine the height numerically, because the peak is very narrow.

The same phenomenon occurs at the frequency corresponding to the points f and f' in Fig. 36. But since this frequency is very close to the lowest natural frequency of the footing-layer system, no separate peak shows up in Fig. 34.

A similar phenomenon to that described above was observed experimentally in steel rods by Oliver [36] and studied theoretically by McNiven [30]. In the rods, very narrow and high response peaks occurred also at those frequencies at which pairs of complex spectral lines for wave numbers became purely real as happens at the points f and f' or g and g' in Fig. 36.

The effect of material damping on the response of footings is to smooth the displacement functions and eliminate natural frequencies. The displacement functions in Fig. 34 and 35 for $\beta=5\%$ and 10% of critical damping therefore show no singularities.

The spectral lines for the wave numbers in the damped case are not much different from those shown in Fig. 36 for the undamped case. But they do not intersect the $\xi$-$\Omega$- plane, as all wave numbers have negative, non-zero imaginary parts in the damped case, and they are smooth with continuous first derivatives at the frequencies at which the spectral lines form right angles in the undamped case.

It is more realistic to include some material damping in the analysis than to assume that the soil behaves purely elastically. Furthermore, the incorporation of damping has the advantage that singularities are avoided.

Response spectra for footings with different mass ratios are presented in Figs. 37 and 38 for $H/r_o = 6$ and $H/r_o = 10$ at $\beta=5\%$. They show peaks at frequencies close to the first natural frequencies of the corresponding undamped cases. The peaks are high for $H/r_o = 6$, but not very significant for $H/r_o = 10$.

Except for these peaks, the response spectra for $H/r_o = 10$ are quite similar to those for the vertical motion of a rigid circular footing on a homogeneous elastic half space, which are shown in Fig. 39 and are based on Lysmer's solution [24]. However, the response spectra for $H/r_o = 6$ differ markedly from those for the half space.

97

The values of the displacement functions in Figs. 34 and 35 were
computed by using rectangular meshes, which were similar to that shown
in Fig. 21 and consisted of 22 x 5 finite elements and 22 sublayers.
The maximum dimension of any element and the maximum thickness of any
layer was less than 1/10 of the length of shear waves at the highest
frequency considered.

To verify the validity of the theory and to check the computer
program, analyses for $H/r_o$ = 6 were repeated at several frequencies with
a different mesh, in which a much larger region, $r<6r_o$ as compared to
$r<r_c$, was represented by finite elements. The results obtained using
the two different meshes were virtually identical. The relative
differences between the computed values of the displacement functions
were less than one percent.

## 12.3  Footing Embedded in Inhomogeneous Layer

Fig. 40 shows an embedded rigid circular footing which is forced
to vibrate in the vertical mode. The shear modulus in the supporting
layer increases with depth as defined in Fig. 26. Poisson's ratio is
$\nu=1/3$ throughout the layer, and 3% of critical damping for shear and
dilatational deformations in the layer is assumed. The damping is
introduced by using a complex shear modulus (Fig. 26 shows only the real
part of the shear modulus). Since Poisson's ratio is real, Lame's
constant $\lambda=2G\nu/(1-2\nu)$ is also complex. The layer has a thickness of
18 footing radii and rests on a rough rigid base.

The displacement function for a massless footing and the response
spectrum for a footing with mass are presented in Fig. 40. The figure
indicates a small peak at a frequency close to that at which the layer,
in the absence of damping, would have its first natural frequency for
vertical displacements.

A comparison with the response spectra in Figs. 37 and 38 suggests
that the response peak in Fig. 40 is small because the layer is thick
with respect to the footing radius, $H/r_o$ = 18. Due to damping, the
displacement function shows no further peaks at the frequencies at

98

which the layer, in the absence of damping, would have higher natural frequencies.

Figs. 41 and 42 show displacement amplitudes along the surface of the layer and displacement amplitudes versus depth at various distances from the axis of the footing. The displacements are caused by vertical vibration of the footing with unit displacement amplitude. The horizontal and vertical components of the displacements along the surface have about equal amplitudes except close to the footing where the vertical component dominates. Fig. 42 shows that the displacement amplitudes decrease with depths at close and far distances from the axis of the footing. This means that most of the energy is propagated in the upper part of the layer, where the material is softer than at greater depth, and also that the rigid base assumed in the analyses has little or no influence on the results.

## 13. SUMMARY AND CONCLUSIONS

A numerical method has been presented for the analysis of steady-state wave propagation problems in linearly elastic or viscoelastic media of infinite extent. The geometries considered are either plane or axisymmetric and consist of a finite, irregular region which is joined to semi-infinite layered regions of the type shown in Figs. 4 and 5. All external loads are applied within the irregular region and vary harmonically with time. Motions both in the plane and perpendicular to the plane of a cross-section through an axisymmetric or plane geometry have been treated.

The irregular region is discretized by the finite element method. Compatible finite elements with quadrilateral cross-sections are employt and the displacements at the nodal joints of the elements are introduced as the degrees of freedom.

The semi-infinite layered region is discretized by subdividing the layers into thin sublayers and by assuming that within each sublayer the displacements vary linearly in the direction normal to the layers. In the direction parallel to the layers, the displacements are required to satisfy the pertinent ordinary differential equations, which are obtained by separation of the variables from the partial differential equations that govern the motion of the continuum.

Compatibility conditions for displacements and equilibrium must be satisfied along the sublayer interfaces, the stress free surface and the fixed base. These conditions constitute an algebraic eigenvalue problem, since no external forces are applied within the layered region. The solutions to the eigenvalue problem describe the propagating and standing waves which can exist in the discretized layered region. These waves serve as shape functions for the displacement expansion. A dynamic stiffness matrix is then developed which uniquely relates the nodal forces to the simultaneous nodal displacements and properly represents the elastic and viscous dynamic response of the semi-infinite layered

region.

The equations of motion for the discrete model are derived from the principle of virtual work which has been formulated to facilitate the use of complex variables in the analysis of harmonic motion.

An important step in the procedure is the determination of the wave modes in the layered region by the solution of the eigenvalue problem. For motions perpendicular to the cross-sectional plane the problem $([A]k^2 + [C])$ $\{v\} = \{0\}$ must be solved in which $[A]$ and $[C]$ are complex, symmetric, tridiagonal matrices. For motions in the cross-sectional plane the problem is $([A]k^2 + i[B]k + [C])$ $\{v\} = \{0\}$ in which $[A]$ and $[C]$ are complex, symmetric matrices with bandwidth 5 and $[B]$ is a complex, skew-symmetric matrix with bandwidth 7. Efficient FORTRAN IV subroutines for solving these problems have been developed and presented.

The method is consistent in that the same displacement expansions are employed for the derivation of the elastic, damping and inertia forces at any nodal joint. The displacement expansions both in the finite element regions and in the layered regions are compatible and thus provide continuous displacements throughout the entire domain. The analysis yields the displacements in the irregular region as well as in the semi-infinite layered regions.


## Accuracy Studies

The accuracy of the method was investigated for the example in which a line load acts on the surface of a homogeneous layer and generates plane generalized Love or Rayleigh waves. In the Love wave case, the numerical results for the discretized layer were compared with the exact solution for the continuous layer. Good agreement was obtained with a relatively coarse mesh and excellent agreement was achieved with a fine mesh. In the Rayleigh wave case, the accuracy of the numerical solutions had to be studied indirectly by comparing solutions obtained with different meshes, because no exact continuum solution is available. For this purpose the boundary between the irregular and the layered

101

region was shifted, replacing the finite element displacement field by the expansion into wave modes and vice versa. The size of the finite elements and the thickness of the sublayers were also varied. The relative differences between numerical solutions obtained with different meshes were insignificant. In addition, exact wave numbers for waves in the continuous layer were computed and compared with the wave numbers for the corresponding waves in the discretized layer. The agreement was highly satisfactory and improved as the discretization was refined. Similar studies of numerical solutions to axisymmetric problems were performed but have not been presented here. In these cases the agreement of solutions obtained with different meshes was equally good.

In another study, a numerical solution for the torsional vibration of a circular footing on a homogeneous layer was computed for comparison with published analytical solutions and test results. The numerical method was again found to yield excellent results.

## Torsional Motion of Circular Footing

The method presented herein was primarily developed for the analysis of steady-stat vibrations of machine foundations. Thus emphasis was placed on applications to this type of problem.

The torsional response of circular footings to vibratory torques about the vertical axes of the footings was studied. The effects of the thickness of a supporting layer, embedment of the footing and increasing shear modulus with depth were investigated. The response of a footing on a homogeneous layer which has a thickness of 4 footing radii or more is, for practical purposes, identical to that of a footing on a homogeneous half space. Footings on layers with a thickness of one footing radius or less respond quite differently and do not benefit from radiation damping at low frequencies.

Embedment may reduce the vibration amplitudes drastically, especially when the footing sides are bonded to the adjacent soil. Several cases were studied in which the shear modulus increased as the square root of the depth below the ground surface. A careful determination of the static stiffness is, as usual, of primary importance. The dynamic

102

effects are similar to those in the case of a homogeneous half space. Therefore, the displacement functions of the half space solution may be utilized in the analysis as a first approximation provided that the shear modulus at a depth of about one half of the footing radius is chosen as the representative shear modulus. A study of displacements in the far field has indicated that, in the typical frequency range, the amplitudes of surface displacements at some distance from the footing depend predominantly on the torque transmitted into the ground and on the layering of the soil.

## Vertical Motion of Circular Footings

The vertical vibration of a circular footing supported by a homogeneous layer over a rigid base was investigated for two ratios of layer thickness to footing radius, $H/r_o = 6$ and $H/r_o = 10$. Displacement functions of massless footings were computed for cases with and without damping. In the undamped case two different resonance phenomena were observed and discussed. Response spectra for footings with typical mass ratios show only one pronounced peak when a realistic amount of damping is assumed. This peak occurs at the fundamental natural frequency for vertically travelling P-waves in the soil layer. For $H/r_o = 6$ or smaller this peak is high, but for $H/r_o = 10$ or larger this peak is insignificant. The response of footings on a thick layer, $H/r_o > 10$, is similar to that of a footing on a homogeneous half space. The vertical response of a circular footing embedded in a layer, in which the moduli increase with depth, was also analyzed.

## Screening Effect of Trenches

The versatility of the method was demonstrated by a further example. The screening effect of trenches on horizontally polarized S-waves was investigated by varying the depth of the trench and the frequency of the wave motion. It was shown that trenches can be quite effective as a barrier against waves of some frequencies but may be

ineffective for waves of other frequencies.

## Possible Additional Applications

It is believed that the method may also be of value in the study of soil-structure interaction during earthquakes. This would require the introduction of a few features in addition to those included in the analyses presented herein. In this type of problem, the rigid base of the model may be subjected to motion in the form of a time-displacement history of the bedrock underlying the soil. The induced transient motion may be analyzed with the assistance of a discretized Fourier transformation.

The method might also find application to wave propagation problems in other fields. In seismology, fault mechanisms of earthquakes and the effect of valleys and mountain ranges on seismic waves may be studied. The interpreation of results from non-destructive vibratory pavement testing may also be improved with the aid of this method of analysis.

# REFERENCES

1. Abel, J.F., "Static and Dynamic Analysis of Sandwich Shells with Viscoelastic Damping," Report No. SESM 68-9, Structural Engineering Laboratory, Univ. of California, Berkeley, 1968.

2. Abramowitz, M., and Stegun, I.A., Handbook of Mathematical Functions, Dover Publications, New York, 1965.

3. Anderson, J.M., "Adaptation of the Finite Element Stiffness Method to Viscoelastic Steady-State Sinusoidal Vibration Solutions," Bull. 5th Meeting ICRPG Working Group on Mechanical Behavior, CPIA 119, vol. 1, p. 297, 1966.

4. Ang., A.H.-S., and Newmark, N.M., "Development of a Transmitting Boundary for Numerical Wave Motion Calculations," Report to Defense Atomic Support Agency, Washington, D.C., Contract DASA-01-69-0040, 1971.

5. Archer, J.S., "Consistent Mass Matrix for Distributed Mass Systems," Jour. Struct. Div., ASCE, vol. 89, no. ST4, pp. 161-178, 1963.

6. Arnold, R.N., Bycroft, G.N., and Warburton, G.B., "Forced Vibrations of a Body on an Infinite Elastic Solid," Jour. Appl. Mech., vol. 22, pp. 391-401, 1955.

7. Awojobi, A.O., and Grootenhuis, P., "Vibration of Rigid Bodies on Semi-infinite Elastic Media," Proc., Royal Soc. London, vol. 287, ser. A, pp. 27-63, 1965.

8. Awojobi, A.O., "Torsional Vibration of a Rigid Circular Body on an Infinite Elastic Stratum," Int. Jour. Solids Structures, vol. 5, pp. 369-378, 1969.

9. Barkan, D.D., Dynamics of Bases and Foundations, McGraw-Hill, New York, 1962.

10. Bycroft, G.N., "Forced Vibration of a Rigid Circular Plate on a Semi-infinite Elastic Space and on an Elastic Stratum," Phil. Trans. Royal Soc. London, ser. A, vol. 248, pp. 327-368, 1956.

11. Chang, T.Y., "Approximate Solutions in Linear Viscoelasticity," Report No. 66-8, Structures and Materials Research, Univ. of California, Berkeley, 1966.

12. Clough, R.W., "The Finite Element Method in Plane Stress Analysis," Proc. 2nd ASCE Conf. on Electronic Computation, Pittsburgh, Pa., 1960.

13. Clough, R. W., "Analysis of Structural Vibrations and Dynamic Response," Proc. of U.S.-Japan Symp. on Recent Advances in Matrix Methods of Structural Analysis and Design, Tokyo, Japan, 1969.

14. DiMaggio, F.L., and Bleich, H.H., "An Application of a Dynamic Reciprocal Theorem," Jour. Appl. Mech., ASME, vol. 29, pp. 678-679, 1959.

15. Dolling, H.J., "Die Abschirmung von Erschütterungen durch Boden-schlitze," Die Bautechnik, vol. 47, pp. 151-158, pp. 193-204, 1970.

16. Ewing, W.M., Jardetsky, and Press, F., Elastic Waves in Layered Media, McGraw-Hill, 1957.

17. Fung, Y.C., Foundations of Solid Mechanics, Prentice-Hall, 1965.

18. Hadala, P.F., "Evaluation of a Transmitting Boundary for a Two-Dimensional Wave Propagation Computer Code," U.S. Army Engineer Waterways Experiment Station, Technical Report S-71-16, 1971.

19. Haskell, N.A., "The Dispersion of Surface Waves on Multilayered Media," Bull. Seism. Soc. Am., vol. 43, pp. 17-43, 1953.

20. Idriss, I.M., Dezfulian, H., and Seed, H.B., "Computer Programs for Evaluating the Seismic Response of Soil Deposits with Non-Linear Characteristics Using Equivalent Linear Procedures," Dept. of Civil Engineering, Univ. of California, Berkeley, 1969.

21. Kaldjian, M.J., "Torsional Stiffness of Embedded Footings," Jour. Soil Mech. Found. Div., ASCE, vol. 97, no.SM7, pp. 969-980, 1971.

22. Kuhlemeyer, R., "Vertical Vibrations of Footings Embedded in Layered Media," Ph.D. Dissertation, Univ. of California, Berkeley, 1969.

23. Luco, J.E., and Westmann, R.A., "Dynamic Response of Circular Footings," Jour. Engineering Mech. Div., ASCE, vol. 97, no. EM5, pp. 1361-1395, 1971.

24. Lysmer, J., and Richart, F.E., Jr., "Dynamic Response of Footings to Vertical Loading," Jour. Soil Mech. Found. Div., ASCE, vol. 92, no. SM1, pp. 65-91, 1966.

25. Lysmer, J., and Kuhlemeyer, R.L., "Finite Dynamic Model for Infinite Media," Jour. Engineering Mech. Div., ASCE, vol. 95, no. EM4, pp. 859-877, 1969.

26. Lysmer, J., "Lumped Mass Method for Rayleigh Waves," Bull. Seism. Soc. Am., vol. 60, pp. 89-104, 1970.

27. Major, A., Vibration Analysis and Design of Foundations for Machines and Turbines, Collet's. London, 1962.

28. Miller, G.F., and Pursey, H., "On the Partition of Energy Between Elastic Waves in a Semi-Infinite Solid," Proc., Royal Soc., London, ser. A, vol. 233, pp. 55-59, 1955.

29. McNeill, R.L., "Machine Foundations, The State of the Art," Proc. Specialty Session 2, Soil Dynamics, 7th Intl. Conf. on Soil Mech. and Found. Engineering, Mexico City, 1969.

30. McNiven, H.D., "Extensional Waves in a Semi-infinite, Elastic Rod," Jour. Acoust. Soc. Am., vol. 33, pp. 23-27, 1961.

31. McNiven, H.D., Sackman, J.L., and Shah, A.H., "An Investigation of Elastic Waves with Imaginary and Complex Wave Numbers in Hollow Rods," Repc t No. SESM 65-14, Univ. of California, Berkeley, 1965.

32. Murray, R.C., "Steady-State Vibrations of Linear Viscoelastic Solids," Graduate Student Research Report No. 331, SESM Div., Dept. of Civil Engineering, Univ. of California, Berkeley, 1968.

33. National Bureau of Standards, Tables of the Bessel Functions $Y_0(z)$ and $Y_1(z)$ for Complex Arguments, Columbia Univ. Press, New York, 1950.

34. National Bureau of Standards, Tables of the Bessel Functions $J_0(z)$ and $J_1(z)$ for Complex Arguments, 2nd Ed., Columbia Univ. Press, New York, 1947.

35. Nickell, R.E., "Stress Wave Analysis in Layered Thermoviscoelastic Materials by the Extended Ritz Method," Technical Report S-175, U.S. Army Missile Command, Redstone Arsenal, Alabama, 1968.

36. Oliver, J., "Elastic Wave Dispersion in a Cylindrical Rod by a Wide-band, Short-duration Pulse Technique," Jour. Acoust. Soc. Am., vol. 29, pp. 189-194, 1957.

37. Ostrowski, A.M., "On the Convergence of the Rayleigh Quotient Iteration for the Computation of the Characteristic Roots and Vectors, I-VI," Arch. Rat. Mech. Anal., vol. 3, 4, 5, 1958-59.

38 Paul, H.S., "Vibration of a Rigid Circular Disk on an Infinite Isotropic Elastic Plate," Jour. Acoust. Soc. Am., vol. 42, no. 2, pp. 412-416, 1967.

39. Reissner, E., "Stationäre, axialsymmetrische, durch eine schüttelnde Masse erregte Schwingungen eines homogenen elastischen Halbraumes," Ingenieur-Archiv, vol. 7, pp. 381-396, 1936.

40. Reissner, E., "Freie und erzwungene Torsionsschwingungen des elastischen Halbraumes," Ingenieur-Archiv, vol. 8, no. 4, pp. 229-245, 1937.

41. Reissner, E., and Sagoci, H.F., "Forced Torsional Oscillations of an Elastic Half-Space," Jour. Appl. Phys., vol. 15, no. 9, pp. 652-662, 1944.

42. Richart, F.F., Jr., Hall, J.R., Jr., and Woods, R.D., <u>Vibrations of Soils and Foundations</u>, Prentice-Hall, 1970.

43. Seed, H.B., and Idriss, I.M., "Soil Moduli and Damping Factors for Dynamic Response Analyses," Report No. EERC 70-10, Earthquake Engineering Research Center, Univ. of California, Berkeley, 1970.

44. Stallybrass, M.P., "On the Reissner-Sagoci Problem at High Frequencies," <u>Intl. Jour. Engineering Sci.</u>, vol. 5, pp. 689-703, 1967.

45. Turner, M.J., Clough, R.W., Martin, H.C., and Topp. L.J., "Stiffness and Deflection Analysis of Complex Structures," <u>Jour. Aeronautical Sci.</u>, vol. 23, no. 9, pp. 805-823, 1956.

46. Warburton, G.B., "Forced Vibrations of a Body on an Elastic Stratum," <u>Jour. Appl. Mech., Transactions, ASME</u>, vol. 24, pp. 55-58, 1957.

47. Weissmann, G.F., "Torsional Vibrations of Circular Footings," <u>Jour. Soil Mech. Found. Div., ASCE</u>, vol. 97, no. SM9, pp. 1293-1316, 1971.

48. Whitman, R.V., and Richart, F.E., Jr., "Design Procedures for Dynamically Loaded Foundations," <u>Jour. Soil Mech. Found. Div., ASCE</u>, vol. 93, no. SM6, pp. 169-193, 1967.

49. Wilkinson, J.H., <u>The Algebraic Eigenvalue Problem</u>, Clarendon Press, Oxford, 1965.

50. Wilson, E.L., "Finite Element Analysis of Two-Dimensional Structures," Structural Engineering Laboratory Report No. 63-2, Univ. of California, Berkeley, 1963.

51. Wilson, E.L., "Structural Analysis of Axisymmetric Solids," <u>Jour. Am. Institute of Aeronautics and Astronautics</u>, vol. 3, no. 12, 1965.

52. Woods, R.D., "Screening of Surface Waves in Soils," <u>Jour. Soil Mech. Found. Div., ASCE</u>, vol. 94, no. SM4, pp. 951-979, 1968.

53. Zienkiewicz, O.C., <u>The Finite Element Method in Engineering Science</u>, McGraw-Hill, 1971.
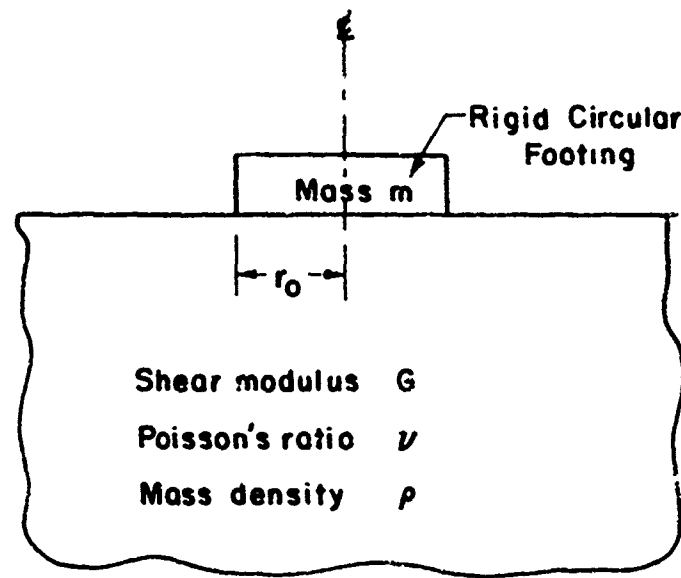
FIG. I-FOOTING ON HOMOGENEOUS
ISOTROPIC HALF SPACE
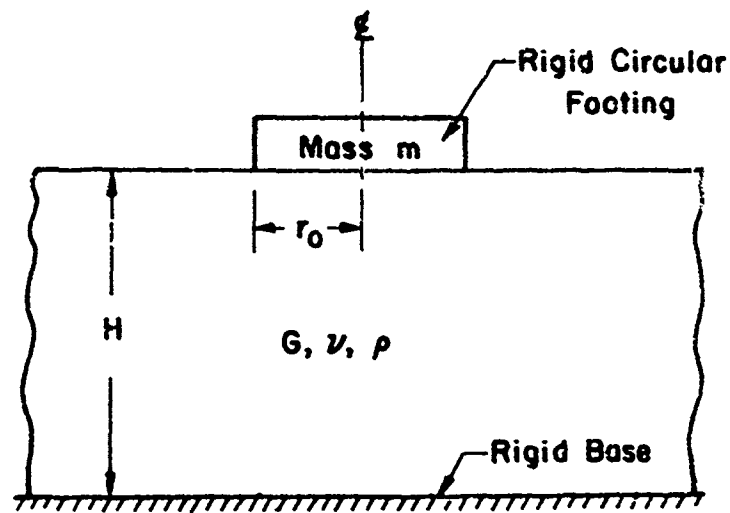


FIG. 2-FOOTING ON HOMOGENEOUS
ISOTROPIC LAYER
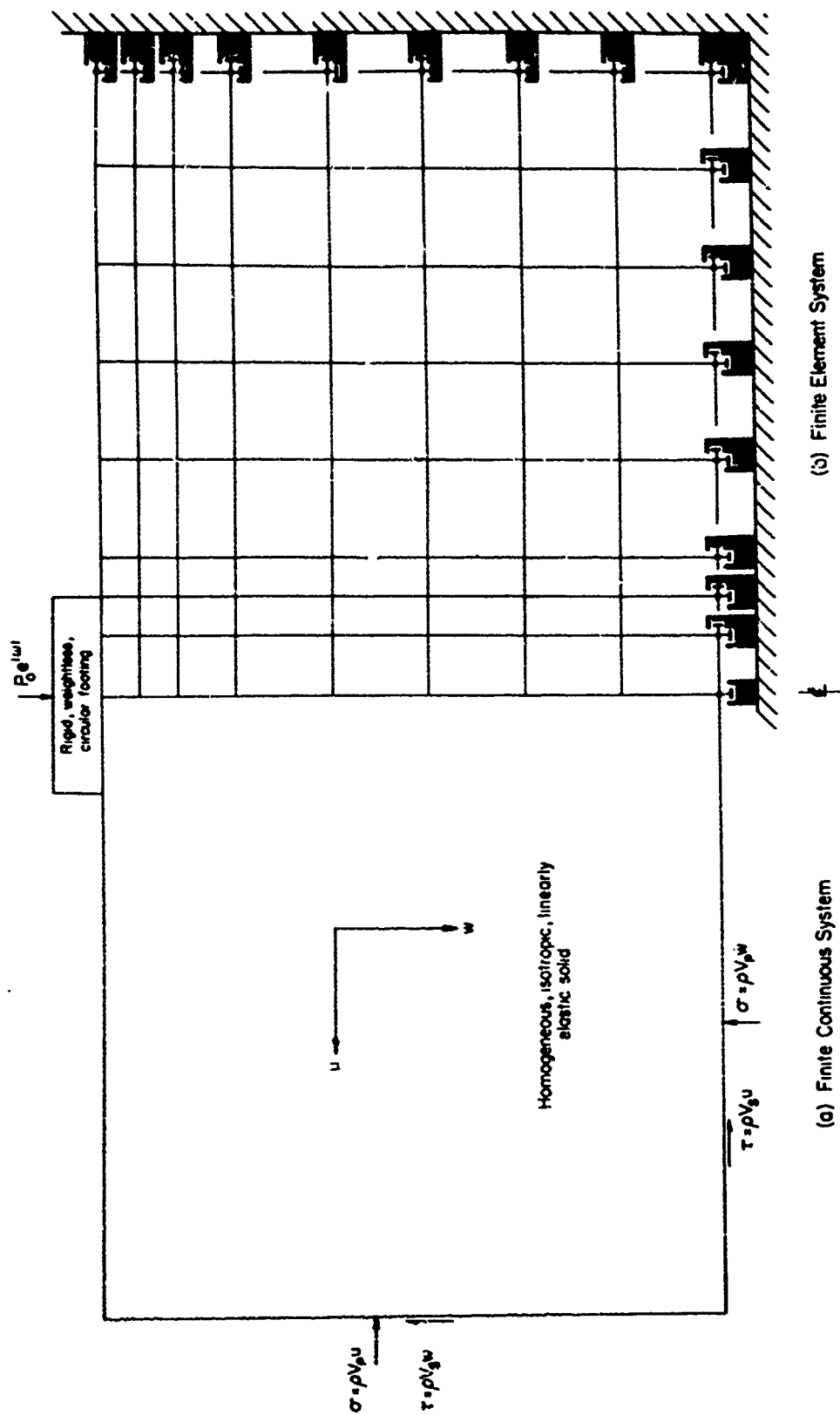
FIG. 3 – FINITE MODEL FOR FOOTING ON A HALF SPACE

(a) Finite Continuous System

(b) Finite Element System
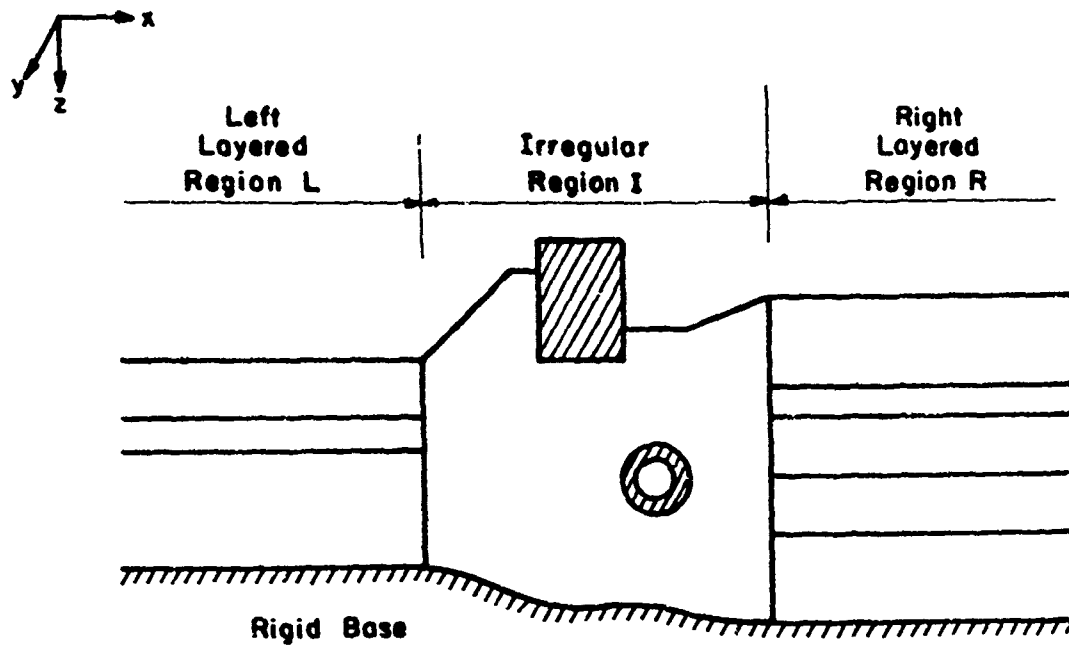
**FIG. 4—TYPICAL PLANE SYSTEM**
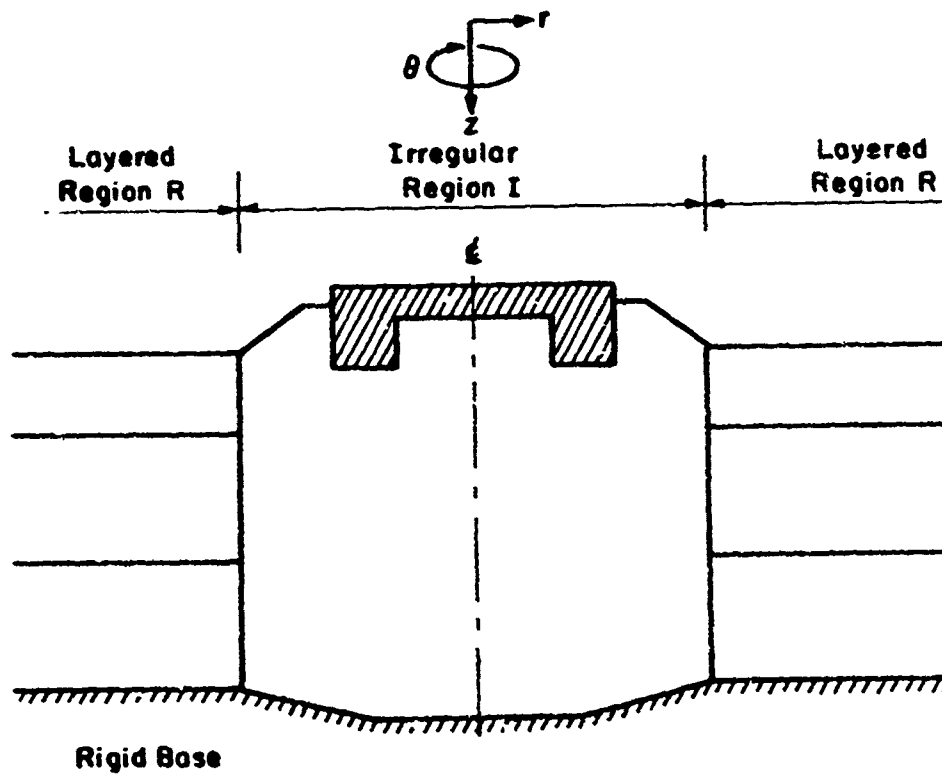


**FIG. 5—TYPICAL AXISYMMETRIC SYSTEM**

111

Region I          Region R

Finite Element

Sublayer

Rigid Base
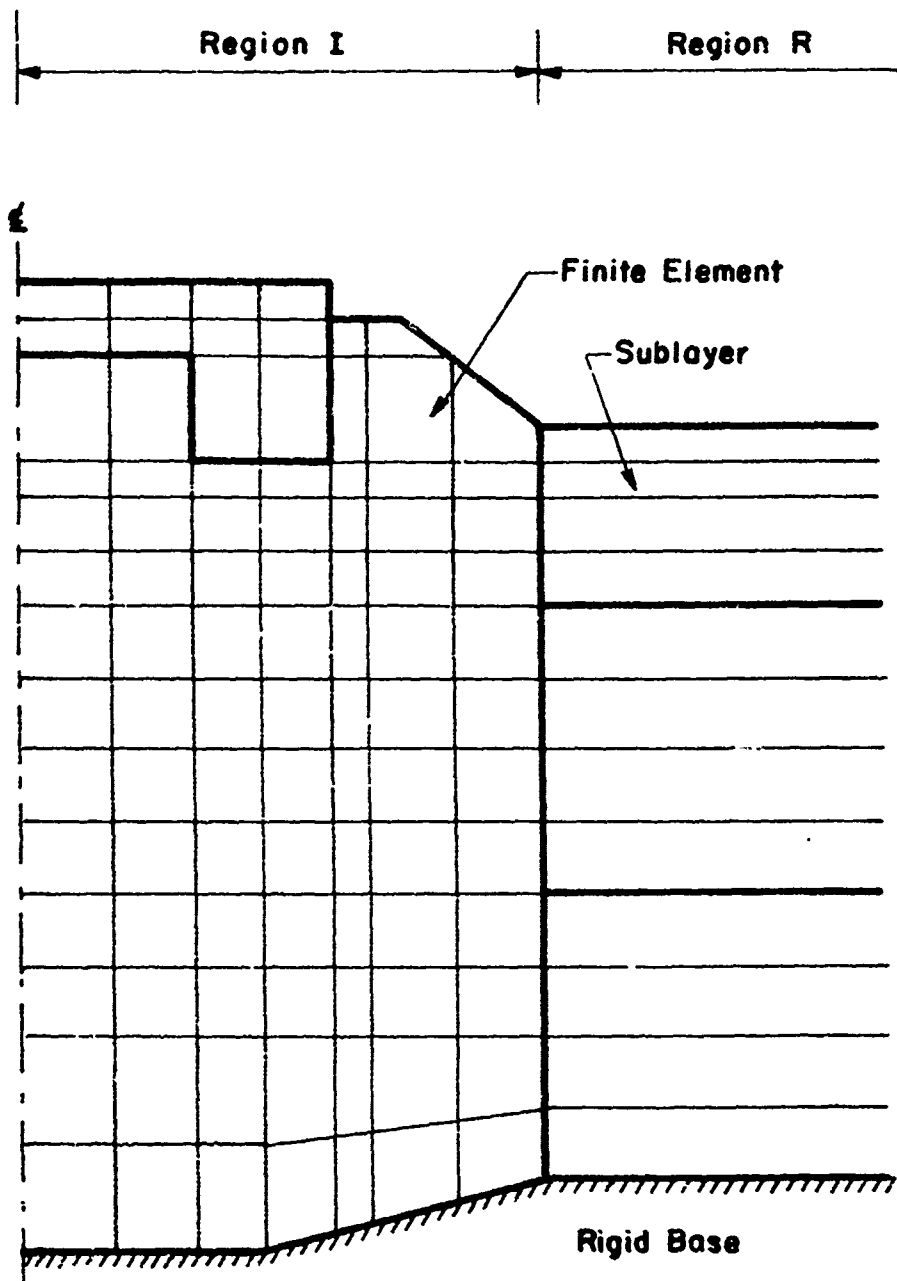
FIG. 6-DISCRETE AXISYMMETRIC MODEL.
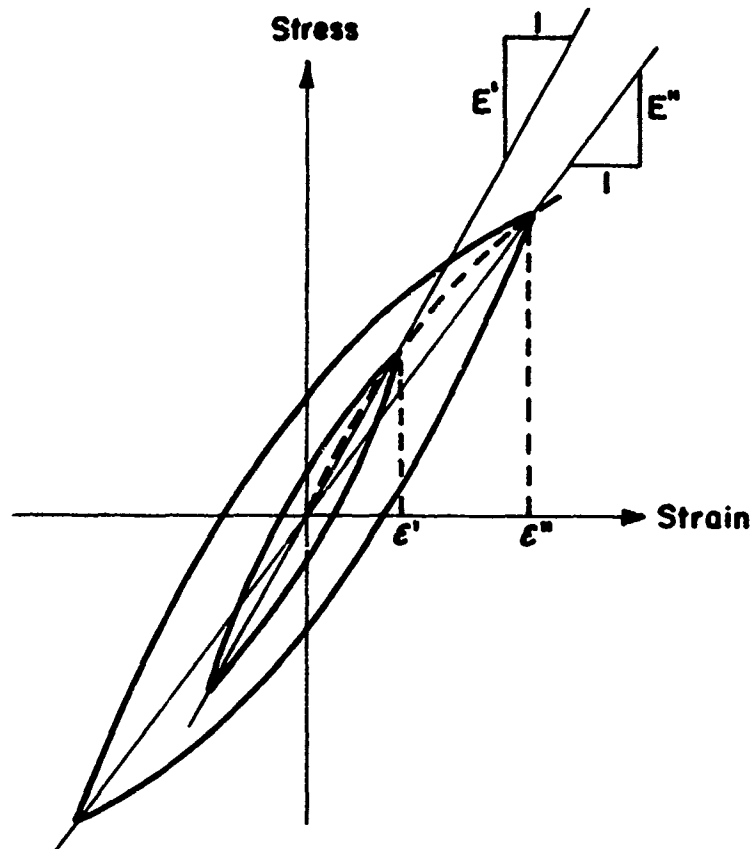
FIG. 7– HYSTERETIC STRESS-STRAIN RELATIONSHIP
AT DIFFERENT STRAIN AMPLITUDES
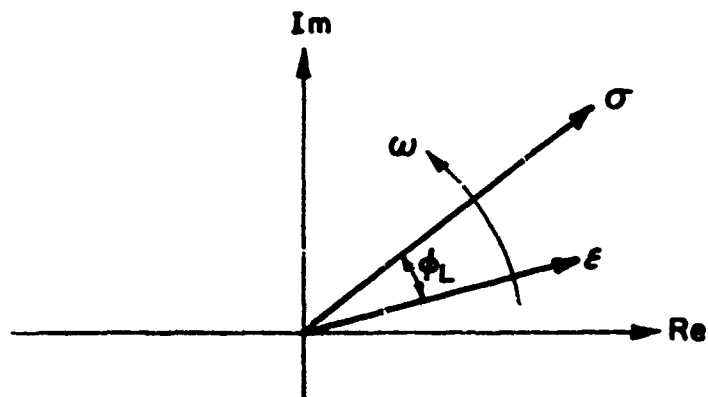


FIG. 8–REPRESENTATION OF STRESS AND STRAIN
IN THE COMPLEX PLANE

113
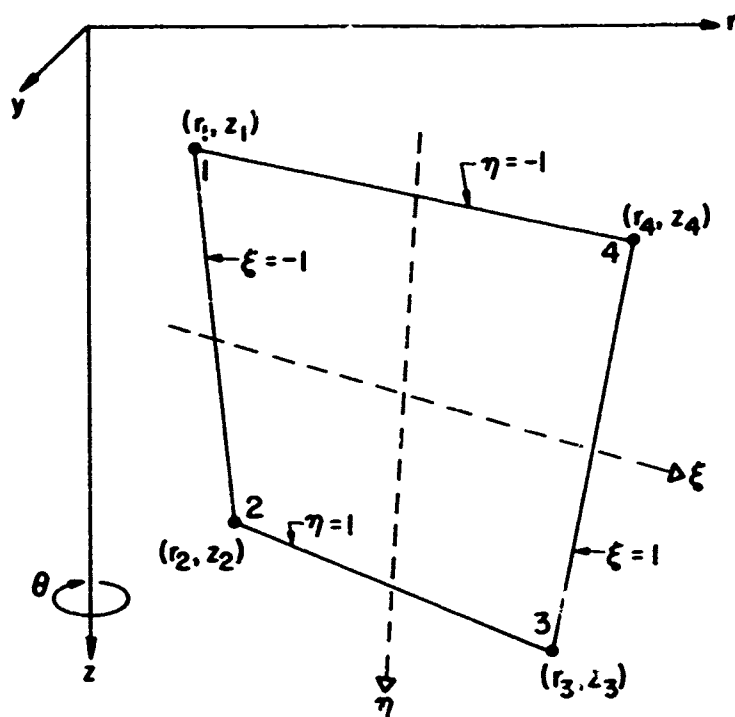
FIG. 9 – QUADRILATERAL CROSS - SECTION OF A
FINITE ELEMENT
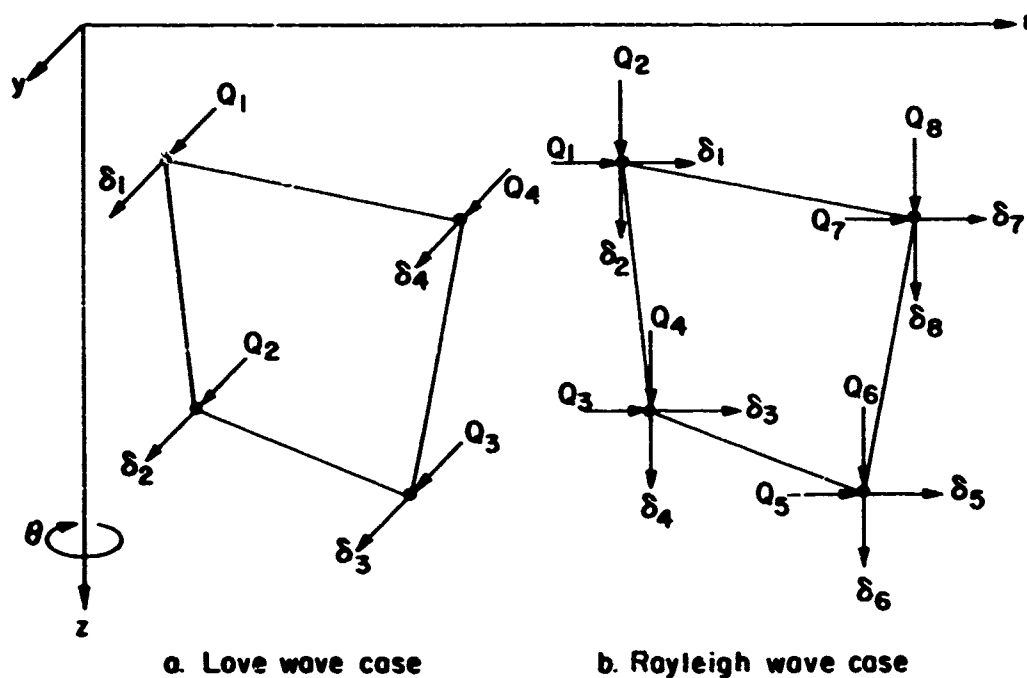


a. Love wave case      b. Rayleigh wave case

FIG. 10 – SIGN RULES FOR FORCES AND DISPLACEMENTS
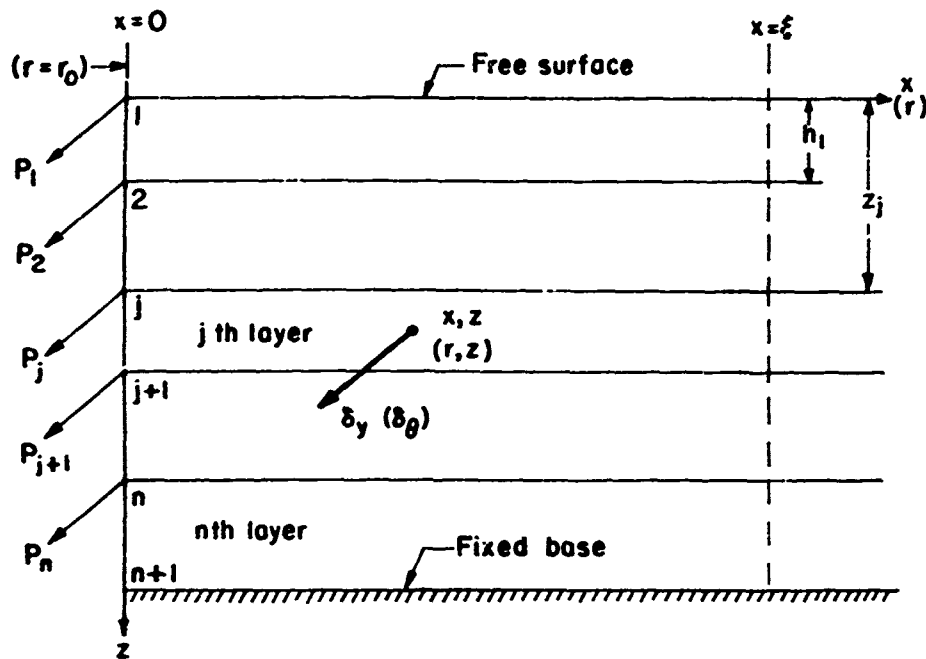
FIG.II TYPICAL LAYERED REGION R IN PLANE
(AXISYMMETRIC) LOVE WAVE CASE
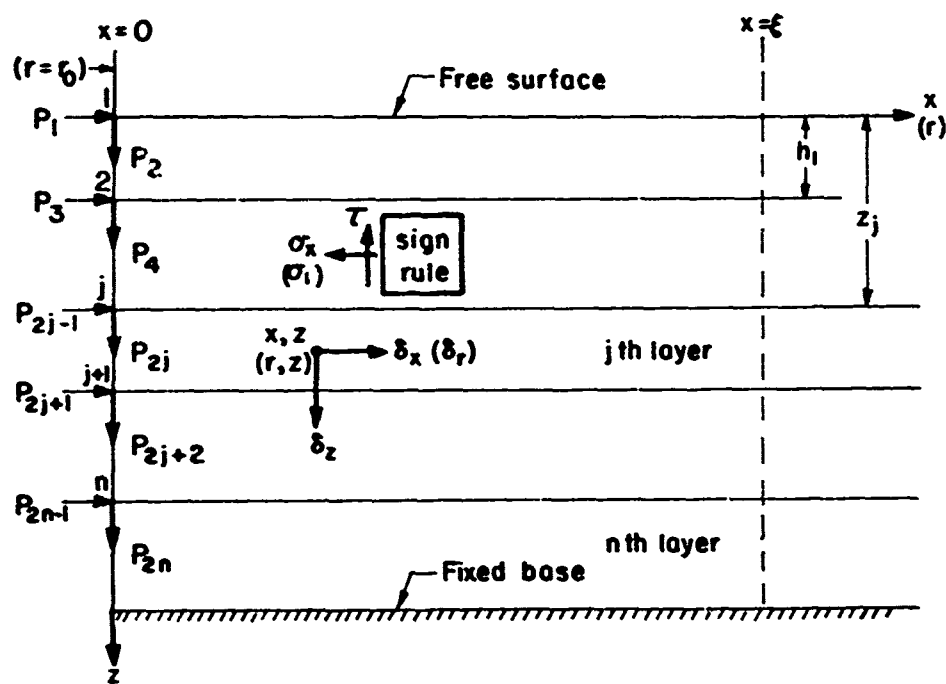


FIG.12-TYPICAL LAYERED REGION R IN PLANE
(AXISYMMETRIC) RAYLEIGH WAVE CASE
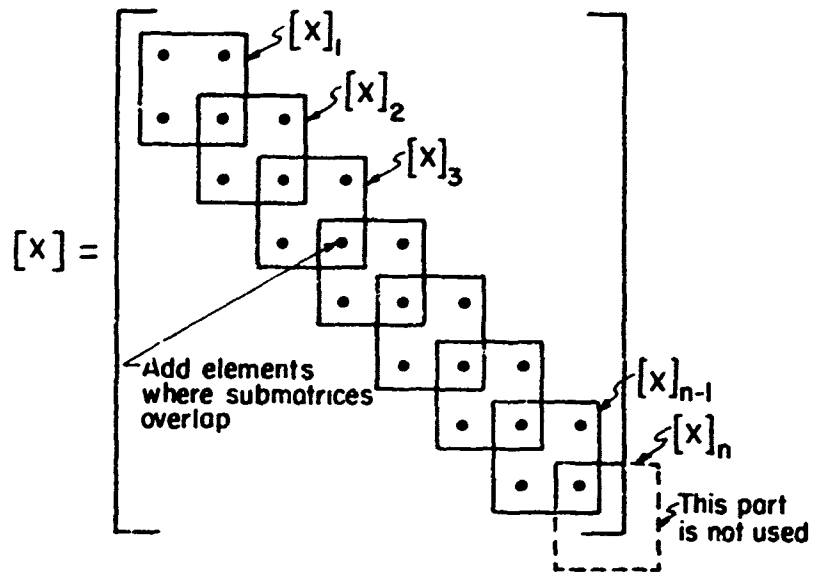
FIG. 13–STRUCTURE OF MATRICES [A], [G], AND [M]
(Love wave case)
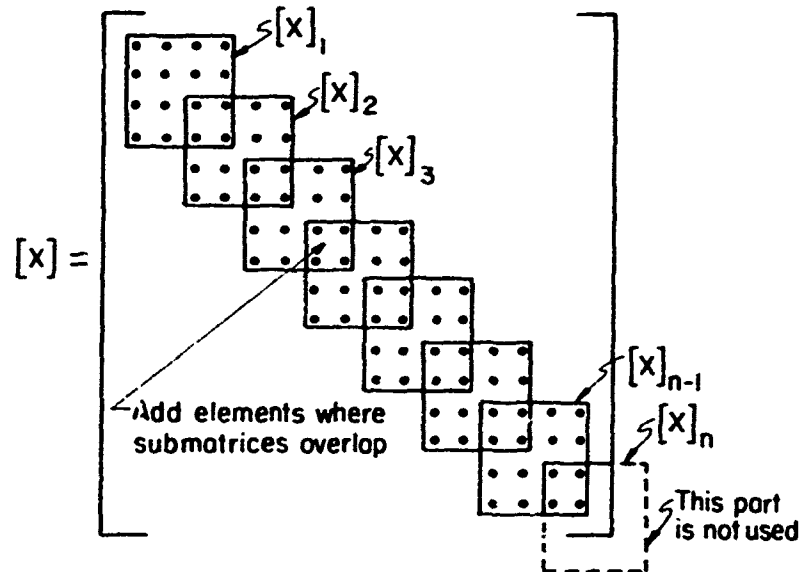


FIG. 14–STRUCTURE OF MATRICES [A], [D], [G], AND [M]
(Royleigh wave case)

116
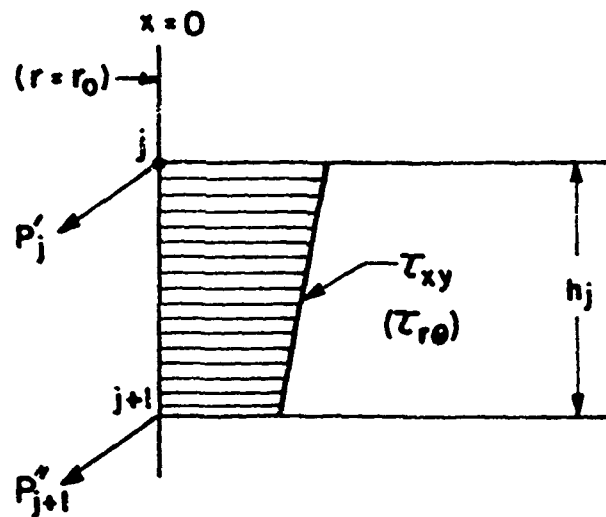
(a) Love Wave Case
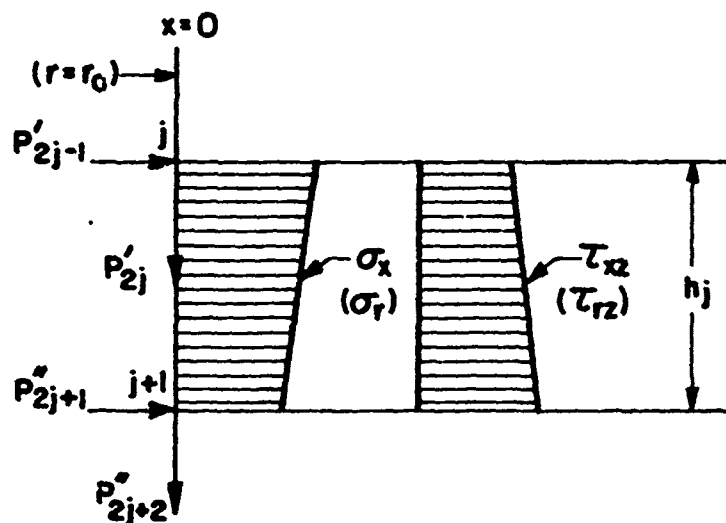


(b) Rayleigh Wave Case

FIG. 15 — FORCES ON VERTICAL BOUNDARY OF
A SUBLAYER AT $x = 0$ ($r = r_0$)
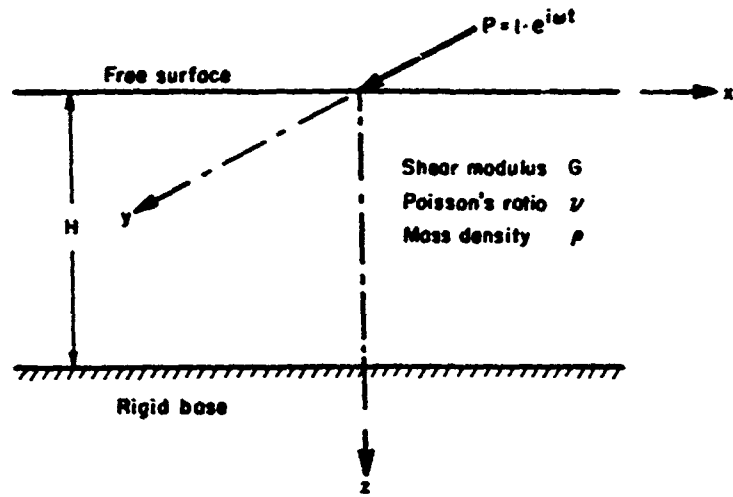
**FIG. 16— LINE LOAD ON HOMOGENEOUS LAYER**
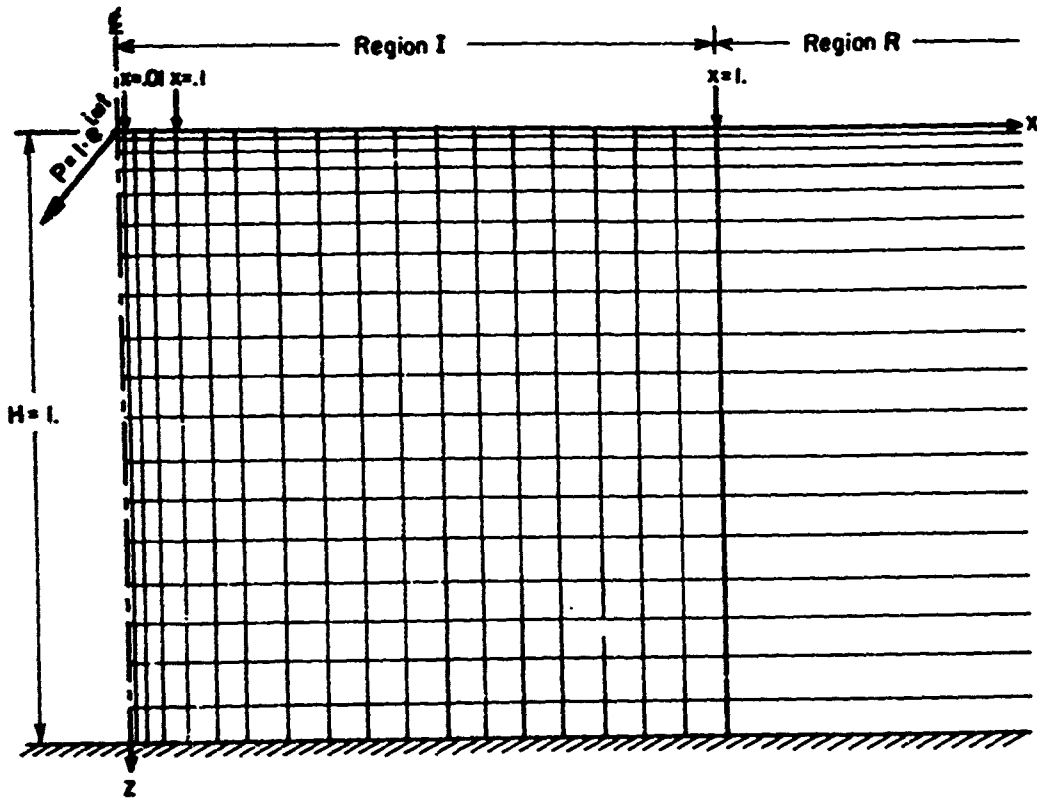


**FIG. 17—FINITE ELEMENT MESH FOR MODEL A.**

118
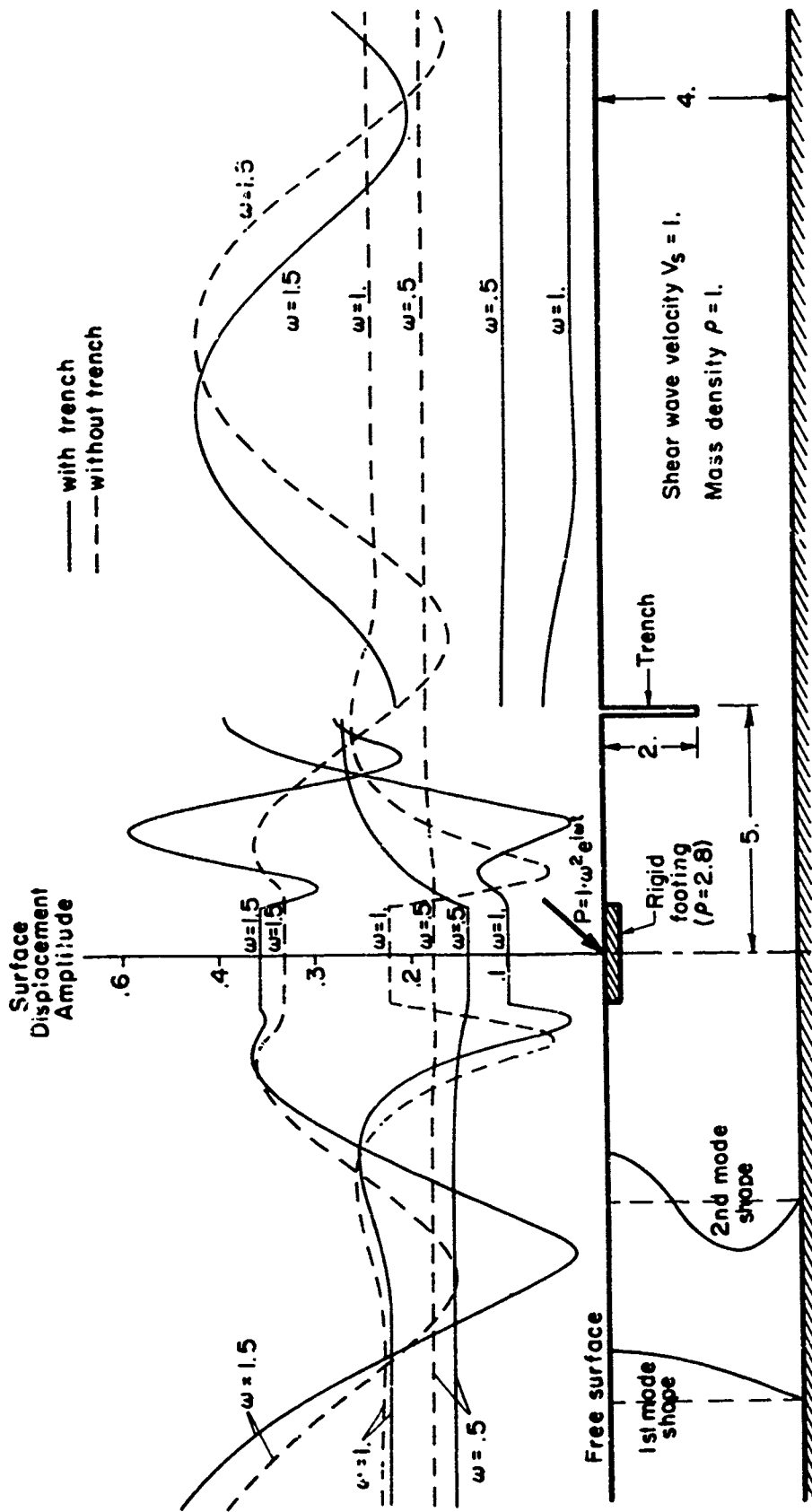
FIG. 18 – SURFACE DISPLACEMENTS WITH AND WITHOUT TRENCH FOR DIFFERENT FREQUENCIES.
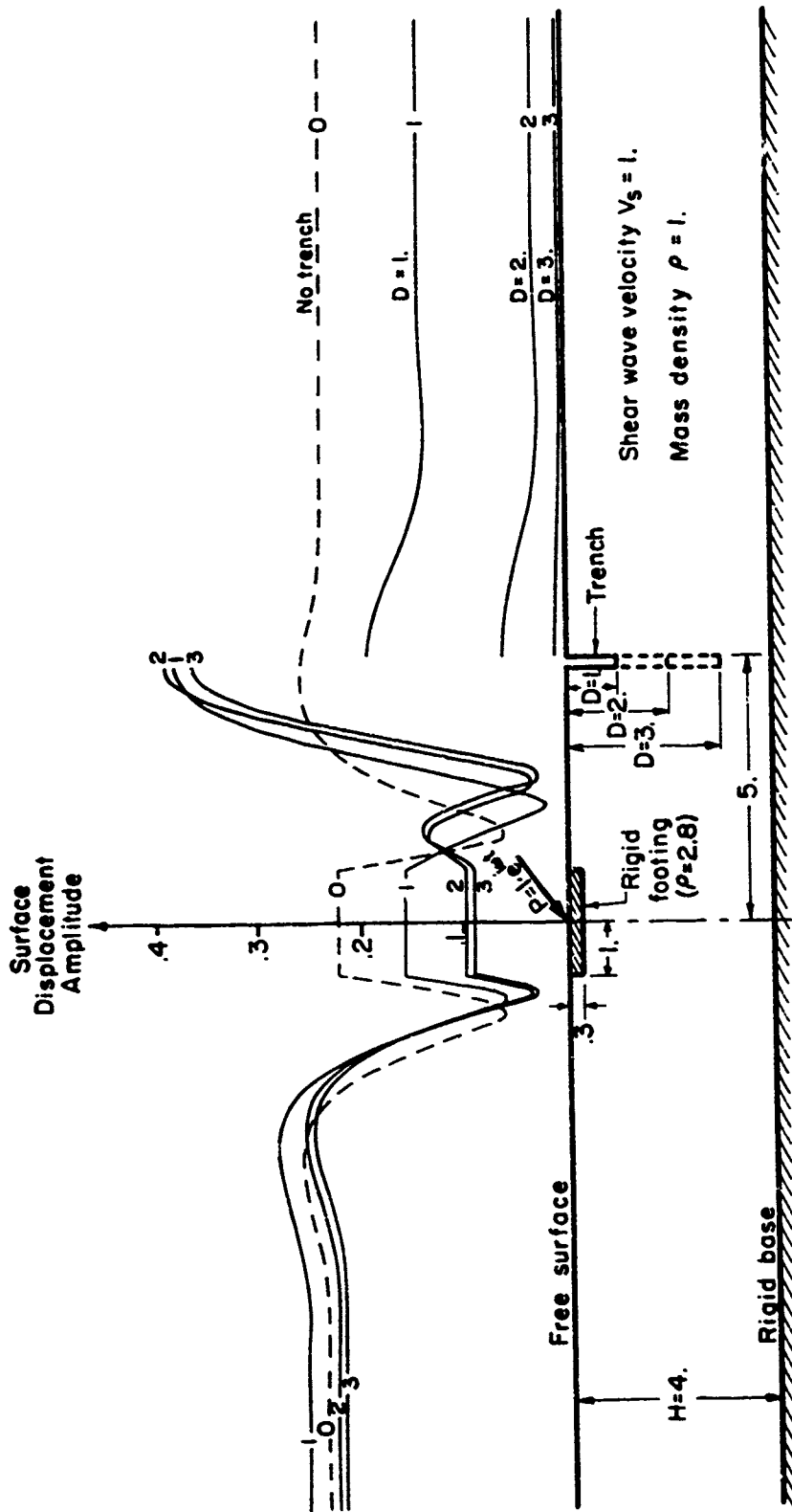
FIG. 19 - SURFACE DISPLACEMENTS AT DIFFERENT TRENCH DEPTHS FOR $\omega = 1.0$

120
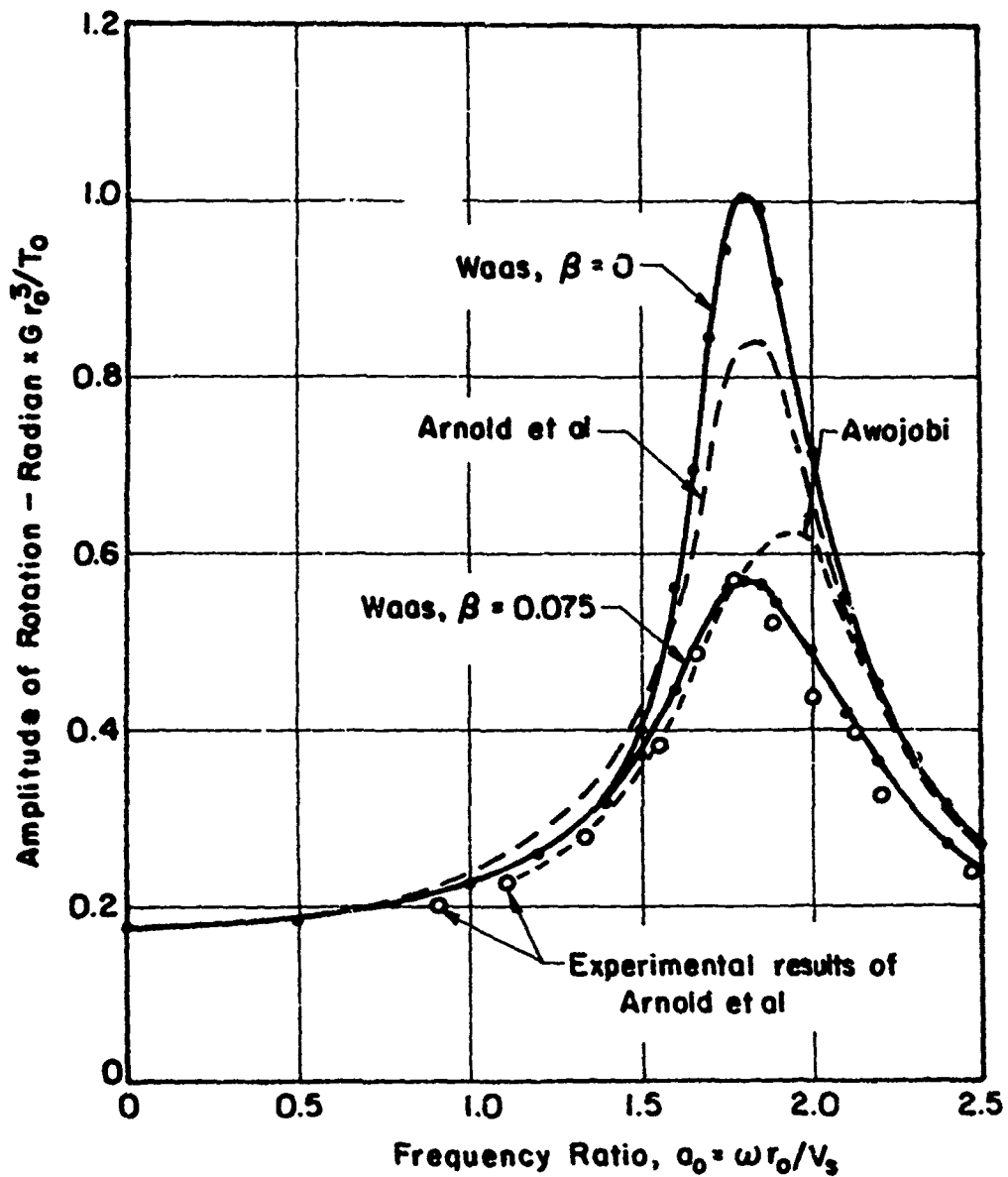
FIG. 20–TORSIONAL MOTION OF A CIRCULAR FOOTING
ON A HOMOGENEOUS LAYER (H/$r_0$ = 0.97;
B$_\theta$ = 0.79)
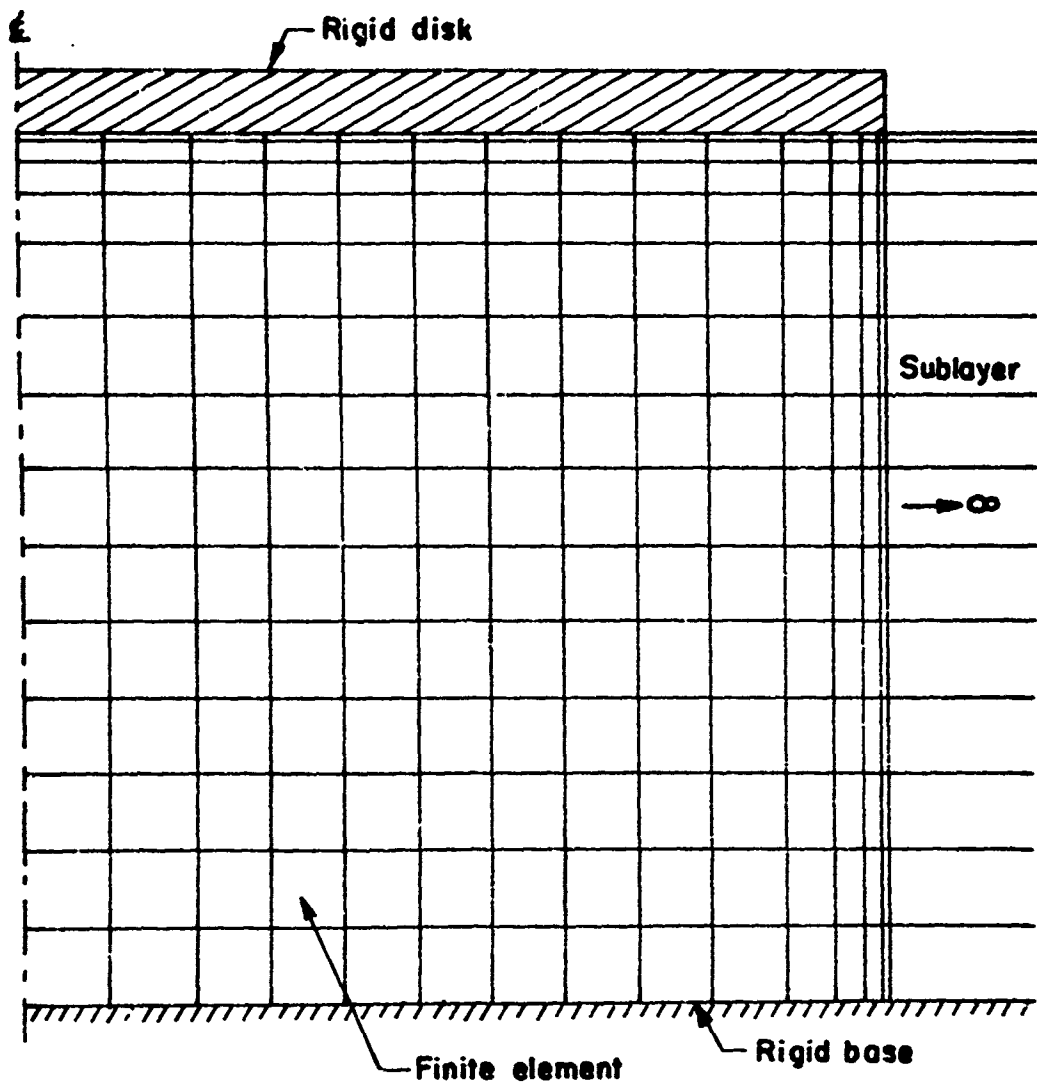
FIG. 21-DISCRETE MODEL FOR CIRCULAR FOOTING ON
HOMOGENEOUS LAYER
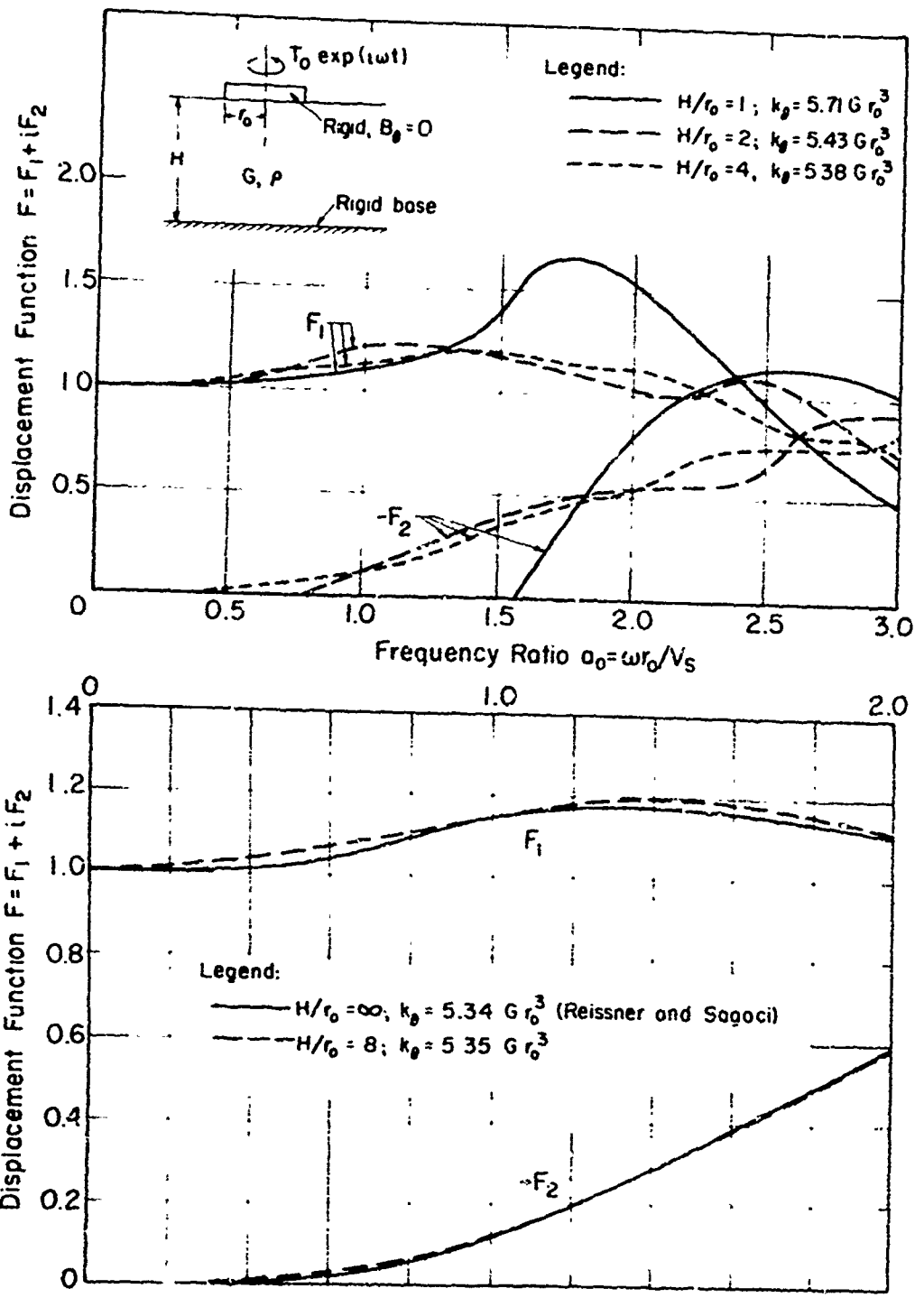
FIG.22- DISPLACEMENT FUNCTIONS FOR TORSIONAL MOTION OF CIRCULAR FOOTING

123
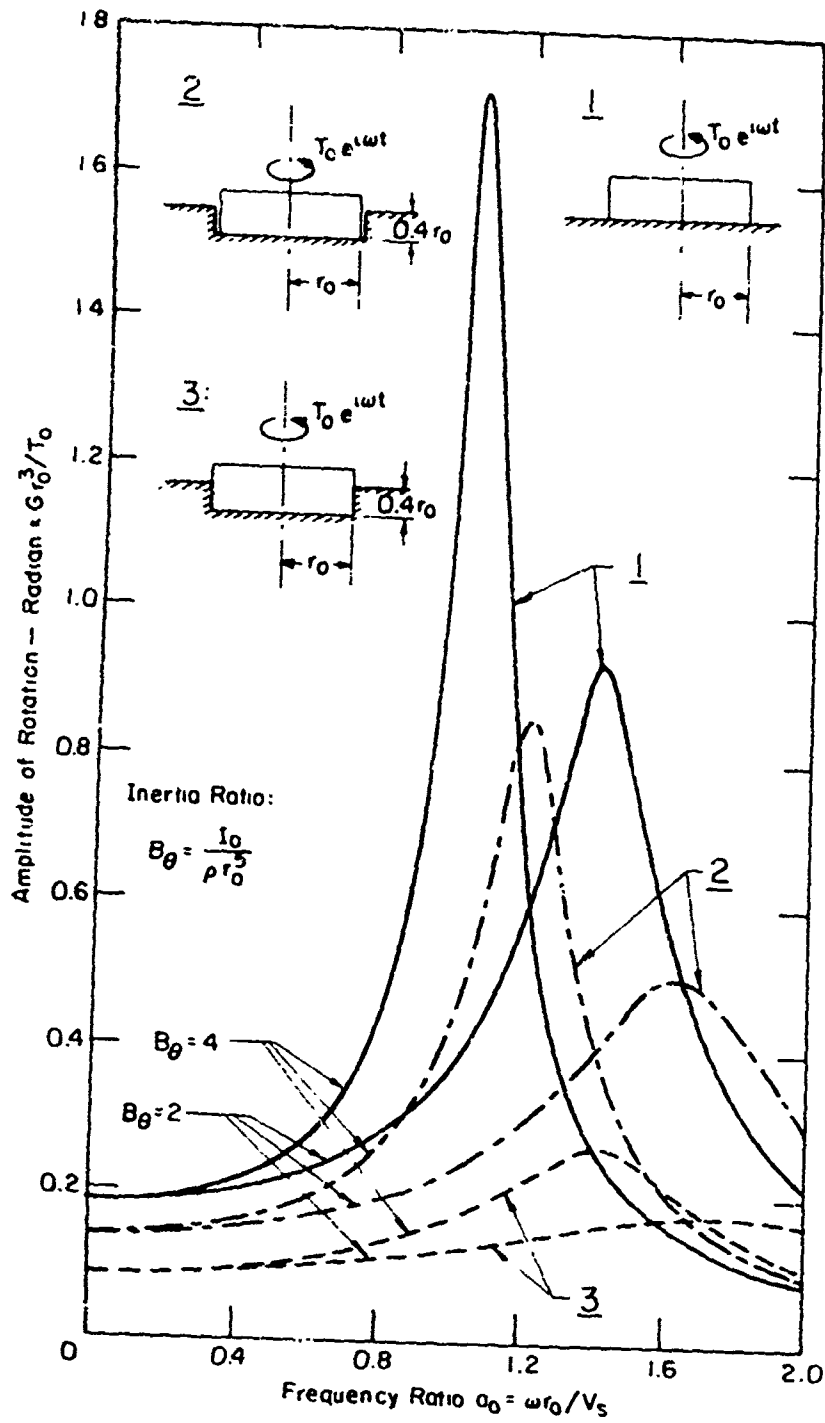
FIG. 23-RESPONSE SPECTRA FOR TORSIONAL MOTION OF CIRCULAR FOOTINGS (H/$r_0$ = 8)

137
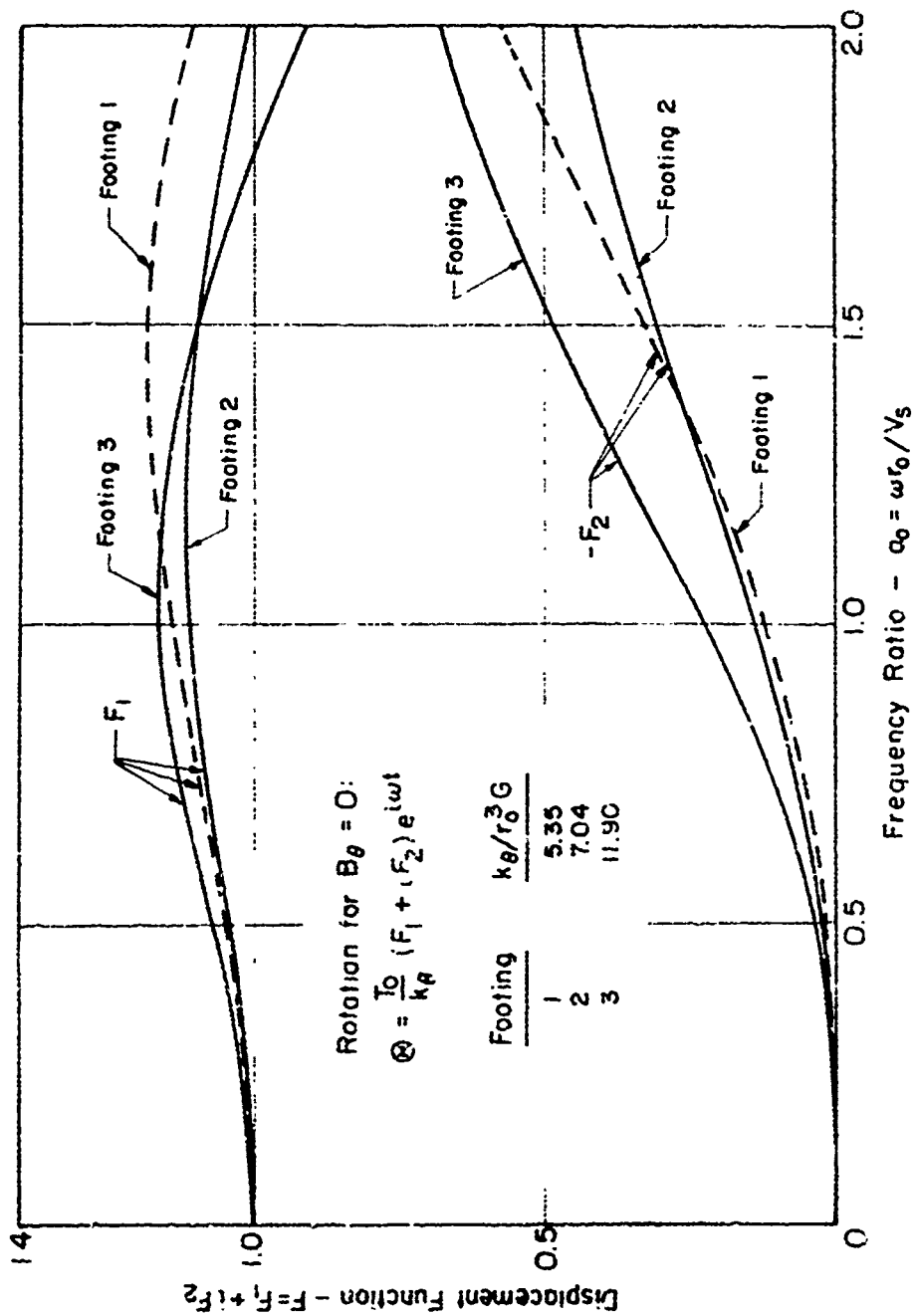
FIG. 24 - DISPLACEMENT FUNCTIONS FOR TORSIONAL MOTION OF CIRCULAR FOOTINGS 1, 2, 3 SHOWN IN FIG. 23

Frequency Ratio – $a_0 = \omega r_0/V_s$

Displacement Function – $F = F_1 + iF_2$

Rotation for $B_\theta = 0$:

$$\Theta = \frac{T_0}{k_\theta}(F_1 + iF_2)e^{i\omega t}$$

| Footing | $k_\theta/r_0^3 G$ |
|---------|--------------------|
| 1       | 5.35               |
| 2       | 7.04               |
| 3       | 11.90              |

Shear Modulus – $G/G_0$

Depth below Surface – $z/r_0$

$p = \frac{1}{2}$  $p = 1$  $p = 2$

for $r < r_0$

$G/G_0 = \sqrt{z/r_0}$

FIG. 25– SHEAR MODULUS INCREASING WITH DEPTH



G for $r < r_0$

G for $r > r_0$

Depth below Surface – $z/r_0$

Shear Modulus – $10^6$ lbs/ft$^2$
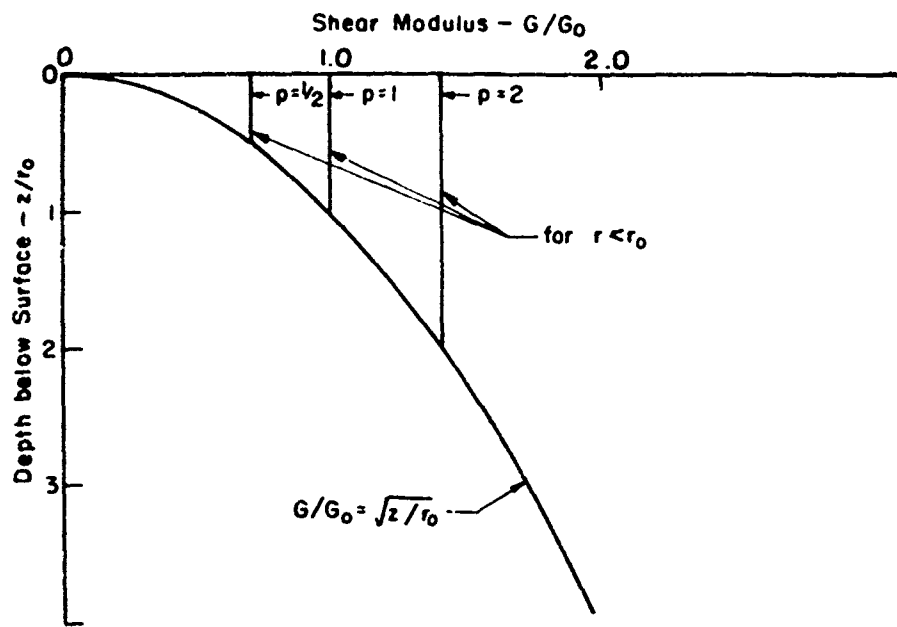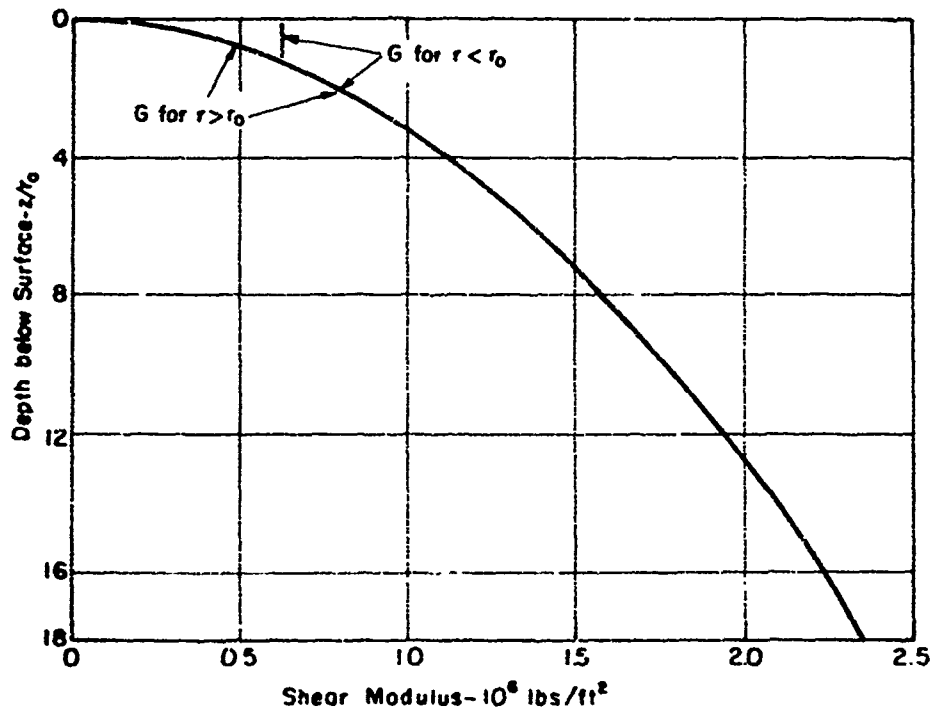
FIG. 26 – SHEAR MODULUS VS. DEPTH FOR INHOMOGENEOUS LAYER
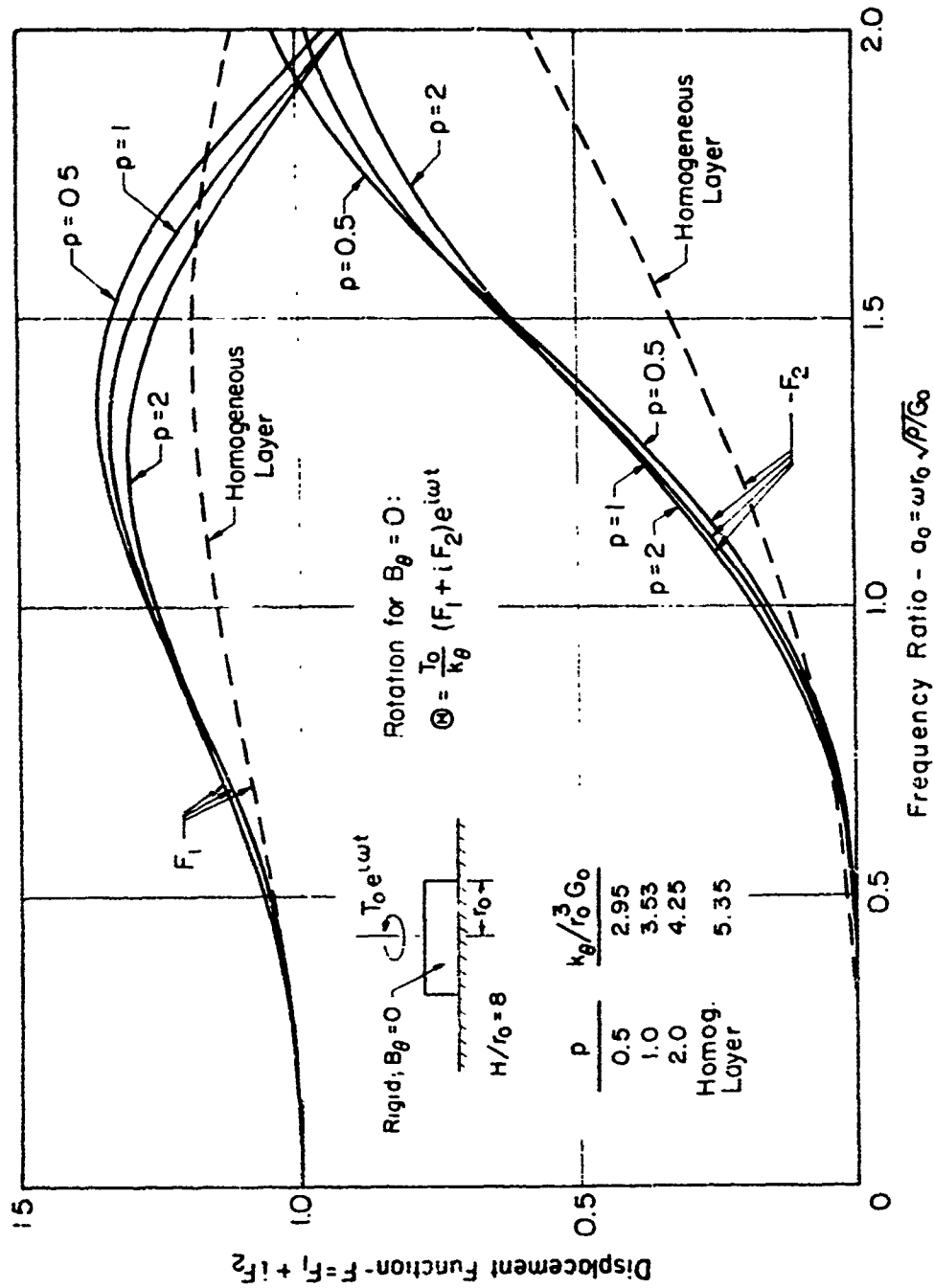
FIG. 27-DISPLACEMENT FUNCTIONS FOR TORSIONAL MOTION OF CIRCULAR FOOTINGS
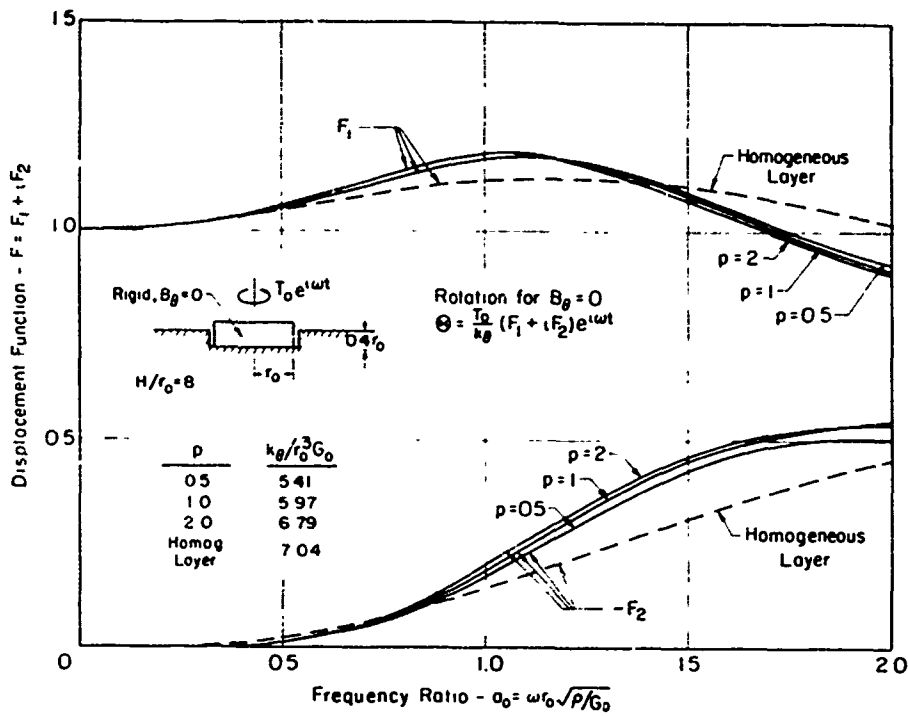
FIG 28-DISPLACEMENT FUNCTIONS FOR TORSIONAL MOTION OF EMBEDDED
CIRCULAR FOOTINGS WITH FREE SIDES
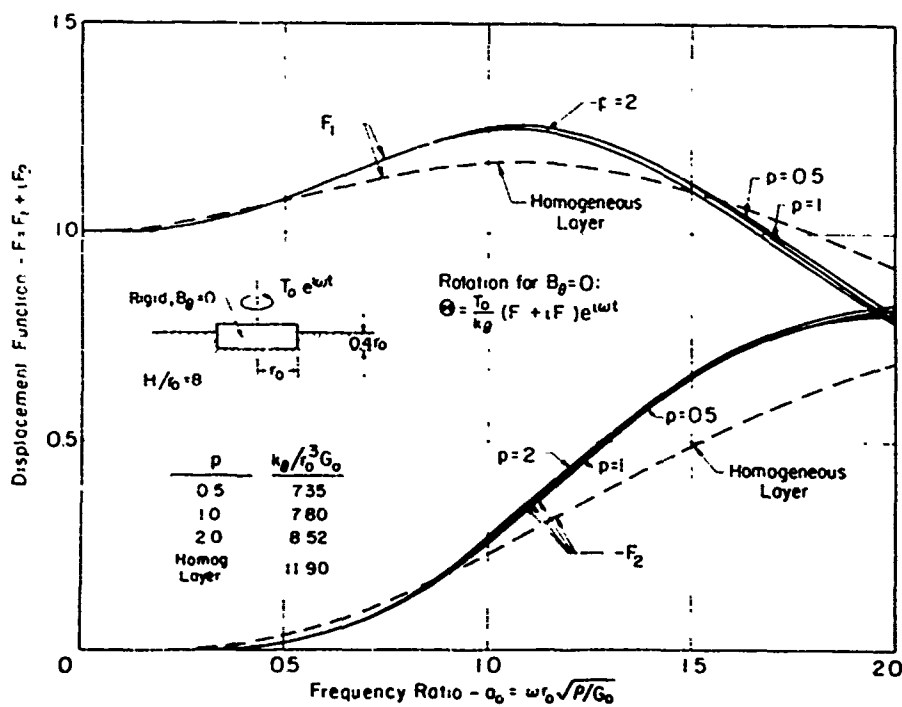


FIG 29-DISPLACEMENT FUNCTIONS FOR TORSIONAL MOTION OF EMBEDDED
CIRCULAR FOOTINGS
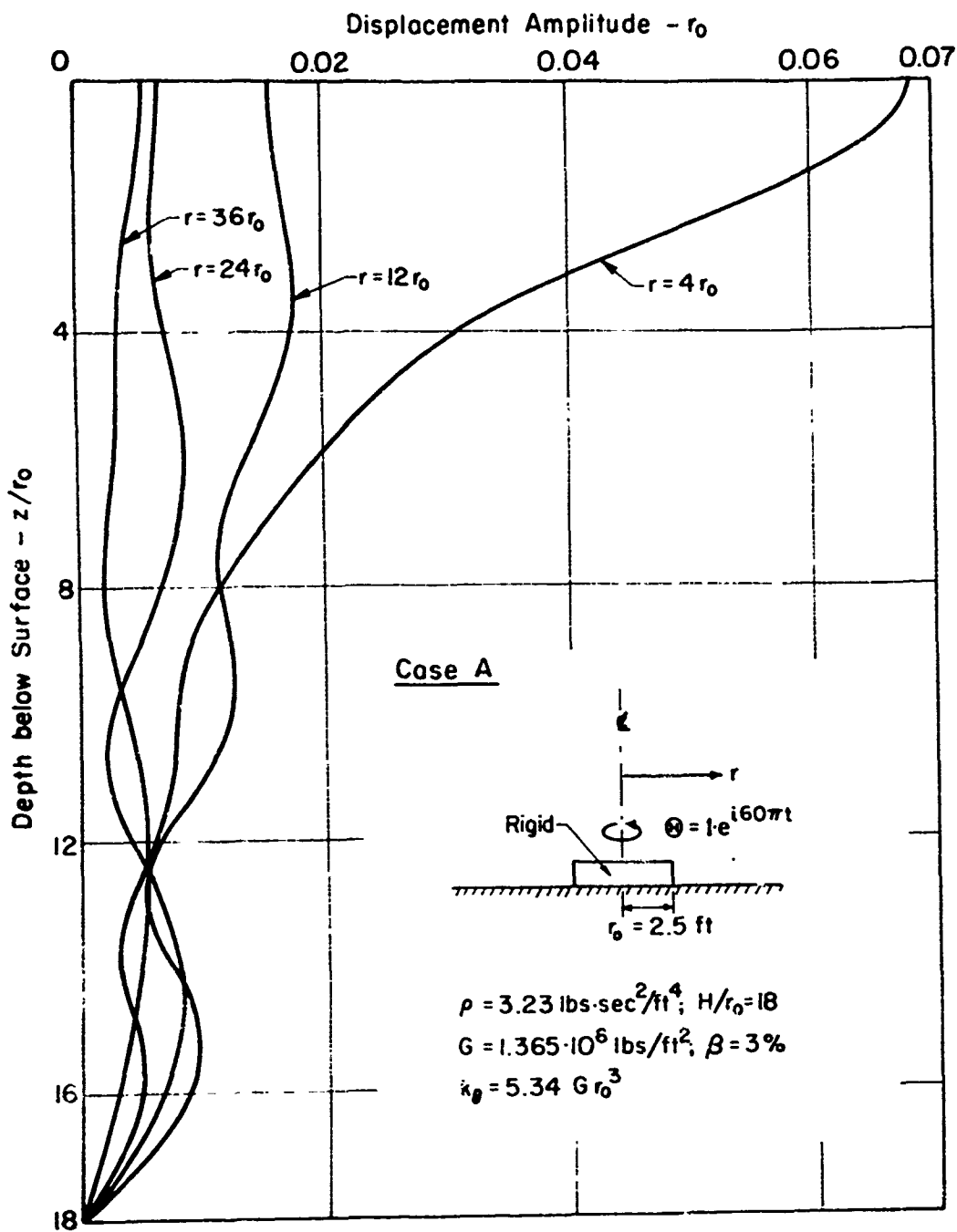
FIG. 30 - DISPLACEMENT AMPLITUDE VS. DEPTH FOR TORSIONAL
MOTION OF CIRCULAR FOOTING ON HOMOGENEOUS
LAYER AT $\omega = 60\pi$
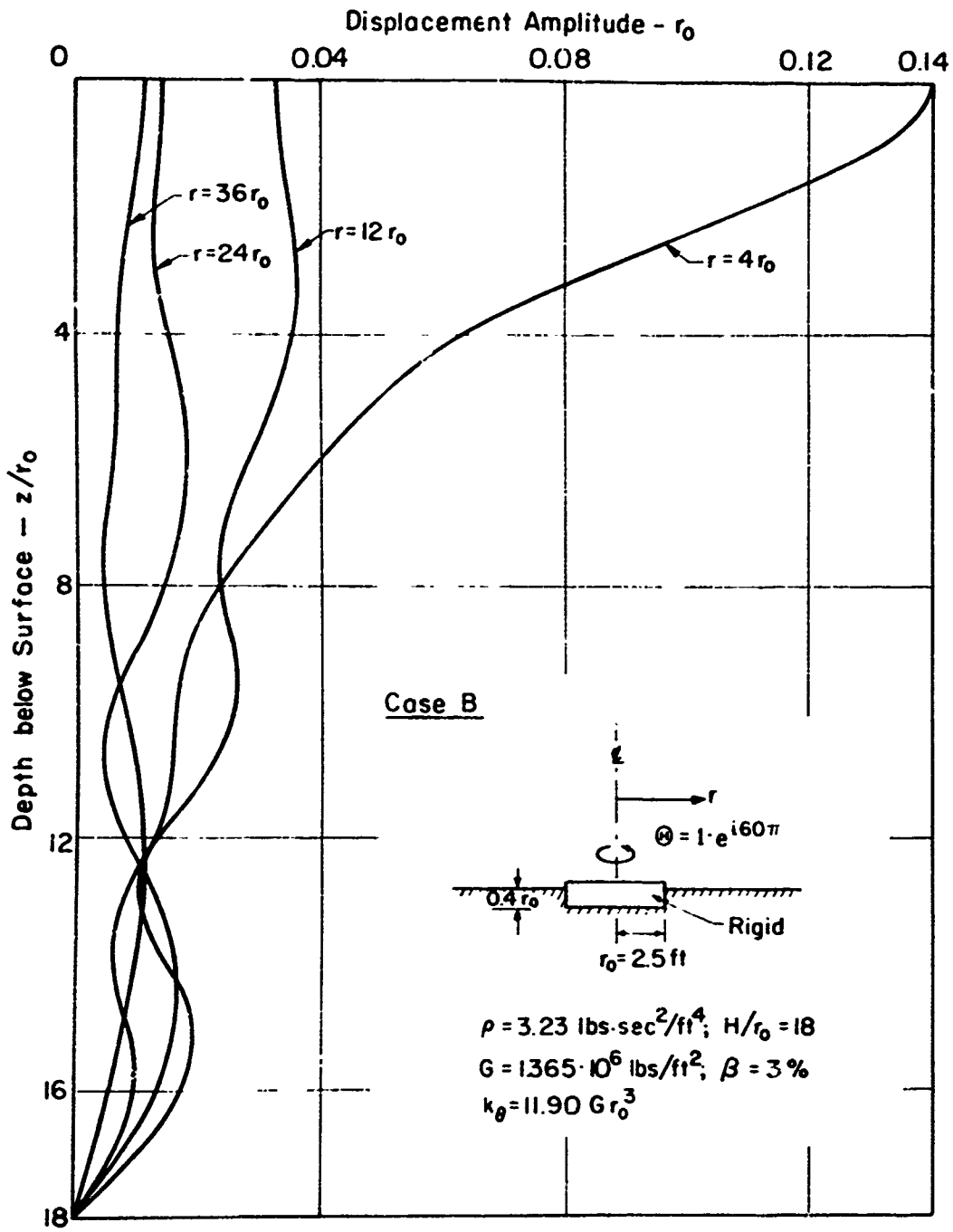
FIG. 31-DISPLACEMENT AMPLITUDE VS. DEPTH FOR TORSIONAL
MOTION OF EMBEDDED CIRCULAR FOOTING ON HOMO-
GENEOUS LAYER AT $\omega = 60\pi$
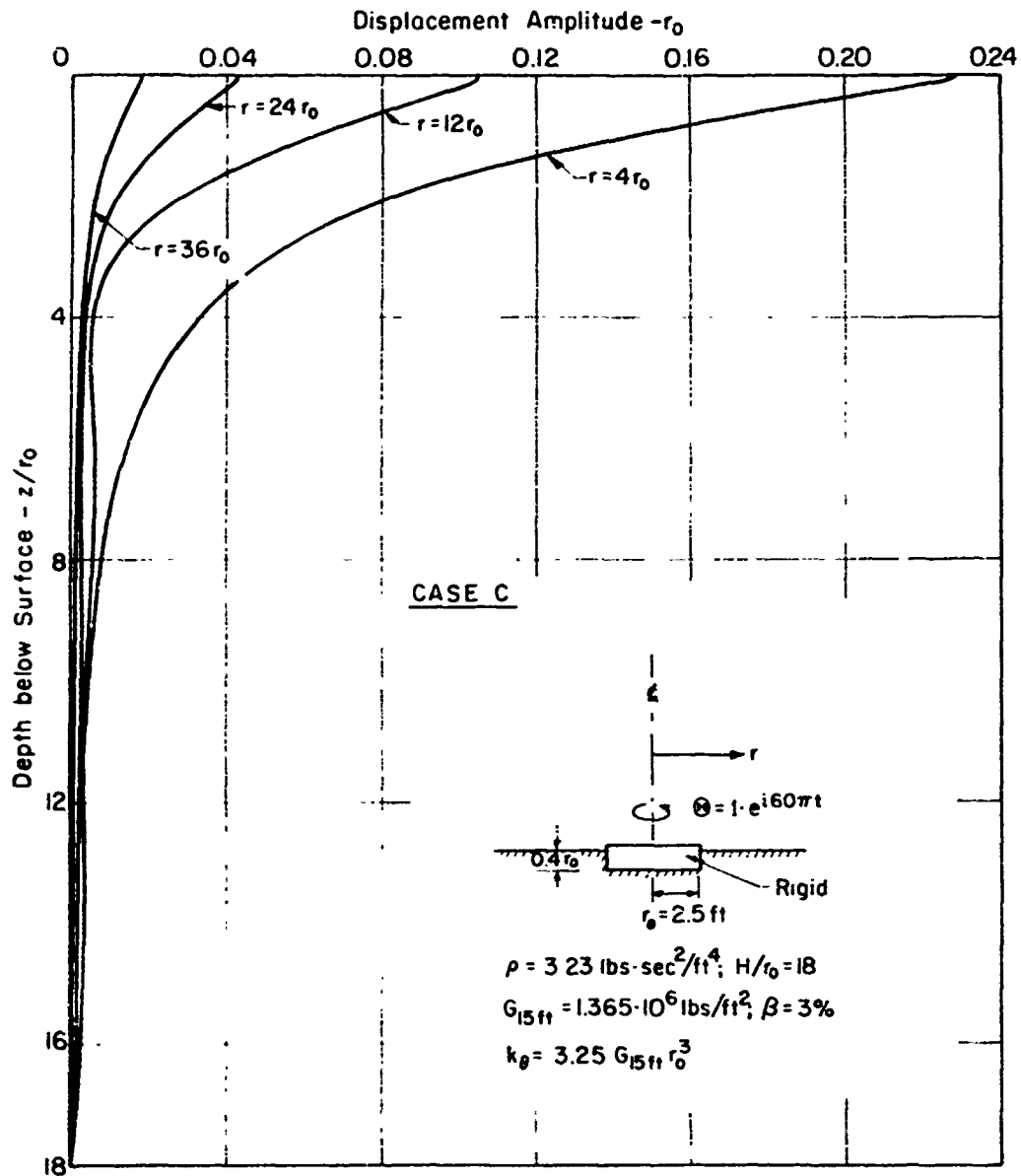
FIG 32- DISPLACEMENT AMPLITUDE VS. DEPTH FOR TORSIONAL MOTION
OF EMBEDDED CIRCULAR FOOTING ON INHOMOGENEOUS LAYER
AT $\omega = 60\pi$

131
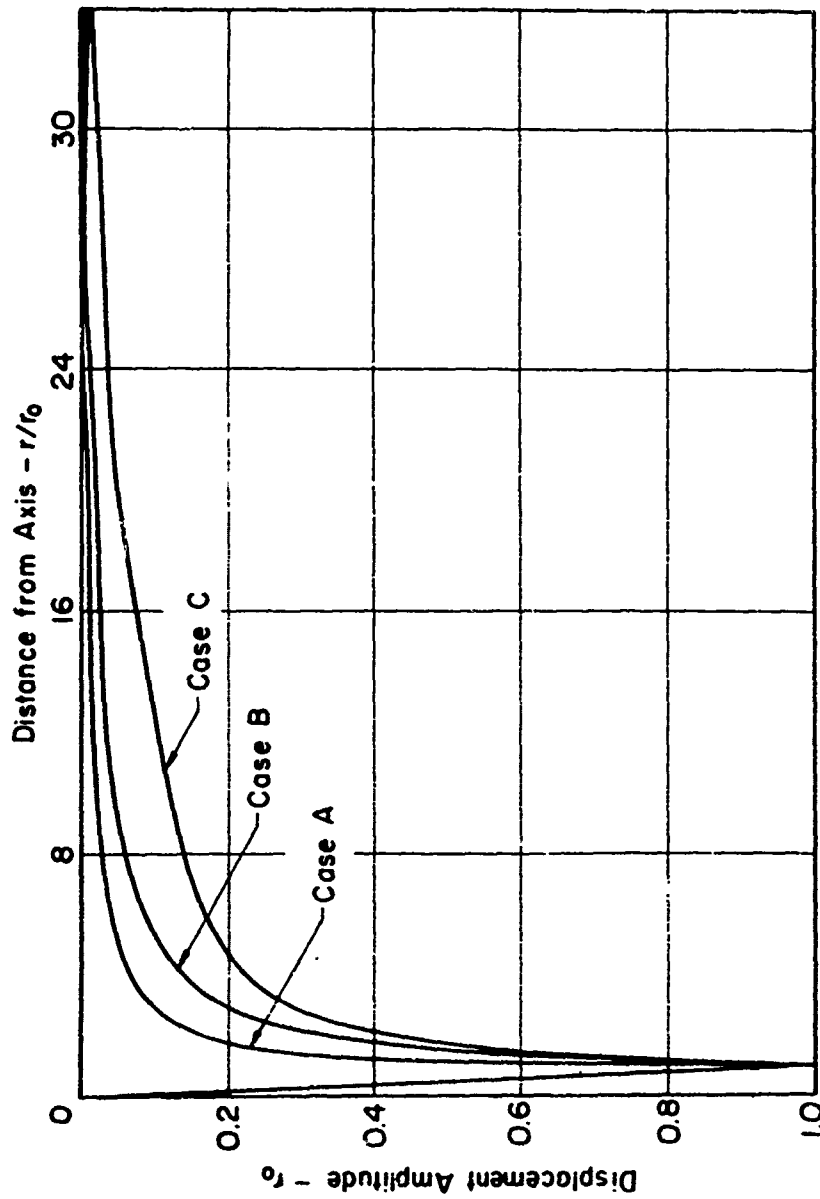
FIG. 33 – DISPLACEMENT AMPLITUDE ALONG SURFACE FOR TORSIONAL MOTION OF CIRCULAR FOOTINGS AT $\omega = 60\pi$ ($H/r_0 = 18$; 3% OF CRITICAL DAMPING)

132
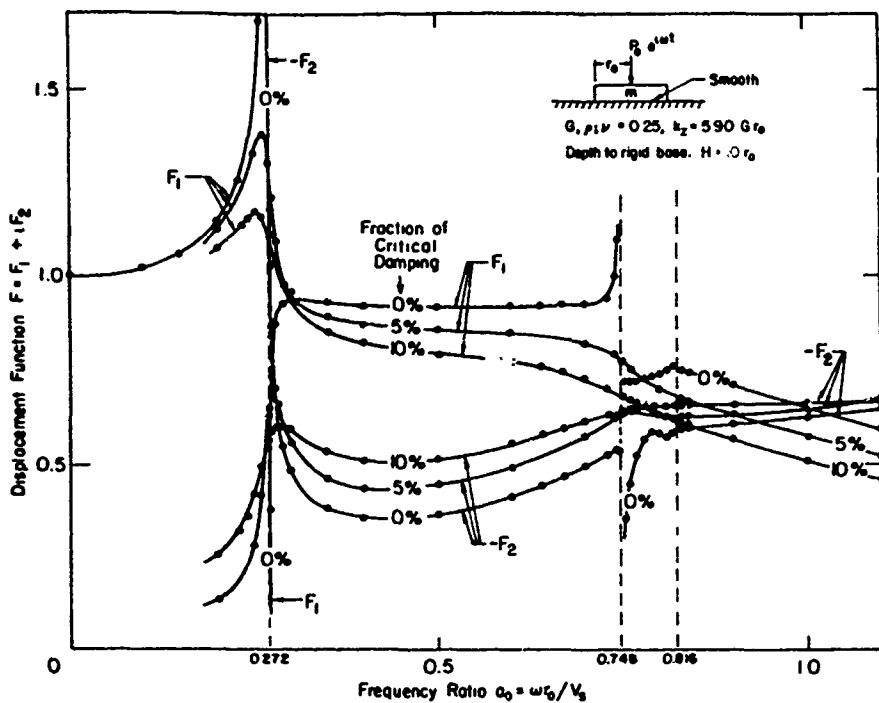
FIG.34 DISPLACEMENT FUNCTIONS FOR VERTICAL MOTION OF CIRCULAR FOOTINGS ON HOMOGENEOUS LAYER (H/r$_0$ = 10)
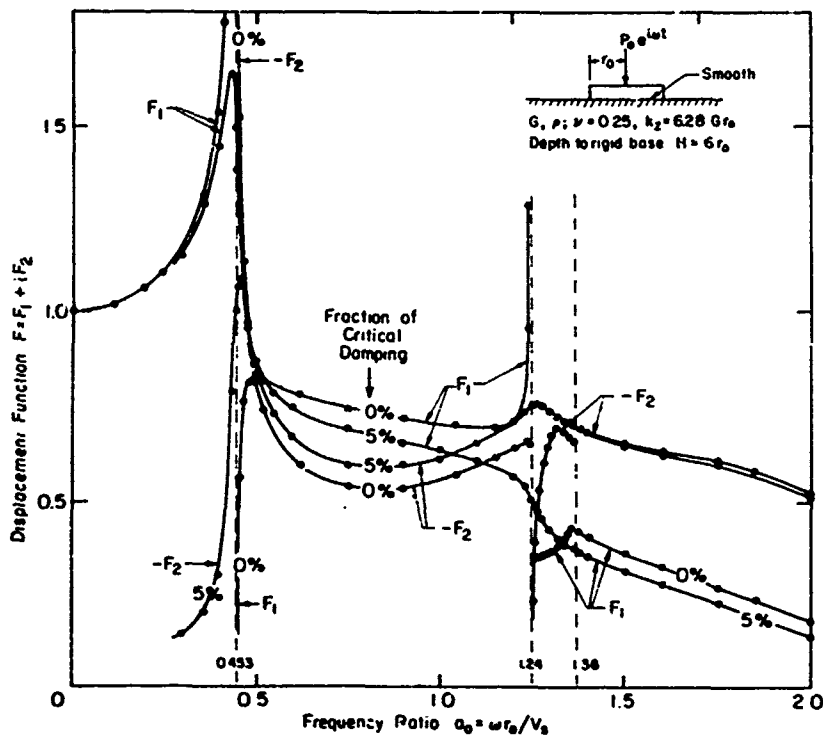


FIG 35 DISPLACEMENT FUNCTIONS FOR VERTICAL MOTION OF CIRCULAR FOOTINGS ON HOMOGENEOUS LAYER (H/r$_0$ = 6)

133
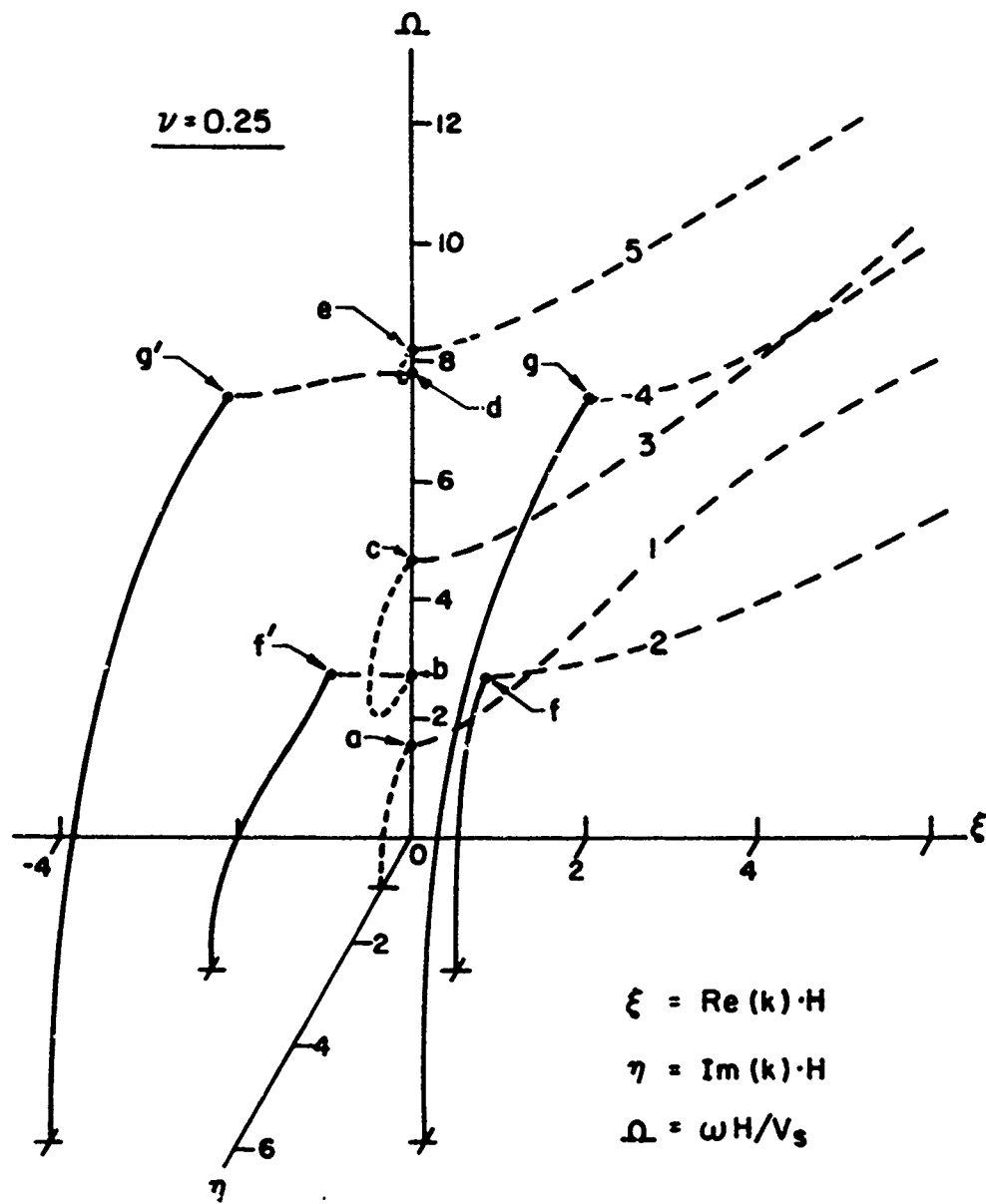
FIG. 36- SPECTRAL LINES FOR WAVE NUMBERS OF
HOMOGENEOUS ELASTIC LAYER OVER ROUGH
RIGID BASE

134
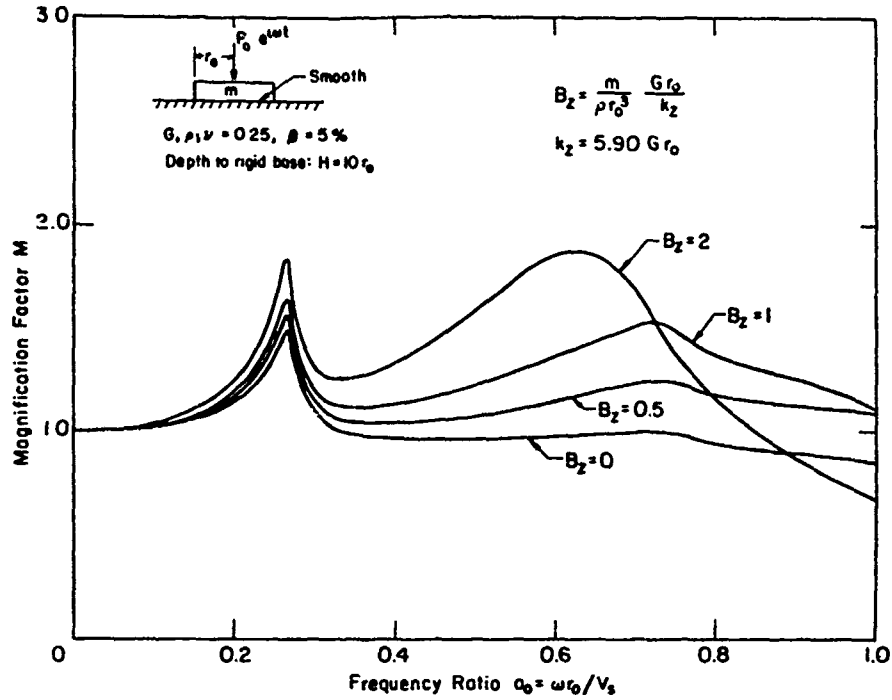
FIG.37- RESPONSE SPECTRA FOR VERTICAL MOTION OF CIRCULAR FOOTINGS ON
HOMOGENEOUS LAYER (H/$r_0$ =10; 5% of critical damping)
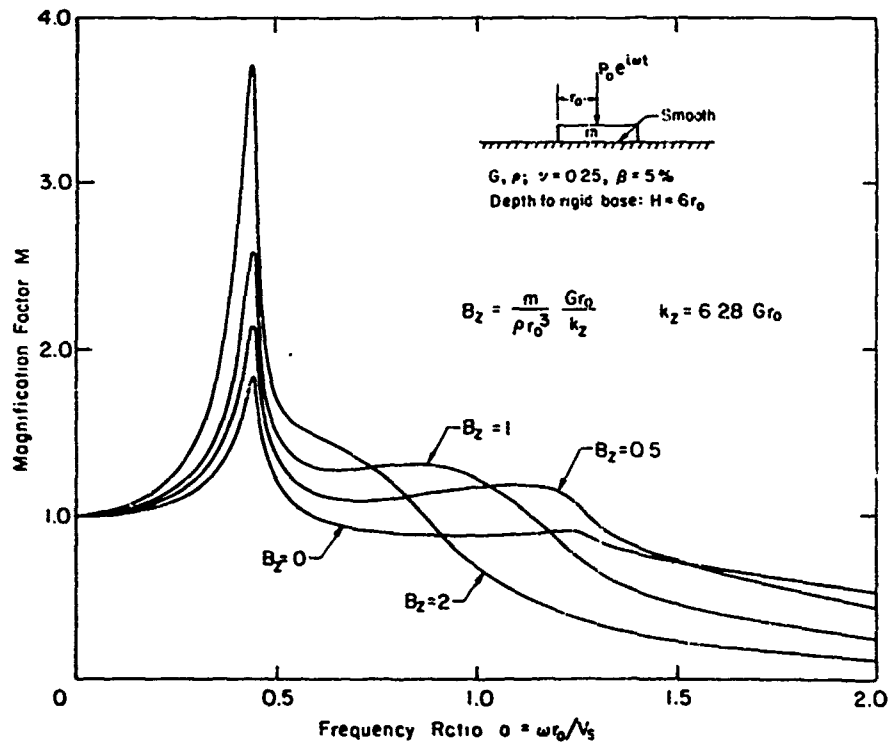


FIG.38-RESPONSE SPECTRA FOR VERTICAL MOTION OF CIRCULAR FOOTINGS
ON HOMOGENEOUS LAYER (H/$r_0$ = 6; 5% of critical damping)

135
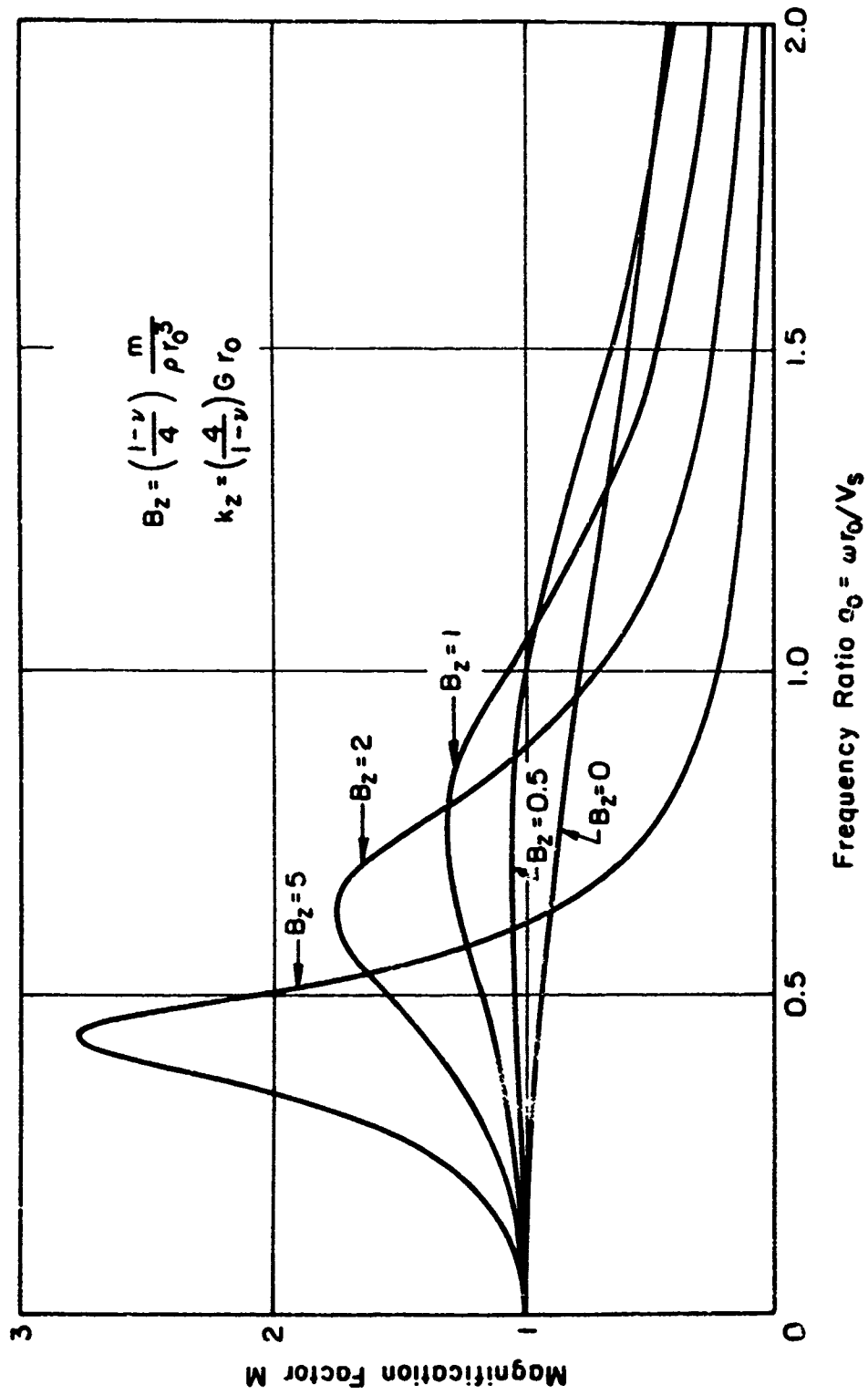
FIG. 39-RESPONSE SPECTRA FOR VERTICAL MOTION OF CIRCULAR FOOTINGS ON HALF SPACE

136
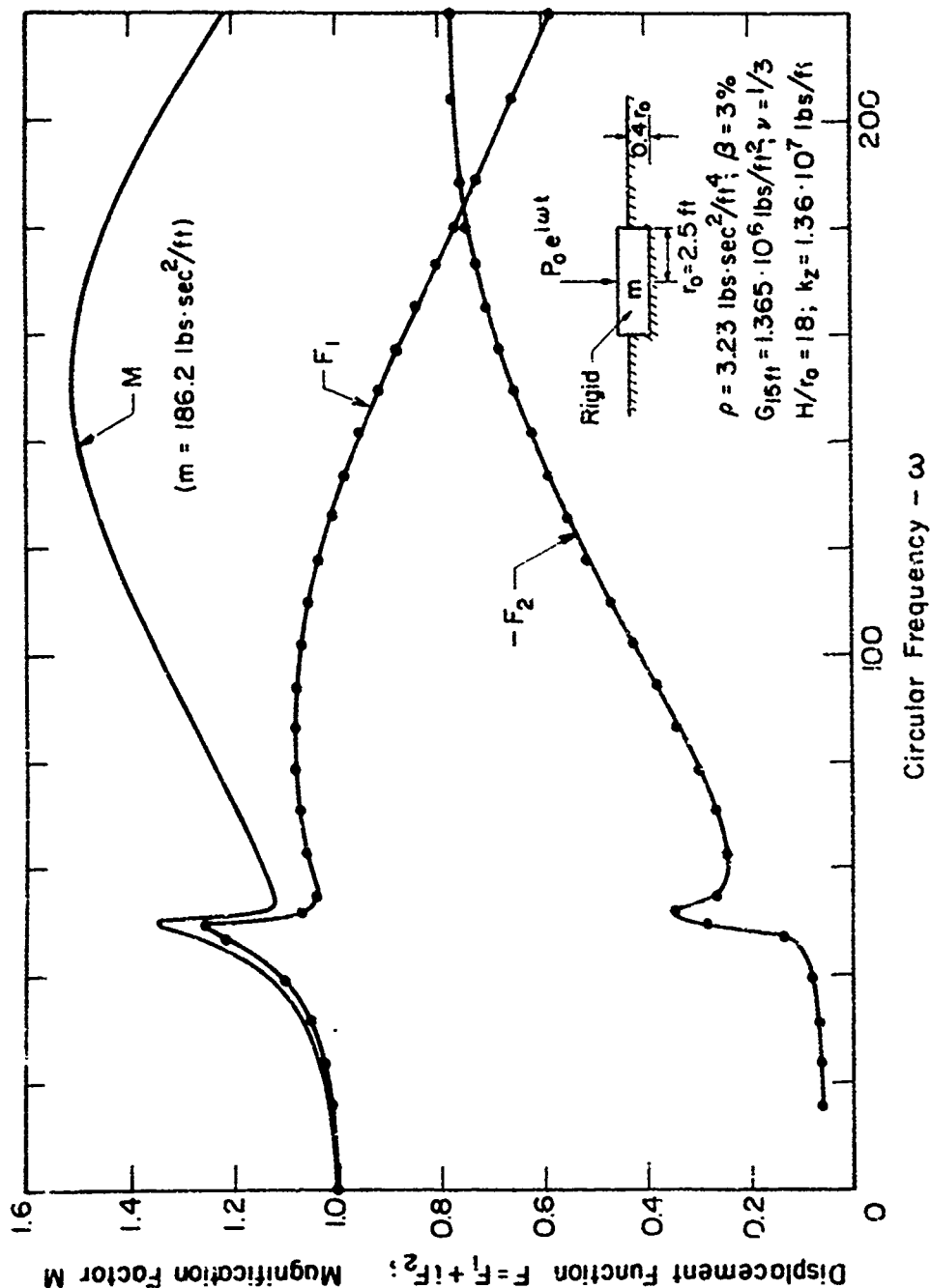
FIG. 40 – DISPLACEMENT FUNCTION AND MAGNIFICATION FACTOR FOR VERTICAL MOTION OF CIRCULAR FOOTING ON INHOMOGENEOUS LAYER

Circular Frequency – $\omega$

Displacement Function $F = F_1 + iF_2$; Magnification Factor M

M

$(m = 186.2 \ lbs \cdot sec^2/ft)$

$F_1$

$-F_2$

$\rho = 3.23 \ lbs \cdot sec^2/ft^4$; $\beta = 3\%$
$G_{15ft} = 1.365 \cdot 10^6 \ lbs/ft^2$, $\nu = 1/3$
$H/r_0 = 18$; $k_z = 1.36 \cdot 10^7 \ lbs/ft$

$P_0 e^{i\omega t}$
$0.4r_0$
$r_0 = 2.5 \ ft$
$m$
Rigid
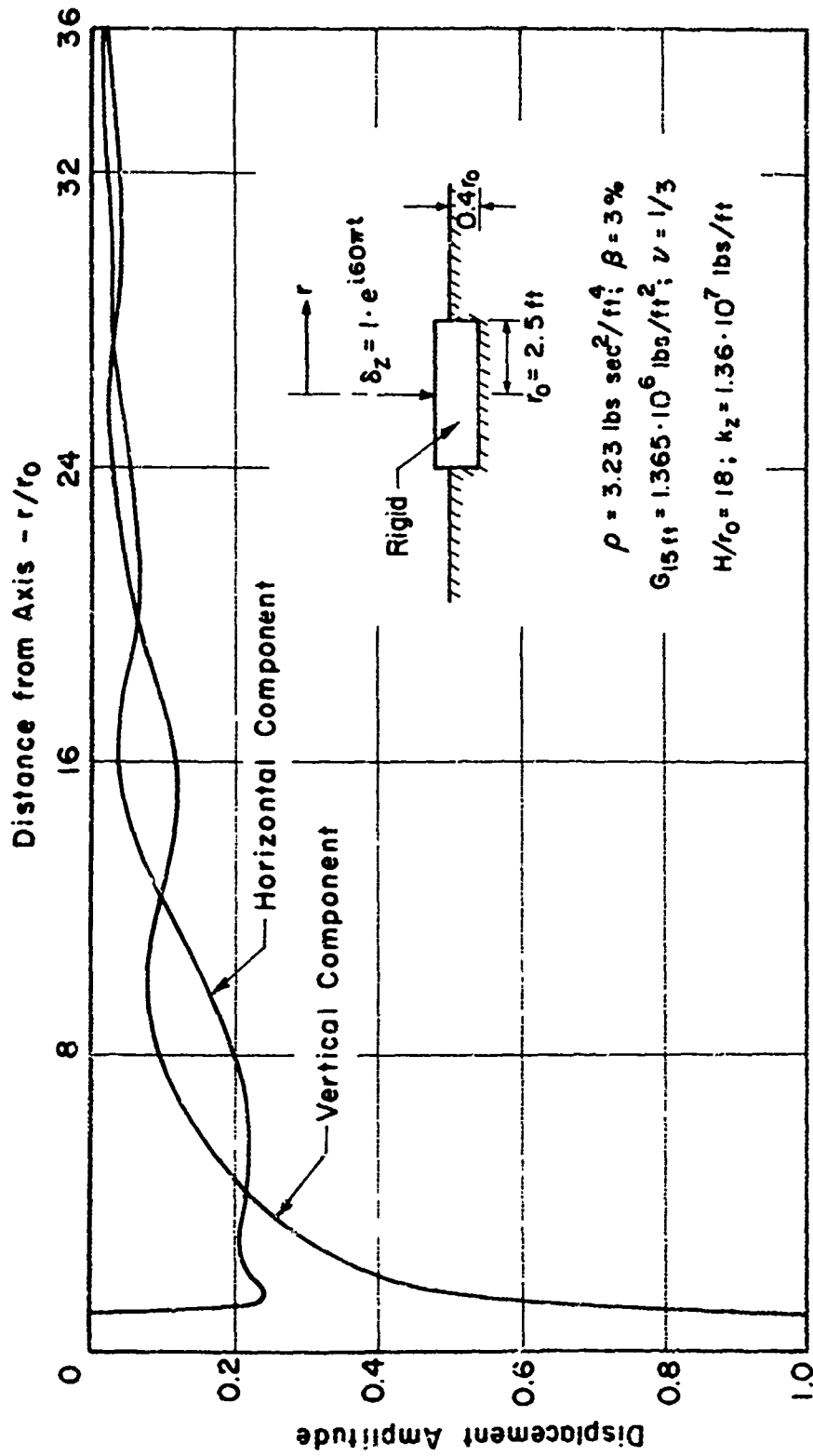
FIG. 41 — DISPLACEMENT AMPLITUDES ALONG SURFACE FOR VERTICAL MOTION OF CIRCULAR FOOTING ON INHOMOGENEOUS LAYER AT $\omega = 60\pi$
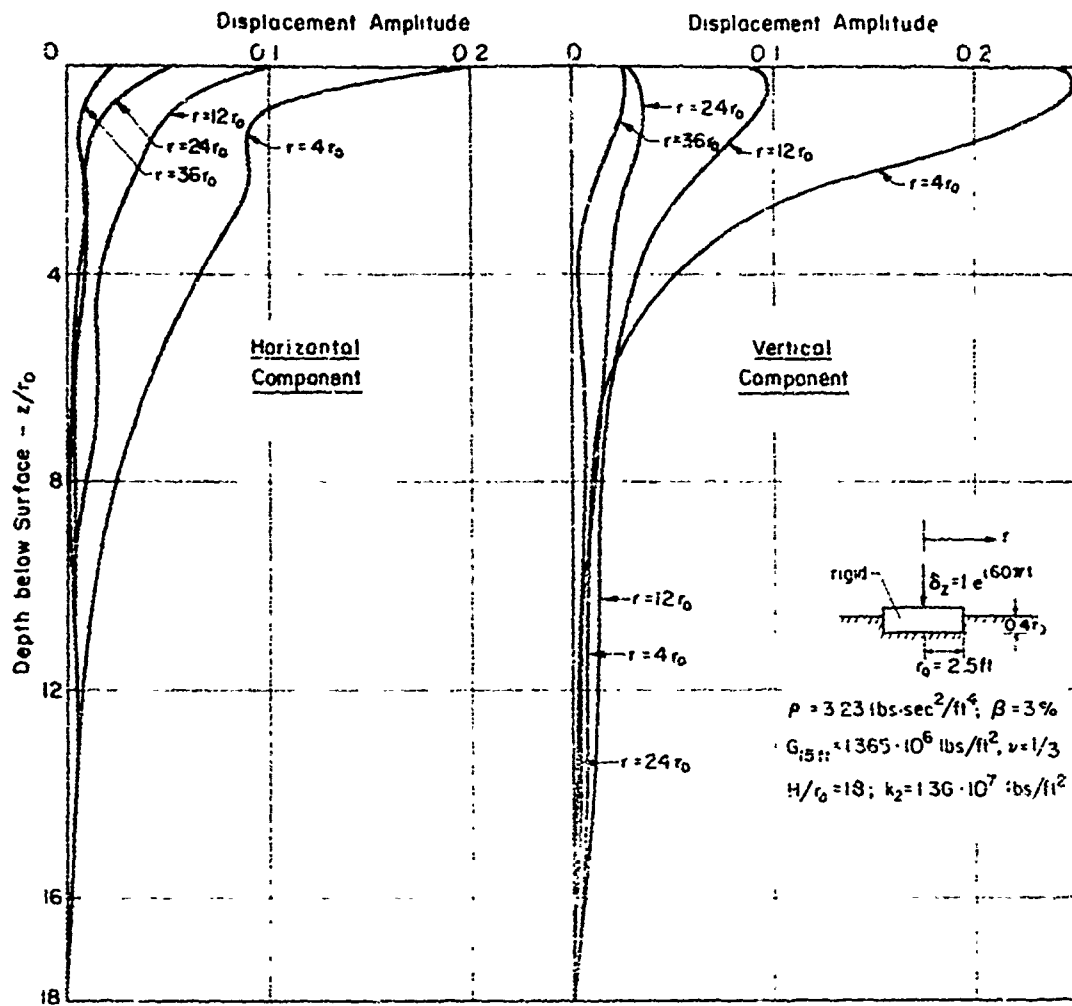
FIG 42 - DISPLACEMENT AMPLITUDES VS DEPTH FOR VERTICAL MOTION OF CIRCULAR
FOOTING ON INHOMOGENEOUS LAYER AT $\omega = 60\pi$

## Table 1

### Displacements for Line Load
### (Love Wave Case)

| Depth z | Solution | Displacement Static Case | | | Displacement Amplitude ω = 2π; β = 0 | | | Displacement Amplitude ω = 2π; β = 0.05 | | |
|---|---|---|---|---|---|---|---|---|---|---|
| | | X = 0.01 | X = 0.1 | X = 1.0 | X = 0.01 | X = 0.1 | X = 1.0 | X = 0.01 | X = 0.1 | X = 1.0 |
| 0.0 | A | 1.4882 | .80605 | .13421 | .8612 | .3601 | .2445 | | | |
| | B | 1.5530 | .81071 | .13436 | .9191 | .3608 | .2414 | .9569 | .3824 | .1505 |
| | C | 1.5451 | .81055 | .13431 | 9147 | .3583 | .2413 | .9522 | .3810 | .1510 |
| | D | 1.5425 | .81049 | .13430 | .9133 | .3575 | .2412 | .9509 | .3805 | .1512 |
| | E | 1.5427 | .81048 | .13430 | 9136 | .3574 | .2412 | .9510 | .3505 | .1512 |
| 0.2 | A | .58442 | .55147 | .12692 | 3448 | .3327 | .1715 | | | |
| | B | .58390 | .55107 | .12704 | .3454 | .3331 | .1692 | .3290 | .3139 | .1114 |
| | C | .58360 | .55156 | .12700 | 3423 | .3305 | .1709 | .3263 | .3117 | .1127 |
| | D | .58617 | .55172 | .12698 | .3413 | .3297 | .1703 | .3254 | .3105 | .1124 |
| | E | .58617 | .55172 | .12698 | .3412 | .3297 | .1703 | .3254 | .3109 | .1124 |
| 0.4 | A | .35718 | .34858 | .10641 | .1825 | .1734 | .1749 | | | |
| | B | .35701 | .34841 | .10647 | .1821 | .1729 | .1763 | .1762 | .1683 | .1228 |
| | C | .35756 | .34881 | .10644 | .1835 | .1745 | .1746 | .1770 | .1694 | .1217 |
| | D | .35774 | .34894 | .10643 | .1840 | .1751 | .1740 | .1773 | .1697 | .1213 |
| | E | .35774 | .34894 | .10643 | .1840 | .1751 | .1740 | .1773 | .1697 | .1213 |
| 0.6 | A | .21437 | .21099 | .07600 | .1484 | .1502 | .2843 | | | |
| | B | .21428 | .21099 | .07603 | .1478 | .1498 | .2831 | .1361 | .1369 | .1842 |
| | C | .21452 | .21109 | .07599 | .1446 | .1465 | .2851 | .1331 | .1340 | .1819 |
| | D | .21460 | .21115 | .07596 | .1435 | .1454 | .2778 | 1321 | .1330 | .1811 |
| | E | .21459 | .21116 | .07595 | .1435 | .1454 | .2778 | .1321 | .1330 | .1811 |
| 0.8 | A | .10159 | .10029 | .03942 | .2088 | .2072 | .2198 | | | |
| | B | .10155 | .10025 | .03943 | .2088 | .2074 | .2206 | .1799 | .1785 | .1413 |
| | C | .10164 | .10033 | .03941 | .2071 | .2057 | .2174 | .1780 | .1766 | .1395 |
| | D | .10167 | .10036 | .03940 | .2066 | .2052 | .2163 | .1775 | .1760 | .1389 |
| | E | .10167 | .10036 | .03940 | .2066 | .2052 | .2163 | .1775 | .1760 | .1389 |

## Table 2

### Phase Shifts for Line Load
### (Love Wave Case)

| Depth z | Solution | Phase Shift in Degrees ω = 2π  β = 0 | | | Phase Shift in Degrees ω = 2π  β = 0.05 | | |
|---|---|---|---|---|---|---|---|
| | | X = 0.01 | X = 0.1 | X = 1.0 | X = 0.01 | X = 0.1 | X = 1.0 |
| 0.0 | A | 28.2 | 85.1 | 5.7 | | | |
| | B | 26.41 | 84.37 | 6.26 | 37.22 | 34.80 | 13.44 |
| | C | 26.32 | 83.61 | 7.77 | 32.21 | 84.20 | 13.42 |
| | D | 26.28 | 83.36 | 8.11 | 32.20 | 85.00 | 14.75 |
| | E | 26.28 | 83.36 | 8.11 | 32.20 | 84.00 | 14.75 |
| 0.2 | A | -119.9 | -128.8 | -25.0 | | | |
| | B | -119.85 | -128.75 | -26.51 | -122.27 | -130.94 | -34.37 |
| | C | -119.50 | -128.64 | -27.23 | -121.90 | -130.82 | -34.93 |
| | D | -119.38 | -128.60 | -27.47 | -121.78 | -130.78 | -35.12 |
| | E | -119.38 | -128.60 | -27.47 | -121.78 | -130.78 | -35.12 |
| 0.4 | A | -162.2 | -167.1 | -101.4 | | | |
| | B | -161.81 | -166.78 | -102.85 | -172.44 | -177.23 | -101.31 |
| | C | -161.56 | -166.51 | -102.85 | -172.11 | -177.04 | -101.86 |
| | D | -161.48 | -166.42 | -102.85 | -172.27 | -177.05 | -101.88 |
| | E | -161.48 | -166.42 | -102.85 | -172.27 | -177.05 | -101.88 |
| 0.6 | A | 67.2 | 63.9 | -127.7 | | | |
| | B | 67.16 | 63.45 | -128.54 | 68.95 | 65.42 | -126.19 |
| | C | 67.14 | 63.44 | -128.96 | 68.91 | 65.38 | -126.62 |
| | D | 67.13 | 63.43 | -129.10 | 68.90 | 65.37 | -126.76 |
| | E | 67.13 | 63.43 | -129.10 | 68.90 | 65.37 | -126.76 |
| 0.8 | A | 45.1 | 42.5 | -133.7 | | | |
| | B | 44.78 | 42.30 | -134.45 | 40.00 | 37.24 | -132.11 |
| | C | 44.28 | 41.83 | -134.97 | 39.26 | 37.03 | -132.60 |
| | D | 44.12 | 41.67 | -135.14 | 39.02 | 36.80 | -132.76 |
| | E | 44.12 | 41.67 | -135.14 | 39.02 | 36.80 | -132.76 |

## Table 3

### Wave Numbers
### (Love Wave Case)

| Solution | $\omega = 2\pi;\ \beta = 0$ Re(k) | $-Im(k)$ | $\omega = 2\pi;\ \beta = 0.05$ Re(k) | $-Im(k)$ |
|---|---|---|---|---|
| B | 6.0835 | 0. | 6.0760 | .32326 |
| C | 6.0836 | 0. | 6.0761 | .32325 |
| D | 6.0836 | 0. | 6.0761 | .32325 |
| E | 6.0836 | 0. | 6.0761 | .32325 |
| B | 4.1378 | 0. | 4.1413 | .47427 |
| C | 4.1514 | 0. | 4.1547 | .47274 |
| D | 4.1559 | 0. | 4.1592 | .47223 |
| E | 4.1559 | 0. | 4.1592 | .47224 |
| B | 0. | 4.8394 | .4028 | 4.8762 |
| C | 0. | 4.7444 | .4107 | 4.7826 |
| D | 0. | 4.7127 | .4133 | 4.7514 |
| E | 0. | 4.7124 | .4134 | 4.7512 |
| B | 0. | 9.2874 | .2112 | 9.3004 |
| C | 0. | 9.0897 | .2158 | 9.1031 |
| D | 0. | 9.0238 | .2173 | 9.0373 |
| E | 0. | 9.0235 | .2173 | 9.0370 |
| B | 0. | 13.183 | .1489 | 13.192 |
| C | 0. | 12.794 | .1534 | 12.803 |
| D | 0. | 12.664 | .1549 | 12.673 |
| E | 0. | 12.664 | .1550 | 12.673 |
| B | 0. | 17.003 | .1155 | 17.009 |
| C | 0. | 16.324 | .1203 | 16.331 |
| D | 0. | 16.098 | .1219 | 16.105 |
| E | 0. | 16.094 | .1220 | 16.102 |
| B | 0. | 20.885 | .0940 | 20.890 |
| C | 0. | 19.798 | .0992 | 19.802 |
| D | 0. | 19.436 | .1009 | 19.441 |
| E | 0. | 19.430 | .1011 | 19.435 |

## Table 4

### Wave Numbers
### (Rayleigh Wave Case)

| Solution | $\omega = 2\pi;\ \beta = 0$ Re(k) | $-Im(k)$ | $\omega = 2\pi;\ \beta = 0.05$ Re(k) | $-Im(k)$ |
|---|---|---|---|---|
| B | 6.7124 | 0. | 6.7051 | .34899 |
| C | 6.7190 | 0. | 6.7117 | .34938 |
| D | 6.7212 | 0. | 6.7139 | .34951 |
| E | 6.7212 | 0. | 6.7139 | .34951 |
| B | 3.8541 | 0. | 3.8321 | .28241 |
| C | 3.8652 | 0. | 3.8422 | .28660 |
| D | 3.8689 | 0. | 3.8456 | .28800 |
| E | 3.8692 | 0. | 3.8457 | .28806 |
| B | 2.2099 | 0. | 2.2088 | .28486 |
| C | 2.2224 | 0. | 2.2212 | .28527 |
| D | 2.2266 | 0. | 2.2253 | .28541 |
| E | 2.2266 | 0. | 2.2253 | .28542 |
| B | 2.3386 | 3.2577 | 2.7047 | 3.2670 |
| C | 2.3421 | 3.1960 | 2.7151 | 3.2029 |
| D | 2.3432 | 3.1755 | 2.7186 | 3.1815 |
| E | 2.3423 | 3.1753 | 2.7104 | 3.1814 |
| B | -2.3386 | 3.2577 | -1.9899 | 3.3129 |
| C | -2.3421 | 3.1960 | -1.9877 | 3.2557 |
| D | -2.3432 | 3.1755 | -1.9869 | 3.2366 |
| E | -2.3429 | 3.1753 | -1.9867 | 3.2366 |
| B | 2.6429 | 7.8605 | 2.8042 | 7.8761 |
| C | 2.7335 | 7.6932 | 2.8977 | 7.7064 |
| D | 2.7637 | 7.6374 | 2.9289 | 7.6498 |
| E | 2.7605 | 7.6383 | 2.9259 | 7.6508 |
| B | -2.6429 | 7.8605 | -2.4832 | 7.8641 |
| C | -2.7335 | 7.6932 | -2.5711 | 7.6997 |
| D | -2.7637 | 7.6374 | -2.6004 | 7.6449 |
| E | -2.7605 | 7.6383 | -2.5972 | 7.6458 |

## Table 5

### Displacements for Line Load
### (Rayleigh Wave Case)

| | Depth z | Solution | Displacement Static Case | | | Displacement Amplitude ω=2π; β=0 | | | Displacement Amplitude ω=2π; β=0.05 | | |
|---|---|---|---|---|---|---|---|---|---|---|---|
| | | | X=0.01 | X=0.1 | X=1.0 | X=0.01 | X=0.1 | X=1.0 | X=0.01 | X=0.1 | X=1.0 |
| Horizontal Component | 0.0 | A | -.08381 | -.08496 | .00147 | .08502 | .08667 | .19462 | .08480 | .08768 | .14113 |
| | | B | -.07569 | -.08416 | .00143 | .07674 | .08520 | .19268 | .07655 | .0862e | .13890 |
| | | C | -.09434 | -.08522 | .00142 | .09563 | .08751 | .19368 | .09540 | .08839 | .13970 |
| | 0.2 | A | .00561 | .04398 | .01394 | .01039 | .08785 | .07334 | .00967 | .08090 | .05117 |
| | | B | .00563 | .04389 | .01398 | .01037 | .08743 | .07307 | .00966 | .08055 | .05100 |
| | | C | .00568 | .04367 | .01396 | .01043 | .08741 | .07392 | .00971 | .08041 | .05145 |
| | 0.4 | A | .00298 | .02790 | .02526 | .00512 | .04742 | .05238 | .00482 | .04458 | .04342 |
| | | B | .00299 | .02800 | .02530 | .00512 | .04748 | .05064 | .00481 | .04462 | .04218 |
| | | C | .00300 | .02802 | .02529 | .00517 | .04796 | .05159 | .00484 | .04493 | .04263 |
| | 0.6 | A | .00191 | .01843 | .02826 | .00311 | .03024 | .08657 | .00286 | .02772 | .06665 |
| | | B | .00191 | .01847 | .02822 | .00311 | .03023 | .08489 | .00286 | .02771 | .06545 |
| | | C | .00191 | .01849 | .02822 | .00311 | .03020 | .08518 | .00285 | .02763 | .06559 |
| Vertical Component | 0.0 | A | .8411 | .3928 | .00106 | .6316 | .2422 | .1329 | .6262 | .2416 | .0932 |
| | | B | .9126 | .3977 | .00122 | .6769 | .2428 | .1350 | .6718 | .2421 | .0932 |
| | | C | .9117 | .3974 | .00118 | .6778 | .2446 | .1341 | .6722 | .2435 | .0928 |
| | 0.2 | A | .3677 | .3358 | .00042 | .2303 | .1918 | .1636 | .2307 | .1915 | .1165 |
| | | B | .3673 | .3352 | .00022 | .2302 | .1919 | .1651 | .2303 | .1913 | .1163 |
| | | C | .3888 | .3350 | .0002? | .2316 | .1929 | .1646 | .2316 | .1922 | .1159 |
| | 0.4 | A | .2259 | .2124 | .00126 | .2003 | .1876 | .1488 | .1848 | .1725 | .1062 |
| | | B | 2260 | .2123 | .00163 | .2004 | .1878 | .1496 | .1847 | .1725 | .1060 |
| | | C | .2265 | .2125 | .00140 | .1998 | .1875 | .1498 | .1838 | .1720 | .1060 |
| | 0.6 | A | .1276 | .1225 | .00343 | .1826 | .1708 | .1116 | .1624 | .1522 | .0791 |
| | | B | .1275 | .1224 | .00354 | .1825 | .1706 | .1121 | .1623 | .1521 | .0792 |
| | | C | .1278 | .1226 | .00352 | .1823 | .1706 | .1125 | .1617 | .1516 | .0796 |

## Table 6

### Phase Shifts for Line Load
### (Rayleigh Wave Case)

| | Depth z | Solution | Phase Shift in Degrees ω=2π; β=0 | | | Phase Shift in Degrees ω=2π; β=0.05 | | |
|---|---|---|---|---|---|---|---|---|
| | | | X=0.01 | X=0.1 | X=1.0 | X=0.01 | X=0.1 | X=1.0 |
| Horizontal Component | 0.0 | A | 176.6 | 149.3 | 170.1 | 170.5 | 140.3 | 166.4 |
| | | B | 176.3 | 148.7 | 168.1 | 170.1 | 139.9 | 164.5 |
| | | C | 177.0 | 149.0 | 167.5 | 170.8 | 140.1 | 164.0 |
| | 0.2 | A | -28.1 | -32.6 | 167.8 | -34.8 | -39.5 | 159.7 |
| | | B | -27.9 | -32.6 | 167.9 | -34.6 | -39.4 | 159.9 |
| | | C | -28.0 | -32.9 | 166.8 | -34.6 | -39.7 | 159.0 |
| | 0.4 | A | -66.4 | -69.4 | 85.2 | -76.5 | -79.5 | 74.6 |
| | | B | -66.2 | -69.2 | 85.4 | -76.2 | -79.2 | 74.6 |
| | | C | -66.4 | -69.4 | 85.3 | -76.4 | -79.5 | 74.2 |
| | 0.6 | A | -146.4 | -149.5 | 48.2 | -152.2 | -155.2 | 66.0 |
| | | B | -145.9 | -148.9 | 4..8 | -151.8 | -154.6 | 45.8 |
| | | C | -146.1 | -149.1 | 47.3 | -152.0 | -154.9 | 45.2 |
| Vertical Component | 0.0 | A | -26.5 | -77.4 | -123.2 | -32.8 | -83.7 | -123.0 |
| | | B | -24.5 | -76.3 | -126.6 | -30.8 | -82.6 | -126.6 |
| | | C | -24.7 | -76.5 | -127.1 | -30.9 | -82.8 | -127.0 |
| | 0.2 | A | -84.7 | -102.2 | -118.4 | -90.1 | -106.5 | -120.4 |
| | | B | -84.9 | -102.5 | -121.7 | -90.2 | -106.8 | -123.9 |
| | | C | -84.5 | -102.5 | -122.2 | -89.9 | -106.8 | -124.3 |
| | 0.4 | A | -144.5 | -151.3 | -117.8 | -148.7 | -155.2 | -122.6 |
| | | B | -144.3 | -151.1 | -120.4 | -148.6 | -155.2 | -125.2 |
| | | C | -144.4 | -151.4 | -1?? 9 | -148.6 | -155.3 | -125.7 |
| | 0.6 | A | -167.0 | -170.4 | -122.7 | -173.9 | -177.0 | -130.5 |
| | | B | -166.8 | -170.2 | -124.7 | -173.7 | -176.9 | -132.6 |
| | | C | -167.3 | -170.7 | -125.3 | -174.1 | -177.3 | -133.2 |

# APPENDIX 1

## SOLUTION METHOD FOR $([A]k^2 + [C])\ \{v\} = \{0\}$

The $n \times n$ matrices $[A]$ and $[C]$ in

$$([A]k^2 + [C])\ \{v\} = \{0\} \tag{A1.1}$$

are tridiagonal, complex symmetric and $[A]$ is well conditioned. The diagonal elements of $[A]$ and $[C]$ are called $a_j$ and $c_j$, $j=1, \ldots, n$, and the off-diagonal elements are called $b_j$ and $d_j$, $j=1, \ldots, n-1$, respectively. The eigenvalues and eigenvectors of Eq. (A1.1) are generally complex.

A determinant search technique employing Newton's iteration method is used to compute the $n$ eigenvalues $\lambda_s = k_s^2$, $s=1, \ldots, n$, of Eq. (A1.1).

The characteristic polynomial to Eq. (A1.1), deflated by the divisors which are already known is

$$f_r = |[A]\ t_r + [C]| \cdot \left( \prod_{s=1}^{m-1} (t_r - \lambda_s) \right)^{-1} \tag{A1.2}$$

in which $t_r$ is the rth approximation to the mth root, $\lambda_m$, and $\lambda_s$, $s=1, \ldots, m-1$, are the roots already calculated.

Newton's iteration scheme is

$$t_{r+1} = t_r - f_r / \dot{f}_r \tag{A1.3}$$

in which $\cdot$ denotes the derivative with respect to $t$. The diagonal elements after triangular factorization of $([A]t_r + [C])$ are

$$u_1 = a_1 t_r + c_1$$
$$u_{j+1} = a_{j+1} t_r + c_{j+1} - (b_j t_r + d_j)^2 / u_j \ ; \quad j=1, \ldots, n-1 \tag{A1.4}$$

Then

$$f_r = \prod_{j=1}^{n} u_j \Big/ \prod_{s=1}^{m-1} (t_r - \lambda_s) \tag{A1.5}$$

143

and

$$\dot{f}_r/f_r = \sum_{j=1}^{n} \dot{u}_j/u_j + \sum_{s=1}^{m-1} 1/(t_r - \lambda_s) \qquad (A1.6)$$

in which

$$\dot{u}_1 = a_1 \qquad (A1.7)$$

$$\dot{u}_{j+1} = a_{j+1} - 2b_j(b_j t_r + d_j)/u_j + (b_j t_r + d_j)^2 \dot{u}_j/u_j^2 \qquad j=1, \ldots, n-1$$

The sth eigenvector corresponding to the eigenvalue $\lambda_s$ is computed by two steps of inverse iteration

$$([A]\lambda_s + [C])\{v_s\}_{r+1} = \{v_s\}_r \quad ; \quad r=1,2 \qquad (A1.8)$$

where $\{v_s\}_1$ is chosen as a full unit vector.

A FORTRAN IV subroutine, ALAMDAB, which is based on the method outlined above is listed in Appendix 5. About 10 iterations are needed on the average to obtain 12 to 14 decimal digits for each eigenvalue.

## APPENDIX 2

## SOLUTION METHOD FOR $([A]k^2 + i[B]k + [C])\ \{v\} = \{0\}$

All eigenvalues $k_s$ and eigenvectors $\{v\}_s$ of

$$([A]k^2 + i[B]k + [C])\ \{v\} = \{0\} \tag{A2.1}$$

are wanted. The matrices [A] and [C] are non-singular, complex symmetric and defined by Eqs. (6.22) and (6.24); [B] is complex skew symmetric and defined by Eq. (6.25). [A], [C], and [B] are of order $m=2n$, typically 30 to 60, and are narrowly banded with bandwidths of 5, 5, and 7, respectively.

Eq. (A2.1) can be transformed into

$$([A]k^2 + [\hat{B}]k + [C])\ \{w_1\} = \{0\} \tag{A2.2}$$

in which

$$[\hat{B}] = i[S][B][S]^{-1} \tag{A2.3}$$

is symmetric and

$$\{w_1\} \propto [S]\ \{v\} \tag{A2.4}$$

The transformation matrix [S] is diagonal and its odd and even numbered diagonal elements are 1 and $i = \sqrt{-1}$, respectively. [A] and [C] are unaltered by the transformation.

Eq. (A2.2) can now be rewritten in the form of a linear eigenvalue problem of double dimension, 2m,

$$([E] - k[F])\ \{w\} = \{0\} \tag{A2.5}$$

in which

$$[E] = \begin{bmatrix} 0 & C \\ C & \hat{B} \end{bmatrix} \tag{A2.6}$$

$$[F] = \begin{bmatrix} C & 0 \\ 0 & -A \end{bmatrix} \tag{A2.7}$$

145

are symmetric 2m x 2m matrices and

$$\{w\} = \begin{Bmatrix} w_1 \\ w_2 \end{Bmatrix} = \begin{Bmatrix} w_1 \\ kw_1 \end{Bmatrix} \tag{A2.8}$$

The 2m eigenvalues of Eq. (A2.4) and their corresponding eigenvectors are in general complex. The row and column eigenvectors are identical because [E] and [F] are symmetric. The eigenvectors are orthogonal to each other with respect to [F] and can be normalized in the sense

$$\{w\}_r^T \ [F] \ \{w\}_s = 0 \quad \text{if } r{\ne}s$$
$$= 1 \quad \text{if } r{=}s \tag{A2.9}$$

The generalized Rayleigh quotient iteration, GRQI, is chosen as solution method because it can take full advantage of the narrow bandwidths of [A], [B], and [C] and it converges rapidly. Ostrowski [37] proved that, under certain conditions, the GRQI's convergence rate is cubic in the limit. GRQI consists of inverse iteration with a shift by the generalized Rayleigh quotient, $\rho$, at each step

$$([E] - \rho_{j-1}[F]) \ \{x\}_j = [F] \ \{x\}_{j-1} \tag{A2.10}$$

$$\rho_j = \frac{\{x\}_j^T \ [E] \ \{x\}_j}{\{x\}_j^T \ [F] \ \{x\}_j} = \rho_{j-1} + \frac{\{x\}_j^T \ [F] \ \{x\}_{j-1}}{\{x\}_j^T \ [F] \ \{x\}_j} \tag{A2.11}$$

where $\{x\}_j^T \ [F] \ \{x\}_j \ne 0$. As $j \to \infty, \{x\}_j$ and $\rho_j$ will go to $\{w\}$ and k, respectively. The generalized Rayleigh Quotient, Eq. (A2.11), is a complex number and is stationary in the neighborhood of an eigenvector [37].

The iteration scheme, Eqs. (A2.10) and (A2.11), is now specialized to take advantage of the structures of [E] and [F]. The steps are

(i) Inverse iteration

$$(\rho_{j-1}^2[A] + \rho_{j-1}[\hat{B}] + [C])\{x_2'\}_j = [C]\{x_1\}_{j-1} - \rho_{j-1}[A]\{x_2\}_{j-1}$$

$$\tag{A2.12}$$

146

$$\{x_1'\}_j = (\{x_2'\}_j - \{x_1\}_{j-1})/\rho_{j=1} \qquad (A2.13)$$

in which the ' indicates a vector which is not normalized;

(ii) Rayleigh Quotient

$$\gamma_j^2 = \{x_1'\}_j^T [C] \{x_1'\}_j - \{x_2'\}^T [A] \{x_2'\}_j \qquad (A2.14)$$

$$\rho_j = \rho_{j-1} + \left(\{x_1'\}_j^T [C] \{x_1\}_{j-1} - \{x_2'\}_j^T [A] \{x_2\}_{j-1}\right)/\gamma_j^2$$

$$(A2.15)$$

(iii) Normalization of vector

$$\{x_1\}_j = \{x_1'\}_j/\rho_j \qquad (A2.16)$$

$$\{x_2\}_j = \{x_2'\}_j/\rho_j \qquad (A2.17)$$

(iv) Check

$$\text{if} \qquad \frac{|\rho_j - \rho_{j-1}|}{|\rho_j|} < \text{tolerance}$$

$$\text{then let} \quad k=\rho_j \text{ and } \{w\} = \begin{Bmatrix} x_1 \\ x_2 \end{Bmatrix}_j$$

otherwise j=j+1 and return to (i).

The matrix in the lefthand side of Eq. (A2.12) has half bandwidth 4, including the diagonal. The triangular factorization is ther fre very fast. The FORTRAN IV subroutine listed in Appendix 6 involves approximately 40 x m complex multiplications and additions per iteration. On the average 7 iterations were needed to find about 12 correct digits of an eigenvalue and its corresponding eigenvector from an arbitrary initial vector.

To avoid convergence towards already known eigenvectors the iteration vector is deflated by Gram-Schmidt's orthogonalization process [49]. In order to keep the computational work involved in the deflation small an arbitrary vector {p} of dimension 2m is selected which is assumed to be complete in the 2m-dimensional space, i.e.

$$\{p\} = \sum_{s=1}^{2m} \{w\}_s \, \alpha_s \quad ; \quad \alpha_s \neq 0 \tag{A2.18}$$

The starting vector $\{x\}_o$ for the iteration towards the rth eigenvector is then obtained by

$$\{x\}_o = \{p\} - \sum_{s=1}^{r-1} \{w\}_s \, \alpha_s \tag{A2.19}$$

with

$$\alpha_s = \{p\}^T \, [F] \, \{w\}_s \tag{A2.20}$$

From the structures of [A], [B], and [C] it follows that if $(k, \{w\})$ is a solution to Eq. (A2.4) then $(-k, \{\tilde{w}\})$ is another solution in which

$$\{\tilde{w}\} = \begin{Bmatrix} \tilde{w}_1 \\ \tilde{w}_2 \end{Bmatrix} = \begin{bmatrix} s^2 & 0 \\ 0 & -s^2 \end{bmatrix} \begin{Bmatrix} w_1 \\ w_2 \end{Bmatrix} \tag{A2.21}$$

Therefore only m eigensolutions to Eq. (A2.4) need to be determined by iteration and the deflation by Eq. (A2.19) can be performed for a pair of eigenvectors, $\{w\}_{2s-1}$ and $\{w\}_{2s} = \{\tilde{w}\}_{2s-1}$, simultaneously.

As Gram-Schmidt's orthogonalization process is sensitive to roundoff errors, the eigenvalues and eigenvectors have to be precise. No difficulties in finding all the eigenvalues and eigenvectors by the presented method have been experienced in a few hundred analyses of problems with dimensions up to 2m = 140 on the CDC 6400 computer, which has a mantissa of 48 binary bits in floating point arithmetic.

The complete solution of a problem with the dimension 2m = 80 takes about 16 seconds on the CDC 6400. The computation time increases with the square of the dimension.

148

# APPENDIX 3

## EXACT SOLUTION FOR LINE LOAD ON HOMOGENEOUS LAYER

The physical system considered is shown in Fig. 16. The loading consists of a harmonic line load, $P = 1 \cdot \exp(i\omega t)$ per unit length.

The motion of the elastic layer is governed by the wave equation

$$\frac{\partial^2 u}{\partial t^2} = \frac{G}{\rho} \left( \frac{\partial^2 u}{\partial x^2} + \frac{\partial^2 u}{\partial z^2} \right) \tag{A3.1}$$

in which u is the displacement in the y-direction, G is the shear modulus, and $\rho$ is the mass density. Eq. (A3.1) has the plane wave solution

$$u(x,z,t) = (A \cos \gamma z + B \sin \gamma z) \exp(i\omega t - ikx) \tag{A3.2}$$

in which A and B are arbitrary constants, k is the wave number, and

$$\gamma = \sqrt{\frac{\omega^2 \rho}{G} - k^2} \tag{A3.3}$$

Satisfaction of the boundary conditions $u(x,H,t) = 0$ and $\tau_{zy}(x \neq 0, z=0, t) = 0$ leads to the eigenfunctions

$$v_s(x,z,t) = \cos(\gamma_s z) \exp(i\omega t - ik_s x) \qquad s=1,2, \ldots \tag{A3.4}$$

in which

$$\gamma_s = \frac{2s-1}{2} \frac{\pi}{H} \tag{A3.5}$$

and

$$k_s^2 = \frac{\omega^2 \rho}{G} - \left( \frac{2s-1}{2} \frac{\pi}{H} \right)^2 \tag{A3.6}$$

An interpretation of the solutions defined by Eqs. (A3.4) to (A3.6) and rules for the choice of the sign on $k_s$ have been given previously in Chapter 4.

The shear stress $\tau_{xy}$ on the plane $x=0$ corresponding to the sth mode is

149

$$\tau_{xy}^{(s)} = G \frac{\partial v_s}{\partial x} = -ik_s G \cos(\gamma_s z) \exp(i\omega t) \tag{A3.7}$$

Because of symmetry about x=0 it is sufficient to consider only the region x>0. The shear stress $\tau_{xy}$ at x=0 vanishes except at the point (0,0) where the load $P = 1 \cdot \exp(i\omega t)$ is applied as a Dirac delta function $\delta(z)$ defined by

$$\delta(z) = 0 \quad \text{for } z \neq 0$$

$$\int_0^\varepsilon \delta(z)dz = \frac{1}{2} \quad \text{for all } \varepsilon > 0 \tag{A3.8}$$

The complete solution is some linear combination of the eigenfunctions given by Eq. (A3.4). The boundary condition at x=0 is therefore

$$\tau_{xy} = \sum_{s=1}^{\infty} \alpha_s \tau_{xy}^{(s)} = -\delta(z) \exp(i\omega t) \tag{A3.9}$$

which by (A3.7) yields

$$iG \sum_{s=1}^{\infty} \alpha_s k_s \cos(\gamma_s z) = \delta(z) \tag{A3.10}$$

The coefficients $\alpha_s$ can be obtained by multiplication of Eq. (A3.10) with $\cos(\gamma_r z)$ and integration over z

$$iG \sum_{s=1}^{\infty} \left[ \alpha_s k_s \int_0^H \cos(\gamma_s z) \cos(\gamma_r z) dz \right] = \int_0^H \delta(z) \cos(\gamma_r z) dz \tag{A3.11}$$

The integral on the right has the value 1/2 and the integrals in the sum vanish except for s=r in which case the value is H/2. Hence Eq. (A3.11) reduces to

$$\alpha_s = \frac{-i}{G H k_s} \quad s=1,2, \ldots \tag{A3.12}$$

which defines the coefficients $\alpha_s$ and the complete solution for x>0 is

150

$$u(x,z,t) = \frac{-i \ \exp(i\omega t)}{G \ H} \sum_{s=1}^{\infty} \frac{\cos(\gamma_s z) \ \exp(-i k_s x)}{k_s} \qquad (A3.13)$$

with $\gamma_s$ and $k_s$ given by Eqs. (A3.5) and (A3.6).

APPENDIX 4

## COMPUTATION OF HANKEL FUNCTIONS

It is not advisable to compute values of the Hankel functions of the second kind and $m$th order, $H_m^{(2)}(z)$, for complex arguments, $z = |z| \exp(i\phi)$, in the range $0 < -\phi < \pi$ from the values of the Bessel functions $J_m(z)$ and $Y_m(z)$ by

$$H_m^{(2)}(z) = J_m(z) - i\, Y_m(z) \tag{A4.1}$$

because severe cancellations occur in the subtraction unless $|z|$ is small (e.g. 9 significant digits would be lost for $|z| = 10$ and $\phi = -5\pi/6$) [2].

The FORTRAN IV subroutine HANKEL, which is listed in Appendix 5, computes $H_0^{(2)}(z)$ and $H_1^{(2)}(z)$ for $0 < -\phi < \pi$ by ascending series if $|z| < 10$ and by asymptotic expansions if $|z| \geq 10$. The computations are based on the following expressions which are taken from [2] and are rewritten. Ascending series:

$$H_0^{(2)}(z) = a + \sum_{k=1}^{\infty} \{a + i2/\pi \cdot (1 + 1/2 + \ldots + 1/k)\}\, b_k^2 \tag{A4.2}$$

$$H_1^{(2)}(z) = [a + i/\pi \cdot (1 + 4/z^2)]\, z/2 \tag{A4.3}$$

$$+ z/2 \cdot \sum_{k=1}^{\infty} \{a + i2/\pi \cdot [1 + 1/2 + \ldots + 1/k + 0.5/(k+1)]\} b_k^2/(k+1)$$

in which $i = \sqrt{-1}$,

$$a = 1 - i2/\pi \cdot [0.577215664901533 + \ln(z/2)] \tag{A4.4}$$

$$b_k = \frac{iz^k}{2k!} \tag{A4.5}$$

Asymptotic expansions:

$$H_m^{(2)}(z) = \sqrt{2/(\pi z)} \cdot \exp(-iz + i\pi m/2 + i\pi/4) \cdot \left(1 + \sum_{k=1}^{\infty} c_k\right) \qquad (A4.6)$$

in which

$$c_k = [k! \ (i8z)^k]^{-1} \cdot \prod_{j=1}^{k} [4m^2 - (2k-1)^2] \qquad (A4.7)$$

In the program, the series, Eqs. (A4.2), (A4.3), and (A4.6), are truncated when $|b_k|$ or $|c_k| < 10^{-8}$. Computed values of $H_o^{(2)}$ and $H_1^{(2)}$ were checked against tables [33, 34] for several values of $|z|$ and $\phi$. The maximum relative error found was about $5 \times 10^{-7}$ and occurred in the transition zone, $|z| \sim 10$, for $\phi \sim -\pi/2$.

# APPENDIX 5

## PROGRAM TORVIB

### Identification:

Analysis of torsional motions of circular footings on, or embedded in, a layered, linearly elastic or viscoelastic medium.

Programmed by Gunter Waas, University of California, Berkeley, June 1972.

### Purpose:

The program is designed to analyze harmonic torsional motions in an axisymmetric system which consists of one or more linearly elastic or viscoelastic layers supported by a rough rigid base. The layered system is subdivided into a finite cylindrical region I and an infinite region R. The two regions are joined together at a cylindrical boundary. The harmonic motions are excited at nodal joints either by harmonic forces acting in the angular direction $\theta$, i.e. perpendicular to the axisymmetric cross-section, or by prescribed displacements in the same direction.

The program consists of the main program TORVIB and the 9 sub-routines: INPUT, BOUNCO, STIFFT, MODIFY, FORCES, DISPLA, ALAMDAB, HANKEL and CYMSOL.

### Discretization:

The region I is discretized by finite elements which are rings with rectangular cross-sections, while the region R is subdivided into sublayers. A typical mesh is presented in the figure below which indicates the order in which elements and nodal joints are numbered.

### Size Limitations:

The program uses dynamic storage allocation for arrays, the length of which is problem dependent. The total storage available for these

154
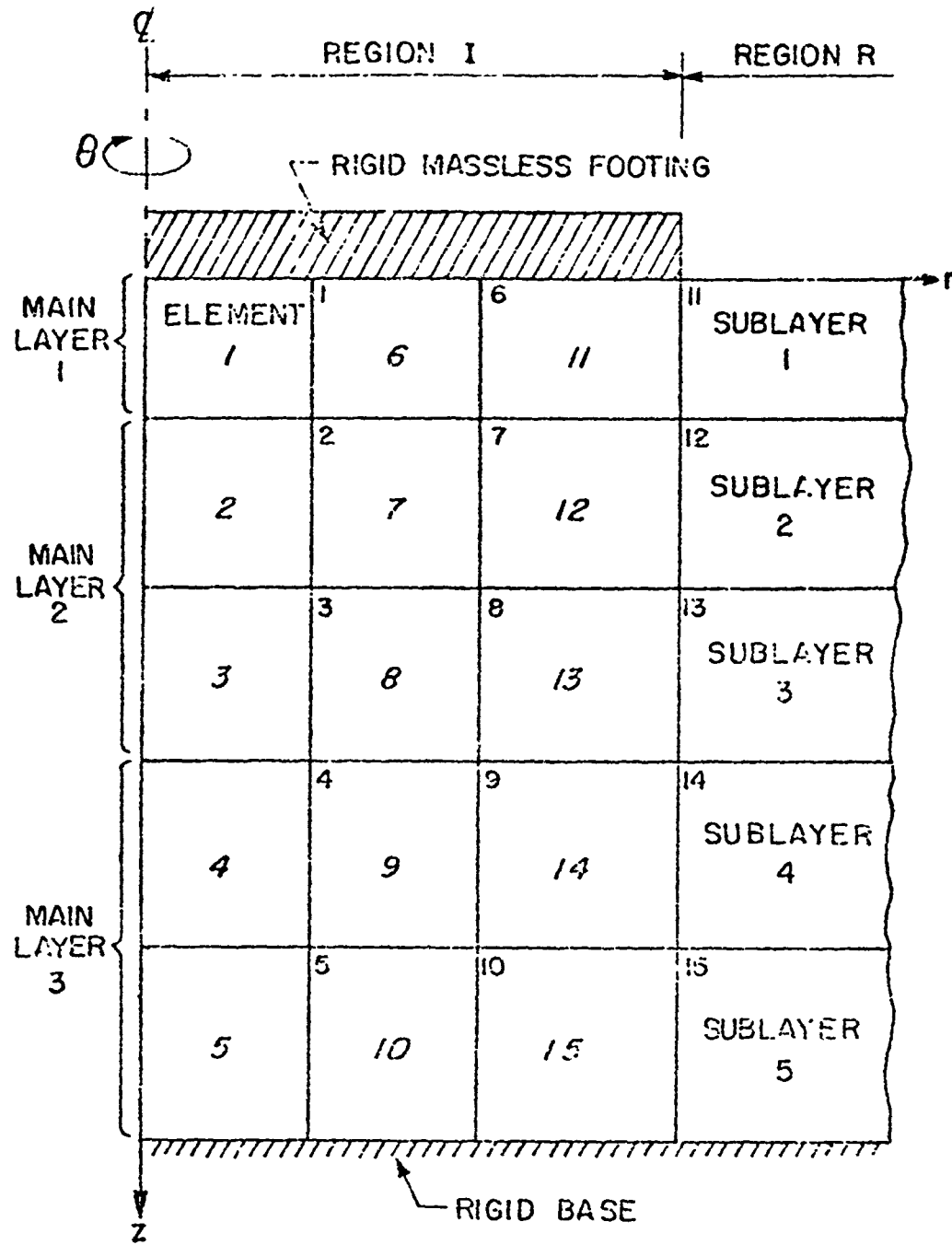
EXAMPLE OF MESH FOR ANALYSIS OF
TORSIONAL MOTION BY PROGRAM TCRVIB

155

arrays is defined by the length, LA, of the array A which appears in the blank COMMON statement of program TORVIB. The required length for any problem is

$$LA > NL^2 (2\ NC + 4) + NL\ (9\ NC + 4\ NDI + 7) + 9\ NDI + 2\ NP + NC$$

in which NL, NC, NDI, and NP are the numbers defined in paragraph B under Input Data.

Input Data:

A. HEADING CARD (12A6) (Read in TORVIB)

Columns 1 to 72 contain alphanumeric data to be printed as titles on the output.

B. CONTROL CARD (8I5) (Read in TORVIB)

Cols. 1-5 No. of main layers, NML
6-10 Total number of sublayers, NL
11-15 No. of columns of elements, NC
16-20 No. of elements, the material properties of which are to be reset, NEC
21-25 No. of nodal loads (external forces or prescribed displacements), NDI
26-30 No. of points in Region R where displacements are to be computed, NP
31-35 Loading parameter, MODE
If MODE=1 loading consists of nodal forces
If MODE=2 loading consists of prescribed nodal displacements
36-40 No. of frequencies at which the system is to be analyzed, NFR

(E.g. in the figure NML=3; NL=5; NC=3, NDI=3; MODE=2)

C. LAYER CARDS (I5,4F10.0) (Read in INPUT)

One card for each main layer commencing with the surface layer and ending with the bottom layer.

Cols. 1-5 No. of sublayers to the main layer, NS
6-15 Thickness of the main layer, X
16-25 Mass density of the main layer, Y
26-35 Real part of the shear modulus, $C_1$
36-45 Imaginary part of the shear modulus, $C_2$

Note: These data also define the thickness and the material properties of the finite elements in Region I.

D. RADIAL COORDINATE CARDS (5F10.0) (Read in INPUT)

As many cards are used as needed to contain the radial coordinates of the vertical grid lines, commencing with the line next to the axis

156

of symmetry and ending with the line which defines the boundary
between Region I and Region R. (E.g., the radial coordinates in
the figure are those of nodal joints 1, 6, and 11) The number of
radial coordinates, NC, is specified in the Control Card.

E.  ELEMENT MODIFICATION CARDS (4I5,3F10.0) (Read in INPUT)

These cards are omitted if NEC=0, c . Control Card. The material
properties of the elements are al $\tau$   .y defined by the Layer Cards.
However, the material properties of some elements may be changed to
any other values including zero. To do this one card must be input
for each rectangular block of elements for which the properties are
to be reset.

Cols.  1-5  No. of uppermost sublayer of block, IB
       6-10 No. of lowermost sublayer of block, IE
       11-15 No. of leftmost column of block, JB
       16-20 No. of rightmost column of block, JE
       21-30 Mass density, RO
       31-40 Real part of shear modulus, $G_1$
       41-50 Imaginary part of shear modulus, $G_2$
(E.g., if the properties of the elements 13 and 14 are to be changed
then IB=3, IE=4, JB=3, JE=3, and NEC=2 in Control Card.

F.  LOAD CARDS FOR FORCES (I5,2F10.0) (Read in INPUT)

These cards are omitted if MODE=2 in Control Card. One card is
needed for each nodal joint at which an external force is applied.

Cols.  1-5  Number of the nodal joint at which force is applied
       6-15 Real part of force per radian
       16-25 Imaginary part of force per radian

G.  LOAD CARDS FOR DISPLACEMENTS (10I5) (Read in INPUT)

These cards are omitted if MODE=1 in the Control Card. The cards
contain the numbers of the nodal joints at which non-zero angular
displacements are prescribed. All displacements are then auto-
matically prescribed to be in phase and have an amplitude equal to
the radius of the respective nodal joint. As many cards are used as
needed to contain all nodal joints with prescribed non-zero displace-
ments. The number of these nodal joints is equal to NDI specified
in the Control Card.
(In the example the nodal joints are 1, 6, and 11)

H.  OUTPUT SPECIFICATION CARDS (I5,F10.0) (Read in INPUT)

Cols.  1-5  Number of the interface passing through the point at
            which the motion in Region R is to be computed, IZ.
            Interfaces are numbered from the surface downward
            commencing with 1.
       6-15 r-ordinate of point at which motion is to be computed, RR
Use one card for each point in Region R. The number of points, NP,
is specified in the Control Card.

1. FREQUENCY CARDS (F10.0) (Read in TORVIB)

   Cols. 1-10 Angular frequency in radians per unit time
   One card for each frequency at which the system is to be analyzed.
   The number of frequencies, NFR, is specified in the Control Card.

Several problems may be analyzed in one run.  The data set for each
problem commences with a Heading Card.


Output Information:

   The program prints the following output:

   (i) Input and generated data.

   (ii) Nodal displacements including amplitudes and phase angles for
        all nodal joints in Region I and for specified points in Region R.

   (iii) Reaction forces for nodal joints at which non-zero displace-
         ments are prescribed, including amplitudes and phase angles.

Listing of Program TORVIB:

```
      PROGRAM TORVIB (INPUT,OUTPUT)
      COMMON/BLOCKA/NL,NC,NDI,NP,MODE,NDF,NB,NEC,NDFN,RAD,NHL
      COMMON/BLOCK5/M,MOI(2)
      COMMON A(300,300)
C
C     THE LENGTH OF THE ARRAY A MUST BE LARGER THAN
C     NL*NL*(2*NS+4)*NL*(9*NC+4*NDI+7)+9*NDI+2**NP*NC
      IF (NHL.LT.1) STOP
100   READ 1000,NEC,NHL,NC,NDI,NP,MODE,NP,MODE,NFR
      PRINT 2000,NEC,NHL,NC,NDI,NP,MODE,NP,MODE,NFR
      RAD=1./NEC
      NHL=NHL*NL
      M1=1
      M2=M1  +NL
      M3=M2  +NL
      M4=M3  +NL
      M5=M4  +NDF
      M6=M5  +NDF*NDF
      M7=M6  +NDI
      M8=M7  +NDI
      M9=M8  +NP
      M10=M9 +AL*NL
      M11=M10+M12*AL*NL
      M12=M11+N2*NL*2
      M13=M12+N2*NL*2
      M14=M13+N5*NHL*(NDF*NB-2)
      M17=M16+NDF*NDF
      L=M17+NDF*NB*2-1
      CALL INPUT   (A(M1),A(M2),A(M3),A(M4),A(M5),A(M6),A(M7),A(M8),
     1             A(M9),A(M10),A(M11),NL)
C
200   READ 1001,OMEGA
      PRINT 2001,OMEGA
      NCOUNT=NCOUNT+1
      OK=OMEGA**2
      CALL BOUNDCO(A(M1),A(M3),A(M2),A(M6-1),OK,A(M12),A(M13),A(M14),
     1             A(M7),NL,NDF)
      CALL STIFFT (A(M6),A(M3),A(M7),A(M5),0.,A(M7),NL,NDF)
      CALL MODIFY (A(M7),A(M6),A(M5),A(M2),A(M7),A(M5),A(M5),NDF)
      CALL CMPSULC(A(M7),A(M7),A(M6),NDF,NDF,NU)
      PRINT 2012
      J=M16-1
      DO 50 K=1,NDF
      I=J+1
      J=J+2
      X=SQRT(A(I)**2+A(J)**2)
      Y=0.
      IF(X.GT.0.) Y=ATA N2(A(J),A(I))*RAD
50    PRINT 2002,K,A(I),A(J),X,Y
      IF(MODE.EQ.2) CALL FORCES (A(M5),A(M6),A(M7),NU2)
      IF(NP.GT.0) CALL DISPLA (A(M13),A(M4),A(M12),A(M16),A(M17),
     1             A(M10),A(M11),A(M4),A(M6-1),NL)
      IF (NCOUNT.LT.NFR) GO TO 200
      GO TO 100
C
1000  FORMAT (12A6,M15)
1001  FORMAT (F10.4)
2000  FORMAT (1H1,12A6/
     1/15.59H MAIN LAYERS
     2/15.59H ROWS OF ELEMENTS OR SUBLAYERS
     3/15.59H COLUMNS OF ELEMENTS
     4/15.59H ELEMENTS WITH PROPERTIES TO BE CHANGED
     5/15.59H NO. OF PRESCRIBED FORCES OR UNIT RADIAN DISPLACEMENTS,
     6/15.59H PRINTS BEFORE BOUNDARY WHERE DISPLACEMENTS ARE REQUESTED
     7/15.30H IF 1 FORCES,IF 2 UNIT RADIAN DISPLACEMENTS ARE PRESCRIBED
     8/15.30H FREQUENCIES WILL BE ANALYZED /)
2001  FORMAT (1H1,30X,20HCIRCULAR FREQUENCY =,E13.6)
2002  FORMAT (15.3X,3E15.6,E13.4)
2012  FORMAT (///10X,33HDISPLACEMENTS OF NODAL JOINTS //
     1             17H JOINT     REAL PART     IMAG. PART     ABS. VALUE     PHASE
     2SHIFT )
C
      END

      SUBROUTINE INPUT (ROL,GL,H,Z,R,RO,G,IDX,F,RP,IZ,N)
C
C     READS AND PRINTS INPUT DATA
C
      COMMON/BLOCKA/NL,NC,NDI,NP,MODE,NDF,NB,NEC,NDFN,RAD,NHL
      DIMENSION RO(N),MIN(N),ZIN(R(1),R(1),ROIN,1),IGN(1),RR(1),IZ(1))
      COMPLEX    GLN,GLN,11,F(1),C
C             LAYER PROPERTIES
C
      ZM=0.
      L=0
      PRINT 2011
      DO 20 I=1,NHL
      READ 1001,NS,X,Y,C
      X=X/NS
      DO 20 J=1,NS
      L=L+1
      Z(L)=ZM
      ZM=ZM+X
```

```
      ML).)<4
      WOL(I)=Y
      GI(L)=C
      DO 10 K=1,NC
      AJ(L,K)=Y
   10 GI(L,K)=C
   20 PRINT 2001,L,R,ZM,Y,C
C     IF (L.LE.N) GO TO 20
      RADIAL COORDINATES OF ELEMENT COLUMNS
      PRINT 2012
      READ 1002,(RR(L),L=1,NC)
      PRINT 1002,(RR(L),L=1,NC)
      PROPERTY CHANGES OF ELEMENTS
      IF (NSC.LT.1) GO TO 45
      PRINT 2013
      DO 30 L=1,NC
      READ 1001,J,C
      ICN(L)=J
      F(L)=C
   30 PRINT 2003,IDN(L),GI(L)
      GO TO 60
C     IF (N=NEC)30,45,90
      INPUT OF DISPLACEMENTS OR FORCES
   45 IF(NODE.EQ.2) GO TO 55
      PRINT 2015
      DO 50 L=1,ND
      READ 1001,J,C
   50 PRINT 2003,IDN(L),L=1,ND))
      READ 1004,((DN(L),L=1,ND))
   55 READ 1004,((IN(L),L=1,ND))
      PRINT 2004,((IN(L),L=1,ND))
      POINTS BEYOND BOUNDARY WHERE DISPLACEMENTS ARE REQUESTED
   60 IF (N.LT.1) GO TO 75
      PRINT 2016
      DO 70 L=1,NP
      READ 2001,(I,RDI(L,J),GI(L,J),J=1,NC)
   70 PRINT 2001,(I,RDI(L,J),GI(L,J),J=1,NC)
      PRINT MATERIAL PROPERTIES OF ELEMENTS
   75 PRINT 2016
      DO 80 I=1,NL
   80 PRINT 2006,(I,RDI(L,J),GI(L,J),J=1,NC)
      GO TO 100
   90 PRINT 2023
  100 CALL EXIT
C
 1001 FORMAT (I5,4F10.4)
 2001 FORMAT (I5,X,5E12.5)
 2023 FORMAT (I5,2X,2E15.5)
 2016 FORMAT (/30 H LAYER PROPERTIES (FROM TOP TO BOTTOM) /
     167H LAYER    THICKNESS    DEPTH BE-    DENSITY    SHEAR MOD.  SHEAR M
     2OD.  /21X.44HLOW LAYER         REAL PART     IMAG.PART )
 2012 FORMAT (/ 30H RADIAL COORDINATES OF COLUMNS )
 1002 FORMAT ( 5F10.4)
 2013 FORMAT (4I5,3F10.4)
 2003 FORMAT (/ 17H EXTERNAL MOMENTS /
     133H JOINT    REAL MOMENT    IMAG.MOMENT )
 1004 FORMAT (10I5)
 2004 FORMAT (/ 47H JOINTS WITH APPLIED UNIT ANGULAR DISPLACEMENTS /
     1 (10I5))
```

```
 2015 FORMAT (/ 57H POINTS BEYOND BOUNDARY WHERE DISPLACEMENTS ARE REQUE
     1STED / 21H DEPTH    RADIAL COORD. )
 2016 FORMAT (/ 32H MATERIAL PROPERTIES OF ELEMENTS /
     143H    FOR COL.  DENSITY    SHEAR MOD.    SHEAR MOD.   /
     248H                                       REAL PART    IMAG.PART )
 2006 FORMAT (2I5,3E12.5)
 2020 FORMAT (//20H ERROR IN INPUT DATA )
      END

      SUBROUTINE BOUNCO (RO,H,G,R,D4,EV,V,V1,BM,N,M,YM)

C     FORMS BOUNDARY MATRIX
C
      COMMON/BLO/XA/NL,NC,NDI,NP,NHUE,NDF,NH,NEC,N)FN
      REAL    RO,N1,M(N)
      COMPLEX  G(I),EV(R),V(N,N),V1(N,N),BM(NM,1)
      COMPLEX  C,CC,D,CD
C     GENERATE MATRICES OF EIGENVALUE PROBLEM
C
      N1=N-1
      C=0.
      X=0.
      D=0.
      DO 10 J=1,N
      CC=G(J)*H(J)/3.
      BM(J)=CC*C
      BM(J+N)=CC*.5
      XX=CM*RO(J)*H(J)/3.
      DD=G(J)/H(J)
      V(I,J)=XX*X-DD-D
      V1(J+N)=XX*.5+DD
      C=CC
      X=XX
   10 D=DD
      BM(N+N)=0.
      V1(N+N)=0.
C                          SOLVE EIGENVALUE PROBLEM
      I=1+N
      J=1+N
      K=J+N
      L=K+N
      M=L+N
      CALL ALAMDAS (V1(1),V1(.),BM(1),BM(1),EV,V,BM(J),BM(K),BM(L),
     1             (1M),V(J),V(K),N)
C                  GET THE WAVE NUMBERS
      PRINT 2000
      DO 15 J=1,N
      C=CSQ.T(EV(J))
      X= REAL(C)
      Y=AIMAG(C)
      IF (Y.EQ.0..AND.X.LT.0.) C=-C
      IF (Y.GT.0.) C=-C
      EV(J)=C
   15 PRINT 2001,J,EV(J)
C                  GENERATE BOUNDARY MATRIX
      DO 20 J=1,N
      V(1,1)=BM(1)*V(1,J)+BM(1+N)*V(2,J)
      V(J,N)=BM(N1)*V(N1,J)+BM(N)*V(N,J)
      DO 20 I=2,N1
      K=I-1
   20 V(I,J,I)=BM(K+N)*V(K,J)+BM(I)*V(I,J)+BM(I+N)*V(I+1,J)
```

```
      M=M+2
      DO 30 K=1,N
      CREVIK)=R
      CALL HANKEL (C,D,CD,CC)
   30 SPFK,L)=2.-C*CC
      DO 50 I=1,N
      L=I-1.
   40 SPK,M)=V(K,I)*SMI(K,L)
      DO 50 J=1,N
      C=C.
   45 C=C+V(K,J)*SM(K,M)
   50 SP(I+V)+Y,J-N))=C
      RETURN
 2000 FORMAT (///,13X,12HWAVE NUMBERS/37H      NO.      REAL PART      IMAGINAR
     1Y PART )
 2001 FORMAT (I5,2X,2E15.8)
      END

C
C
      SUBROUTINE STIFFT (KO,H,G,R,OM,A,N,NM)
C
C     SCANS GLOBAL DYNAMIC STIFFNESS MATRIX
C
      COMMON/BLOCKA/NL,NC,NDI,NP,MODE,NDF,NB,NEC,NDFN
     #F&L
      COMPLEX RC(*,1),H(1),R(1)
      COMPLEX GIN(1),AINM,1)
      COMPLEX C,CA,CB,CC,CD,CE,CF
      N1=N-1
      N2=N+1
      CM3=OM/3.
C
C     INITIALIZE STIFFNESS MATRIX
C
      IF (NDI.GT.1) GO TO 5
      DO 4 I=1,NDFN
      DO 4 J=1,NB
    4 A(I,J)=C.
    5 L=NDFK+1
      K=NN
      DO 6 I=1,NM
      K=K-2
    20 6 J=K,NB
    6 A(I,J)=0.
C
C     FIRST ELEMENT COLUMN
C
      R=R(1)*2/4.
      DO 10 J=1,N1
      C=G(J,1)/H(J)*RA
      X=CM3*RO2(J,1)*H(J)*RA
      K=J+1
      A(J,1)=A(J,1)*C-X
      A(J,2)=A(J,2)-C-X*.5
   10 A(K,1)=A(K,1)*C-X
      A(N,1)=A(N,1)*(G(N,1)/H(N)-CM3*RO(N,1)*H(N))*RA
      IF (NC.LT.2) GO TO 40
C     SECOND TO LAST ELEMENT COLUMN
C
      L=0
      DO 30 I=2,NC
      K=J-1
      RD=RD(I)-R(K)
      PG=RD/12.
      X=(ALOG(R(I)/R(K))
      G=(R(I)/R(J))**2*X
```

```
      RB=R(K)*R(1)/RD**2*X
      RC=(R(K)/RD)**2*X
      RD=R(I)*3.*R(K)
      RE=R(I)+R(K)
      PF=R(K)*3.*R(I)
      DO 20 J=1,N1
      L=L+1
      LA=L+1
      LN=L+N
      LO=L+N1
      CA=G(J,1)*H(J)/3.
      CB=.5*CA
      G  =G(J,1)/H(J)*RG
      X  =OM3*RO(J,1)*H(J)*RG
      CC= C.- X
      CD=-C-X*.5
      CE= CA*RA+CC*RD
      CF=-CA*HB+CC*RE
      A(L ,1 )=A(L ,1 )+CE
      A(L ,2 )=A(L ,2 )+CB*RA+CC*RD
      A(L ,NA)=A(L ,NA)+CF
      C=CB*PC+CC*RF
      A(LL,1 )=A(LL,1 )+CE
      A(LA,1 )=A(LA,1 )+CE
      A(LO,1 )=A(LO,1 )+C
   20 A(LN,2 )=A(LN,2 )+CB*PC+CC*RF
      L=L+1
      LN=L+N
      CC=(G(K,1)/H(N)-OM3*RC(N,1)*H(N))*RG
      C =G(N,1)*H(N)/3.
      A(L ,1 )=A(L ,1 )+C*RA+CC*RD
      A(L ,NA)=A(L ,NA)-C*RB+CC*RE
      A(L ,NA)=A(L ,NA)+C*RC+CC*RF
   30 A(LN,1 )=A(LN,1 )+C*PC+CC*RF
   40 RETURN
      END

C
C
      SUBROUTINE MODIFY (A,B,ION,F,S,R,NOFD)
C
C     MODIFIES MATRIX EQUATION FOR PRESCRIBED DISPLACEMENTS
C
      COMMON/BLOCKA/NL,NC,NDI,NP,MODE,NDF,NB,NEC,NDFN,P'D
      DIMENSION ION(1),R(1)
      COMPLEX A(NOFD,1),S(1),B(1),F(1)
C
      DO 10 J=1,NDF
   10 B(J)=0.
      IF (MODE.EQ.1) GO TO 60
      K=0
      DO 50 ID=1,NDI
      L =ION(ID)
      L+L+1
      L9=L-1
      I=(C/NL+1
      DIS=F(I)
      DO 20 J=1,NB
      I=L9+J
      IF (I.GT.NDF) GO TO 30
```

161

```
            K=K+1
            SIN)=AI(L,J)
   20       R(I)=B(I)=- DIS *A(L,J)
   50       DO 40 J=2,NB
            I=L(-J
            IF (I.LT.1) GO TO 50
            K=K+1
            SIN)=A(I,J)
   40       R(I)=B(I)=- DIS *A(I,J)
   50       CONTINUE
            DO 150 ID=1,NDI
            L=IDN(ID)
            LI=L-I
            I=(L-1)/NL+1
            B(I)=R(I)
   120      DO 120 J=1,NB
            AI(L,J)=0.
            I=L1-J
            IF(I.LT.1) GO TO 150
            I=L1-J
   140      IF(I.LT.1) GO TO 150
   150      CONTINUE
            GO TO 100
   50       DO 70 ID=1,NDI
            L=IDN(ID)
   70       B(L)=F(ID)
  100       RETURN
            END

C
            SUBROUTINE FORCES (S,B,IDN,R)
C
            COMPUTES REACTION MOMENTS
C
            COMMON/BLOCKA/NL,NC,NDI,NP,MODE,NIF,NB,NEC,NDFN,RAD
            DIMENSION IDN(1),R(1)
            COMPLEX S(1),B(1),FT,C
C
            PRINT 2011
            K=0
            FT=0.
            DO 60 ID=1,NDI
            L =IDN(ID)
            L1=L+1
            L9=L-1
            I=L9/NL+1
            DIS=R(I)
            C=0.
            DO 2) J=1,NB
            Y=K+1
            IF (I.GT.NDF) GO TO 30
            Y=K+1
   20       C=C+S(K)*B(I)
   30       DO 40 J=2,NB
            I=L1-J
            IF (I.LT.1) GO TO 50
            K=K+1
   40       C=C+S(K)*B(I)
   50       X=CABS(C)
            Y=0.
            IF(X.GT.0.) Y=ATAN2(AIMAG(C),REAL(C))*RAD
```

```
   60       PRINT 2001,L,C,X,Y
            FT= C
            PRINT 2012
            X=CABS(FT)
            Y=0.
            IF(X.GT.0.) Y=ATAN2(AIMAG(FT),REAL(FT))*RAD
            PRINT 2002,FT,X,Y
            PRINT 2013
            C=1.,FT
            X=CABS(C)
            Y=0.
            IF(X.GT.0.) Y=ATAN2(AIMAG(C),REAL(C))*RAD
            PRINT 2002, C,X,Y
            RETURN
C
 2001 FORMAT (I5,3X,3E15.6,F13.4)
 2002 FORMAT (3E15.6,F13.4)
 2011 FORMAT (//10X,24H MOMENTS AT NODAL JOINTS          //       ABS. VALUE       PHASE
     1 2DH JOINT          REAL PART          IMAG. PART       )
 2012 FORMAT (//40H TOTAL MOMENT TO PRODUCE A UNIT ROTATION /
     1 61H      REAL PART          IMAG. PART          ABS. VALUE      PHASE SHIFT )
 2013 FORMAT (//35H ROTATION PRODUCED BY A UNIT MOMENT /
     1 61H      REAL PART          IMAG. PART          ABS. VALUE      PHASE SHIFT )
            END

C
            SUBROUTINE DISPLA (V,VI,EV,REAL,RR,IZ,P,V)
C
C           COMPUTES DISPLACEMENTS IN REGION R (BEYOND THE BOUNDARY)
C
            COMMON/BLOCKA/NL,NC,NDI,NP,MODE,NDF,NB,NEC,NDFN,RAD
            DIMENSION RR(1),IZ(1) ,Z(N)
            COMPLEX   VIN,NJ,VI(5,N),B(1),AL(N),EV(N)
            COMPLEX   C,CC,AR,H0,H1
            NN=NDF-NL
            C=0.
            DO 20 I=1,NL
   10       C=C+B(IN+J)*EV(I,J)
            AR=EV(I)*R
            CALL HANCEL (AR,H0,H1,CC)
   20       AL(I)=C/A1
            PRINT 2012
            DO 50 L=1,NP
            I=IZ(L)
            C=0.
            DO 40 J=1,NL
            AR=EV(J)*RR(L)
            CALL HANKEL (AR,H0,H1,CC)
   40       C=C+V(I,J)*AL(J)*H1
            X=CABS(C)
            Y=0.
            IF(X.GT.0.) Y=ATAN2(AIMAG(C),REAL(C))*RAD
   50       PRINT 2002,RR(L),Z(I),C ,X,Y
            RETURN
C
 2002 FORMAT (2F10.4,3E15.6,F13.4)
 2012 FORMAT (//34H DISPLACEMENTS BEYOND THE BOUNDARY /
     1 83H R-COORD.     DEPTH          REAL PART          IMAG. PART      ABS. VAL
     2UE      PHASE SHIFT )
            END
```

162

```
      SUBROUTINE ALAMDAB (A1,A2,B1,B2,E,V,B22,P,Q,R,W,INT,N)
C
C      SOLVES EIGENVALUE PROBLEM
C
      COMPLEX C,D,EV,F,G,S,V,Y,Z
      COMPLEX A1(N),A2(N),B1(N),B2(N),E2(N),B22(N),E(N),P(N),Q(N),R(N),W(N)
      COMPLEX V(N,N)
      LOGICAL INT(N)
      TAU=1.E-7
      EPS=1.E-9
      T,I=CABS(A1(1))*1.E-20
      V1=V-1
      N..=N-2
      DO 20 J=1,N
   20 C22(J)=B2(J)*2.
      T=0.
C      SEARCH FOR ROOT OF DETERMINANT BY NEWTONS METHOD
      PRINT 2000
      DO 500 NV=1,N
      NV1=NV-1
      TP=1.
      IT=0
      .,IT=0
      EV=C,0.999
  105 EV=EV*(1.+TAU)
      TP=0.
  108 IT=IT+1
      IF (IT.GE.100) GO TO 20
      D=-C
      IF (NV1.EQ.0) GO TO 115
      DO 110 J=1,NV1
      C=EV-E(J)
  110 D=D-1./C
  115 X=A1(1)-EV*B1(1)
      IF (ABS(REAL(X))+ABS(AIMAG(X)).LT.TOL) X=TOL
      Y=-B1(1)*(B22(1)+B22(1)+2*V)*C1)/X
      C=Y*Y
      DO 120 J=2,N
      I=J-1
      Z=A2(I)-EV*B2(I)
      C=Z*X
      X=A1(J)-EV*B1(J)-Z*C
      Y=(-B1(J)-EV*B2(1)+2*V)*C)/X
  120 C=Y-Y
      D=-1./D
      EV=EV-D
      T=ABS(REAL(C))+ABS(AIMAG(C))
      IF (T.GT.EPS) GO TO 108
      IF (INT.EQ.1) GO TO 200
      NIT=1
      TP=1.
      GO TO 108
  200 PRINT 2001,NV,EV,T,IT
      E(NV)=EV
C
C      COMPUTE EIGENVECTOR BY INVERSE ITERATION
      DO 210 J=1,N
  210 W(J)=1.
C      REDUCTION OF MATRIX
      X=A1(1)-EV*B1(1)
      Y=A2(1)-EV*B22(1)
      R(1)=Y
      DO 250 I=1,N1
      J=I+1
      C=A1(J)-EV*B1(J)
      S=R(I)
      R(J)=A2(J)-EV*B22(J)
      T=ABS(REAL(X))+ABS(AIMAG(X))
      IF (T.GT.(ABS(REAL(S))+ABS(AIMAG(S)))) GO TO 230
      P(I)=1./S
      Q(I)=C
      INT(I)=1
      Z=-X*P(I)
      X=Y+Z*C
      Y=Z*R(J)
      GO TO 250
  230 IF (T.LT.TOL) X=TOL
      P(I)=S/X
      Q(I)=Y
      INT(I)=0
      Z=-S*P(I)
      X=C+Z*Y
      Y=R(J)
  250 IF (ABS(REAL(X))+ABS(AIMAG(X)).LT.TOL) X=TOL
      NITER=0
C      REDUCTION OF VECTOR
  300 NITER=NITER+1
      Z=V(1,NV)
      DO 330 I=1,N1
      IF (INT(I).EQ.1) GO TO 320
      W(I+1)=W( +1)+Z*W(I)
      GO TO 330
  320 Y=W(I)
      W(I)=W(I+1)
      W(I+1)=Y+Z*W(I)
  330 CONTINUE
C      BACKSUBSTITUTION
      W(N)=W(N)/X
      W(N1)=(W(N1)-Q(N1)*W(N))*P(N1)
      DO 350 L=2,N1
      I=N-L
      Y=W(I)-Q(I)*W(I+1)
      IF (INT(I).EQ.1) Y=Y-R(I(+1)*W(I+2)
  350 W(I)=Y*P(I)
      IF (NITER.LT.2) GO TO 300
C      NORMALIZE EIGENVECTOR
      C=W(1)*(A1(1)*W(1)+B2(1)*W(2))
      DO 420 J=2,N1
  420 C=C+W(J)*(B2(J-1)*W(J-1)+A1(J)*W(J)+B2(J)*W(J+1))
      C=C+W(N)*(B2(N1)*W(N1)+B2(N)*W(N))
      C=1./CSQRT(C)
      DO 440 J=1,N
  440 V(J,NV)=W(J)*C
  500 CONTINUE
C
      RETURN
```

163

```fortran
C
520 PRINT 2020,IT
    STOP
2000 FORMAT (//10X,5HEIGENVAUE (SQUARE OF THE WAVE NUMBER)          LAST
    1 NO. OF /11X, 9HREAL PART,14X,14HIMAGINARY PART, 4X,20HCORRECTIO
    2CN ITERATION )
2001 FORMAT (15,2F23,15,I9,2, I8)
2020 FORMAT (15HNO CONVERGENCE IN,14,58H NEWTON STEPS TO A CORRECTION
    1SMALLER THAN 1.E-9 THE ROOT)
    END

    SUBROUTINE HANKEL (Z,H0,H1,C)
C
C -  COMPUTATION OF HANKEL FUNCTION
C  Z - COMPLEX ARGUMENT,-3.1415,..LE.ARG(Z).LE. 0.
C  H0- HANKEL FUNCTION OF SECOND KIND AND FIRST ORDER
C  H1- HANKEL FUNCTION OF SECOND KIND AND SECOND ORDER
C  C - H0/H1.
C
    COMPLEX Z,H0,H1,C,A,E,E2,ZM,P
    X=REAL(Z)
    Y=AIMAG(Z)
    R=SQRT(X**2+Y**2)
    PHI=ATAN2(Y,X)
    IF(R.LE.10.) GOTO 20
    C=(10.,.125)/Z
    K=2
    P=C**2
    A=.5*P
    P=7.5*P
    H0=1.+C*A
    H1=1.-3.*C-P
10  I=4*K
    K=K+1
    A=A*C*( +1./K)
    P=P*C*(-3./K)
    H0=H0+A
    H1=H1-P
    IF(ABS(REAL(P))+ABS(AIMAG(P)).GT.1.E-8 ) GOTO 10
    C=H0/H1(10.,-1.)
    AR=.7953981633974-X-PHI/2.
    E=.7979456080802865/SQRT(R)*EXP(Y)*CMPLX(COS(AR),SIN(AR))
    IF(X.EQ.0.) E=CMPLX(0.,AIMAG(E))
    H0=H0*E
    H1=H1*C*(0.,1.)
    GOTO 30
20  ZM=Z/2.
    C=-ZM**2
    E=CMPLX(0.,.31830986,037911)
    E2=E*2.
    A=1.-E2*(.5772156649901533+ALOG(R/2.))+PHI*.6365197723675882
    P=1.
    K=1
    H0=A
    H1=A+E*(1.-1./C)
25  K=K+1
    P=P*C
    H0=H0+A*P

    IF(ABS(REAL(P))+ABS(AIMAG(P)).GT.1.E-16) GOTO 25
    H1=H1*ZM
    IF(X.NE.0.) GOTO 29
    H0=CMPLX(0.,AIMAG(H0))
    H1=CMPLX(REAL(H1),0.)
29  C=H0/H1
33  RETURN
    END

    SUBROUTINE CYMSOLC(A,B,NPI,NN,MM)
C
C   SOLVES EQUATIONS IN CORE
C
    COMPLEX A(NML,1),B(1),C
C   REDUCE MATRIX AND VECTOR
    DO 280 N=1,NN
    IF(A(N,1).EQ.0.) GO TO 280
    DO 260 L=N,MM
    C=A(N,L)/A(N,1)
    L = N+L-1
    IF(1.GT.NN) GOTO 260
    J=0
    DO 250 K=L,MM
    J=J+1
250 A(I,J)=A(I,J)-C*A(N,K)
260 A(N,L)=C
    B(I)=B(I)-C*B(N)
    B(N)=B(N)/A(N,1)
280 CONTINUE
C   BACK SUBSTITUTION
    N=NN
300 N = N-1
    IF(N.EQ.0) GOTO 500
    DO 400 K=2,MM
    L = N+K-1
    IF(L.GT.NN) GOTO 400
    B(N) = B(N) - A(N,K) * B(L)
400 CONTINUE
    GO TO 300
500 RETURN
    END
```

164

APPENDIX 6

PROGRAM PLAXLY

Identification:

Analysis of plane and axisymmetric layered media of infinite extent
subjected to harmonic loads which act within the plane of the cross-section.

Programmed by Gunter Waas, University of California, Berkeley,
June 1972.

Purpose:

Program PLAXLY is designed for the analysis of harmonic motion in
plane and axisymmetric systems of the type shown in Figs. 4 and 5.
Materials may be either linearly elastic or viscoelastic. The loads
(prescribed nodal forces and nodal displacements) vary harmonically with
time. Static loads may be analyzed by setting the frequency zero. The
program consists of a main program PLAXLY and 15 subroutines: INPUTD,
ELSTIF, QUAD, BUUMAT, GENEP, SECEVA, BOMAP, INVERTC, HANKEL, STIFF,
BLOCKS, MODIFY, OUTPUTD, RFORCE and OUTDIS.

Discretization:

The irregular region I, see Figs. 4 and 5, is subdivided into finite
elements with quadrilateral cross-sections as shown in Fig. 6. The
layered regions are subdivided into thin sublayers such that the layer
interfaces coincide with the finite element nodes at the plane or
cylindrical boundaries between the irregular and the layered regions.
Any finite element, except those adjacent to the boundaries between the
irregular and layered regions, may have zero moduli and zero mass density,
while the sublayers of the layered regions must always have non-zero
property values.

The numbering of the finite element nodes is arbitrary with the
following restriction. If it exists the left layered region L, see

165

Fig. 4, is connected to the first NUMLL+1 nodes, where NUMLL is the number of sublayers in the left layered regions. The surface layer is connected to nodes 1 and 2, the second layer to nodes 2 and 3, ..., and the bottom layer (numbered NUMLL) to nodes NUMLL and NUMLL+1. The right layered region R, if existing, is connected to the last NUMLR+1 nodes, where NUMLR is the number of sublayers in the right layered region. The surface layer is connected to the nodes NUMNP-NUMLL and NUMNP-NUMLL+1, ..., and the bottom layer to NUMNP-1 and NUMNP, where NUMNP is the total number of nodes. Because the system is supported by a rough rigid base, see Figs. 4 and 5, zero displacements must be specified for the nodes at the bottom.

## Size Limitations:

The program uses dynamic storage allocation for arrays the lengths of which are problem dependent. The total storage available for these arrays is the length, MTOT, of the array A which appears in the blank COMMON statement of program PLAXLY. The length requirement is

$$\text{MTOT} > \text{MBAND} \, (5 \, \text{MBAND}+7) + 3 \, \text{NUMNP} + 2 \, \text{NPBB}$$

in which

MBAND = maximum half-bandwidth of global stiffness matrix, i.e. twice the maximum difference between nodal point numbers of nodes belonging to any element +2
NUMNP = total number of nodal points
NPBB = number of points outside the finite element region at which motion is to be computed.

MTOT is set 15000 in the version of the program listed below. If the value of MTOT is reset then the dimension of the array A in the blank COMMON statement of program PLAXLY must also be adjusted.

## Output Information:

The program prints the following output:

i) Input and generated data.

ii) Nodal point displacements including amplitudes and phase angles.

iii) Reaction forces for nodes at which non-zero displacements are prescribed, including amplitudes and phase angles.

166

Input Data:

A. START CARD (5H) (Read in PLAXLY)

The word START must be punched in columns 1 to 5 on a separate card at the beginning of each problem. Several problems can be analyzed in one run.

B. HEADING CARD (12A6) (Read in program PLAXLY)

Columns 1 to 72 contain alphanumerical data to be printed as title on the output.

C. CONTROL CARD (8I5) (Read in PLAXLY)

Cols. 1-5 No. of nodal points, NUMNP
 6-10 No. of finite elements, NUMEL
 11-15 No. of different materials, NUMMAT
 16-20 No. of sublayers in Region L, NUMLL, less or equal 40
 21-25 No. of sublayers in Region R, NUMLR, less or equal 40
 26-30 No. of points outside of Region I where displacements are to be computed, NPBB
 31-35 No. of frequencies at which the model is to be analyzed, NFRQ
 36-40 If column 40 is left blank problem is taken to be axisymmetric and NUMLL must be zero. 1 in column 40 indicates a plane problem.

Note: If NUMLR is input as minus NUMLL Region R is understood to be a mirror image of Region L, and some computation can be saved.

D. MATERIAL CARDS (2I5,5F10.0) (Read in INPUTD)

One card for each different material; not more than 40 materials.

Cols. 1-5 Material number, M
 6-10 Interpretation parameter, INTPR
 If INTPR=0 Cols. 21-60 contain moduli
 If INTPR=1 Cols. 21-60 contain wave velocities
 11-20 Mass density, RHO
 21-30 Real component of shear modulus or S-wave velocity, $G_1$
 31-40 Imaginary part of shear modulus or S-wave velocity, $G_2$
 41-50 Real part of Poisson's ratio or P-wave velocity, $NU_1$
 51-60 Imaginary part of Poisson's ratio or P-wave velocity, $NU_2$

E. LAYER CARDS (10I5) (Read in INPUTD)

Cols. 1-5 Material number for sublayer 1
 6-10 Material number for sublayer 2
 etc.

Note: This data is grouped in sets, one set for each layered region. If there are two layered regions the first sets describes Region L and the second set Region R. If NUMLL=0 or NUMLR=0 the respective set is omitted. In the axisymmetric case NUMLL should be zero. Each set consists of as many cards as necessary to contain the material numbers of the layers sequentially, starting with the surface layer and ending with the bottom layer.

F. NODAL POINT CARDS (2I5,4F10.0,I5) (Read in INPUTD)

Cols. 1-5 Nodal point number, NL
      6-10 Parameter indicating if displacements or forces are specified, ICODE
      11-20 r-ordinate, (x-ordinate in plane case), R(NL)
      21-30 z-ordinate, Z(NL)
      31-40 U(1,NL) see below
      41-50 U(2,NL) see below
      51-55 Parameter for nodal point generation, INCL

If ICODE is
      0 U(1,NL) is specified force in r-direction and U(2,NL) is specified force in z-direction
      1 U(1,NL) is specified displacement in r-direction and U(2,NL) is specified force in z-direction
      2 U(1,NL) is specified force in r-direction and U(2,NL) is specified displacement in z-direction
      3 U(1,NL) is specified displacement in r-direction and U(2,NL) is specified displacement in z-direction

Note: Nodal point cards need not be input in numerical sequence. Suppose cards for nodes NA and NB are input sequentially. If (NA − NB) < 1 then nodal point data will be generated for nodes NA+INCL, NA+2INCL, ..., NB-INCL where INCL is the integer specified on the card for node NA. The coordinates for these nodal points will be obtained by linear interpolation between nodes NA and NB. The value of ICODE for the generated nodes is 0. if (NA − NB) > 0 no data are generated. If left blank INCL is taken as 1.

G. OUTPUT SPECIFICATION CARDS (F5.0,F10.0) (Read in INPUTD)

Cols. 1-5 Number of the interface passing through the point at which motion in Region L or Region R is to be computed, RZ. Interfaces are numbered from the surface downward commencing with 1.
      6-15 Absolute r-ordinate (horizontal) of point at which motion is to be computed, RZ.

Use one card for each point in Region L and Region R. Cards for points in Region L are placed first. The number of points, NPBB, is specified by the Control Card, see C.

H. ELEMENT CARDS (7I5) (Read in ELSTIF)

Cols. 1-5 Element number, MMM
      6-10 Nodal point i, IY(1)
      11-15 Nodal point j, IY(2)
      16-20 Nodal point k, IY(3)
      21-25 Nodal point l, IY(4)
      26-30 Material identification number for element, IY(5). If left blank it is taken as 1.
      31-35 Element generation parameter, INCL

Note: Order nodal points counter clockwise when the r-axis points horizontally to the right and the z-axis points vertically downward.

168
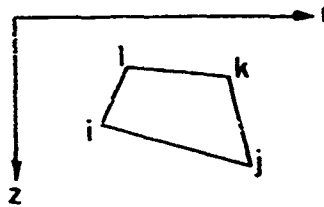
Note: Element data may be generated automatically if the material number is the same for all elements in a series and the nodal point numbers can be obtained as follows:

$$IY(1)_i = IY(1)_j + INCL$$
$$IY(2)_i = IY(2)_j + INCL$$
$$IY(3)_i = IY(3)_j + INCL$$
$$IY(4)_i = IY(4)_j + INCL$$

where j refers to an element for which the element number $MMM_j$ is one less than the element number $MMM_i$. In this case only the element card for the first element of the series need be input. However, the last element (highest element number) must always be input. If INCL is left blank then INCL=1.

I. FREQUENCY CARDS (F10.0) (Read in PLAXLY)

Cols. 1-10 Frequency of the exciting forces and displacements, CPS

Note: If CPS is positive it is interpreted as the frequency in cycles per second. If CPS is negative it is interpreted as the angular frequency in radians per second. The number of frequency cards is equal to NFRQ specified in the Control Card, see C.

J. STOP CARD (4H) (Read in PLAXLY)

For normal termaintion of execution the complete data deck (not each individual problem) finishes with a card with the word STOP punched in columns 1 to 4.

# Listing of Program PLAXLY:

```fortran
      PROGRAM PLAXLY (INPUT,OUTPUT,TAPE5=INPUT,NUMEL,NUMMP,NERJ,RADM,HED(12),
     1    TAPE3,TAPE6,TAPE1)
C
C
      COMMON/SING. 1/NUMMP,NUMEL,NUMMA*,NUMMP,NUMLL,NERJ,NPBB,HED(12),
     1      (BLAX,ISY4,P2,COL(2),MSJ,ISY4,NPBB,OMEGA,CPS
      COMMON A(13000)
      DATA /A2 /CONSTANT ,6.8270 /
C
C     ASSIGN MESH EQUAL TO LENGTH OF BLANK COMMON
C     ISYMMETRIC IF IPLNAX=0.  PLANE PROBLEM IF IPLNAX=1
C
      MTC1=13000
      P1=4.DATA*(1.-0)
      P2=3.142.6/PI
C     READ AND PRINT CONTROL INFORMATION
      IF ( MC40) .EQ. MJ001) ) GO TO 1
      IF ( MC40) .EQ. MJ0(2) ) STOP
      GO TO 10
    1 ISTOP=0
      READ (5,1020) HED,NUMNP,NUMEL,NUMEL,NUMMAT,NUMLL,NUMMR,NPB3,NFRQ,IPLNAX
      IF ( NUMNP .EQ. 0 ) STOP
      IF ( NUMNP .EQ. 0 ) STOP
      ISY4=0
      IF (NJ,NX,LO.0.-NJMLL) ISY4=1
      NUMLA=IABS(NJMLR)
      WRITE (6,2000) HED,NUMNP,NUMEL,NUMEL,NUMMAT,NUMLL,NUMMR,NPBB,NFRQ
      IF ( IPLNAX .EQ. 0 ) WRITE (6,2001)
      IF ( IPLNAX .EQ. 1 ) WRITE (6,2002)
C     DIMENSION BLANK COMMON
      NO=1
      N1=NO+NPBB*NPBB
      N2=N1+NUMNP*NUMNP
      N3=N2+NUMNP
      N4=N3+NUMNP
      N5=N4+NUMNP
```

```fortran
      I=N3+N36
      IF (I.GT.MTC1) GO TO 20
C
      CALL INPUT (A(N0),A(N1),A(N2),A(N3),A(N4),A(N5))
      IF ( ISTOP .EQ. 1 ) GO TO 15
      REWIND 1
      CALL FILTER (A(N1),A(N3),A(C..),A(N5))
      IF ( ISTOP .EQ. 1 ) GO TO 19
      N6=N(N1)-3N,MSJ,NPBB) P2=N(MEGA1/202
      IF(N2.GT.MSJ03) GO TO 66
      IF(N3.GT.N1/2
      WRITE (6,3204) NJ,MBA,O,N,R,NPBLK
      N1=N1+2
      N3=N1/2
      N3=N(N1/2)
      IF (N1.GT.NDMAP) NJ=N2+3N
      REWIND 1
      REWIND 2
      CALL STIFF (A(N3),A(N5),A(N3),A(N4),A(N5),A(N7),A(N1),A(N2),
     1                                    A(N3),AN,MBA,O,HCAN'')
C
      N3=N2+N4
      IC*48=0
  100 READ (5,1003) CPS
      IF (CPS.GE.0.) OMEGA=CPS*P1=2.
      IF (CPS.LT.0.) OMEGA=-CPS
      IF (CPS.LT.0.) CPS=OMEGA/P1/2.
      WRITE (6,7000) HCU,CPS,OMEGA
      OMSQ=OMEGA*2
      REWIND 1
      REWIND 2
      REWIND 3
      IF (NUMLL*NUMLR.LT.1) GO TO 16
      REWIND 4
      IF (NUMLL.GT.0) CALL ROUMAT  (A(N2),NUMLL,1,IPLNAX,ISY4,OMSQ)
      IF (ISY4.EQ.1) GO TO 15
      IF (NUMLR.GT.0) CALL ROUMAT  (A(N7),NUMLR,2,IPLNAX,ISY4,OMSQ)
      REWIND 4
   15 CONTINUE
   16 CALL BLOCKS (A(N1),A(N2),A(N3),A(N4),A(N5),A(N6),A(N7),A(N8),A(N9)
     1                        ,NN,MBA,O,N84NN)
C
      REWIND 1
      REWIND 7
      CALL OUTPUT (A(N0),A(N1),A(N2),A(N4),A(N6),A(N7),A(N8),A(N9),NN)
      IF(ICTFR.LT.NFRQ) GO TO 100
      GO TO 10
   20 WRITE (6,3000) 1,MTGT
      GO TO 10
   30 WRITE (6,3000) N11,MTGT
      GO TO 19
   60 WRITE (6,3003) MBAND
```

```
      GO TO 10
 1000 FORMAT (12A6/8I5)
 1001 FORMAT(A6)
 1002 FORMAT (F10.0)
 2000 FORMAT (1H1,12A6/)
    1 13H0 NUMBER OF NODAL POINTS------   I3 /
    2 13H0 NUMBER OF ELEMENTS-------       I3 /
    3 13H0 NUMBER OF DIFF. MATERIALS----   I3 /
    4 13H0 NUMBER OF LEFT LAYERS------     I3 /
    5 13H0 NUMBER OF RIGHT LAYERS------    I3 /
    6 13H0 NUMBER OF OUTSIDE POINTS------  I3 /
    7 13H0 NUMBER OF CONVERGENCES         I3 /  )
 2001 FORMAT (///  40H AXISYMMETRIC LINEARLY VISCOELASTIC SOLID )
 2002 FORMAT (///  34H PLANE STRAIN OF LINEARLY VISCOELASTIC SOLID )
 2003 FORMAT(1H0 12A6/20H CYCLES PER SECOND =E13.5/
     1       16H FREQUENCY (2H3.5)
 2004 FORMAT(1H0 26H BAND WIDTH OF BLOCK COMMON=,I5/
     1       22H ASSIGNED LENGTH OF BLANK COMMON=,I5/
     2       24H INSUFFICIENT STORAGE FOR THIS(EQ) )
 2005 FORMAT(16H STORAGE INSUFFICIENT FOR BANDWIDTH OF,I5)
     1  /36H TOTAL NUMBER OF EQUATIONS          =,I5,
     2  /36H NUMBER OF EQUATIONS TO A BLOCK     =,I5,
     3  /36H NUMBER OF BLOCKS                   =,I5)
      END

      SUBROUTINE INPUTD (RZ,U,ICODE,R,Z)
C
C     READS AND PRINTS INPUT DATA
C
      COMMON/GENC/NP,NUMNP,NUMEL,NUMMAT,NUMLL,NUMLK,NFRQ,RADN,HED(12),
     1            IPLNA,IST,3,NCODE(2),GVS4,ISYM,NPRB
      COMMON/MAT/CM,VS,VP,TYPE,PK,MAT(15,10),LHF(40,2),THL(40,2),RK(21),ZZ(2)
      DIMENSION RZ(1),U(2,1),ICODE(1),R(1),Z(1)
      COMPLEX  G,NU,VS,VP,LAMDA
C
C     READS AND PRINT MATERIAL PROPERTIES
C
      WRITE (6,2000)
      DO 10  J=1,NUMMAT
      READ (5,1000) M,INTPR,RHO,G,NU
      IF (INTPR.EQ.1) GO TO 5
      VS=CSQRT(G/RHO)
      VS=CSQRT(2.*G*(1.-NU)/(1.-2.*NU)/RHO)
      GO TO 6
    5 G=VS*VS*RHO
      VP=VP
      G=VS*VS*2.*RHO
      NU=(VP-VS )**2
      LAMDA=2.*G*NU/(1.-2.*NU)
      G=VS*(1.)/RHO
      PK=MAT(J,1)*LAMDA(J)
      PK=MAT(J,1)*LAMDA(J)
      PRCMAT(5,MAT,LAMDA,LAMDA)
   10 WRITE (6,2001) M,RHO,G,NU,VS,VP
C
C     READ AND PRINT LAYER DATA
```

      IF (NUMLL.LT.1) GO TO 20
      READ (5,1005) (LHT(N,1),N=1,NUALL)
      WRITE (6,2005) (N,N=1,NUMLL)
   20 IF (NUMLR.LT.1) GO TO 40
      READ (5,1005) (LHT(N,1),N=1,NUMLR)
      WRITE (6,2006) (N,N=1,NUMLR)
      WRITE (6,2007) (LHT(N,2),N=1,NUMLR)
   40 IF (ISYM.EQ.1) WRITE (6,2009)
C
C     READ AND PRINT NODAL DATA
C
      WRITE (6,4001) HED
      WRITE (6,2004)
      IF CON=0
   50 READ (5,1002) NL,(ICODE(N),U(N,1),N=1,2)
    1 IF ( N .NE. L ) GO TO 60
      ICCUNT=ICCUNT+1
      IF ( ICCUNT .NE. 1 ) GO TO 70
      N=NL
      ZX=(NL-NF)/INCF
      IF (ZX .NE. 0.0 ) GO TO 70
      DR=(R(NL)-R(N))/ZX
      DZ=(Z(NL)-Z(N))/ZX
   65 N=N+INCF
   70 NF=NL
      L=CF+INCL
      IF ( ICRDNT .LT. NUMNP ) GO TO 50
      IF ( ICCUNT .GT. NUMNP ) GO TO 100
      GO TO 110
  100 WRITE (6,2000) N
      ISTOP=1
  110 WRITE (6,2002) (N,ICODE(K),R(K),Z(K),U(1,K),U(2,K),K=1,NUMKP)
C
      IF (NUMLL.LT.1) GO TO 140
      DO 130 N=1,NUMLL
      THL(N,1)=(BS(Z(N+1)-Z(N))
      RP(I)=R(I)
      ZZ(1)=Z(1)
      NUMLL=NUMLL*2
  140 IF (NUMLR.EQ.0) GO TO 160
      J=NUMNP-NUMLR
      DO 150 N=1,NUMLR
      I=J
      J=J+1
      THL(N,2)=ABS(Z(J)-Z(I))
      RR(2)=R(1)
      ZZ(1)=Z(1)
      GO TO K.NUMRK*2
  160 IF (NPRM.LE.0) GO TO 200

171

```
      A=NPROC2
      READ (5,1003) (R2(J),J=1,K)
  200 RETURN
C
 1001 FORMAT (215,5F10.0)
 1002 FORMAT (215,4F10.0,I5)
 1003 FORMAT (F5.0,F10.0)
 1004 FORMAT (I3I5)
 1005 FORMAT (//12H MATERIAL NO.   DENSITY     REAL(G)    IMAG(G)
     1     REAL(NU)    IMAG(NU)    REAL(VS)    IMAG(VS)    REAL(VP)    IMAG(VP)
 2001 FORMAT (18,6X,9E12.4)
 2002 FORMAT (2I12,2F12.3,2E24.7)
 2003 FORMAT ( 9H7 VOL. PRINT
 1005 FORMAT //12H CONTACLE NT  Z-LOAD ON DISPLACEMENT )
 2035 FORMAT ///13H LEFT LAYER NO.,40(3)            TYPE  R-CRDINATE   Z-CRDINATE   R-LO
 2036 FORMAT ///13H RIGHT LAYERS//LCH LAYER NO.,40(3)
 2037 FORMAT ( 9H4 MATERIAL   40(3) )
 2050 FORMAT //45H LEFT AND RIGHT LAYERED SYSTEMS ARE IDENTICAL )
 2021 FORMAT 26H NODAL POINT CARD ERROR N= I5)       (LEFT LAYER NO.,40(3)
 2031 FORMAT(1H1,12A6///)
      END
C

      SUBROUTINE ELSTIF (...,...)
C
C     READS ELEMENT CARDS,GENERATES DATA AND COMPUTES ELEMENT MATRICES
C
      COMMON/GC=CON/ASP=MP,NUMEL,NUMAT,NUPEL,NUMLR,NFRQ,RADN,HED(12),
     1    IPCMAX,ISTOP,NUMNLK,MBAND,MBANDL,NR2,N4,NS,NT,VD
      COMMON/VE=YCCN/NQ,NUMSLK,MTYPE,PRCMAT(5,40),LMT(40,2),RR(2),ZZ(2)
      COMMON/VE=ECCN/LM(8),S(3,8),S4(4,4),VMIN,SHAPE,RHO,G,ELA,IPX,VOL
      COMPLEX S,G,ELA
      DIMENSION U(12),H(11),Z(11),Q(5,3),IX(5),IY(5)
C
C     READS AND PRINT ELEMENT PROPERTIES,DETERMINE MAX. BANDWIDTH
C
      WRITE (6,4001) HED
      WRITE (6,2001)
      MBAND=0
      NUMBLK=0
  100 IPX=IPLMAX
      READ (5,1003) NUM,(IY(J),J=1,5),INCL
      IF ( INCL .EQ. 0 ) INCL=1
      SHAPE=1.0
      IF ( IY(4) .EQ. 0 ) SHAPE=0.0
      IF ( IY(5) .EQ. 0 ) IY(5)=1
      IF ( SHAPE .EQ. 0.0 ) IY(4)=IY(3)
  110 N=NUM
      IF(NUM-N) 200,120,130
  120 DO 125 I=1,5
  125 IX(I)=IY(I)
      GO TO 140
  130 DO 135 I=1,4
  135 IX(I)=IX(I)+INCF
  140 K=0
      NI=IX(1)
      NJ=IX(2)
      NK=IX(3)
      NL=IX(4)
```

              172

```
      MTYPE=IX(5)
      DO 160 J=1,4
      DO 160 J=1,4
      L=JAN=(IX(I))-IX(J))
      IF(L.GT.K) K=L
  160 CONTINUE
      K=2*K+2
      IF IX,GT,MBAND) MBAND=K
  170 N=IN=NJ
      IF ( NJ .LT. NNIK ) NJ=N=NJ
      IF ( NK .LT. NNIK ) NJ=N=NK
      IF ( NL .LT. NPIK ) N=N=NNL
      DO 171 I=1,4
  171 L=MI(12)=2*IX(I)
      LMI(12)=2*IX(I)
  171 MI(I)=2*(I2I-1)
C
      RHO=PRCMAT(1,MTYPE)
      G  =CMPLX(PRCMAT(2,MTYPE),PRCMAT(3,MTYPE))
      ELA=CMPLX(PRCMAT(4,MTYPE),PRCMAT(5,MTYPE))
C
C     FORM MATRICES FOR QUADRILATERAL ELEMENTS
C
      CALL QUAD (R1(NI),R(NJ),R(NK),R(NL),Z(NI),Z(NJ),Z(NK),Z(NL),
     1                                    Q(1),Q(40))
      WRITE (6,2003) V,(IX(I),I=1,5)
      IF (VOL.GT.0.0) GO TO 175
      ISTOP=1
  200 WRITE (6,2002) NUM
      WRITE (6,2004) N
      GO TO 180
  175 WRITE (1, (LMI(I),I=1,154)
  180 IF(N.EQ.NUMEL) GO TO 150
      IF ( N .NE. MNM ) GO TO 110
      INCL=INCL
      GO TO 100
  150 MBAND=MBAND/2
      RETURN
 1003 FORMAT(I5)
 2001 FORMAT (4IH ELEMENT NO.         I      J      K      L    MATERIAL
     1 (VOLUME )
 2002 FORMAT(I7I2H40 ELEMENT CARD IN ERROR,I5)
 2003 FORMAT (I11I3,4I6,I112)
 2004 FORMAT(34H0 NEGATIVE OR ZERO AREA OF ELEMENT,I5)
 4001 FORMAT(1H1,12A6///)
      END
C

      SUBROUTINE QUAD (R1,R2,R3,R4,Z1,Z2,Z3,Z4,R,Q)
C
C     CALCULATES STIFFNESS MATRIX S1 AND MASS MATRIX SM FOR AN AXISYM.
C     (IPX=0) OR PLANE (IPX=1) QUADRILATERAL ELEMENT- 4 POINT INTEGRATION
C
      COMMON/ELECON/LP(3),ST(8,8),SI(4,4),NMIN,SHAPE,RHO,G,ELA,IPX,VOL
      COMPLEX ST,ELA,G,GGL,D1,D2,D3,D6,Q0(12,12)
      DIMENSION TT(4),SS(4),H(6),B(4,12)
      DATA SS/-.5773503,+.5773503,+.5773503,-.5773503/,
     1       TT/-.5773503,-.5773503,+.5773503,+.5773503/
C
      GGL=G+G+ELA
      R=1.
```

```
      DO 10 I=1,16
   10 ST(I)=0.
      DO 20 I=1,48
   20 UE(I)=0.
      DO 30 I=1,144
   30 SE(I)=0.
      R1=R1-R2
      R2=R1-R3
      R3=R2-R3
      R4=R3-R4
      S2=R4-R2-R3
      S3=R3-R3-R4
      S2=R2-R3
      R3=R2-R3
      S4=R2-R3-R4
      IF(R1.EQ.0.0) R=(R1*R2+R3+R4)/4.
      V=(-R1*R2+R3*R2+R3)*R/2.

C
      DO 500 I=1,6
      S=SS(I)
      T=T(I)
      S=S1.,5
      S=S1.,5
      TP=1.0-T
      TP=1.0-T
      S=2.,C=TST
      S=R1.0-SBS
      H(1)=S*RTM
      H(2)=SP*TM
      H(3)=SP*TP
      H(4)=SP*TP
      H(5)=TP*T/2.
      H(6)=S*-.2/2.
      IF(IPX.EQ.0) R=(H(1)*R1*H(2)*R2*H(3)*R3*H(4)*R4)/4.
      PT=-(S*P2(4+SP*R.23)/4.0
      P2=-(T*P2(2-TP*R34)/4.0
      PR5=-(TM*R12-TP*R34)/4.
      XJ=PAS*PZT-PRT*PZS
      X1=P2T/XJ
      X2=-P4S/XJ
      X3=-RJT/XJ
      R=-P5S/XJ
      FA.=-XJ*W/16.
      R1(1,1)=-TM*X1-SM*X2
      R1(1,3)= TM*X1-SP*X2
      R1(5)= TP*X1+SP*X2
      R1(7)=-TP*X1+SM*X2
      R1. 9)=-S*X1
      R1. 1)= T*X2
      B1(2,2)=-TM*X3-SM*X4
      B1(2,4)= TM*X3-SP*X4
      R1(2,6)= TP*X3+SP*X4
      B1(2,8)= TP*X3+SM*X4
      B1(2,1)=-S*X3
      B1(2,1)= T*X4
      B1(4,1)=-S*X3
      B1(4,3)=-S(,,)
```

```
      B(4,5)=B(2,6)
      B(4,7)=B(2,8)
      B(4, 9)=B(2,1)
      B(4,10)=B(2,12)
      B(4,2)=B(1,1)
      B(4,4)=B(1,3)
      B(4,6)=B(1,5)
      B(4,8)=B(1,7)
      B(4,11)=B(1, 9)
      B(4,12)=B(1,10)

C
      IF(IPX.EQ.0) GO TO 350
      DO 300 J=1,12
      D1=(GL*H(1,J)+ELA*B(2,J))*FAC
      D2=(GL*B(2,J)+ELA*B(1,J))*FAC
      D3=.,* B(4,J)*FAC
  300 QQ(J,1)=QQ(J,1)+D1*B(1,1)+D2*B(2,1)+D3*B(4,1)
      GO TO 420

C
  350 B(3,1)=H(1)/R
      B(3,3)=H(2)/R
      B(3,5)=H(3)/R
      B(3,7)=H(4)/R
      B(3,1)=H(5)/R
      B(3,1)=H(6)/R
      DO 400 J=1,12
      D1=(GL*B(1,J)+FLA*B(2,J)+B(3,J))*FAC
      D2=(GL*B(2,J)+FLA*B(1,J)+B(3,J))*FAC
      D3=(GL*B(3,J)+FLA*B(1,J)+B(2,J))*FAC
      D4=    G  B(4,J)*FAC
  400 QQ(J,1)=QQ(J,1)+B(1,1)*D1+B(2,1)*D2+B(3,1)*D3+B(4,1)*D4
C                              INERTIA COEFFICIENTS
  420 FAC=FAC*RHO
      DO 450 I=1,4
      DO 450 J=1,4
      S(I,J)=S(I,J)+H(I)*H(J)*FAC
  450 S(I,J)=S(I,J)+H(I)*H(J)*FAC
  500 CONTINUE
C                  ELIMINATE EXTRA DEGREES OF FREEDOM
      IF (IPX.EQ.0) GO TO 500
      DO 60 N=1,4
      L=12-N
      M=L+1
      Q2=QQ(M,M)
      IF(ABS(REAL(Q2))*ABS(AIMAG(Q2)).EQ.0.) GO TO 60
      DO 50 J=1,L
      D1=QQ(1,M)/Q2
      DO 50 J=1,L
   50 QQ(I,J)=QQ(I,J)-Q1*QQ(J,M)
   60 CONTINUE
C                  WRITE STIFFNESS INTO ST
  590 DO 600 I=1,8
      DO 600 J=1,8
      ST(I,J)=QQ(I,J)
  600 S*(J,I)=ST(I,J)
      RETURN
      END

      SUBROUTINE BOUMAT (A,NN,LR,IPA,ISYM,CMS)
```

173

```
C     FORMS MATRICES OF EIGENVALUE PROBLEM,SOLVES PROBLEM
C     AND COMPUTES BOUNDARY MATRIX
      COMMON/MATCON/MTYPE,PROMAT(15,40),LMT(40,2),THL(40,2),RK(2),ZZ(2)
      DIMENSION A(1)
      NUP=NN/2
      NN2=2*NN+N
      M1=1
      M2=M1+NN
      M3=M2+NN
      M4=M3+NN2
      M5=M4+NN2
      M6=M5+NN2
      M7=M6+NN2
      M8=M7+NN2
      M9=M8+NN2
      M10=M9+NN
      N1=NN
      N2=N1+NN2
      N3=N2+NN2*NN
      N4=N3*NN2*2*NN
      N5=N4+NN2*2*NN
      N6=N5+NN2
      N7=N6+NN2
      N8=N7+NN2
      N9=N8+NN2
      N10=N9+NN2
      N11=N10+NN2
      N12=N11+NN2
      N13=N12+NN2
      DO 10 N=1,NUML
      K=LMT(N,LR)
      L=N+1
      J=N+N
      I=J-1
      A(I)=PROMAT(2,K)
      A(J)=PROMAT(3,K)
      A(I+NN)=PROMAT(4,K)
      A(J+NN)=PROMAT(5,K)
      A(I+N2)=P2CMAT(1,K)
      A(J+N2)=THL(N,LR)
   10 CALL GENEP  (A(M1),A(M2),A(M3),A(M4),A(M5),A(M6),A(M7),A(M8)
     .             A(M9),A(M10),OMS,NUML)
C
      IF (LR.OR.ISYM.EQ.1) WRITE (6,2001)
      IF (LR.EQ.2) WRITE (6,2002)
      IF (ISYM.EQ.1) WRITE (6,2003)
      CALL SECEVA (A(M3),A(M4),A(M5),A(M6),A(M7),A(M8),A(1),A(N2),
     1 ,A(N3),A(N6),A(N5),A(N8),A(N7),A(N8),A(N9),A(N11),A(N12),
     2 A(N13),NN)
      CALL BOMAP  (A(M1),A(M2),A(M3),A(M4),A(M5),A(M6),A(N1),A(N2),A(N3)
     .            ,NN,LR,IPA,ISYM,RR(LR))
      RETURN
C
 2001 FORMAT(///3H  WAVE NUMBERS OF LEFT LAYERED SYSTEM )
 2002 FORMAT(///3H  WAVE NUMBERS OF RIGHT LAYERED SYSTEM )
 2003 FORMAT(///4H  WAVE NUMBERS OF LEFT AND RIGHT LAYERED SYSTEMS )
      END
C
      SUBROUTINE GENEP (SM,LAM,A1,A3,B2,B4,C1,C3,RHO,TH,OMS,NUML)
```

```
C     GENERATES MATRICES OF EIGENVALUE PROBLEM
C
      DIMENSION RHO(1),TH(1)
      COMPLEX   A1(1),A3(1),B2(1),B4(1),C1(1),C3(1),SM(1),LAM(1)
      COMPLEX   AH,AHO,AV,AVO,BH,RHO,BV,CH,CHO,CV,CVO,AL
C
      AH=0.
      AV=0.
      BH=0.
      CH=0.
      CV=0.
      I=0
      DO 105 J=1,NUML
      TH3=THL(J)/3.
      AL=SM(J)*.5+SM(J)
      C=RHO(J)*TH3*OMS
      AH=AL*TH3
      AV=C*AL(J)*TH3
      CH=CH(J)/TH(J)-CM
      CV=AL/TH(J)-LAM(J)*CM
      AH=(SM(J)-LAM(J))*.5
      BV=(SM(J)+LAM(J))*.5
      I=I+1
      A1(I)=AH+AHO
      A3(I)=AH-.5
      B2(I)=BH-RHO
      B4(I)=BV
      C1(I)=CH-CHO
      C3(I)=-CH-1.5*CM
      I=I+1
      A1(I)=AV+AVO
      A3(I)=AV-.5
      B2(I)=BV
      B4(I)=0.
      C1(I)=CV-CVO
      C3(I)=-CV-1.5*CM
      AHO=AH
      AVO=AV
      BHO=BH
      CHO=CH
      CVO=CV
  105 CONTINUE
      RETURN
      END
```

```
      SUBROUTINE SECEVA (A1,A3,B2,B4,C1,C3,E,V,A,V1,V2,U1,U2,U3,R1,R2,
     1 S1,S2,MVB,NN)
C
C     SOLVES EIGENVALUE PROBLEM
C
      DIMENSION MVB(1)
      COMPLEX A(1),A3(1),B2(1),B4(1),C1(1),C3(1)
      COMPLEX A(NN,1),V1(1),V2(1),U1(1),U2(1),U3(1),S1(1),S2(1)
      COMPLEX E(1),V(NN,NN),P(1),R2(1),EOLD(1),EV,EVS,CE,CD,DEV,C,D,CF
      DATA EPS1/1.0E-5/,EPS2/1.0E-10/
      N1=NN-1
      N2=NN-2
      DO 10 J=1,N2
      MVB(J)=J+3*NN
   10 MVB(N1)=N1+NN
```

```
          XA=0.
          DO 15 J=1,NN
          X=C1(J)/A1(J)
15        XN=X+ABS(X)
          XA=SQRT(XA/XN)
          X=C*PLX(XN,XN*XN)
          DO 20 J=1,NN
          S1(J)=1.
          S2(J)=C
          V(J)=-S1(J)
          V2(J)=S2(J)
          A1(J)=0.
20        X7(J)=0.
          FV=XA/XN
          ISM=0
          NC=0
          NC=3
440       KC=KC+1
          DO 50 N=1,NN
          U1(N)=C1(N)*V1(N)
          U1(N)=U1(N)*C3(L)*V1(L)
          U2(L)=U2(L)*A3(L)*V2(N)
50        U2(N)=U2(N)*A3(L)*V2(L)
          DO 25 N=3,NN
          L=N-2
          IF(ISM.EQ.1) GO TO 95
          X=CA0.(EV)*2.
          EV=CMPLX(X,X+X)
          GO TO 87
55        EV=C0*G(EV)
          ISM=2
          IO=1.
87        IK=0
          DO 200 IT=1,30
          EVS=EV**2
          DO 90 N=1,NN
          A(N,1)=EVS*A1(N)*C1(N)
          A(N,2)=EVS*B2(N)
          A(N,3)=EVS*A3(N)*C3(N)
          A(N,4)=EV*B4(N)
90        V2(N)=(U1(N)-U2(N)*EV)*CD
          DO 150 N=1,N1
          I=N
          J=N+NN
          M=MVB(N)
          DO 120 L=J,M,NN
          C=A1(L)/A(N)
          A1(L)=C
          I=I+1
          DO 110 K=L,M,NN
110       A(K)=A(K)-C*A(K)
          A1(J)=V2(J)-C*V2(N)
120       V2(L)=V2(L)/A(N)
130       V2(N)=V2(N)/A(N)

          DO 160 K=1,N1
          N=N-1
          L=N
          J=N+NN
          M=MVB(N)
          DO 160 L=J,M,NN
          I=I+1
160       V7(I)=V2(N)-A1(I)*V2(I)
          CE=0.
          DO 170 N=1,NN
          V1(N)=(V2(N)-V1(N)*C0)/EV
          CF=CE-U1(N)*V1(N)+U2(N)*V2(N)
          U1(N)=C1(N)*V1(N)
170       V2(N)=A1(N)*V2(N)
          CF=CE*CD
          DO 180 N=3,NN
          L=N-7
          U1(L)=U1(L)+C3(L)*V1(N)
          U1(N)=U1(N)+C3(L)*V1(L)
          U2(L)=U2(L)+A3(L)*V2(N)
180       U2(N)=U2(N)+A3(L)*V2(L)
          CD=0
          DO 190 N=1,NN
190       CD=CD-U1(N)*V1(N)+U2(N)*V2(N)
          DEV=CE/C0
          IF(IT.GT.15) DEV=DEV*0.5
          EV=EV+DEV
          CF=CD
          CD=CSQRT(Z./CD)
          C=DEV/EV
          X=ABS(REAL(C))+ABS(AIMAG(C))
          IF(IK.EQ.1.AND.X.LT.EPS2) GO TO 300
          IF(X.LT.EPS1) IK=1
200       CONTINUE
          PRINT 2030
          STOP
300       E(KC)=EV
          ICP=0
          X=ABS(REAL(EV))
          Y=ABS(AIMAG(EV))
          Z=X+Y
          IF(Y/Z.LT.EPS2) ICR=1
          IF(X/Z.LT.EPS2) ICR=2
          IF(ICR.EQ.1) E(KC)=REAL(EV)
          IF(ICR.EQ.2) E(KC)=AIMAG(EV)*(0.,1.)
          DO 310 N=1,NN
310       V(N,KC)=V2(N)*V2(N)*CD
C     IF THE EIGENVALUE IS REAL CHOOSE THE SIGN SUCH THAT THE GROUP VELOCIT
C     BECOMES POSITIVE
          IF(ICR.NE.1) GO TO 316
          X=(V1(1)*2*V1(2))*EV
          IF(X.GT.0.)        GOTO 315
          E(KC)=-E(KC)
          DO 315 N=2,NN,2
315       V(N,KC)=-V(N,KC)
C     CHECK THE SPECIAL ORTHOGONALITY OF THE NEWLY FOUND EIGENVECTOR AND
C     THE SUM OF THE PREVIOUSLY FOUND EIGENVECTORS
316       CE=0.
          DO 330 I=1,NN
330       CE=CE-R1(N)*U1(N)+R2(N)*U2(N)
          CE=CE*CD
          Y=ABS(REAL(CE))+ABS(AIMAG(CE))
```

```
      XA=0.
      DU 15 J=1,NN
      X=C1(J)/A1(J)
15    XM=X+ABS(X)
      XA=SQRT(XA/XN)
      2.0 .PLX(XN,XN*XN)
      DU 20 J=1,NN
      S1(J)=1.
      S2(J)=C
      V1(J)=S1(J)
      V2(J)=S2(J)
      A1(J)=0.
20    A7(J)=0.
      FV=X*V/XN
      ISN=0
      IC=0
      NC=0
      PRINT 2007
400   IC=KC+1
      DG 50 N=1,NN
      U1(N)=C1(N)*V1(N)
50    U2(N)=S1(N)*V2(N)
      DU 55 N=3,NN
      L=A-2
      U1(L)=U1(L)+C3(L)*V1(N)
      U1(N)=U1(N)+C3(L)*V1(L)
      U2(L)=U2(L)+A3(N)*V2(N)
55    U2(N)=U2(N)+A3(L)*V2(L)
      IF (ISN*E2.1) GO TO 95
      ISN=0
      C0=1.
      R=CABS(EV)*2.
      EV=CMPLX(X,Y+X)
      GJ TO R7
85    EV=CC(NJG(EV)
      ISN=2
      C0=1.
87    IK=0
      DO 200 IT=1,30
      EVS=EV**2
      DC 90 N=1,NN
      A1(N,1)=EVS+A1(N)+C1(N)
      A(N,2)=EV*B2(N)
      A1(N,3)=EVS+A3(N)+C3(N)
      A1(N,4)=EV*B4(N)
90    V2(N)=(U1(N)-U2(N)*EV)*CD
      DO 150 N=1,N1
      J=N+NN
      M=MVB(N)
      DC 120 L=J,M+N
      A(J)=A(J)-C*A(K)
      C=A(L)/A(N)
      1=1+1
      J=1
      DO 110 A=L,M,NN
      A(J)=A(J)-C*V2(N)
      C=A(L)/A(N)
      A(L)=C
110   V2(L)=V2(L)-C*V2(N)
      1=J4
120   V2(J)=V2(I)-C*V2(N)
150   V2(J)=V2(M)/A(N)

      DO 160 K=1,N1
      N=N-1
      1=N
      J=A+NN
      M=MVB(N)
      DO 160 L=J,M,NN
      1=1+1
160   V2(N)=V2(N)-A(L)*V2(L)
      CC=0.
      DO 170 N=1,NN
      V1(N)=(V2(N)-V1(N)*CO)/EV
      CF=CE-U1(N)*V1(2)+U2(N)*V2(N)
      U1(N)=C1(N)*V1(N)
170   V2(N)=A1(N)*V2(N)
      CF=CE*CD
      DO 180 N=3,NN
      L=N-2
      U1(L)=U1(L)+C3(L)*V1(N)
      U1(N)=U1(N)+C3(L)*V1(L)
180   U2(N)=U2(N)+A3(L)*V2(L)
      CO=0.
      DO 190 N=1,NN
190   CD=CO-U1(N)*V1(N)+U2(N)*V2(N)
      DEV=CE/CO
      IF (IT.GT.15) DEV=DEV*0.5
      EV=EV-DEV
      CF=CD
      CD=CSQRT(2./CO)
      C=DEV/EV
      X=ABS(REAL(C))+ABS(AIMAG(C))
      IF (IK.EQ.1.AND.X.LT.EPS2) GO TO 300
      IF (X.LT.EPS1) IK=1
200   CONTINUE
      PRINT 2020
      STOP
300   E(KC)=EV
      ICP=0
      X=AP(REAL(EV))
      Y=ABS(AIMAG(EV))
      Z=X+Y
      IF (Y/Z.LT.EPS2) ICR=1
      IF (X/Z.LT.EPS2) ICR=2
      IF(ICR.EQ.1) E(KC)=REAL(EV)
      IF(ICR.EQ.2) E(KC)=AIMAG(EV)*(0.,1.)
      DO 310 N=1,NN
310   V1(N,KC)=V2(N)*CD
C     IF THE EIGENVALUE IS REAL CHOOSE THE SIGN SUCH THAT THE GROUP VELOCIT
C     BECOMES POSITIVE
      IF (ICR.NE.1) GO TO 316
      X=(V1(1)**2+V1(2)**2)*EV
      IF(X.GT.0.) GOTO 316
      E(KC)=-E(KC)
      DO 315 N=2,NN,2
315   V1(N,KC)=-V1(N,KC)
C     CHECK THE SPECIAL ORTHOGONALITY OF THE NEWLY FOUND EIGENVECTOR AND
C     THE SUM OF THE PREVIOUSLY FOUND EIGENVECTORS
316   CE=0.
      DO 330 N=1,NN
      CL=CE-R1(N)*U1(N)+R2(N)*U2(N)
      CE=CE*CD
330   Y=ABS(REAL(CE))+ABS(AIMAG(CE))
```

175

```
      PRINT 2008,KC,IT,E(KC),DEV,X
      IF (X.LT.EPS) GO TO 335
      PRINT 2021
      STOP
335   C=1./F(KC)
      DO 340 N=1,NN
      R1(N)=R1(N)+V(N+KC)*C
C     FIND A STARTING VECTOR ORTHOGONAL TO ALL EIGENVECTORS FOUND FOR THE
C     ITERATION TOWARD THE NEXT EIGENVECTOR
340   F2(N)=F2(N)+V(N)*V(N+KC)
      C=0.
      D=0.
      DO 342 N=2,NN,2
      M=N-1
342   C=C-U1(M)*S1(M)+U2(N)*S2(N)
      CF=2./F
      C=C+CE
      D=D+CE
      DO 343 N=2,NN,2
      M=N-1
      S1(M)=S1(PI-C*V1(M)
      S1(N)=S1(N)-D*V1(N)
      S2(M)=S2(M)-D*V2(M)
      S2(N)=S2(N)-C*V2(N)
      V1(N)=S1(M)
      V1(N)=S1(N)
      V2(M)=S2(M)
343   V2(N)=S2(N)
      IF (ICK+ISM.EQ.0) ISM=1
      MC=MC+1
      IF (MC.GE.NN ) GO TO 350
      GOTO 400
C     FORM VECTORS FOR DISPLACEMENT EXPANSION
350   DO 610 N=1,NN
      C=(0.,-1.)
      X =A1MAG(F(N))
      IF (X.LE.C.) GO TO 600
      E(N)=-L(N)
      C=J-C
600   DO 610 J=2,NN,2
610   V(J,N)=-V(J,N)*C
100   RETURN
C
2007  FORMAT(//,12H  NO. NO.OF,19X,11HWAVE NUMBER,27X,15HLAST CORRECTIO
     1 N,12X,14HDEVIATION FROM/
     2 7X,5HITER.,5X,9HREAL PART,1X,9HIMAG. PART,16X,9HREAL PART
     3 ,3X,10HIMAG. PART,8X,14HORTHOGONALITY /)
2008  FORMAT( I5,I6,6X,2F23.15,4X,2E12.5,8X,2E12.5)
2020  FORMAT(43H1 FAILURE TO CONVERGE IN 30 ITERATION STEPS )
2021  FORMAT(6PH1 FAILURE TO FIND AN EIGENVECTOR ORTHOGONAL TU THE ONES
     1 FOUND BEFORE )
      END

      SUBROUTINE SOMAP (SM,LAM,A1,A3,S,T,V,M,NN,LR,IPA,ISYM,R)
C
C     COMPUTES BOUNDARY MATRIX
C
      COMPLEX SM(1),LAM(1),A1(1),A3(1),S(1),T(1),V(1),E(NN)
      COMPLEX V(NN,NN),W(NN,NN),C,CC,D,DD,H,HH
      N1=NN-1
```

```
      N2=NN-2
      N3=NN-3
      C=.5
      C=0.
      IF (IPA.GT.0) GO TO 20
      F=F+R
      G=2.
      DO 10 J=1,NN
      F(J)=E(J)+R
      CALL HANKEL (E(J),M,HH,C)
      CC=C+(0.,1.)
      U =C+E(.)
      DD=F(J)+(0.,1.)
      DO 10 I=1,NN
      W(I,J)=CD*V(I,J)
10    V(I,J)=CC*V(I,J)
      GO TO 40
20    DO 30 J=1,NN
      C=E(J)+(0.,1.)*C
30    W(I,J)=CC*V(I,J)
40    DO 60 J=1,NN
      I=1,1
      W(1,J)=A1(1,J)+A3(1)*W(3,J)
      S(1)=A1(1)*W(1,J)+A3(2)*W(4,J)
      S(2)=A1(2)*W(2,J)+A3(N3)*W(N3,J)
      S(N)=A1(N)*W(N1,J)+A3(N3)*W(N3,J)
      S(NN)=A1(N)*W(NN,J)+A3(N2)*W(N2,J)
      DO 50 I=3,N2
50    S(I)=A3(I-2)*W(I-2,J)+A1(I)*W(I,J)+A3(I)*W(I+2,J)
      DC 60 I=1,NN
60    W(I,J)=S(I)
C
      WRITE (1) E,V
      CALL INVERT (V,NN,NN,S,T,DET)
      WRITE (1) V
C
      DO 80 I=1,NN
      DO 70 J=1,NN
      S(J)=0.
      DO 70 K=1,NN
70    S(J)=S(J)+W(I,K)*V(K,J)
      DO 80 J=1,NN
80    W(I,J)=S(J)
      CC=0.
      DD=0.
      HH=0.
      M=0
      DO 100 I=2,N2,2
      K=I-1
      M=M+1
      C=F+LAM(M)
      D=F+SM(M)
      H=G*A3(I)
      W(K,I)=W(K,I)+C-CC
      W(K,K+2)=W(K,K)+H+H+HH+HH
      W(K,K+3)=W(K,K+2)+H
      W(K,K+3)=W(K,K+3)-C
      W(I,I+1)=W(I,I+1)-D
      CC=C
      DD=D
100   HH=H
```

176

```
      M(N1,MI)=M(N1,MI)+G*A1(NN)
      M(N1,NN)=M(N1,NN1-CC*F*LAN(M*1)
C
      L=0
      DO 150 I=1,NN
      DO 150 J=1,NN
      V(I)=M(I,J)
150   M(I)=V(I)
      M=0
      K=A*A*N+2
      DO 200 I=1,NN,2
      A=K-4
      L=M+1
      M=L*K
      IF (L9,EQ.2) GO TO 190
173   V(I)J=-V(J)
      GO TO 200
190   WRITE (4) (M(J),J=1,M)
200   CONTINUE
      IF (L5,EQ.1) WRITE (4) (V(J),J=1,K)
      IF (ISYM.NE.,1) GO TO 300
      M=0
      K=A*A*N+2
      DO 250 I=1,N,2
      K=K-4
      L=L+1
      M=L*K
256   WRITE (4) (M(J),J=1,M)
300   RETURN
      END


      SUBROUTINE INVERTC(A,NN,N,M,C,DET)
C
C     GENERAL INVERSION OF COMPLEX MATRIX
C     METHOD = GAUSS-JORDAN WITH COMPLETE PIVOTING
C
      DIMENSION M(1)
      COMPLEX A(N,1),C(1),D,TEMP,DE
      CE=1.
      IF (NN-1) 300,350,100
100   DO 110 I = 1,NN
110   M(I) = -1
      DO 200 I = 1,NN
C     LOCATE LARGEST ELEMENT
      X=0.
      DO 135 L = 1,NN
      IF (M(L),GT.0) GO TO 130
      DO 120 K = 1,NN
      IF (M(K),GT.0) GO TO 120
      D=A(L,K)
      Y=A*P*(BF/L(D))+ABS(AIMAG(D))
      IF (X,GT.Y) GO TO 120
      LO = L
      KO = K
      X=Y
120   CONTINUE
130   CONTINUE
      D=A(LO,KO)
```

```
C     CF=DE*D
C     INTERCHANGE ROWS
      L = -M(L)
      M(LO) = M(KO)
      M(KO) = L
      DO 140 J = 1,NN
      C(J) = A(LO,J)
      A(LO,J) = A(KO,J)
140   A(KO,J) = C(J)
C     DIVIDE COLUMN BY LARGEST ELEMENT
      DO 150 K = 1,NN
150   A(K,KO) = A(K,KO)/D
C     REDUCE REMAINING ROWS AND COLUMNS
      DO 170 J = 1,NN
      IF (J.EQ.KO) GO TO 170
      DO 160 K = 1,NN
160   A(K,J) = A(K,J) - C(J)*A(K,KO)
170   CONTINUE
C     REDUCE ROW
      C(KO) = -1.
      DO 180 K = 1,NN
180   A(KO,K) = -C(K)/D
200   CONTINUE
C     INTERCHANGE COLUMNS
      DO 240 I = 1,NN
      L = 0
220   L = L + 1
      IF (M(L).NE.I) GO TO 220
      M(L) = M(I)
      M(I) = L
      DO 240 K = 1,NN
      TEMP = A(K,L)
      A(K,L) = A(K,I)
240   A(K,I) = TEMP
      DET=C*ABS(DE)
300   RETURN
350   A(1,1) = 1./A(1,1)
      DET=C*ABS(A(1,1))
      GO TO 300)
      END


      SUBROUTINE HANKEL (Z,H0,H1,C)
C
C     COMPUTATION OF HANKEL FUNCTION
C     Z - COMPLEX ARGUMENT,-3.1415...LE.ARG(Z) .LE. 0.
C     H0- HANKEL FUNCTION OF SECOND KIND AND FIRST ORDER
C     H1- HANKEL FUNCTION OF SECOND KIND AND SECOND ORDER
C     C - H0/H1
C
      COMPLEX Z,H0,H1,C,A,E,E2,2H,P
      X=REAL(Z)
      Y=AIMAG(Z)
      R=SQRT(X**2+Y**2)
      PH=ATAN2(Y,X)
      IF(R.LE.1C.) GOTO 20
      C=(0.,.1251)/Z
      K=2
      P=C**2
      A=4.5*P
      P=7.5*P
      H0=1.+C+4
```

177

```
      MIN1.=3.*C-R
10    I=AOK
      A=AO1
      A=AO.C=(I+1./K)
      P.PO.C=(I-3./K)
      ..Q=MO+A
      M(M)=P
      IF(A.1)(R.EAL(P))+ABS(AIMAG(P)).GT.1.E-8 ) GOTO 10
      C=AO/M(=(O..-1.)
      A=..TA935M16)19748-X-PMI/2.
      I=.7/797+24002865/SQRT(R)*EXP(Y)*CMPLX(COS(AR),SIN(AR))
      IF(K.EQ.O.) R=CMPLX(O..AIMAG(E))
      MO=MO+E
      M=M(M=E=(O..1.)
      GCTO 30
40    Z=M2/2.
      C=-2*M+2
      *=CMPLX(O...3183U986618.17+01)
      *Z=E+2.
      A=1.-E2=(.977215664901533*ALOG(R/2.))+PM*0.6366197723674982
      P=1.
      M=1
      M2=A
      M1=A+E=(1.-1./C)
25    A=-A=E2/K
      *=-D=C
      MO=MO+AB
      R=M+1
      P=P/(K*K)
      M1=M1+(AOK+P)*P
      IF(ABS(REAL(P))+ABS(AIMAG(P)).GT.1.E-10) GOTO 25
      M(=M1)=2M
      IF(X.NE.O.) GOTO 29
      MO=CPPLX(O..AIMAG(MO))
      M1=CMPLX(R=REAL(M1),0.)
29    C=MO/M1
30    RETURN
      END

      SUBROUTINE STIFF   (U,ICODE,MVB,B,BB,A, .,A,AM,AMM,ND,MM,MMM)
C
C     ASSEMBLES GLOBAL STIFFNESS AND MASS MATR..... ND DETERMINES
C     VARIABLE BANDWIDTH
C
      COMMON/VGFKCON/KUNMP,NUMEL,NUMMAT,NUMKL,NUMLR,NFRQ,RADN,MED(12),
     1      IPLNAX,ISTOP,NDRD(2),OMSQ,ISVM,NPUB
      COMMON/EQNCON/KO,NUMBLK,MBAND,KBAI,H,NR2,NN,NS,NT,NB
      COMMON/ELECON/LM(8),S(8,8),SPI4,S),NNIK,SHAPE
      DIMENSION U(2,1),ICODE(1),A1(MM,ND),AM(MM,ND),MVB(ND)
      CCMPLEX C,B(ND),BB(ND),A(MM,ND),AA(MM,ND)
      CCMPLEX S
      MPREVR=1
      NDP=NT.2
      NUPMLK=O
      20    IO A=1,ND
      B(N)=0.
10    BB(N)=0.
      DO 20 M=1,NT
      A(N)=0.
      AA(M)=0.
```

```
20    AMIN)=O.
Coooo=FORM STIFFNESS AND MASS MATRICES IN BLOCKS
50    NUMALK=NUMBLK+1
      NS=NS=NUMBLK
      MP=AM=NC
      ML=NM-NS+1
      KSHIFT=N*NL-2
      REWIND 1
      DO 120 I=1,NUMEL
      NEAD(1) (LM(I),I=1,154)
      KA=(NM K-1)/NS+1
      IF(NB.NE.NUMALK) GO TO 120
      GO 110 I=1,8
      II=LM(I)-KSHIFT
      L=(I+1)/2
      DO 100 J=1,8
      JJ=LM(J)-LM(I)+1
      IF(JJ.LE.C) GO TO 100
      A(JJ,II)=A(JJ,II)+S(I,J,1)
      M=(J+1)/2
      IF(K.GT.JJ/2) AM(K,II)=AM(K,II)+SM(M,L)
100   CONTINUE
110   CONTINUE
120   CONTINUE
Coooo=DETERMINE VARIABLE BANDWIDTH
      MPREV=MPREVR
      DO 230 N=1,ND
      MPRCV=MPREV-1
      J=MBAND+1
      11=MBAND+N+1
      DO 210 I=1,MBAND
      J=J-1
      II=II-1
      C=A(I,I)
      IF(ABS(REAL(C)).NE.0..OR.ABS(AIMAG(C)).NE.0.0) GO TO 220
210   CONTINUE
      J=J-1
      GO TO 230
220   IF (J.LT.MPREV) J=MPREV
      IF (J.GT.MPREV) MPREV=J
230   MVB(I)=J
      MPREV=MPREV
Coooo=ADD FORCES, FOR DISPLACEMENT B.C.. SET MVB(I)=0
      DO 350 M=N,NM
      IF (N.GT.NUMNP) GO TO 400
      J=2*M-KSHIFT
      1=J-1
      JJ=ICODE(M)+1
      GO TO (310,320,330,340),JJ
310   B(II)=U(1,M)
      H(J)=U(2,M)
      U(1,M)=0.
      U(2,M)=0.
      GO TO 350
320   MVB(I)=0
      B(II)=U(2,M)
      U(2,M)=0.
      GC TO 350
330   B(II)=U(1,M)
      MVB(J)=0
      U(1,M)=0.
```

178

```
      GO TO 350
350   MVRI=IJ
352   CONTINUE
C*****WRITE UPPER BLOCK ON TAPE AND SHIFT UP LOWER BLOCK
310   FORMAT (//11X,A,21)
400   WRITE (2) A,AP,B,MVB
      IF (A.GE.NUMIP) GO TO 900
      DO 420 N=1,NO
      B(N)=C(N)
420   B(N)=0.
      DO 430 N=1,NT
      AI(N)=AI(N)
430   AA(N)=C.
      DO 440 N=1,NTH
      AM(N)=AM(N)
      AM(N)=AMIN,
410   AM(N)=0.
450   RETURN
      END

      SUBROUTINE BLOCKS (U,MVA,MVBB,B,3B,BBB,A,AA,AM,NO,MM,NMM)
C4005 BOUNDARY MATRICES,MODIFIES EQUATIONS FOR PRESCRIBED
C     DISPLACEMENTS AND SOLVES EQUATIONS
      COMMON /GENCON/KUNNP,NUMEL,NUMNP,MUMMAT,NUMLL,NUMLR,NFRQ,RAON,IIED(12),
     1IPLMAX,ISTUP,NORD(21),OMEGO,ISYM,NPBB
      COMMON/IDA/GL/NO/NUMBLR,MBAND,MBAM,NR2,NN,NS,NT,MB
      DIMENSION U(1),MVB(NO),MVRI(NO),AI(NMM,NO)
      DC/OLER  C=0.,B(NO),BB(NO),MB(N,1),AA(N,1),A(MM,NO),AA(MM,NO)
      N1=MVB+1
      N1=N1+1
C*****READ FIRST BLOCK
      NO=1
      NA=NN
      READ (2) A,AM,B,MVB
      L=0
10    AI(L,AI(N)-OMSQ*AM(L)
      DO 10 N=1,NT,2
12    AM(N)=0.
C*****ADD LEFT BOUNDARY MATRIX
      IF (A.NE.1.EQ.0) GO TO 25
      N=NUMEL+1)/NUPLL/2
      READ (6) (AA(L),L=1,M)
      L=0
      N1=N1-NN
      DO 20 N=1,NUMLL
      J=1+NN
      DO 20 K=1,J
20    AI(L)=AI(K)+AA(L)
C*****READ SECOND BLOCK
25    IF (NUMBLR.EQ.1) GO TO 195
      N1=N1-NN
      READ (2) AA,AM,BB,MVBB
      L=0
      DO 30 N=1,NT,2
```

```
      L=L+1
30    AA(N)=AA(N)-OMSQ*AM(L)
      GO TO 135
C*****SHIFT UP LOWER BLOCK
100   NA=NA-1
      NA=NA+NN
      DO 110 N=1,NT
110   AI(N)=AA(N)
      DO 120 N=1,NN
      B(N)=BB(N)
120   MVRI(N)=MVM(N)
C*****READ NEXT B.C.
      IF (NS.(2.NUPLR) GO TO 160
      READ (2) AA,AM,BB,MVBB
      L=0
      DO 130 N=1,NT,2
      L=L+1
130   AA(N)=AA(N)-OMSQ*AM(L)
      DO 132 N=1,NN
      BB(N)=MB(N)+BUB(N)
132   BB(N)=C.
C*****ADD RIGHT BOUNDARY MATRIX
135   IF (NUMLP.EQ.O.OR.NA.LT.NM) GO TO 160
      KSHIT=J-2-NN
      IF (NR.EQ.1) J=2
      IF (J.EQ.O) KSHIT=2
      DO 150 N=1,NUMLR,2
      N=NN+N-1
      IF (N.LE.J.OR.N.GT.NA) GO TO 150
      JJ=NUMLP-N
      L=(I-KSHIT)*N+NO
      M=JJ-JJ+NT
      READ (6) (AA(L),L=1,NT),M)
      L=NT
      DO 140 I=1,L,2
      L=L+NN
      M=L+JJ-1
      DO 140 K=L,M
      L=L+1
140   AI(N)=A(K)+AA(L)
150   CONTINUE
C*****MODIFY FOR DISPLACEMENT B.C.
160   N=N+1
      IF (NO.EQ.1) N=1
      NA=NA+2-1
      CALL MODIFY (U,MVB,A,A,AM,N,MB)
C*****REDUCE BLOCK OF EQUATIONS
200   N=1
      DO 300 N=1,NN
      MV=MV,(N)-1
      IF (MV) 300,290,225
225   C=A(M)
      J=M+1
      MV=MV+M
      I=M+MM
      I=M
      DO 275 L=J,NV
      IF(L.EQ.1
      C=A(L)
      IF(ABS(R(IA(C))-GGS(AIMAGIC))).EQ.0.0) GO TO 275
      C=C/D
```

```
      L=U
      M=M1
      DO 10 I=J,K
      L=L+1
      B(M)=B(M)-A(I)*U(I)
   15 S(L)=A(I)
      R(M)=JU
      IF (M.GE.1) GO TO 30
      K,M=M1
      M=M-1
      L=L+1
      R(M)=B(M)-A(I)*U(I)
   20 S(L)=A(I)
   3C WRITE (7) S
   40 IF (N,FQ,1) GO TO 10C
      K=M1
      DO 50 I=1,K
      J=J-M1
   50 A(J)=0.
  100 CONTINUE
      I=150 N=1,ND
      I=NDBND-NUBN
      IF (MVBIN).EQ.0.AND.I.LE.NQ) B(N)=U(I)
  150 CONTINUE
      RETURN
      END

      SUBROUTINE OUTPUTO (RZ,U,AL,B,E,V,VI,NN)
C
C     COMPUTES REACTION FORCES,OUTPUTS FORCES AND DISPLACEMENTS
C
      COMMON/GINCON/NUMNP,NUMEL,NUMAT,NUMLR,NUMLR,NFRQ,RADN,HED(12),
     1PLNAX,ISTOP,MOD(12),OMSQ,ISYM,NFBB,OMEGA,CPS
      COMMON/ENCOK/NQ,NUMBLK,MBAND,MBANH,MR2,N4,NS,NT,NB
      DIMENSION RZ(1),U(1)
      COMPLEX AL(1),B(1),C(1),V(1),VI(1)
C
      MB=MBAND2-1
      CALL RFORCE (U,B,VI,MBAND,MB)
      WRITE (6,2300) HED , CPS
      DO 10 N=1,NUMNP
      J=NN
      I=J-1
      AHR= REAL(A(I))
      AHI=AIMAG(B(I))
      AHV=SQRT(AHR**2+AHI**2)
      PHH=0.
      IF (AHV.GT.0.) PHH=ATAN2(AHI,AHR)*RADN
      AVR= REAL(B(J))
      AVI=AIMAG(B(J))
      AVV=SQRT(AVR**2+AVI**2)
      PHV=0.
      IF (AVV.GT.0.) PHV=ATAN2(AVI,AVR)*RADN
   10 WRITE (6,2001) N,AHR,AHI,AHV,PHH,AVR,AVI,AVV,PHV
```

```
      JJ=1
      DO 290 K=1,NV
      A(JJ)=A(JJ)-C*A(K)
  290 JJ=JJ+1
      B(I)=B(I)-C*B(K)
      A(I)=C
  2/5 I=1,KM
  20C B(N)=B(M)/A(N)
  220 M=M-MM
C.....WRITE REDUCED BLOCK ON TAPE 3
      IF (N.EQ.NUMBLK) GO TO 400
      WRITE (3) A,B,MVB
      GO TO 130
C.....BACKSUBSTITUTION
  400 JJ=NUMBLK*N-1
  410 M=NT1
      JK
      JJ=JJ-1
      J=K
      N=N-1
      N=N-NN
      C=B(N)
      MV=MVB(N)-1
      IF (MV.LE.1) GO TO 450
      NV=NV+N
      I=1-N
      DO 420 L=J,NV
  420 C=C-A(L)*B(RL)
  450 AA(JJ)=C
      NB=NN-1
      IF (N.EQ.0) GO TO 500
      DO 460 N=1,NN
  460 R(N)=R(N)
  462 B(N)=R(N)
      BACKSPACE 3
      READ (3) A,B,MVB
      BACKSPACE 3
      GO TO 410
C.....INSERT DISPLACEMENTS IN B-ARRAY
  530 DO 600 N=1,NQ
  600 B(I)=A(N)
      RETURN
      END

      SUBROUTINE MODIFY (U,MVB,B,A,S,NJ,MB)
C
C     MODIFIES EQUATIONS FOR PRESCRIBED DISPLACEMENTS
C
      COMMON/EQNCON/NQ,NUMBLK,MM,NMM,NM,NO,NS,NT,NB
      DIMENSION U(1),MVB(1)
      COMPLEX B(1),A(1),S(MM)
      M1=NM-1
      DO 100 N=N,NJ,NM
      I=NBND-NDBM
      IF (MVB(N).GT.0.OR.I.GT.NQ) GO TO 100
      UU=U(I)
      M1=N-1
      K=N+NM
      JK=MM
      IF (UU.EQ.0.0) GO TO 40
```

```
        IF (NPORE.EQ.3) GO TO 200
        L=NUMLR+1
        K=NUMR+2
        L=2*NPP-NUMLR-2
        DO 120 M=L,K
        L=L=1
        WRITE (6,2010) MED,CPS
        IF(NUMLL.GT.0) CALL OUTDIS (R2,AL,B(1),C,V,VI,NUMLL,1)
        IF(NUMLR.GT.0) CALL OUTDIS (R2,AL,B(1),R,V,VI,NUMLR,2)
120 RETURN
C
2000 FORMAT(1H1,12A6//30H NODAL POINT DISPLACEMENTS AT ,F8.6,18H CYCLES
     1 PER SECOND //5X,11HNODAL POINT
     2,11X,17HR - DISPLACEMENTS,37X,17HZ - DISPLACEMENTS//21X,10H  REAL
     3 VALUE   IMAG. VALUE   ABS. VALUE   PHASE SHIFT    REAL VALUE  IMAG.
     4 VALUE   ABS. VALUE   PHASE SHIFT /)
2001 FORMAT (I10,2X,3E13.5,3X,2A,3E13.5,F10.3)
2010 FORMAT (1H1,12A6//47H DISPLACEMENTS OF POINTS BEYOND THE BOUNDARY
     1,43H ,F8.6,18H CYCLES PER SECOND //7H  R-ORD.  Z-ORD.
     2,11X,17HR - DISPLACEMENTS,37X,17HZ - DISPLACEMENTS//21X,10H  REAL
     3 VALUE   IMAG. VALUE   ABS. VALUE   PHASE SHIFT    REAL VALUE  IMAG.
     4 VALUE   ABS. VALUE   PHASE SHIFT /)
        END

        SUBROUTINE BFORCE (J,B,S,MM,MU)
C
C       COMPUTES AND OUTPUTS REACTION FORCES
C
        COMMON/CFCOM/NUMMAT,NUMMAT,NUMLL,NUMLR,NFRQ,RAON,MED(12),
     1  IPLNAX,ISTOP,MTYPE,OMSQ,ISYM,MPBB,OMEGA,CPS
        DIMENSION U(1)
        COMPLEX  B(1),S(MM),C,CV,CV
        NEG=2*NUMP
        C=0.
        CV=0.
        IF (CO.1.NE.0)
        IF (U(1).EQ.0.0) GO TO 130
        N=M1
        IF (M.EQ.1) WRITE (6,2002) MED,CPS
        READ (7) S
        C=0.
        I=I-1
        DO 10 J=1,MM
        K=M1
        IF (K.GT.NEG) GO TO 20
        C=C+S(J)*B(K)
10      C=C+S(J)*B(K)
20      J1
        J=MM
        DO 30 J=2,MM
        K=K+1
        IF (K.LT.1) GO TO 40
30      C=C-S(J)*B(K)   C=C-C*6.2831833
40      IF (IPLNAX.EQ.0)
        MR= REAL(C)
        MI=AIMAG(C)
        VV=SQRT(MM**2+MI**2)
        V=3.
```
(code continues)
```
        IF (MV.GT.0.) HP=ATAN2(MI,MR)/RADN
        R=(1)/2
        IF (L1/2.EC.K) GO TO 90
        CHK=-C
        WRITE (6,2001) R,MR,MI,MV,MP
        GO TO 100
90      CV=CV+C
        WRITE (6,2002) R,MR,MI,MV,MP
100     CONTINUE
        MA= REAL(CV)
        MI=AIMAG(CV)
        MV=SQRT(MM**2+MI**2)
        MP=3.
        IF (MV.GT.0.) HP=ATAN2(MI,MR)/RADN
        VR= REAL(CV)
        VI=AIMAG(CV)
        VV=SQRT(VR**2+VI**2)
        VP=3.
        IF (VV.GT.0.) VP=ATAN2(VI,VP)/RADN
        WRITE (6,2003) MR,MI,MV,MP,VR,VI,VV,VP
        RETURN
C
2000 FORMAT(1H1,12A6//32H NODAL POINT REACTION FORCES AT ,F8.6,18H CYCL
     1ES PER SECOND //5X,11HNODAL POINT
     2,11X,18HR - REACTION FORCE,37X,18HZ - REACTION FORCE//21X,10H  REAL
     3VALUE   IMAG. VALUE   ABS. VALUE   PHASE SHIFT /)
2001 FORMAT (I10,2X,3E13.5,F10.3)
2002 FORMAT (I10,60X,3E13.5,F10.3)
2003 FORMAT (///16H THE SUM OF THE      /16H REACTION FORCES
     1,4X,3E13.5,F10.3,5X,3E13.5,F10.3)
        END

        SUBROUTINE OUTDIS (R2,AL,B,C,V,VI,NN,LR)
C
C       COMPUTES AND OUTPUTS DISPLACEMENTS IN LEFT AND RIGHT
C       LAYERED REGIONS
C
        COMMON/GENCON/NUMMAT,NUMMAT,NUMLL,NUMLR,NFRQ,RADN,MED(12),
     1  IPLNAX,ISTOP,MTYPE,PROM,CMSQ,ISYM,MPBB,OMEGA,CPS
        COMMON/PHYCON/MTYPE(5,40),LM(40,2),IM(40,2),KG(2),KG(2),ZZ(2)
        DIMENSION A(12)(1)
        COMPLEX  AL(1),B(1),E(NN),V(NN,NN),VI(NN,NN),C,CM,CV,D,+MM
        IS=LR*LR-3
        NUMLPNN/2
        IF (LR.EQ.1*M.EQ.3) GO TO 5
        READ (1) E,V
        READ (1) VI
        IF (LR.NE.1) GO TO 5
        DO 7 J=2,NN+2
7       B(J)=-B(J)
5       DO 10 I=1,NN
        AL(I)=0.
        DO 10 J=1,NN
        AL(I)=AL(I)+V(I,J)*B(J)
10      AL(I)=AL(I)+V(I,J)*B(J)
        OM=SQRT(OMSQ)
        IF (IPLNAX.NE.0) GO TO 15
        DO 12 J=1,NN
        CALL HANKEL (E(J),MM,C)
12      AL(J)=AL(J)/MM
```

```
15   DO 100 M=1,NPBD
     WL=(RZ12,N)=AM(LR);=15.
     IF (NO.LT.O.) GO TO 10C
     L=/Z(LR)
     IF (I.GT.NUM.GR.I.LT.1) GO TO 100
     L=I-1
     IF (I.EQ.1) GO TO 25
     DO 20 K=1,L
20   Z=.4*THL(K,LR)
25   IV=I+1
     IH=IV-1
     CM=O.
     CV=O.
     IF (IPL(NAX.EQ.O) GO TO 32
     D=D0(0.,-1.)
     DO 30 K=1,NN
     C=E(K)*D
     C=CEXP(C)*AL(K)
     CH=CH+C*CV(IH*K)
     CV=CV+C*CV(IV*K)
30   CONTINUE
     IF (LR.EQ.1) CV=-CV
     GO TO 35
32   X=(RD*RR(LR))/RR(LR)
     DO 35 K=1,NN
     C=E(K)*X
     CALL HANKEL (C,M,MH,C)
     CH=CH+MHV(IH,K)*AL(K)
     CV=CV+ MHV(IV,K)* B(K)
35   CONTINUE
38   AHR= REAL(CH)
     AMI=AIMAG(CH)
     AMI=SQRT(AHR**2+AHI**2)
     PHI=O.
     IF (AMV.GT.O.) PHV=ATA42(AMI,AHH),BRADN
     AVR= REAL(CV)
     AVI=AIMAG(CV)
     AVV=SQRT(AVR**2+AVI**2)
     PHV=O.
     IF (AVV.GT.O.) PHV=ATA=2(AVI,AVV),BRADN
40   WRITE (6,2003) RZ12,N1,2,CH*AHV,PHH,CV,AVV,PHV
100  CONTINUE
     RETURN
2003 FORMAT (2F6.3,2X,2E13.6,F10.7,5X,3E13.5,F10.3)
     END
```